REPORT DOCUMENTATION PAGE

Form Approved
OMB No. 0704-0188

1. AGENCY USE ONLY *(Leave blank)*	2. REPORT DATE	3. REPORT TYPE AND DATES COVERED
	11.Jan.99	DISSERTATION

4. TITLE AND SUBTITLE
DEVELOPMENT OF A METHOD FOR KINEMATIC GPS CARRIER-PHASE AMBIGUITY RESOLUTION USING MULTIPLE REFERENCE RECEIVERS

5. FUNDING NUMBERS

6. AUTHOR(S)
CAPT RAQUET JOHN F

7. PERFORMING ORGANIZATION NAME(S) AND ADDRESS(ES)
UNIVERSITY OF CALGARY

8. PERFORMING ORGANIZATION REPORT NUMBER

9. SPONSORING/MONITORING AGENCY NAME(S) AND ADDRESS(ES)
THE DEPARTMENT OF THE AIR FORCE
AFIT/CIA, BLDG 125
2950 P STREET
WPAFB OH 45433

10. SPONSORING/MONITORING AGENCY REPORT NUMBER
FY99-62

11. SUPPLEMENTARY NOTES

12a. DISTRIBUTION AVAILABILITY STATEMENT
Unlimited distribution
In Accordance With AFI 35-205/AFIT Sup 1

12b. DISTRIBUTION CODE

13. ABSTRACT *(Maximum 200 words)*

14. SUBJECT TERMS

15. NUMBER OF PAGES
0

16. PRICE CODE

17. SECURITY CLASSIFICATION OF REPORT	18. SECURITY CLASSIFICATION OF THIS PAGE	19. SECURITY CLASSIFICATION OF ABSTRACT	20. LIMITATION OF ABSTRACT

THE UNIVERSITY OF CALGARY

Development of a Method for Kinematic GPS Carrier-Phase Ambiguity Resolution Using Multiple Reference Receivers

by

John F. Raquet

A DISSERTATION

SUBMITTED TO THE FACULTY OF GRADUATE STUDIES

IN PARTIAL FULFILLMENT OF THE REQUIREMENTS FOR THE

DEGREE OF DOCTOR OF PHILOSOPHY

DEPARTMENT OF GEOMATICS ENGINEERING

CALGARY, ALBERTA

MAY, 1998

THE UNIVERSITY OF CALGARY

FACULTY OF GRADUATE STUDIES

The undersigned certify that they have read, and recommend to the Faculty of Graduate Studies for acceptance, a dissertation entitled "Development of a Method for Kinematic GPS Carrier-Phase Ambiguity Resolution Using Multiple Reference Receivers" submitted by John F. Raquet in partial fulfillment of the requirements for the degree of Doctor of Philosophy.

Supervisor, Prof. G. Lachapelle, Department of Geomatics Engineering

---

Prof. M. E. Cannon, Department of Geomatics Engineering

Prof. P. Maybeck, Air Force Institute of Technology

Prof. R. Johnston, Department of Electrical Engineering

Prof. P. Enge, Stanford University

Date

ABSTRACT

To perform the most precise relative positioning using GPS, it is necessary to resolve the carrier-phase integer cycle ambiguities. This process becomes increasingly difficult as the distance between the mobile and reference GPS receivers increases, due to the decorrelation of the GPS errors with distance, resulting in a practical limit on the distance over which ambiguity resolution can be performed when using a single reference receiver.

This thesis proposes a novel method, called NetAdjust, which uses multiple reference receivers to reduce code and carrier-phase differential measurement errors and improve the ability to resolve carrier-phase ambiguities. The NetAdjust method is based upon an optimal linear minimum error variance estimator, and it "encapsulates" all of the network information into the measurements of a single reference receiver, so standard single-reference differential GPS processing algorithms can be used. The geometry of the reference receiver network is embedded within the error covariance matrix, and a functional form of this covariance matrix is described.

The NetAdjust method was tested using two different GPS networks—an 11-receiver network covering a 400 km $\times$ 600 km region in southern Norway, and a 4-receiver network covering a 50 km $\times$ 150 km region at Holloman AFB in New Mexico. The results for L1 code, L1 phase, and widelane phase measurements are analyzed in the measurement domain and the position domain, showing improvements in RMS errors of up to 50% when using NetAdjust. Significant improvements in the ability to resolve carrier-phase ambiguities are also demonstrated for the Holloman and Norway test networks. Issues relating to development of an operational, real-time NetAdjust system are discussed.

Also, a covariance analysis method is developed which can be used to predict NetAdjust effectiveness under various conditions and network configurations. This covariance analysis demonstrates that, for the conditions present during the Norway test, the network of eleven reference receivers is sufficient to perform widelane ambiguity resolution, but it is not sufficiently accurate for L1 ambiguity resolution throughout the network.

ACKNOWLEDGEMENTS

As I complete this dissertation I am filled with gratitude to those who have enabled this work to be done. At the risk of inadvertantly missing some, I'd like to express appreciation those that have had especially significant impact on me over the past few years.

- First and foremost, to God who has given me all that I have, including my family, friends, teachers, abilities, vocation, and new life through His Son (which is most important). I do not consider anything in this document to be my own creation. Rather, it is a discovery of what He has already created, and I have found great joy in this discovery process.

- To my wife, Cindy, who has been a constant source of encouragement ever since I met her. She is the person most responsible for encouraging me to aim for a doctorate, and she has supported me through the entire endeavor. I would especially like to recognize her Herculean efforts over the last few months of writing, when she shouldered much of the load at home during my long hours in the office. (She even read the *whole* dissertation!) She is my perfect complement, and I can't imagine what life would be like without her.

- To my children, Anna, Nathan, Ellen, and Carol, who probably don't realize how much our wrestling matches and stories before bed helped to keep things in perspective. They are truly gifts from God.

- To my parents, who freely gave everything they had to support and encourage me for many, many years. They taught me to love God, respect others, and work diligently, and they can take the credit for much of what I am today. They are the best teachers I've ever had.

- To my advisor, Dr. Gérard Lachapelle. He is the primary reason that I came to The University of Calgary, and I have had no regrets about that decision. His office door was always open, and I especially appreciate the countless hours that he spent

talking with me about this research and other important matters. My only complaint is that he still doesn't seem to know the correct spelling for the word "meter."

- To *all* of my fellow students, especially Richard, Chris, Sun, and Rob. Interacting with each of you has been an enriching experience, and a highlight of my time in Calgary.

- To Professors M.E. Cannon, P. Maybeck, P. Enge, and R. Johnston, the members of my examining committee. Your efforts at reading through this dissertation and your feedback are greatly appreciated.

- To Tor Egil Melgård and Kværner Marine Automation for collecting and giving me access to the data from the Norwegian network.

- To the U.S. Air Force and the Killam Memorial Scholarship, for providing the financial support for this research.

- Finally, to all the teachers that have invested their lives into their students, including me. In particular, I'd like to thank Mrs. Levtzow, Mr. Fenske, and Lt. Col. Cloud for pushing me as far as possible.

DEDICATION

To Cindy — my perfect puzzle piece.

He who finds a wife finds a good thing

Proverbs 18:22

A wife of noble character, who can find? She is worth far more than rubies. Her husband has full confidence in her and lacks nothing of value. She brings him good, not harm, all the days of her life. ... She watches over the affairs of her household and does not eat the bread of idleness. Her children arise and call her blessed; her husband also, and he praises her: **"Many women do noble things, but you surpass them all."**

Proverbs 31

♡

Contents

List of Tables

List of Figures

Notation

List of Symbols

Symbol	Description
A	Design matrix
$\mathcal{B}$	Bayes risk.
B	Double difference matrix (see section 3.1.2).
B_1	The double difference matrix [$\mathrm{B}_{n,n}$ **0**] used to generate double differences between only the network reference stations.
B_2	The double difference matrix [B_{cp_1} B_{cp_2}] used to generate double differences between the network reference stations and a mobile receiver at the "computation point".
$\boldsymbol{C}$	Covariance matrix.
$\boldsymbol{C}_{\delta\ell}$	Covariance matrix of the measurement errors $\delta\ell$. These are the errors that are not cancelled in the double-differencing process.
$C_{\hat{\mathbf{x}}}$	Covariance matrix of the estimated parameters.
Δt	Time interval (between measurements).
$\mathbf{I}$	Identity matrix.
I	Ionospheric delay factor ($= 40.30TEC$) ($\mathrm{Hz}^2\mathrm{m}$).
L	Loss function.
ℓ_{true}	True measurement-minus-range vector.
L1	Relating to the GPS signal transmitted at a frequency of 1575.42 MHz.
L2	Relating to the GPS signal transmitted at a frequency of 1227.60 MHz.
N	Carrier-phase cycle ambiguities (usually an integer) (cycles).
N_e	Local electron density (electrons/m^3).
P_{rec}	Receiver position.
$\mathbb{P}_{rec}$	True receiver position (at receive time).
$\Psi_{xx}(\tau)$	Autocorrelation function.
P_{sv}	Satellite position.
$\mathbb{P}_{sv}$	True satellite position (at transmit time).
R	Range between the receiver and the satellite (m).
$\mathbb{R}$	The true range between the GPS receiver position at the time it received the signal and the satellite position at the time it transmitted the signal.

Symbol	Description
S	Total signal at GPS receiver antenna, including direct and reflected components.
S_D	Direct carrier-phase signal from satellite to receiver.
SOSr	Sum of squares of the residuals.
SOS_{ratio}	Ratio of the second best sum of squares of the residuals to the best sum of squares of the residuals.
S_R	Reflected carrier-phase signal (which causes multipath).
T	Delay of the GPS signal due to the troposphere (m).
TEC	Total Electron Content—the electron density integrated along the signal path (electrons/m^2).
WL	Widelane—formed by subtracting the L2 value from the L1 value of the item being described, i.e. WL = L1 - L2.
$\boldsymbol{Y}$	Vector of observations.
α	Attenuation factor of reflected signal.
α_m	Attenuation of the phase due to multipath.
c	Speed of light (299792458.0 m/sec).
d	Distance between two points on the ground (km).
δ	Sum of correlated errors and uncorrelated errors.
$\boldsymbol{\delta P_{rec}}$	Error in receiver position.
$\boldsymbol{\delta R}$	Error in computed range.
δ_c	Correlated errors (includes satellite position, receiver position, troposphere, and ionosphere errors).
d_c	Correlated errors, relative to the reference point $\boldsymbol{p}_0$.
$\delta\phi_M$	Phase shift due to multipath.
δp_{rec}	Projection of the nominal receiver position error onto the line-of-sight vector to the satellite ($\boldsymbol{e} \cdot \boldsymbol{\delta P_{rec}}$).
δp_{sv}	Projection of the satellite position error onto the line-of-sight vector to the satellite ($\boldsymbol{e} \cdot \boldsymbol{\delta P_{sv}}$).
$\boldsymbol{\delta P_{sv}}$	Error in computed satellite position.
δt_{rec}	Receiver clock error (sec).
δt_{sv}	Satellite clock error (sec).
δ_u	Uncorrelated errors (includes multipath and receiver noise).
δx	X position error (m).
δy	Y position error (m).
δz	Z position error (m).
ε	Satellite elevation.
$\mathbf{e}$	Estimator function.
$\boldsymbol{e}$	Unit line-of-sight vector.
err	Error (estimated minus true value).
f	Frequency (Hz).

Symbol	Description
$\boldsymbol{\ell}$	Measurement-minus-range vector.
$\boldsymbol{l}$	Measurement vector.
λ	Carrier-phase wavelength (m).
m	Delay of the GPS signal caused by multipath (could be positive or negative) (m).
μ	Elevation mapping factor.
ϕ	GPS receiver phase measurement (cycles).
$\boldsymbol{p}$	Position vector.
ρ	GPS receiver code measurement (m).
v	Measurement noise (m).
$\boldsymbol{x}$	Parameter vector.

List of Acronyms

Acronym	Description
AFM	Ambiguity Function Method
CA	Coarse Acquisition (code)
DGPS	Differential GPS
ECEF	WGS-84 Earth Centered Earth Fixed reference frame
FARA	Fast Ambiguity Resolution Approach
FASF	Fast Ambiguity Search Filter
GPS	Global Position System
PRN	Pseudo-Random Noise code (used to identify the signal from a particular satellite)
RMS	Root Mean Squared value
SA	Selective Availability
SNR	Signal-to-Noise Ratio
SV	Satellite Vehicle
TEC	Total Electron Content–the electron density integrated along the signal path
UTC	Coordinated Universal Time
WAAS	Wide Area Augmentation System
WADGPS	Wide Area Differential GPS
WGS-84	World Geodetic System – 1984
WL	Widelane–formed by subtracting the L2 value from the L1 value of the item being described, i.e. WL = L1 - L2

List of Operators and Other Notation

Operator	Description
$\Diamond^{-1}$	Matrix inverse.
$\hat{\Diamond}$	Estimated value of $\Diamond$.
$\tilde{\Diamond}$	Unavailable measurement (one which does exist, but is not available for use in the NetAdjust algorithm).
$E[\Diamond]$	Expected value of $\Diamond$.
$\Delta\nabla\Diamond_{ab}^{xy}$	Double difference of $\Diamond$, which is $(\Diamond_a^x - \Diamond_a^y) - (\Diamond_b^x - \Diamond_b^y)$.
$\Diamond_1 \cdot \Diamond_2$	Dot (inner) product of $\Diamond_1$ and $\Diamond_2$.
$\bar{\Diamond}$	Bar over the symbol represents a measurement-minus-range observable (the range measurement minus a nominal calculated range).
$\Diamond^T$	Matrix or vector transpose.
$\lvert\Diamond\rvert$	Magnitude (2-norm) of the vector $\Diamond$.
$\mathbf{\Diamond}$	Boldface indicates a matrix or vector.

Chapter 1

Introduction

In this thesis, a novel and effective approach is presented for using a network of reference receivers to perform kinematic carrier-phase positioning.

1.1 Background

To improve the attainable accuracy using GPS, many differential GPS (DGPS) techniques have been developed which perform relative positioning between two or more GPS receivers. The basic premise of these DGPS techniques is that many of the sources of GPS measurement errors are correlated between receivers. By only performing relative positioning between receivers, rather than absolute positioning of the receivers, the correlated portions of the measurement errors are reduced, resulting in a significant increase in accuracy and precision.

Differential GPS techniques can be classified according to the type of GPS measurement that is used:

- *Code* differential techniques use the GPS pseudorange measurement which is obtained by locking onto the pseudorandom code for a given satellite and measuring the time difference between transmit and receive time to determine satellite range. The code measurement is an absolute range measurement, which provides a value of the true range between the satellite and the receiver, after removal of clock errors

and other error sources. It is relatively easy to implement differential GPS for code measurements, because it is an absolute measurement.

- *carrier-phase* differential techniques rely upon a measurement of the accumulated phase of the GPS carrier. It is not an absolute measurement, because the number of carrier-cycles at the start of the accumulation (known as the phase ambiguity) is not known. Due primarily to the different wavelengths of the code and carrier-phase measurements (about 290 m for C/A code and 0.2 m for carrier-phase), carrier-phase measurements are much more precise. The phase ambiguities must be determined, however, to use carrier-phase measurements for positioning.

Because the phase ambiguities are integer values, the most accurate differential techniques resolve these integer ambiguities, resulting in relative positioning accuracies at the cm level. Carrier-phase ambiguity resolution is limited, however, by measurement errors that are not removed in the double-differencing process. These measurement errors are grouped into spatially correlated errors (atmospheric and satellite position errors) and uncorrelated errors (receiver noise and multipath). Because differential atmospheric errors increase with the distance between the mobile and reference receivers, the ability to perform carrier-phase ambiguity resolution successfully decreases with distance as well.

This requirement to be close to a reference receiver is a significant operational constraint for many precise positioning applications. For example, suppose that there is a requirement to provide cm-level positioning over 100 km $\times$ 100 km area around a medium sized city. If the mobile receiver needs to be within 10 km of a reference receiver to guarantee rapid single-frequency integer ambiguity resolution, then one approach would be to place 25 reference receivers around the city as shown in Figure 1.1. In this figure, the small dark dots are reference receivers, and the grey circles are the areas that they effectively cover. This is obviously a poor approach, for a large number of receivers (and reference sites) are required, and some areas still remain uncovered. Another approach would be to increase the maximum distance over which ambiguities can be resolved by

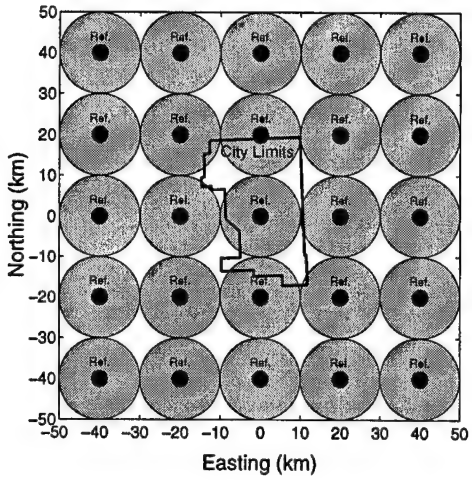

Figure 1.1: *Use of many independent reference stations to cover desired area. A mobile receiver would use reference data from just the nearest reference receiver.*

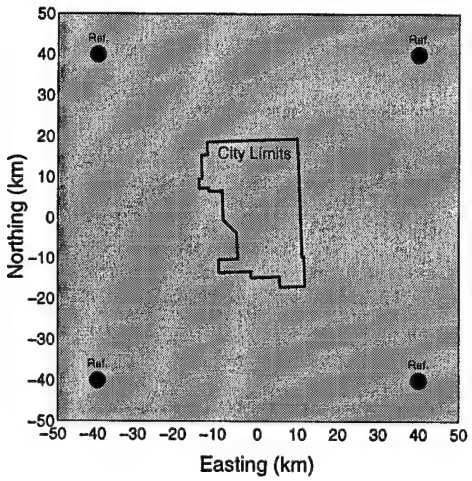

Figure 1.2: *Use of network of reference stations to cover desired area. A mobile receiver would use reference data combined from all four reference receivers.*

using more advanced data processing techniques (such as better error models or combinations of dual frequency measurements). This approach has merit and is commonly used, but there remains an effective (albeit larger) maximum radius for accurate ambiguity resolution.

A different approach is shown in Figure 1.2, where instead of using a single reference receiver, data from multiple reference receivers are used together in a carrier-phase network. In this hypothetical example, only four reference receivers (represented by black dots) are required to provide coverage for the entire area. Note that this example refers to coverage of an area the size of a city, but this approach can be scaled up to the size of a state or province or even a country (as will be shown in Chapter 4).

It is not immediately obvious how to use a network of reference receivers effeciently for performing carrier-phase ambiguity resolution, without solving for separate sets of integer ambiguities to each reference receiver. In this thesis, one promising approach to this problem is presented.

1.1.1 Related Research

1.1.1.1 Carrier-Phase Ambiguity Resolution

One of the simplest ambiguity resolution algorithms is to use code measurements to determine the carrier-phase ambiguities directly (code/carrier smoothing) (Hatch, 1982). This method alone is not adequate generally to determine integer ambiguities. An early effort to resolve integer carrier-phase ambiguities was the Ambiguity Function Method (AFM) (Counselman and Gourevitch, 1981; Mader, 1990; Remondi, 1991). The AFM is a coordinate domain search technique that is computationally intensive and is not commonly used in its original form.

Next, the least squares search method was developed (Hatch, 1990; Lachapelle et al., 1992). With a least squares search, sets of integer ambiguities are tested by calculating the least squares position estimate and residuals. If one set of ambiguities has significantly lower residuals than the rest, then it is considered the correct ambiguity set. While more efficient than the AFM, in its most basic form it can still be computationally intensive and require a large amount of memory. A number of improvements to this method have been proposed which greatly increase efficiency and reduce memory requirements (Euler and Landau, 1992; Borge and Forssell, 1994).

Another class of ambiguity resolution techniques involves the use of a covariance matrix of the ambiguities, which is normally calculated by a Kalman filter or a weighted least-squares algorithm. One of the earliest such techniques was the Fast Ambiguity Resolution Approach (FARA) (Frei and Beutler, 1990). Other ambiguity covariance methods include the Fast Ambiguity Search Filter (FASF) (Chen and Lachapelle, 1995), an integer nonlinear programming method (Wei and Schwarz, 1995), and the Z-transform method (Teunissen, 1994). A more statistically precise method for choosing the best ambiguity is given by Han (1996). Dual frequency data can also be used to aid the ambiguity resolution process (Hatch, 1989; Abidin, 1991; Lu et al., 1995).

Recently, interest has been shown in single-epoch integer ambiguity resolution tech-

niques (Han and Rizos, 1996; Pratt et al., 1997). These require high quality dual frequency GPS receivers, and they are very sensitive to uncancelled differential errors.

Some have developed algorithms which are specifically designed to perform precise carrier-phase positioning over long baselines. One method calculates the dual-frequency (widelane) ambiguities at the start and end of the mission by taking off and landing near the reference receiver (Sonntag et al., 1995). Ambiguities in mid-flight are then estimated, holding the known ambiguities fixed. This is performed after the mission is completed, using forward and backward filtering, and it would fail if the mobile receiver was reinitialized mid-flight (or if there were excessive cycle slips).

Colombo studied precise GPS positioning over long baselines using a software simulation (Colombo, 1991). A high-order Kalman filter/smoother was used to estimate satellite position errors, reference receiver position errors, atmospheric refraction errors, mobile receiver position, and phase ambiguities using dual frequency carrier-phase and single frequency L1 Coarse Acquisition (CA) code measurements. There were no multipath errors in this simulation. He showed that using the high-order model (versus estimating only position and velocity) significantly improved positioning accuracy, especially when there were large satellite orbit errors. He also showed that using two reference receivers improved the results. The smoothing portion of this near-optimal method can only be performed in post-mission mode.

Each of these methods have their own strengths and weaknesses, and there is no question that having a robust, well-designed algorithm can improve ambiguity resolution results. Nevertheless, there remains a limit to the time required and the distance over which ambiguities can be resolved correctly due to the presence of uncancelled differential measurement errors (such as multipath, satellite position errors, and unmodeled atmospheric errors). Even a method that optimally calculates the integer ambiguities is limited by the presence of these uncancelled errors. The approach in this thesis is to reduce the errors, rather than to develop an improved ambiguity resolution technique. If the errors are reduced, then all of the ambiguity resolution techniques listed above will show improved

performance.

1.1.1.2 Reducing Uncancelled Differential Errors

Uncancelled differential errors are those errors which are not eliminated by measurement double differencing. These include satellite position errors, atmospheric propagation errors, multipath, and receiver noise. Receiver noise is primarily a function of receiver design tradeoffs, and it is relatively small and benign (since it is more or less zero-mean white noise). Efforts to reduce the other three uncorrelated error sources explicitly are given below. Reducing any of these errors will enhance the ability to perform carrier-phase ambiguity resolution.

1.1.1.2.1 Reducing Satellite Position Errors For real-time, non-differential users, the satellite position error includes errors in the broadcast ephemerides and the effects of Selective Availability (SA), which introduces both a clock and satellite position error. The contribution of SA error to the user range error is 24 m (1-σ) (Zumberge and Bertiger, 1996). The non-clock portion of the SA error can cause an error when the double difference measurements are generated for integer ambiguity resolution. Even when SA is turned off, errors in the broadcast ephemerides remain which impact positioning accuracy. The U.S. National Research Council recommended improving the satellite ephemeris and clock estimates by increasing the satellite navigation data update frequency, increasing the number of GPS reference stations, and using a non-partitioned Kalman filter for the orbit estimation (Committee on the Future of the Global Positioning System, 1995).

Simply using differential GPS significantly reduces orbital errors, even over long baselines. For example, an orbital error of 2.5 m will result in only a 1 cm positioning error over a 100 km baseline (Rothacher, 1997).

A number of organizations also use worldwide reference receiver networks to calculated post-mission precise orbits at a very high accuracy (20 cm or better) (Kouba et al., 1993). These precise orbits are used to help isolate the various errors sources in Chapter 2.

1.1.1.2.2 Reducing Atmospheric Propagation Errors Spatial variations in the ionosphere and the troposphere introduce errors into the double difference measurements that increase with the distance between the two receivers. A standard ionospheric model can be used to remove approximately 50% of the ionospheric error in mid-latitude regions (Klobuchar, 1987). For greater accuracy, an ionospheric contour or ionospheric grid can be calculated using a network of ground receivers. This grid can then be used to provide accurate ionospheric corrections for any receiver/satellite combination with a receiver-to-satellite line of sight that pierces the grid (Skone et al., 1996; Kee, 1996; Enge and Van Dierendonck, 1996). Another method for modeling the ionosphere using tomography is presented by Hansen et al. (1997). Dual frequency users can determine the ionospheric effect directly, using the difference between the pseudorange measurements of the two frequencies (ICD-GPS-200C, 1993). Other methods have been devised to estimate ionospheric delays as well (Goad, 1990; Cohen et al., 1992).

A great number of models have been developed for estimating the delay induced by the troposphere (Hopfield, 1969; Goad and Goodman, 1974; Santerre, 1987; Marini, 1972; Baby et al., 1988; Mendes and Langley, 1994). These work fairly well, but they do generally require input of meteorological parameters which may have errors. Also, the troposphere is at times not homogeneous (such as when a storm front is moving through), which can result in errors. Some have modeled the tropospheric error as part of the ambiguity estimation process, with some success (Brown et al., 1995).

1.1.1.2.3 Reducing Multipath The most basic method for reducing multipath is to place the GPS antenna in a low-multipath environment, away from any potential reflectors and with a good ground plane or choke ring (Tranquilla et al., 1994). Another common method for reducing code multipath is to smooth the code measurements with the carrier-phase measurements (Hatch, 1982). Some have attempted to model the multipath environment around a fixed antenna using simulated or real data (Hajj, 1990; Cohen, 1992; Hardwick and Liu, 1995). Others have used the signal-to-noise ratio in combina-

tion with the antenna gain pattern to estimate the carrier-phase multipath (Axelrad et al., 1996). A number of techniques involve signal processing methods internal to the GPS receiver (Townsend and Fenton, 1994; Townsend et al., 1995; Kumar and Lau, 1996). Filtering techniques have also been used to estimate and correct for the multipath errors (Johnson and King, 1996). Using multiple reference receivers for multipath reduction has also been demonstrated (Raquet, 1996; Raquet and Lachapelle, 1996).

1.1.1.3 Use of Multiple Reference Receivers

1.1.1.3.1 Code Based Positioning It has long been recognized that using multiple reference receivers improves differential positioning results. Multiple reference systems have been implemented for code (or carrier-smoothed code) positioning in many different applications, normally in the context of a Wide-Area Differential GPS (WADGPS) system for positioning (Kee and Parkinson, 1992; Lapucha and Huff, 1992; Ashkenazi and Hill, 1992; Spradley, 1993; Szabo and Tubman, 1994). Because the code measurement is an absolute measure of range and time (i.e., there are no ambiguities), most of these methods generate individual measurement corrections as a function of the mobile receiver position. One way to do this is to estimate code measurement corrections at each reference receiver and then use an estimation (i.e., interpolation) algorithm to determine the corrections at the mobile receiver location.

This approach has been implemented using a Kalman filter with a one-dimensional (Gauss-Markov) spatial decorrelation function (Tang et al., 1989). A similar approach using least-squares adjustment techniques is presented in Loomis (1991). In Mueller (1994), all of the individual pseudorange corrections for a given satellite are combined using a weighting function which explicitly minimizes the variance of the errors. This also relies upon a spatial decorrelation (or covariance) function, and it is very similar (if not identical) to the approaches by Tang and Loomis et al., because Kalman filters and least-squares estimators also minimize the error variance. All three of these methods essentially interpolate the whole-valued corrections for the mobile receiver position.

An alternative method is to estimate explicitly three-dimensional satellite position errors, ionospheric errors (using an ionospheric grid, for example), and SV clock errors, and then transmit these to the mobile user who then calculates the corresponding errors at their specific location. An example of this approach is the Wide Area Augmentation System (WAAS) (Enge and Van Dierendonck, 1996; Enge et al., 1996; Enge, 1997). This approach would be applicable to carrier-phase positioning, as described in the next section. However, because small (10–20 cm) errors are not very significant for code-based positioning, systems that are designed for code positioning often would not have the accuracy required to significantly aid in carrier-phase positioning.

1.1.1.3.2 Carrier-Phase Based Positioning Lapucha and Barker (1996) have used a network of two reference receivers applied to carrier-phase ambiguity resolution, but only to improve the code positioning accuracy (which reduces the size of the ambiguity search space), and to provide a quality check of the ambiguities which are solved separately between the mobile receiver and each reference receiver. Checking the ambiguities between multiple reference receivers has also been performed in an aircraft-to-aircraft test (Lachapelle et al., 1994) and in a shipborne mode (Weisenburger, 1997).

An approach to reducing the distance dependence of carrier-phase positioning errors has been proposed by Wübbena et al. (1996).. This approach involves generation of a geometric model for carrier-phase corrections, using horizontal coordinates as parameters. The "network coefficients" of the geometric model are calculated by performing a least squares adjustment of a network of reference stations. Using the network coefficients, it is then possible to interpolate the DGPS carrier-phase corrections for specific locations within the area covered by the network. While this method has been described, it apparently has not yet been successfully implemented, as the results in W ubbena et al. (1996) use a full network adjustment software package to "simulate" what could be done by this approach.

A similar approach proposed by Varner generates partial derivative corrections for

each individual phase double difference measurement, and it has shown promising results (Varner, 1997). An advantage of this method over the estimation of the single geometric model given in (Wübbena et al., 1996) is that the uncorrelated errors (like multipath) can be accounted for. In this approach, the differential errors between a base reference receiver and each of the other reference receivers are used as measurements to estimate multipath at each site and to estimate the differential phase error as a function of position, by fitting it to a polynomial of position variables. The user then uses the error polynomial (and the estimated multipath error) to calculate the estimated differential error at their location. A simplified version of this same approach is given by Han (1997).

Another approach to this problem presented by Wanninger is to model the differential ionosphere explicitly, using a linear interpolation algorithm (Wanninger, 1995). As originally presented, this method involves calculation of differential ionospheric delays among network of three reference stations surrounding the mobile receiver. The differential ionosphere is then linearly interpolated to the mobile user position (hence the name linear interpolation algorithm).

Gao et al. (1997) improved upon this algorithm by extending it to any number of reference stations. They also modeled the satellite ephemeris error, and demonstrated a significant improvement in positioning accuracy over the uncorrected case.

1.2 Statement of the Problem

1.2.1 Objective

Using a network of reference receivers (rather than a single reference receiver) should improve the ability to resolve carrier-phase integer ambiguities by reducing the differential errors. Evidence of the improvement would take three different forms:

- Use of a network should improve the performance of ambiguity resolution algorithms, relative to the single reference case at the same distance. Performance is

measured in terms of the ability to determine the correct ambiguities and the time required to do this.

- Use of a network should increase the distance over which ambiguities can be accurately resolved, relative to the single reference case.

- Use of a network should reduce the errors in the differential code and carrier-phase measurements for the mobile user. The differential errors that should be reduced are all errors that are not cancelled in the double differencing process (except for the integer ambiguities). Reducing these errors improves the ability to resolve the carrier-phase ambiguities, and provides better positioning performance once the ambiguities are known.

The primary objective for this research is to develop and test a methodology for using multiple reference receivers which a) reduces differential errors, b) improves ambiguity resolution performance (for a given inter-receiver distance), and c) increases the inter-receiver distance (for a fixed level of performance).

1.2.2 Requirements

As in most engineering problems, many different approaches can meet the stated objective to some degree or another. The goal of this research is to develop a method which meets the primary objective *and* which is practically realizable in real-world and real-time situations. To this end, there are four requirements in addition to the primary objective, as described in the following sections.

1.2.2.1 Real-Time Capability

It must be possible to implement this methodology in a real-time mode (with a small data latency) as well as in post-mission mode. While this research will not involve actually

implementing a real-time system, the approach should be developed with consideration of real-time implementation at a future time.

There are many applications in which real-time processing is absolutely necessary. The most obvious example is navigation, in which (users need to know their position in order to make real-time decisions about how to proceed. Landing an aircraft is one such application.

1.2.2.2 Network Details Hidden

This method should accept any number of reference stations at arbitrary locations. In addition, the real-time user should not be required to have to know the number of reference receivers, or their positions. In this way, the task of maintaining an operating network can be separated from the use of that network.

Any network set up within a particular geographic region would probably begin with a minimal number of reference receivers (perhaps using receivers that currently exist). If the system is designed around this initial network (by requiring transmission of all of the raw data from the reference receivers to the mobile receiver, for example), then adding more reference receivers could be difficult. If there is a desire to add more receivers to the network (which commonly happens), then it is important to allow for seamless incorporation of new reference receivers into the network. If the network details are hidden from the mobile user, then additional reference stations will affect improved performance without any additional computational load on the mobile user.

1.2.2.3 Minimal Ambiguity Set

This method should require solving for only a single set of integer ambiguities, as would be the case if there were only a single reference receiver. Again, the desire is to make it as easy as possible for the mobile user to resolve the carrier-phase integer ambiguities.

1.2.2.4 Minimize Data Link Bandwidth Requirement

In any real-time differential system, the bandwidth of the differential data link is often a limiting factor. This method should be chosen with consideration to minimizing data link bandwidth requirements. For example, it would be unacceptable to require transmission of the raw data from all of the reference receivers to the mobile receiver.

1.2.3 Assumptions

The assumptions listed in the sections below are top-level assumptions which help to define the scope of this research. Many of these assumptions are actually topics for additional, complementary research.

1.2.3.1 Reference Receiver Coordinates Known

The locations of the reference stations are assumed to be known to a very high level of accuracy (e.g., $<$ 1cm). This can be done off-line using many days of GPS data, if necessary.

1.2.3.2 Centralized Data Collection

It is assumed that the data from all of the reference receivers can be collected at one central location to be processed (in real-time, for real-time mode). This is a common approach for real-time network differential GPS systems (Lapucha and Huff, 1992).

1.2.3.3 Large Data Processing Ability on Network Data

While computational load of the mobile user should be minimized (as stated above), it is assumed that there is much computational capability for processing the data from the network prior to transmission to the mobile user. Because all of the data is sent to a central processing location (see above), it will be possible to have this data processed by sufficiently powerful computers at this location.

1.2.3.4 Network Ambiguities Known

It is assumed that L1 and widelane carrier-phase integer ambiguities have been resolved between each of the reference stations. This is a considerable challenge to implement in real-time, and this issue is discussed further in Chapter 6.

1.3 Contributions of This Research

In this thesis, a novel and effective approach is presented for kinematic carrier-phase positioning using a reference receiver network. In this approach, code and carrier-phase measurement corrections are generated which minimize the sum of the variances of the differential measurement errors (i.e., the trace of the error covariance matrix). As stated earlier, a minimum error variance approach for code measurements was given in Mueller (1994), which calculates corrections based upon network code measurement errors. For carrier-phase measurements, individual measurement errors are not directly available from the network (because of the unknown cycle ambiguities), so double differencing must be used as part of the minimum variance estimation process.

This minimum error variance approach is equivalent to a least squares condition adjustment on the measurements from each of the reference stations, and insight into the method is gained by interpreting it as such. The method presented in this thesis, which minimizes the sum of the differential error variances, will be referred to as the "NetAdjust" method.

The most distinguishing feature of the NetAdjust method relates to the assumptions about the characteristics of the errors as a function of position. Each of the other carrier-phase methods discussed in the previous section explicitly assumes a functional form which relates the error to position, and then calculates the coefficients of this functional form using the reference receiver data. In contrast, the NetAdjust approach does not force the errors themselves into a particular functional form (of position). Rather, the error *covariance* is expressed in a functional form (with coefficients based upon data from

the reference receiver network), and then this covariance is used to calculate the actual errors for any given mobile user position. In this way, the NetAdjust method is based upon determination of an accurate expression of the second moment (covariance) of the network errors.

One advantage the NetAdjust approach is that it enables a realistic covariance analysis to predict performance under various network conditions, including various reference network configurations (number/position of reference stations), satellite configuration (number/direction of satellites), positions of the mobile user, and different levels of correlated errors (atmospheric and satellite position errors).

The specific contributions of this research can be stated as follows:

1. Development of a new method for performing kinematic carrier-phase positioning using multiple reference receivers (the NetAdjust method), which minimizes the sum of the differential error variances (the trace of the error covariance matrix).
   (a) Mathematical description of the carrier-phase network problem.
   (b) Development of a functional form of the covariance matrix of the measurement errors from the reference network (using double-difference data).
   (c) Methodology for determining the elevation dependence of a measurement using double difference data.
2. Development of covariance analysis methodology for predicting performance of relative code and carrier-phase positioning using a reference network.

1.4 Dissertation Outline

This thesis consists of seven chapters and two appendices.

Chapter 1 states the overall research objectives, requirements, and assumptions. It provides the motivation for using a carrier-phase reference network and outlines other

research that has been performed in this area. Finally, it describes the contributions of this thesis.

Chapter 2 is an overview of differential GPS error sources, especially as they relate to the use of a reference receiver network. Included are definitions of phase and code errors, double differencing, and the errors that result from various carrier-phase measurement combinations. Each of the differential error sources is then described, including ionosphere, troposphere, multipath, measurement noise, satellite position error, receiver position error, and clock errors.

Chapter 3 derives and describes the NetAdjust method for both code and phase measurements. It covers the derivation of the functional form of the error covariance matrix, and demonstrates how actual field data is used in this process. It also derives how a covariance analysis is performed once the functional form of the covariance matrix is determined.

In Chapter 4, the NetAdjust method is applied to data from a network of reference stations covering the southern portion of Norway. The results are analyzed in the measurement domain and the position domain. The effect of using NetAdjust on the ability to calculate carrier-phase integer ambiguities is also analyzed. In addition, results from a smaller network in the southern United States are also presented.

In Chapter 5, the covariance analysis procedure is used to examine the relationship between differential GPS performance and various factors, including the number and geometry of the reference stations, the position of the mobile user, and the level of various error sources.

Chapter 6 deals with operational considerations for an implementation of the NetAdjust method in a real-world situation. This includes topics such as parameterizing the corrections as a function of the mobile user position, time filtering of the corrections and the effect on data link bandwidth requirements, calculation of the ambiguities between reference receivers, and continuous calculation of the covariance parameters.

Chapter 7 provides a summary of the results and presents recommendations for further

research.

Appendix A is a general description of the two different reference receiver field networks that are used in this research, including a discussion of the methods used to determine the reference receiver coordinates. Data from these networks are used in Chapters 3, 4, 5, and 6.

Appendix B describes how the ambiguities between the reference receiver networks were calculated.

Chapter 2

Analysis of Differential GPS Error Sources

In order to use a network of reference receivers or simulate GPS measurements, one must understand the nature of the errors present in GPS measurements. In this chapter, error equations are defined for both code and phase measurements. Double differencing is described as a method for eliminating or reducing many of the errors, and each significant error source that remains after double differencing is described and analyzed.

In Chapter 3, error sources will be treated in two groups—correlated errors (atmospheric and satellite position errors), and uncorrelated errors (multipath and noise). The error analysis shown below provides the background necessary to describe the statistical characteristics of both groups of errors accurately and precisely.

2.1 Double Difference Error Equations

There are two primary observables generated by most GPS receivers—the range measurement based upon tracking of the GPS signal code, and a measurement of the phase of the beat frequency between the received GPS carrier signal and the carrier signal generated within the receiver. These are referred to as the code measurement (represented as ρ) and the phase measurement (represented as ϕ).

The double difference error equations for both the code and phase measurements will

be derived below.

2.1.1 Code Measurements

The GPS code measurement ρ is a linear measurement in units of metres, and it can be represented as

$$\rho = \mathbb{R} + \frac{I}{f^2} + T + m + c\delta t_{rec} - c\delta t_{sv} + v, \tag{2.1}$$

where

$\mathbb{R} \triangleq$ True range between SV (at transmit time) and receiver (at receive time) (m)

$I \triangleq$ Ionospheric delay parameter (= 40.30 TEC—see note below) (Hz^2m)

$f \triangleq$ Carrier signal frequency (1575.42 MHz for L1, 1227.60 MHz for L2)

$T \triangleq$ Measurement delay due to troposphere (m)

$m \triangleq$ Measurement delay due to multipath (m)

$c \triangleq$ Speed of light (m/s)

$\delta t_{rec} \triangleq$ Receiver clock error (sec)

$\delta t_{sv} \triangleq$ Satellite clock error (sec)

$v \triangleq$ Measurement noise (m).

Note that in the above definitions, TEC is the Total Electron Content, which is the integration of the electron density along the signal path. The TEC is in units of electrons/m^2, and 40.3 is an empirically derived constant (with units m^3s^{-2}electrons^{-1}) which relates the TEC to physically useful units.

Most DGPS processing involves generating a nominal, "computed" range between the receiver and the satellite which is calculated from the best known coordinates of the receiver and the satellite. The true range vector $\mathbf{R}$ is

$$\mathbf{R} = \mathbf{P}_{sv} - \mathbf{P}_{rec}, \tag{2.2}$$

where $\mathbb{P}_{sv}$ is the true position of the satellite at transmit time and $\mathbb{P}_{rec}$ is the true position of the receiver at receiver time. The computed range vector $\boldsymbol{R}$ is then

$$\boldsymbol{R} = \boldsymbol{P}_{sv} - \boldsymbol{P}_{rec}, \tag{2.3}$$

where $\boldsymbol{P}_{sv}$ is the computed position of the satellite at transmit time (from the ephemeris), and $\boldsymbol{P}_{rec}$ is the nominal position of the receiver at receive time. The three-dimensional error in the computed range vector ($\delta\boldsymbol{R}$) is

$$\begin{aligned} \delta\boldsymbol{R} &\equiv \boldsymbol{R} - \mathbb{R} \\ &= (\boldsymbol{P}_{sv} - \mathbb{P}_{sv}) - (\boldsymbol{P}_{rec} - \mathbb{P}_{rec}) \\ &\equiv \delta\boldsymbol{P}_{sv} - \delta\boldsymbol{P}_{rec} \end{aligned} \tag{2.4}$$

or, equivalently

$$\boldsymbol{R} = \mathbb{R} + \delta\boldsymbol{P}_{sv} - \delta\boldsymbol{P}_{rec}, \tag{2.5}$$

where $\delta\boldsymbol{P}_{sv}$ and $\delta\boldsymbol{P}_{rec}$ are the errors in the "known" (or computed) satellite and receiver positions relative to the true positions.

If the magnitudes of the satellite position error and the receiver position error are very small relative to the magnitude of the true range vector (which is normally true in GPS positioning), then the errors can be projected onto the range vector to make them scalar quantities. In equation form, if

$$|\delta\boldsymbol{P}_{sv}| \ll |\mathbb{R}| \quad \text{and} \quad |\delta\boldsymbol{P}_{rec}| \ll |\mathbb{R}|$$

then

$$\begin{aligned} R = |\boldsymbol{R}| &= |\mathbb{R} + \delta\boldsymbol{P}_{sv} - \delta\boldsymbol{P}_{rec}| \\ &= |\mathbb{R}| + \delta p_{sv} - \delta p_{rec} \end{aligned} \tag{2.6}$$

where

$$\delta p_{sv} = \boldsymbol{e} \cdot \delta\boldsymbol{P}_{sv}, \tag{2.7}$$

$$\delta p_{rec} = \boldsymbol{e} \cdot \delta\boldsymbol{P}_{rec}, \tag{2.8}$$

and

$$\boldsymbol{e} = \frac{\mathbb{R}}{|\mathbb{R}|}. \tag{2.9}$$

The magnitude R of the computed range vector can be subtracted from the actual code measurement to generate the measurement-minus-range observable $\bar{\rho}$:

$$\bar{\rho} = \rho - |\boldsymbol{R}| = \rho - R. \tag{2.10}$$

Note that if there are no errors (i.e. $\rho = \mathbb{R}$ and $R = \mathbb{R}$), then $\bar{\rho} = 0$. Any errors in either the computation of the range vector or the pseudorange measurement itself will result in a non-zero value for $\bar{\rho}$.

When performing standard GPS or DGPS code positioning, the method normally used is to calculate $\bar{\rho}$ (either explicitly or implicitly) based upon a nominal receiver position. In doing so, $\bar{\rho}$ provides a measure of the error in the nominal receiver position ($\boldsymbol{\delta P_{rec}}$), and it can be used to estimate that error and correct the nominal position until convergence is obtained.[1]

In this research, the measurement-minus-range observable is used in a slightly different manner. Instead of using $\bar{\rho}$ to calculate $\boldsymbol{\delta P_{rec}}$, the reference receiver positions are assumed to be known exactly (i.e. $\boldsymbol{\delta P_{rec}}$ is assumed to be zero), and $\bar{\rho}$ is used as a measurement of the errors themselves.

In order to significantly reduce or eliminate many of the error sources for precision differential GPS, a "double-difference" observable is generated.

2.1.1.1 Double Differencing

For the discussion that follows, subscripts are used to identify the receiver and superscripts are used to identify the satellite. For example, $\bar{\rho}_a^x$ would be the code measurement-minus-range observable between receiver a and satellite x.

[1]This simplified explanation of GPS positioning is intended to provide insight into the nature of the measurement-minus-range observable. Certainly, other considerations that must be taken into account (such as estimation of clock errors for single point positions) in order to successfully perform GPS positioning.

First, a single difference observable is generated by differencing simultaneous measurements between two satellites and one receiver: [2]

$$\nabla\bar{\rho}_a^{xy} = \bar{\rho}_a^x - \bar{\rho}_a^y. \tag{2.11}$$

Next, single difference observables between two receivers are themselves differenced in order to form the double difference observable

$$\begin{aligned}\Delta\nabla\bar{\rho}_{ab}^{xy} &= \nabla\bar{\rho}_a^{xy} - \nabla\bar{\rho}_b^{xy} \\ &= (\bar{\rho}_a^x - \bar{\rho}_a^y) - (\bar{\rho}_b^x - \bar{\rho}_b^y) \\ &= [(\rho_a^x - \rho_a^y) - (\rho_b^x - \rho_b^y)] - [(|\boldsymbol{R}_a^x| - |\boldsymbol{R}_a^y|) - (|\boldsymbol{R}_b^x| - |\boldsymbol{R}_b^y|)]\end{aligned} \tag{2.12}$$

Combining Equation 2.12 with Equations 2.1 and 2.6 results in

$$\begin{aligned}\Delta\nabla\bar{\rho}_{ab}^{xy} = [\ & (\mathbb{R}_a^x - \mathbb{R}_a^y) - (\mathbb{R}_b^x - \mathbb{R}_b^y) && \text{(2.13a)}\\ & + \frac{1}{f^2}[(I_a^x - I_a^y) - (I_b^x - I_b^y)] && \text{(2.13b)}\\ & + (T_a^x - T_a^y) - (T_b^x - T_b^y) && \text{(2.13c)}\\ & + (m_a^x - m_a^y) - (m_b^x - m_b^y) && \text{(2.13d)}\\ & + [(\delta t_{rec_a}{}^x - \delta t_{rec_a}{}^y) - (\delta t_{rec_b}{}^x - \delta t_{rec_b}{}^y)]c && \text{(2.13e)}\\ & + [(\delta t_{sv_a}{}^x - \delta t_{sv_a}{}^y) - (\delta t_{sv_b}{}^x - \delta t_{sv_b}{}^y)]c && \text{(2.13f)}\\ & + (v_a^x - v_a^y) - (v_b^x - v_b^y)] && \text{(2.13g)}\\ - [\ & (\mathbb{R}_a^x - \mathbb{R}_a^y) - (\mathbb{R}_b^x - \mathbb{R}_b^y) && \text{(2.13h)}\\ & + (\delta p_{sv_a}{}^x - \delta p_{sv_a}{}^y) - (\delta p_{sv_b}{}^x - \delta p_{sv_b}{}^y) && \text{(2.13i)}\\ & - (\delta p_{rec_a}{}^x - \delta p_{rec_a}{}^y) + (\delta p_{rec_b}{}^x - \delta p_{rec_b}{}^y)] && \text{(2.13j)}\end{aligned}$$

Several simplifications can be made in Equation 2.13. First, lines a and h completely cancel. Also, line e disappears with the assumption that the measurements were collected

[2] In reality, the measurements are not simultaneous but are very close in time. As a result, different satellite positions are calculated for each receiver, which to first order removes the errors induced by non-simultaneous measurements.

at simultaneous receive times ($\delta t_{rec_a}^{\ x} = \delta t_{rec_a}^{\ y}$ and $\delta t_{rec_b}^{\ x} = \delta t_{rec_b}^{\ y}$). In a similar manner, line f disappears if the measurements were transmitted at the same time from satellites x and y ($\delta t_{sv_a}^{\ x} = \delta t_{sv_a}^{\ y}$ and $\delta t_{sv_b}^{\ x} = \delta t_{sv_b}^{\ y}$).[3] After performing these cancellations and applying double difference notation, Equation 2.13 can be simplified to the final form of the code double difference error equation

$$\Delta\nabla\bar{\rho}_{ab}^{xy} = \frac{\Delta\nabla I_{ab}^{xy}}{f^2} + \Delta\nabla T_{ab}^{xy} + \Delta\nabla m_{ab}^{xy} + \Delta\nabla v_{ab}^{xy} + \Delta\nabla\delta p_{sv}{}_{ab}^{xy} - \Delta\nabla\delta p_{rec}{}_{ab}^{xy}. \quad (2.14)$$

This equation shows each of the error sources that are present in a double differenced code measurement-minus-range observable. These error sources will be described in sections 2.2 through 2.6.

2.1.2 Carrier-Phase Measurements

The L1 or L2 GPS phase measurement ϕ, in units of cycles, can be represented as

$$\phi = \frac{1}{\lambda}(\mathbb{R} - \frac{I}{f^2} + T + m + c\delta t_{rec} - c\delta t_{sv} + v) + N \quad (2.16)$$

where $\mathbb{R}$, I, f, T, m, δt_{rec}, δt_{sv}, v, and c are defined as in Equation 2.1, and

$\lambda \triangleq$ Wavelength of L1 or L2 carrier

$N \triangleq$ Integer carrier-phase cycle ambiguity (cycles)

Note that there are many similarities between the code measurement equation (2.1) and this phase measurement equation. First, the true range $\mathbb{R}$, tropospheric delay T, and clock errors δt_{rec} and δt_{sv} are identical (i.e. they have the same values). The ionospheric error I has an opposite sign than in the code equation, reflecting the fact that the ionosphere effects a *delay* of the code measurement and an *advance* of the phase measurement (Klobuchar, 1996). The multipath m and measurement noise v are also defined as

[3] As stated earlier, small differences in measurement times can be handled effectively by calculating separate satellite positions for each receiver.

in the code case, only here they refer to the phase measurements (so the actual values will be different).

There is one additional term in Equation 2.16, which is the carrier-phase integer ambiguity N. This is necessary because, unlike the code observable, the carrier-phase observable is not truly a whole-valued range measurement. Rather, the carrier-phase observable is a measurement of the accumulated Doppler since a particular time epoch, at which time there was an unspecified (N) number of carrier cycles between the satellite and the receiver which could not be output as part of the carrier-phase measurement. In essence, N can be thought of as a constant, initially unknown bias added in each of the carrier-phase measurements which happens to be an integer number of cycles. The values for N are different and independent for measurements between different receivers or different satellites. However, the values for N are constant for the same measurements taken at different time epochs (assuming no cycle slips between those epochs).

Using the same procedure presented in Section 2.1.1.1 with the phase measurement equation results in the phase double difference equation

$$\Delta\nabla\bar{\phi}_{ab}^{xy} = \frac{1}{\lambda}\Big(- \frac{\Delta\nabla I_{ab}^{xy}}{f^2} + \Delta\nabla T_{ab}^{xy} + \Delta\nabla m_{ab}^{xy} + \Delta\nabla v_{ab}^{xy} + \Delta\nabla \delta p_{sv}{}_{ab}^{xy} - \Delta\nabla \delta p_{rec}{}_{ab}^{xy}\Big) + \Delta\nabla N_{ab}^{xy}, \tag{2.17}$$

where f refers to the frequency of the carrier (L1 or L2), and $\lambda = c/f$.

2.1.3 Carrier-Phase Measurement Combinations

It is possible to generate a measurement denoted $\phi_{j,k}$ which is a linear combination of the L1 and L2 phase measurements

$$\phi_{j,k} \triangleq j\phi_{L1} + k\phi_{L2}. \tag{2.18}$$

After applying Equation 2.15, the $\phi_{j,k}$ observable can be described as

$$\begin{aligned}\phi_{j,k} =& \frac{1}{\lambda_{j,k}}(\mathbb{R} + T + c\delta t_{rec} - c\delta t_{sv}) \\ &+ \frac{j}{\lambda_1}(m_{L1} + v_{L1}) + \frac{k}{\lambda_2}(m_{L2} + v_{L2}) \\ &- \frac{I}{c}\left(\frac{jf_2 + kf_1}{f_1 f_2}\right) + jN_1 + kN_2,\end{aligned} \tag{2.19}$$

where

$$\lambda_{j,k} \triangleq \left(\frac{\lambda_1\lambda_2}{j\lambda_2 + k\lambda_1}\right). \tag{2.20}$$

Finally, following the developments of the previous section, the double difference equation of the measurement-minus-range observable is

$$\begin{aligned}\Delta\nabla\bar{\phi}^{xy}_{ab_{j,k}} =& \frac{1}{\lambda_{j,k}}\left(\Delta\nabla T^{xy}_{ab} + \Delta\nabla\delta p_{sv}{}^{xy}_{ab} - \Delta\nabla\delta p_{rec}{}^{xy}_{ab}\right) \\ &+ \frac{j}{\lambda_1}\left(\Delta\nabla m^{xy}_{ab_{L1}} + \Delta\nabla v^{xy}_{ab_{L1}}\right) + \frac{k}{\lambda_2}\left(\Delta\nabla m^{xy}_{ab_{L2}} + \Delta\nabla v^{xy}_{ab_{L2}}\right) \\ &- \frac{\Delta\nabla I^{xy}_{ab}}{c}\left(\frac{jf_2 + kf_1}{f_1 f_2}\right) + j\Delta\nabla N_1 + k\Delta\nabla N_2\end{aligned} \tag{2.21}$$

There are many different L1-L2 phase combinations that can be used. Two key combinations that are used in this research are shown in the first two entries of Table 2.1. The widelane observable $\phi_{1,-1}$ (also denoted ϕ_{WL}) is often used for carrier-phase ambiguity resolution, for several reasons. First, the widelane ambiguity remains an integer quantity,

Table 2.1: *Linear combinations of phase measurements*

Description	j	k	$\lambda_{j,k}$	Ambiguity
Widelane (WL)	1	-1	0.8619 m	$\Delta\nabla N_1 - \Delta\nabla N_2 = \Delta\nabla N_{WL}$
Ionospheric Free (IF)	1	$-\frac{f_2}{f_1}$	0.4844 m	$\Delta\nabla N_1 - \frac{f_2}{f_1}\Delta\nabla N_2 = \Delta\nabla N_{IF}$
L1 only (L1)	1	0	0.1903	$\Delta\nabla N_1$
L2 only (L2)	0	1	0.2442	$\Delta\nabla N_2$

which is necessary for any sort of integer search technique. The widelane observable also has a much longer wavelength than single frequency (L1 or L2) measurements, which helps to reduce the effect of some of the errors, as shown in Table 2.2. In this table, the second and third columns are the L1 and WL magnitudes of the differential GPS errors, *expressed in cycles*. The fourth column is the ratio between the WL errors and the L1 errors, again expressed in cycles. This WL/L1 ratio describes how much the errors are reduced by using the WL measurement, relative to the cycle wavelength. Ambiguity resolution algorithms attempt to determine the integer cycle ambiguities, so a reduction in the errors relative to the cycle wavelength (i.e. a WL/L1 ratio less than 1) aids in the ambiguity resolution process. Table 2.2 shows that the SV position, receiver position, and tropospheric errors are reduced the most, followed by ionospheric errors which are still reduced by over 70%. Note, however, that the multipath and measurement noise are not reduced at all. (It's not represented in the table, but the total multipath and noise actually increases, since it is a combination of L1 *and* L2 errors).

Table 2.3 shows the differential GPS errors expressed in *metres*, and the WL/L1 ratio is calculated as in Table 2.2. This shows that for SV position, receiver position, and tropospheric errors the total error magnitude (expressed in m, such as used for positioning) stays the same when going from L1 to WL observables, the total ionospheric error increases slightly, and the multipath and noise are increased significantly. Tables 2.2 and 2.3 taken together demonstrate that the total errors, expressed in m, are the same or are amplified when using a WL measurement, but due to the increased wavelength, the errors are generally reduced when expressed in cycles.

A second carrier-phase combination is called the ionospheric-free observable $\phi_{1,-\frac{f_2}{f_1}}$. This measurement has the distinct advantage that it completely removes the ionospheric

Table 2.2: *Comparison between L1 phase error and WL phase error, expressed in cycles*

Error	L1 error (cycles)	WL error (cycles)	$\frac{\text{WL}}{\text{L1}}$ ratio
SV Position	$\frac{1}{\lambda_1}\Delta\nabla\delta p_{sv}$	$\frac{1}{\lambda_{WL}}\Delta\nabla\delta p_{sv}$	$\frac{\lambda_1}{\lambda_{WL}} \approx 0.221$
Rec. Position	$\frac{1}{\lambda_1}\Delta\nabla\delta p_{rec}$	$\frac{1}{\lambda_{WL}}\Delta\nabla\delta p_{rec}$	$\frac{\lambda_1}{\lambda_{WL}} \approx 0.221$
Troposphere	$\frac{1}{\lambda_1}\Delta\nabla T$	$\frac{1}{\lambda_{WL}}\Delta\nabla T$	$\frac{\lambda_1}{\lambda_{WL}} \approx 0.221$
Ionosphere	$-\frac{1}{\lambda_1 f_1^2}\Delta\nabla I$	$-\frac{(f_1-f_2)}{cf_1f_2}\Delta\nabla I$	$\frac{(f_1-f_2)}{f_2} \approx 0.283$
L1 Multipath	$\frac{1}{\lambda_1}\Delta\nabla m$	$\frac{1}{\lambda_1}\Delta\nabla m$	1
L1 Noise	$\frac{1}{\lambda_1}\Delta\nabla v$	$\frac{1}{\lambda_1}\Delta\nabla v$	1

Table 2.3: *Comparison between L1 phase error and WL phase error, expressed in metres*

Error	L1 error (m)	WL error (m)	$\frac{\text{WL}}{\text{L1}}$ ratio
SV Position	$\Delta\nabla\delta p_{sv}$	$\Delta\nabla\delta p_{sv}$	1
Rec. Position	$\Delta\nabla\delta p_{rec}$	$\Delta\nabla\delta p_{rec}$	1
Troposphere	$\Delta\nabla T$	$\Delta\nabla T$	1
Ionosphere	$-\frac{1}{f_1^2}\Delta\nabla I$	$-\frac{\lambda_{WL}(f_1-f_2)}{cf_1f_2}\Delta\nabla I$	$\frac{f_1}{f_2} \approx 1.283$
L1 Multipath	$\Delta\nabla m$	$\frac{\lambda_{WL}}{\lambda_1}\Delta\nabla m$	$\frac{\lambda_{WL}}{\lambda_1} \approx 4.529$
L1 Noise	$\Delta\nabla v$	$\frac{\lambda_{WL}}{\lambda_1}\Delta\nabla v$	$\frac{\lambda_{WL}}{\lambda_1} \approx 4.529$

errors.[4] However, the ambiguity is no longer an integer quantity, so it cannot be calculated using integer search techniques. The ionospheric free observable can be used in conjunction with the widelane observable to calculate the L1 ambiguities, as described in Appendix B.

2.2 Ionospheric Errors

The ionosphere is a region of the atmosphere extending roughly from 50 to 1500 km, and it is characterized by a significant number of free electrons (with negative charge) and positively charged ions (Leick, 1995). The free electrons affect the propagation of radio waves, so they are of interest to users of GPS. The creation of free electrons is caused primarily by ultraviolet light from the sun, so the amount of ultraviolet light determines the state of the ionosphere. When there is no ultraviolet light, the free electrons and positive ions recombine, reducing the number of free electrons. The free electron density is then a function of the relative position of the sun, which makes it vary in a 24-hour cycle when observed from earth. The total amount of ultraviolet light emitted by the sun tends to be correlated with observations of the number of sunspots, have have historically varied on an approximately 11-year cycle. Times of high ultraviolet radiation (high number of sunspots) create a large number of free electrons in the ionosphere, resulting in relatively large induced errors in the radio signals. The next peak of the 11-year cycle is expected sometime in the year 2000.

[4]To be more precise, the ionospheric-free observable removes all of the *first order* ionospheric effects. Higher order effects do exist, but they contribute less than 0.1% error, even under the worst case ionospheric conditions (Klobuchar, 1996). Nonetheless, 0.1% error can contribute several cm of error under these worst case conditions, and accounting for the higher order terms can yield improved results under these conditions (Brunner and Gu, 1991).

2.2.1 Effect on Code and Carrier-Phase Measurements

By definition, the total electron content (TEC) along the path from the receiver to the GPS satellite is

$$\text{TEC} = \int_{path} N_e \, ds, \tag{2.22}$$

where N_e is the local electron density, expressed in electrons/m^3. Then, to first order, the ionospheric group delay I, expressed in Hz^2m is

$$I = \frac{40.30\text{TEC}}{f^2}, \tag{2.23}$$

were f is the frequency of the signal. The code measurement experiences a delay of $I/(f^2c)$ seconds, which is equivalent to an elongation of the pseudorange measurement of I/f^2 metres.

The phase of the GPS signal is advanced by the ionosphere by the same amount (when converted to m) that the code delay was delayed. As shown in Equation 2.16, the phase measurement is advanced by -I/cf cycles.

2.2.2 Evaluation of Ionospheric Error from Phase Measurement Combination

For a differential GPS positioning application, it is the uncancelled error (i.e. the portion of the error that is not cancelled by double differencing) that is of interest (as given in Equation 2.17). The value for $\Delta\nabla I$ can be measured directly using a phase measurement combination $\phi_{\lambda_1,-\lambda_2}$ as defined in Equation 2.18. The result, after double differencing is performed and the ambiguities are removed, is a direct measurement of the double difference ionosphere (plus multipath and noise). This can be seen by using $j = \lambda_1$ and

$k = -\lambda_2$ in Equation 2.21, resulting in the error observable

$$\Delta\nabla\bar{\phi}^{xy}_{ab_{\lambda_1,-\lambda_2}} = \left(\Delta\nabla m^{xy}_{ab_{L1}} + \Delta\nabla v^{xy}_{ab_{L1}}\right) - \left(\Delta\nabla m^{xy}_{ab_{L2}} + \Delta\nabla v^{xy}_{ab_{L2}}\right) - \Delta\nabla I^{xy}_{ab}\left(\frac{f_1^2 f_2^2}{f_2^2 - f_1^2}\right) + j\Delta\nabla N_1 + k\Delta\nabla N_2. \quad (2.24)$$

Under normal conditions, multipath and noise are much smaller than the ionospheric error, so when the integer ambiguities are known, the $(\lambda_1, -\lambda_2)$ combination of phase measurements is a very good way to measure the double differenced ionosphere.

The primary data set used in this thesis was from 11 receivers spread throughout the southern portion of Norway, as described in Appendix A. To demonstrate ionospheric error effects, four different baselines with lengths of 0.01 km, 67 km, 192 km, and 461 km were chosen. The values of $\Delta\nabla\bar{\phi}_{\lambda_1,-\lambda_2}$ were calculated and scaled for the L1 frequency for every possible PRN combination over two different three-hour periods. A 12° elevation cutoff was used. The first time period was from 12:00 to 15:00 local time, which would normally be the time of the day with the peak ionospheric errors. Another three-hour period was selected during the ionospherically stable night hours of 03:00 to 06:00 local time. The data was collected at latitudes between 60° N and 65° N on September 30, 1997, which is in the mid-point in the 11 year solar cycle.

Because the ionospheric errors grow as the satellite elevation decreases, it is useful to map the errors to zenith (vertical), using a mapping function. The time series of ionospheric phase advances was mapped to zenith using the equation

$$I = F_I(\varepsilon) I_z, \quad (2.25)$$

where I_z is the value of I mapped to zenith, ε is the satellite elevation, and $F_I(\varepsilon)$ is the mapping function from the Klobuchar ionospheric model (Klobuchar, 1987)

$$F_I(\varepsilon) = 1 + 16\left(0.53 - \frac{\varepsilon}{180^\circ}\right)^3 \quad (2.26)$$

(ε is expressed in degrees). A plot of this mapping is shown in Figure 2.1. For double difference measurements between satellites x and y, the mapping function is a combination

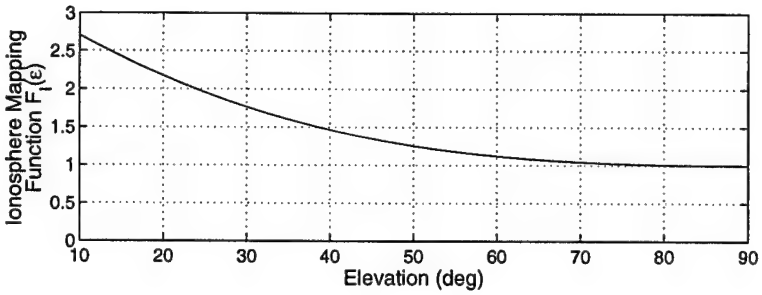

Figure 2.1: *Zenith mapping function for ionosphere (Klobuchar model)*

of the two individual mapping functions

$$\Delta\nabla I^{xy} = \left(\frac{F_I(\varepsilon^x) + F_I(\varepsilon^y)}{2}\right) I_z^{xy}. \tag{2.27}$$

For more details on the justification of the above equation, see Section 3.4.3.2.

The L1 zenith differential ionospheric phase advance was calculated for the three-hour periods, and the results are shown in Figures 2.2 and 2.3. The axis limits are consistent for each of the plots in order to make the comparison clear. As would be expected, the ionospheric errors increase with baseline distance in the afternoon case, with an RMS value of around 0.7 cm at 0.01 km (which is from multipath and noise), to RMS values of 21.9 cm at 461 km. During the ionospherically stable nighttime conditions shown in Figure 2.3, the RMS values for the 461 km case was only 8.0 cm. The intermediate baselines also showed this same trend. As described in Appendix A, the ionosphere during this test showed no significant irregularities.

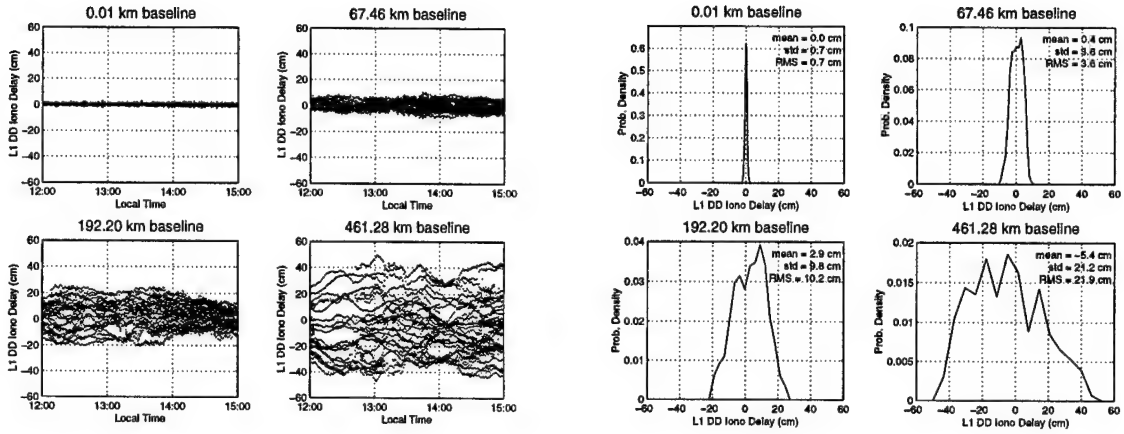

Figure 2.2: *Time series and probability density functions of double difference zenith L1 ionospheric delay for four different baseline lengths during* ***afternoon*** *(generated from* $\Delta\nabla\bar{\phi}_{\lambda_1,-\lambda_2}$ *observable), southern Norway, September 1997*

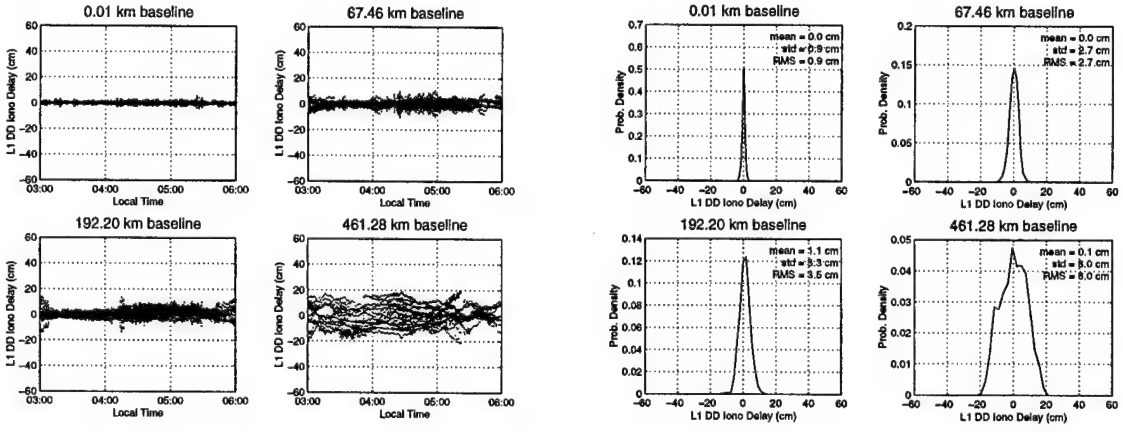

Figure 2.3: *Time series and probability density functions of double difference zenith L1 ionospheric delay for four different baseline lengths during* ***night*** *(generated from* $\Delta\nabla\bar{\phi}_{\lambda_1,-\lambda_2}$ *observable), southern Norway, September 1997*

2.3 Tropospheric Errors

The GPS measurement errors discussed in this section are those caused by the neutral atmosphere, primarily consisting of the troposphere (around 0–10 km altitude).[5] At GPS frequencies, the troposphere is a non-dispersive medium, so the delay effects are not frequency dependent, and therefore are the same for both the code and phase measurements.

There are two major delay effects of the troposphere, referred to as the dry delay (caused by the non-water portion of the atmosphere) and the wet delay (caused by water in the atmosphere). The dry delay is the larger of the two effects, and is caused primarily by the presence of O_2 and N_2 in the atmosphere. While the largest effect (contributing 80%–90%), it can be modeled to an accuracy of 1% or better, so it is not much of a problem. The wet delay, on the other hand, only contributes to 10%–20% of the total delay, but it is difficult to model accurately, and zenith errors in wet delay models are at the level of 10–20% (Lachapelle, 1994). At zenith, the dry delay is about 2.3 m and the wet delay varies between 1–80 cm (Spilker Jr., 1996a).

The tropospheric delay T can be expressed mathematically as

$$T = \int_{path} (n-1)ds + \Delta_g, \tag{2.28}$$

where n is the refractive index of the atmospheric gases (which is a function of position), and Δ_g is the difference between the curved and free-space paths (since the signal does not actually travel in a straight-line path). The value of Δ_g is less than 3 mm for elevations greater than 20°, and increases to around 2 cm for elevations of 10° (Spilker Jr., 1996a).

There are numerous tropospheric delay models that have been developed over the years, with varying levels of performance (Mendes and Langley, 1994). The model that

[5] Actually, the troposphere accounts for about 75% of the neutral atmosphere delay effect. The other 25% is caused by regions above the troposphere, namely, the tropopause (around 10–16 km) and the stratosphere (around 16–50 km) (Spilker Jr., 1996a). Nonetheless, the total neutral atmosphere delay is referred to as the tropospheric error.

has been used for this research is the modified Hopfield model (Goad and Goodman, 1974), which has input parameters of atmospheric pressure, temperature, relative humidity, and satellite elevation. The pressure and temperature are determined from the receiver altitude (using standard temperature and pressure tables), and the relative humidity is set to a fixed value of 50%.

The ionospheric free carrier-phase measurement combination is useful for studying the tropospheric error. If precise satellite coordinates are used (which eliminate the satellite position error), the receiver coordinates are assumed to be known, and the ambiguities are removed (all of which are post-processing mode), then the ionospheric free ($\Delta\nabla\bar{\phi}_{IF} = \Delta\nabla\bar{\phi}_{1,-f_2/f_1}$) measurement errors from Equation 2.21 can be simplified to

$$\Delta\nabla\bar{\phi}_{IF} = \frac{1}{\lambda_{IF}}(\Delta\nabla T) + \frac{1}{\lambda_1}(\Delta\nabla m_{L1} + \Delta\nabla v_{L1}) - \frac{f_2}{f_1\lambda_2}(\Delta\nabla m_{L2} + \Delta\nabla v_{L2}) \tag{2.29}$$

For longer baseline distances, the troposphere term ($\Delta\nabla T$) will dominate the multipath and noise terms, which means that $\Delta\nabla\bar{\phi}_{IF}$ is a useful tool for measuring differential tropospheric error (assuming that the above conditions regarding precise orbits, receiver coordinates, etc. are met).

Figure 2.4 shows a 24-hour time series of the double differenced tropospheric errors, as calculated from the $\Delta\nabla\bar{\phi}_{IF}$ observable (so it includes amplified multipath and noise). Precise (post-processed) ephemerides and an elevation cutoff of 12° were used. (Surface weather conditions during the test are given in Table A.1 in Appendix A). Data is presented from the same four baselines as shown in the previous analysis of ionospheric errors. Figure 2.5 shows the probability density function for each of the time series, as well as the mean, standard deviation, and RMS value. As expected, the RMS value increases as the baseline distance increases. The increase is not as pronounced as in the ionospheric case, however.

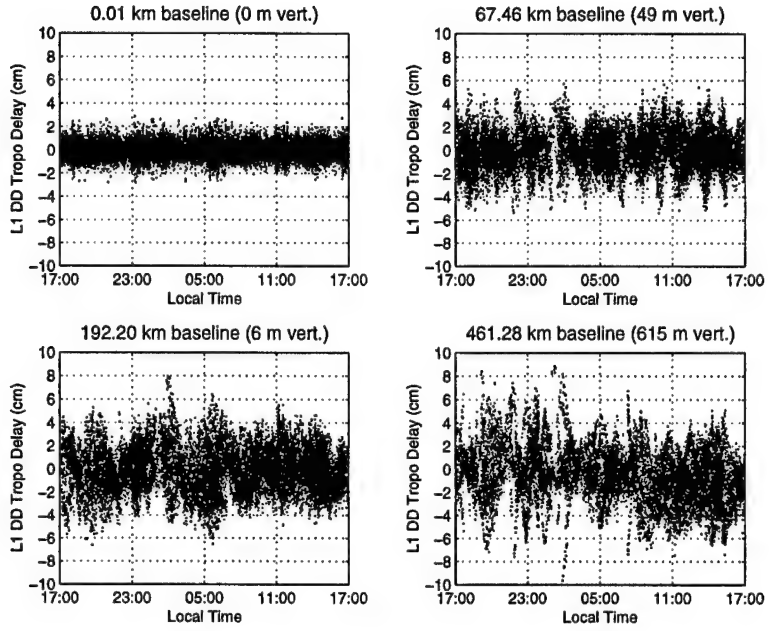

Figure 2.4: *Time series of double difference zenith troposphere delay (from $\Delta\nabla\bar{\phi}_{IF}$ measurement) over 24-hour period for four different baselines*

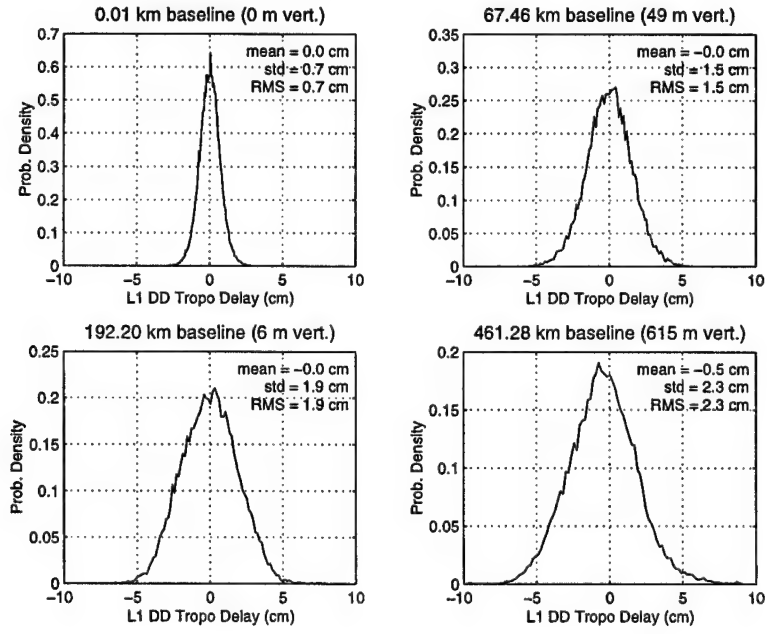

Figure 2.5: *Statistics of double difference zenith troposphere delay (from $\Delta\nabla\bar{\phi}_{IF}$ measurement) over 24-hour period for four different baselines*

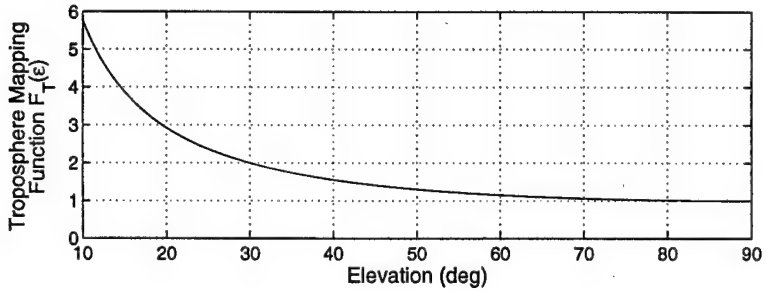

***Figure 2.6:** Zenith mapping function for troposphere*

Each of the values is mapped to zenith using the relation

$$\Delta\nabla T^{xy} = \left(\frac{F_T(\varepsilon^x) + F_T(\varepsilon^y)}{2}\right) T_z^{xy}, \tag{2.30}$$

where $F_T(\varepsilon)$ is the simplified troposphere mapping function (Spilker Jr., 1996a)

$$F_T(\varepsilon) = \frac{1}{\sin\varepsilon}. \tag{2.31}$$

This function is plotted in Figure 2.6.

2.4 Measurement Noise

Measurement noise is any noise which is generated by the receiver itself in the process of taking code or phase measurements. It is considered to be white noise for the sampling interval normally present in GPS receivers (maximum of 20Hz). There is also no correlated noise between separate measurements taken at the same point in time, because independent tracking loops are used for each separate measurement, and the noise is primarily generated by tracking loop jitter.

White noise can be effectively measured through the use of a "zero-baseline" test. In this test, the GPS signal from a single antenna is split and sent to two different GPS receivers. When measurement-minus-range values are calculated using data from these two receivers, then all error terms in Equations 2.14 and 2.17 cancel, except for measurement noise. (The carrier-phase ambiguities also remain, but these can easily be determined and

eliminated by rounding the double differenced measurement-minus-range values). The resulting equation for the phase measurement is

$$\Delta\nabla\bar{\phi}_{ab}^{xy} = \Delta\nabla v_{ab}^{xy} = v_b^x - v_b^y - (v_b^x - v_b^y), \tag{2.32}$$

and the equation for the code measurement is

$$\Delta\nabla\bar{\rho}_{ab}^{xy} = \Delta\nabla v_{ab}^{xy} = v_b^x - v_b^y - (v_b^x - v_b^y). \tag{2.33}$$

Note that in the above two equations, the v variables represent independent realizations of measurement noise, which are completely uncorrelated between measurements.

Measurement noise is increased as the signal-to-noise ratio (SNR) decreases (Spilker Jr., 1996b). Because the SNR tends to decrease with elevation, measurement noise can be expected to increase with elevation.

In order to characterize the measurement noise, data was collected for a period of six hours in a zero-baseline test using two Ashtech Z-12 receivers. Measurement-minus-range values were double differenced, and the phase measurement integer ambiguities were removed by rounding. The highest visible satellite was used as the base satellite in all cases.

The top plot in Figure 2.7 shows the raw double differenced measurement noise as a function of the elevation of the lower satellite. To analyze the measurement noise as a function of elevation, the raw data was divided into separate 2° elevation bins. The first bin included all measurements in which the lowest satellite elevation was between 10° and 12°, the second bin was between 12° and 14°, and so on. Statistics were calculated for the samples in each elevation bin. The second plot in Figure 2.7 shows the number of double differenced measurements in each elevation bin, and the third plot shows the standard deviation of the *double-differenced* measurement noise between the high-elevation satellite and the low-elevation satellite. While this is useful, what is really desired is the statistics of the measurement noise for an *individual* measurement.

To calculate this, an assumption is made that the variance (i.e. square of the standard deviation) of the measurement noise is constant at elevations greater than 50°. This

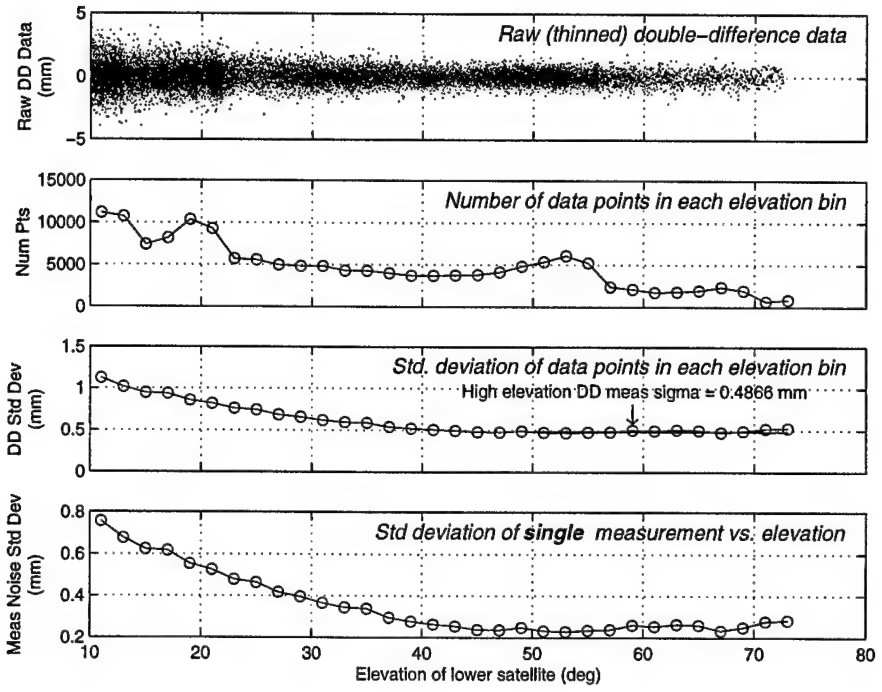

Figure 2.7: *L1 phase zero baseline test results using Ashtech Z-12 receiver*

assumption is supported by the third plot in Figure 2.7. Using the covariance law (and the fact that the measurements are uncorrelated), the variance of the double differenced high-elevation satellites ($\sigma^2_{DD_{high}}$) can then be expressed as the sum of the four single measurement variances in Equation 2.32

$$(\sigma^2_{DD_{high}})^{xy}_{ab} = (\sigma^2_{v_{high}})^{x}_{a} + (\sigma^2_{v_{high}})^{y}_{a} + (\sigma^2_{v_{high}})^{x}_{b} + (\sigma^2_{v_{high}})^{y}_{b}, \tag{2.34}$$

where $\sigma^2_{v_{high}}$ is the measurement noise variance of a single high elevation satellite. Because the variance of the measurement noise is constant for high elevation satellites (by assumption), this can be rewritten as

$$\sigma^2_{DD_{high}} = 4\sigma^2_{v_{high}} \tag{2.35}$$

or, equivalently,

$$\sigma^2_{v_{high}} = \frac{\sigma^2_{DD_{high}}}{4}. \tag{2.36}$$

The high elevation satellite was at an elevation greater than 50° for all of the data that was collected. Applying Equation 2.34 to the case of any double difference measurement between a high satellite (x) and another satellite (y) results in

$$(\sigma^2_{DD})^{xy}_{ab} = (\sigma^2_{v_{high}})^x_a + (\sigma^2_v)^y_a + (\sigma^2_{v_{high}})^x_b + (\sigma^2_v)^y_b \tag{2.37}$$

$$= 2\sigma^2_{v_{high}} + 2\sigma^2_v \tag{2.38}$$

The variance of the measurement noise for a single measurement (σ^2_v) can then be solved using

$$\sigma^2_v = \frac{\sigma^2_{DD} - 2\sigma^2_{v_{high}}}{2} \tag{2.39}$$

The standard deviations corresponding with the values of σ^2_v vs. elevation are shown in the bottom plot of Figure 2.7.

The same procedure was repeated for the L2 phase measurement and the three code measurements from the Ashtech Z-12, and the standard deviations of the single measurement noise are shown in Figure 2.8. Note that the code measurement noise is on the order of metres, while the phase measurement noise is on the order of millimetres. For both code and phase measurements, the signals generated from the P codes are significantly noisier than the signals generated from the CA code. This is because the Ashtech receiver (and other non-authorized dual-frequency receivers) can only track P-code measurements in a semi-codeless mode (Van Dierendonck, 1994), and it relies upon cross-correlation to remove the encryption code (Van Dierendonck, 1994).

A probability distribution function was also calculated for L1 CA-code, L1 semicodeless P-code, L1 phase, and L2 phase double differenced noise measurements, and the results are shown in Figure 2.9. Note that they each appear to follow a Gaussian distribution and are zero-mean. The zero-baseline test was also performed on other dual-frequency receivers, with no significant differences in the results.

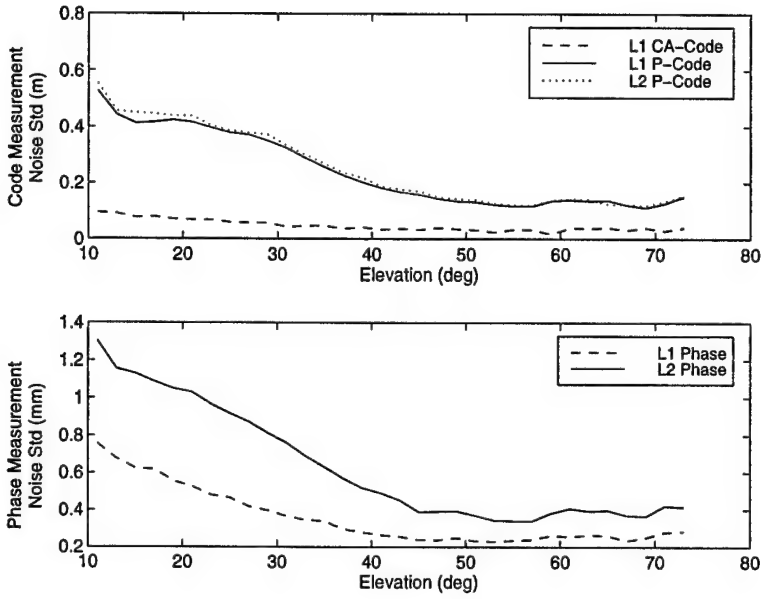

Figure 2.8: Measurement noise statistics vs. elevation for Ashtech Z-12 receiver

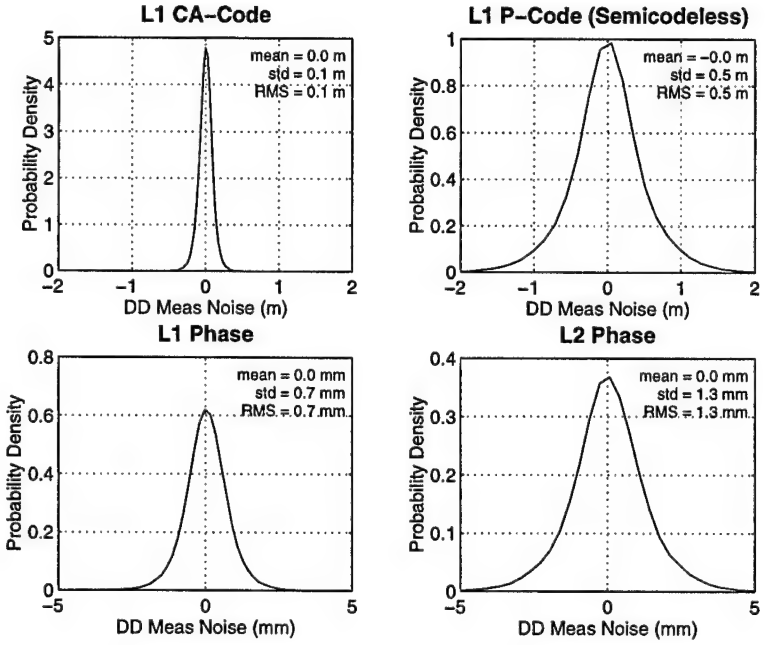

Figure 2.9: Statistics of double differenced zero-baseline measurement noise

2.5 Multipath

Multipath is the error caused when the GPS signal arrives at the receiver via more than one path, normally caused by reflections near the receiver. As a result, it is highly dependent upon the conditions surrounding the receiver antenna, the type of antenna that is used, and the internal tracking loop algorithms of the receiver. This makes multipath a difficult error to remove, because there is no model that can be used for the general case.

2.5.1 Carrier-Phase Multipath

The direct signal from the GPS satellite to the receiver (S_D) can be expressed as

$$S_D = A\cos\varphi. \tag{2.40}$$

Then, each reflected signal (S_R) will be attenuated and shifted in phase (as a function of the geometric configuration), and this is represented by the equation

$$S_R = \alpha A\cos(\varphi + \delta\varphi). \tag{2.41}$$

In the general case, there can be any number (n) of reflected signals with different attenuation factors α and phase shifts $\delta\varphi$. The total signal at the receiver antenna (S) is then the superposition of all of these signals

$$S = A\cos\varphi + \sum_{j=1}^{n} \alpha_j A\cos(\varphi + \delta\varphi_j). \tag{2.42}$$

It is useful to examine the simple case of one reflected signal to gain insight into multipath errors. Starting with the superimposed direct and reflected signal

$$S = A\cos\varphi + \alpha A\cos(\varphi + \delta\varphi) \tag{2.43}$$

(following the development in Hoffman-Wellenhof et al. (1994)), application of the cosine theorem yields

$$S = A\cos\varphi + \alpha A\cos\varphi\cos\delta\varphi - \alpha A\sin\varphi\sin\delta\varphi \tag{2.44}$$

$$= (1 + \alpha\cos\delta\varphi)A\cos\varphi - (\alpha\sin\delta\varphi)A\sin\varphi. \tag{2.45}$$

Because the direct and reflected signals have the same frequency, the superposition of them can also be written in the form

$$S = \alpha_M A \cos(\varphi + \delta\varphi_M), \tag{2.46}$$

where α_M is the attenuation factor of the signal due to multipath, and $\delta\varphi_m$ is the induced phase shift of the signal due to multipath.

Comparing the coefficients for $A \sin\varphi$ and $A \cos\varphi$ in Equations 2.45 and 2.46 results in the two simultaneous equations

$$\begin{aligned} \alpha_M \sin\delta\varphi_m &= \alpha \sin\delta\varphi \\ \alpha_M \cos\delta\varphi_m &= 1 + \alpha \cos\delta\varphi, \end{aligned} \tag{2.47}$$

which, when solved for $A \sin\varphi$ and $A \cos\varphi$ yields

$$\alpha_m = \sqrt{1 + \alpha^2 + 2\alpha \cos\delta\varphi} \tag{2.48}$$

and

$$\tan\delta\varphi_m = \frac{\alpha \sin\delta\varphi}{1 + \alpha \cos\delta\varphi} \tag{2.49}$$

The variation in amplitude for a variety of attenuation factors (α) and reflected signal phase shifts is shown in Figure 2.10. Note that the amplitude is actually larger when the reflected signal phase shift is small. More importantly (in terms of measurement errors), the phase shift in the combined signal induced by the reflected signal is shown in Figure 2.11. In general, the tracking loops within the receiver will track the combined signal, and any induced phase error will show up as a multipath error in the phase measurement.

According to Figure 2.11, the maximum multipath error (for a reflected signal with the same strength as the direct signal, i.e. $\alpha = 1$) is 90°, which would correspond to about 5 cm when converted from L1 cycles to metres. However, in most real-world applications, the reflected signal will be attenuated to some extent, and typical phase multipath values are more on the order of 1 cm or less (Lachapelle, 1994).

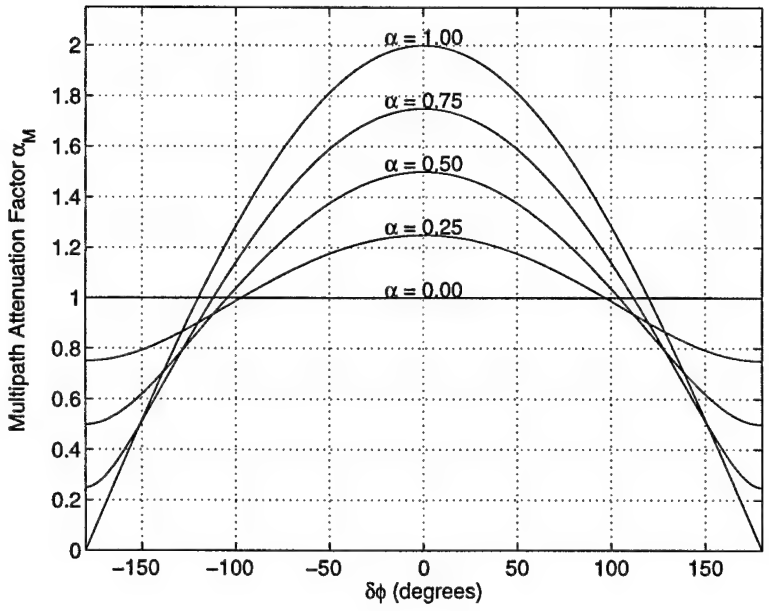

Figure 2.10: *Theoretical effect of single reflected signal on the combined signal amplitude*

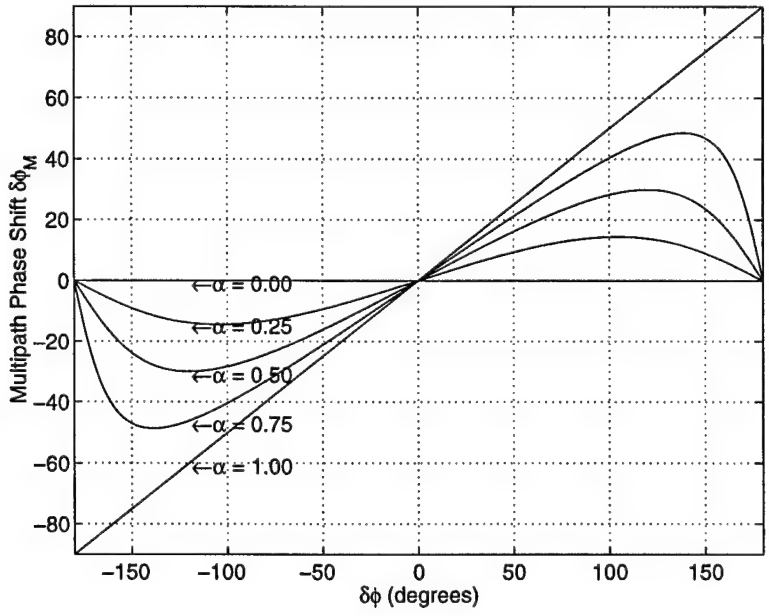

Figure 2.11: *Theoretical effect of single reflected signal on the combined signal phase offset (from the direct phase)*

2.5.2 Code Multipath

Code multipath is similar to carrier-phase multipath, only its magnitude tends to be several orders of magnitude larger. Just as the carrier-phase multipath is a fraction of the wavelength, code multipath is limited by the chipping rate. The higher the chipping rate, the lower the maximum multipath (Leick, 1995). As a result, code multipath tends to be much smaller for P-code pseudorange measurements (which have a chipping rate of 10.23 MHz) than for CA-code measurements (which have a chipping rate of 1.023 MHz). Several signal processing techniques within the receiver can be used to reduce the code multipath, such as narrow correlator spacing (Van Direndonck et al., 1992).

2.5.3 Samples of Multipath from Field Data

If two receivers are separated by a short enough baseline to remove all of the correlated (atmospheric and satellite position) errors, but long enough to assure that the multipath is decorrelated between the receivers, then double difference measurements will be primarily a measure of multipath and measurement noise. For short baselines, Equations 2.17 and 2.14 reduce to

$$\Delta\nabla\bar{\phi}_{ab}^{xy} = \Delta\nabla m_{ab}^{xy} + \Delta\nabla v_{ab}^{xy} \tag{2.50}$$

$$\Delta\nabla\bar{\rho}_{ab}^{xy} = \Delta\nabla m_{ab}^{xy} + \Delta\nabla v_{ab}^{xy} \tag{2.51}$$

Two different short baseline tests were conducted at The University of Calgary. In the first test, two Trimble 4000 SSi receivers were placed at sites separated by approximately 600 m. One receiver was mounted on a concrete pillar on the roof of the 3-story Engineering building, and the other was mounted on the roof of a 1-story weather station using a tripod. Both receivers used standard Trimble dual frequency groundplane antennas. Data was collected at two second intervals over a period of six hours on Jan 13th, 1998. The double differenced measurement-minus-range values were calculated for the code measurements ($\Delta\nabla\bar{\rho}$) and the phase measurements ($\Delta\nabla\bar{\phi}$).

The analysis described by Equations 2.34–2.39 in Section 2.4 was applied in the same manner for this short baseline data. The only difference was that in this case, the $\Delta\nabla\bar{\rho}$ and $\Delta\nabla\bar{\phi}$ values included both multipath and noise.

Results for the Trimble test are shown in Figure 2.12. The top plot shows the single measurement L1 CA-code and semicodeless L2 P-code multipath + noise as a function of elevation. These particular measurements were carrier-smoothed, which resulted in relatively low multipath + noise values. The bottom plot shows the phase multipath + noise values. Note that these are an order of magnitude higher than the pure measurement noise values seen in Figure 2.8.

A second test was performed the following day during the same time period using Ashtech Z-12 receivers with standard dual-frequency Ashtech antennas. Results are shown in Figure 2.13. The Ashtech Z-12 generates L1 P-code (semicodeless) in addition to the L1 CA-code and L2 P-code (semicodeless). The top plot shows all of the code measurement statistics, and the bottom plot shows that phase measurement statistics. Recall from Figure 2.8 that the CA-code measurement noise was significantly lower than either of the P-code measurement noises, because the P-code measurements are semicodeless. When multipath is added, however, the semicodeless P-code measurements are slightly better than the CA-code measurements. This demonstrates that CA-code multipath is significantly higher than P-code multipath in this case. The Ashtech phase multipath + noise values are somewhat higher than the Trimble values, but still have maximum standard deviations of only 12 mm at low elevations.

Finally, probability distribution functions were generated for the short baseline Trimble data, and the results are shown in Figure 2.14. Note that in all cases, the distribution appears Gaussian and the errors are double difference errors are close to zero-mean.

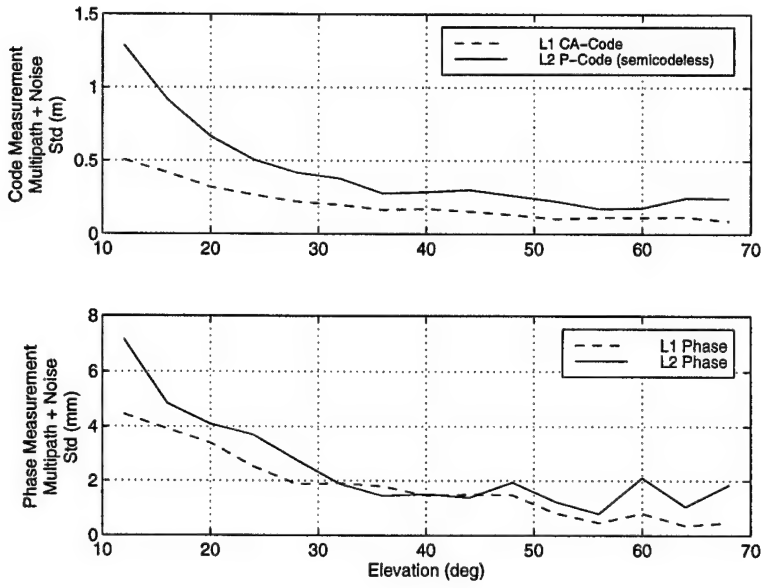

Figure 2.12: *Single measurement multipath + noise statistics vs. elevation for Trimble 4000 SSi receiver (600 m baseline)*

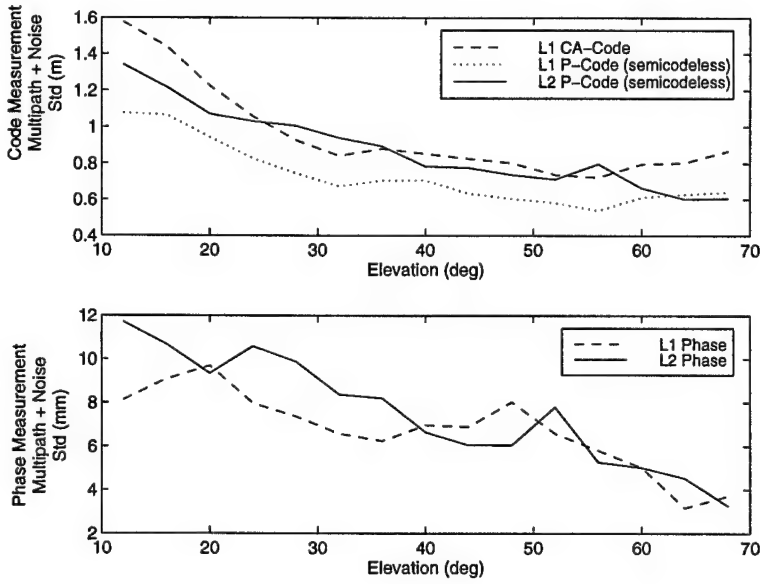

Figure 2.13: *Single measurement multipath + noise statistics vs. elevation for Ashtech Z-12 receiver (600 m baseline)*

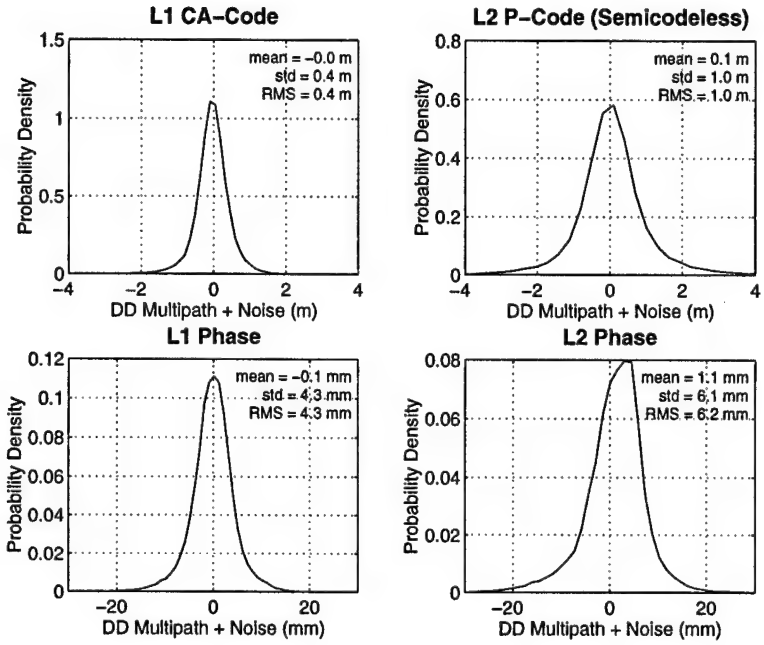

Figure 2.14: *Statistics of double differenced short baseline multipath + measurement noise using Trimble 4000 SSi (600 m baseline)*

2.6 Satellite Position Error

In order to generate measurement-minus-range values, the positions of the satellites are calculated using the broadcast navigation message, which includes Keplerian orbital elements and time derivatives for some of these elements. The broadcast navigation message is generated using measurements from five monitor stations located around the world, and it is updated once every two hours (nominally). This broadcast orbit has a slant range RMS accuracy of approximately 2.1 m (Bowen et al., 1986).

Errors in the broadcast orbits will cause errors in the double differenced measurement-minus-range values. It is possible to determine what the orbital errors were for a particular period of time through the use of precise orbits, which are calculated using many reference stations and many days of data before and after the time period. These precise orbits typically have an RMS accuracy of 6 cm (Rothacher, 1997). The satellite position error can be calculated by differencing the position generated from the broadcast navigation

messages and the position generated from the precise orbits. The double differenced satellite position error is then calculated by projecting the 3-dimensional orbital error onto the line of site vectors between the receivers and the satellites, and then double differencing.

Double differenced satellite position errors were calculated over a 24 hour period, using the same data set presented in Section 2.3. Results for a 461 km baseline are shown in Figure 2.15. Note that the errors make step jumps at two hour intervals, corresponding to a new broadcast navigation message upload. Note also the unusually large errors between 23:00 and 24:00. These are due to an unusually large position error in the PRN 14 satellite, and the error is corrected at the 24:00 update.

The same plot was generated for three additional baselines, and the results (along with the 461 km baseline) are presented in Figure 2.16. The corresponding probability distribution functions and statistics are shown in Figure 2.17. These figures show that the satellite position error is clearly a function of baseline distance.

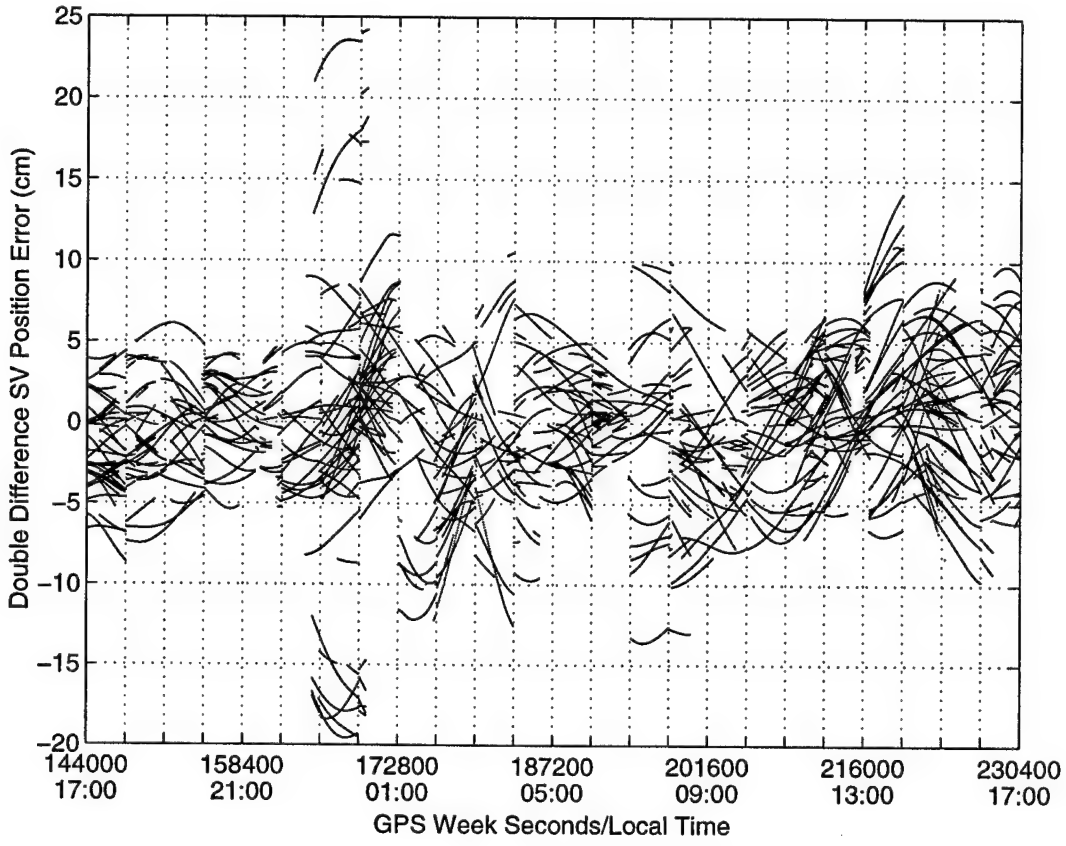

Figure 2.15: *Double differenced satellite position error (projected onto line of sight vectors) over a 461 km baseline*

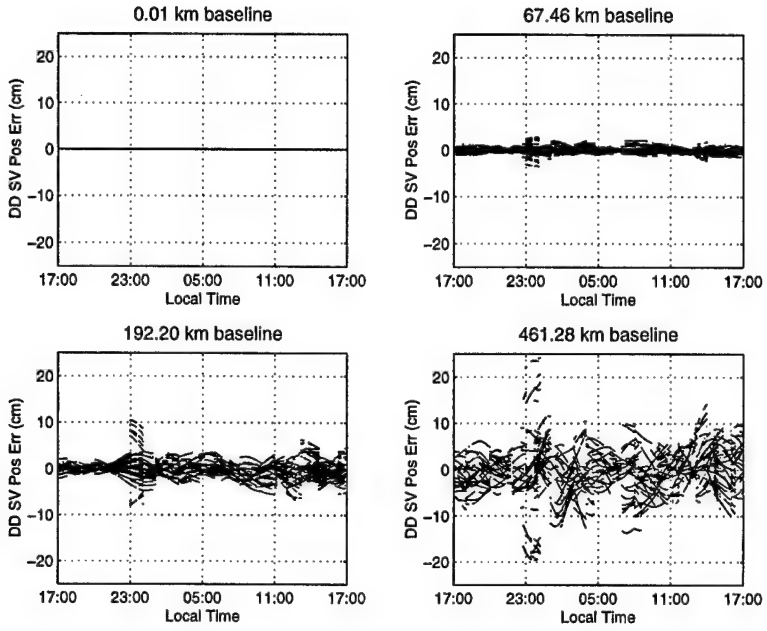

Figure 2.16: *Time series of double differenced satellite position error over four different baselines*

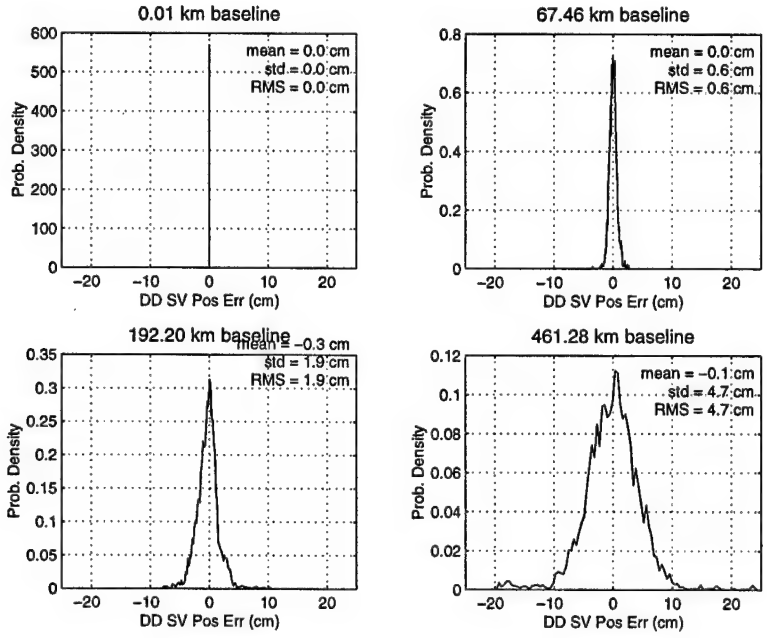

Figure 2.17: *Probability density functions of double differenced satellite position error over four different baselines*

Chapter 3

The NetAdjust Method

This chapter begins with a discussion of optimal estimation, showing that a Linear Minimum error Variance (LMV) estimator is the optimal minimum error variance estimator under certain conditions. A full derivation of the optimal LMV estimator is not given—rather, the emphasis is on describing the estimation problem, defining the conditions of optimality and presenting the final result.

After this mathematical background, a description of the NetAdjust method is presented. This begins by carefully defining the values to be estimated for performing network differential GPS, followed by the application of the optimal LMV estimator to the problem.

Next, a covariance analysis method is described. This covariance analysis predicts what the performance of the network will be when positioning a mobile receiver, and it forms the basis for all of the analysis that is performed in Chapter 5.

The key element in the NetAdjust method is the measurement covariance matrix which contains the information about the reference network geometry. The fourth section in this chapter shows how a functional form of this covariance matrix can be generated, in order to calculate the covariance elements for any *general* receiver configuration within the network. A method for using field data to determine the parameters of the covariance function is then presented.

Finally, the NetAdjust approach will be interpreted in the least squares context, in-

cluding the least squares condition adjustment and least squares prediction (collocation). The least squares condition adjustment interpretation is particularly useful to help provide insight into how the NetAdjust method works.

All of the equations in this chapter refer to phase measurements, which can be either single frequency or widelane phase measurements. The equations apply equally well to GPS code measurements, except that with code measurements there are no cycle ambiguities, so the ambiguity terms (N or $\Delta\nabla N$) can be ignored. (There is also a sign change in the ionospheric errors which is explicitly considered when applicable). When applied, the NetAdjust method is used to correct the L1 code, L1 phase, and WL phase errors *independently* (see Chapter 4 for more details). However, the underlying algorithms presented in the current chapter are the same for all three types of measurements.

3.1 Mathematical Background

3.1.1 Optimal Estimation

The basic elements of a statistical estimation problem include (Minkler and Minkler, 1993)[1]:

- An unknown parameter (vector) $\boldsymbol{x}$, whose value is to be estimated.
- Observations $\boldsymbol{Y}$ containing information about $\boldsymbol{x}$.
- An estimator $\mathbf{e}(\boldsymbol{Y})$ which provides an estimate of $\boldsymbol{x}$ from $\boldsymbol{Y}$. It is essentially a function which assigns every set of observations $\boldsymbol{Y}$ to an estimate of the parameters $\hat{\boldsymbol{x}}$, i.e. $\hat{\boldsymbol{x}} = \mathbf{e}(\boldsymbol{Y})$ as shown in Figure 3.1.
- The estimate of the $\boldsymbol{x}$, $\hat{\boldsymbol{x}}$, which is the output of the estimator $\mathbf{e}(\boldsymbol{Y})$.

[1]The references presented in this section are those used by the author, and they are not necessarily the original sources.

- A loss function $L(\boldsymbol{x}, \hat{\boldsymbol{x}})$ that provides a value representing the loss incurred when an estimate $\hat{\boldsymbol{x}}$ is assigned to the true value $\boldsymbol{x}$. (Sometimes this is called a cost function).
- Criteria for optimal estimation.

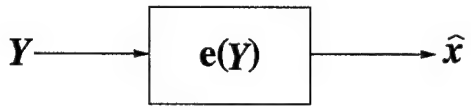

Figure 3.1: *Definition of estimator*

In the following sections, a Linear Minimum error Variance (LMV) estimator (i.e., an estimator that minimized the estimation error variance) will be defined. In contrast, "least squares" estimation techniques explicitly minimize a quadratic form of the measurement residuals. Both the least squares and the LMV frameworks result in the same final estimator, but the LMV framework will be the one presented, because it fits more naturally into the context of the differential GPS network problem.

3.1.1.1 Bayesian Estimators

The loss function $L(\boldsymbol{x}, \hat{\boldsymbol{x}})$ given in the previous section is used to determine the criterion for optimal estimation. It is called the loss function, because it represents the loss incurred by the estimator $\mathbf{e}(\cdot)$ in its estimate of $\boldsymbol{x}$.

In Bayes estimation theory, it is assumed that either $\boldsymbol{x}$ or $\boldsymbol{Y}$ are random quantities, with a joint probability density function $f_{\boldsymbol{x},\boldsymbol{Y}}(\boldsymbol{\xi}, \boldsymbol{\psi})$ (where $\boldsymbol{\xi}$ and $\boldsymbol{\psi}$ are dummy variables used in the definition of probability distribution/density functions). The "Bayes risk" $\mathcal{B}(\mathbf{e})$ for any estimator $\mathbf{e}(\cdot)$ is defined as the expected value of the loss function (Minkler and Minkler, 1993):

$$\mathcal{B}(\mathbf{e}) \triangleq E[L(\boldsymbol{x}, \mathbf{e}(\boldsymbol{Y}))] \tag{3.1}$$

$$= \int_{\boldsymbol{x}} \int_{\boldsymbol{Y}} L(\boldsymbol{\xi}, \mathbf{e}(\boldsymbol{\psi})) f_{\boldsymbol{x},\boldsymbol{Y}}(\boldsymbol{\xi}, \boldsymbol{\psi}) d\boldsymbol{\xi} d\boldsymbol{\psi} \tag{3.2}$$

Then, among a set of all possible estimators S for a given estimation problem, a Bayes estimator is an estimator in S that minimizes the Bayes risk (which is defined by the loss function).

3.1.1.2 Minimum Error Variance Estimators

Many reasonable loss functions can be generated. A loss function which is of particular interest is the squared error loss function, which is defined as

$$L(\boldsymbol{x}, \mathbf{e}(\boldsymbol{Y})) \triangleq |\boldsymbol{x} - \mathbf{e}(\boldsymbol{Y})|^2, \tag{3.3}$$

where $|\boldsymbol{x} - \mathbf{e}(\boldsymbol{Y})|$ is the magnitude of the vector $\boldsymbol{x} - \mathbf{e}(\boldsymbol{Y})$.

Then, combining Equations 3.1 and 3.3, an estimator $\mathbf{e}(\boldsymbol{Y})$ is a minimum variance of error estimator of $\boldsymbol{x}$ if it minimizes

$$E[|\boldsymbol{x} - \mathbf{e}(\boldsymbol{Y})|^2] = E[(\boldsymbol{x} - \mathbf{e}(\boldsymbol{Y}))^T(\boldsymbol{x} - \mathbf{e}(\boldsymbol{Y}))]. \tag{3.4}$$

The error covariance matrix for an estimator $\mathbf{e}(\boldsymbol{Y})$ is defined as the matrix

$$E[(\boldsymbol{x} - \mathbf{e}(\boldsymbol{Y}))(\boldsymbol{x} - \mathbf{e}(\boldsymbol{Y}))^T]. \tag{3.5}$$

Note that minimizing $E[|\boldsymbol{x} - \mathbf{e}(\boldsymbol{Y})|^2]$ is the same as minimizing the trace[2] of the error covariance matrix, because

$$E[|\boldsymbol{x} - \mathbf{e}(\boldsymbol{Y})|^2] = \text{trace}E[(\boldsymbol{x} - \mathbf{e}(\boldsymbol{Y}))(\boldsymbol{x} - \mathbf{e}(\boldsymbol{Y}))^T]. \tag{3.6}$$

It can be shown that the optimal minimum variance of error estimator $\mathbf{e}_{\text{op}}(\boldsymbol{Y})$ is (Maybeck, 1994; Minkler and Minkler, 1993)

$$\mathbf{e}_{\text{op}}(\boldsymbol{Y}) = \int \boldsymbol{\xi} f_{\boldsymbol{x}|\boldsymbol{Y}}(\boldsymbol{\xi}|\boldsymbol{Y}) d\boldsymbol{\xi} = E[\boldsymbol{x}|\boldsymbol{Y}], \tag{3.7}$$

where $f_{\boldsymbol{x}|\boldsymbol{Y}}(\boldsymbol{\xi}|\boldsymbol{Y})$ is the conditional probability density function of $\boldsymbol{x}$ and $E[\boldsymbol{x}|\boldsymbol{Y}]$ is the conditional mean of $\boldsymbol{x}$, conditioned on the observations taking on the realized value $\boldsymbol{Y}$.

[2]The trace of a matrix is defined to be the sum of the diagonal elements.

3.1.1.3 Linear Minimum Error Variance (LMV) Estimators

A *linear* minimum error variance (LMV) estimator is any estimator that minimizes the Bayes risk

$$\mathcal{B}(\mathbf{e}) = E[|\boldsymbol{x} - \mathbf{e}(\boldsymbol{Y})|^2] \tag{3.8}$$

from all estimators that are of the form

$$\mathbf{e}(\boldsymbol{Y}) = \boldsymbol{\alpha} + \boldsymbol{\beta}\boldsymbol{Y} \tag{3.9}$$

(which is the form of a linear estimator). An LMV estimator results in a squared error Bayes risk which is greater than or equal to that of a minimum variance of error estimator $E[\boldsymbol{x}|\boldsymbol{Y}]$. However, it can be shown that if $\boldsymbol{x}$ and $\boldsymbol{Y}$ are jointly Gaussian,[3] then the LMV estimator is equal to the minimum variance of error estimator $E[\boldsymbol{x}|\boldsymbol{Y}]$, and it is therefore also the *optimal* estimator for minimizing the squared error Bayes risk (Maybeck, 1994; Minkler and Minkler, 1993). Therefore, under these conditions,

$$\hat{\boldsymbol{x}} = \mathbf{e}_{\text{op}}(\boldsymbol{Y}) = \boldsymbol{\alpha} + \boldsymbol{\beta}\boldsymbol{Y}. \tag{3.10}$$

Finally, the solutions for $\boldsymbol{\alpha}$ and $\boldsymbol{\beta}$ are (Minkler and Minkler, 1993)

$$\boldsymbol{\alpha} = E[\boldsymbol{x}] - \boldsymbol{C}_{\boldsymbol{x},\boldsymbol{Y}}\boldsymbol{C}_{\boldsymbol{Y}}^{-1}E[\boldsymbol{Y}] \tag{3.11}$$

$$\boldsymbol{\beta} = \boldsymbol{C}_{\boldsymbol{x},\boldsymbol{Y}}\boldsymbol{C}_{\boldsymbol{Y}}^{-1}, \tag{3.12}$$

where

$$\boldsymbol{C}_{\boldsymbol{x}} \triangleq E[(\boldsymbol{x} - E[\boldsymbol{x}])(\boldsymbol{x} - E[\boldsymbol{x}])^T], \tag{3.13}$$

$$\boldsymbol{C}_{\boldsymbol{Y}} \triangleq E[(\boldsymbol{Y} - E[\boldsymbol{Y}])(\boldsymbol{Y} - E[\boldsymbol{Y}])^T], \text{ and} \tag{3.14}$$

$$\boldsymbol{C}_{\boldsymbol{x},\boldsymbol{Y}} \triangleq E[(\boldsymbol{x} - E[\boldsymbol{x}])(\boldsymbol{Y} - E[\boldsymbol{Y}])^T]. \tag{3.15}$$

---

[3] *Jointly Gaussian* means that the joint distribution function $f_{\boldsymbol{x},\boldsymbol{Y}}(\xi, \psi)$ is Gaussian, or equivalently, the vector $\begin{bmatrix} \boldsymbol{x} \\ \boldsymbol{Y} \end{bmatrix}$ is Gaussian.

If both $\boldsymbol{x}$ and $\boldsymbol{Y}$ are zero-mean ($E[\boldsymbol{x}] = \mathbf{0}$ and $E[\boldsymbol{Y}] = \mathbf{0}$), then the above equations are simplified to

$$\hat{\boldsymbol{x}} = \mathbf{e}_{\text{op}}(\boldsymbol{Y}) = \boldsymbol{C}_{\boldsymbol{x},\boldsymbol{Y}}\boldsymbol{C}_{\boldsymbol{Y}}^{-1}\boldsymbol{Y}, \tag{3.16}$$

where

$$\boldsymbol{C}_{\boldsymbol{x}} = E[\boldsymbol{x}\boldsymbol{x}^T] \qquad \boldsymbol{C}_{\boldsymbol{Y}} = E[\boldsymbol{Y}\boldsymbol{Y}^T] \qquad \boldsymbol{C}_{\boldsymbol{x},\boldsymbol{Y}} = E[\boldsymbol{x}\boldsymbol{Y}^T]. \tag{3.17}$$

3.1.2 Double Difference Matrix (B)

In a differential GPS scenario, two or more receivers collect nearly simultaneous measurements from common satellites at each time epoch. In a single reference case, there is one reference receiver and one "mobile" receiver.[4] In a network case, there are two or more reference receivers, and one mobile receiver. The network case (which is more general) will be used here. First, all phase measurement-minus-range-observables from the reference receivers are placed into a single vector $\boldsymbol{\ell}_n$ (standing for $\boldsymbol{\ell}$-network)

$$\boldsymbol{\ell}_n = [\bar{\phi}_1^1 \ldots \bar{\phi}_1^{n_{sv}}, \bar{\phi}_2^1 \ldots \bar{\phi}_2^{n_{sv}}, \ldots, \bar{\phi}_{n_{rec}}^1 \ldots \bar{\phi}_{n_{rec}}^{n_{sv}}]^T \tag{3.18}$$

where $\bar{\phi}_a^x$ is the phase measurement-minus-range observable from receiver a to satellite x, n_{rec} is the number of receivers in the network, and n_{sv} is the number of visible satellites. Note that the derivation in this chapter is performed using phase measurements (ϕ). The same operations apply to code measurements (ρ) as well. Note also that Equation 3.18 implies that all reference receivers receive measurements from exactly the same satellites. This is not true, in general, and the actual $\boldsymbol{\ell}_n$ vector may not be of the exact form as that shown in Equation 3.18.

Next, all of the linearly independent[5] double difference combinations of $\boldsymbol{\ell}_n$ are placed

[4] In this thesis, the "mobile" receiver refers to the receiver to be positioned. In some special applications, the receiver to be positioned may actually be stationary.

[5] Linear independence means that no double difference can be expressed as a linear combination of any of the other double differences.

into the vector $\Delta\nabla\boldsymbol{\ell}_n$

$$\Delta\nabla\boldsymbol{\ell}_n = [\Delta\nabla\bar{\phi}_{12}^{12}\ldots\Delta\nabla\bar{\phi}_{12}^{1n_{sv}}, \Delta\nabla\bar{\phi}_{13}^{12}\ldots\Delta\nabla\bar{\phi}_{13}^{1n_{sv}}, \ldots, \Delta\nabla\bar{\phi}_{1n_{rec}}^{12}\ldots\Delta\nabla\bar{\phi}_{1n_{rec}}^{1n_{sv}}]^T \tag{3.19}$$

where $\bar{\phi}_{ab}^{xy}$ is the double difference of the measurement-minus-range observables from receivers a and b and satellites x and y (as defined in Equation 2.12). As before, some of these elements may be missing if not all of the satellites are visible to all of the reference receivers.

The double difference matrix B_n for the network is then defined as

$$\mathrm{B}_n \triangleq \frac{\partial\Delta\nabla\boldsymbol{\ell}_n}{\partial\boldsymbol{\ell}_n}. \tag{3.20}$$

Since double difference measurements ($\Delta\nabla\boldsymbol{\ell}_n$) are direct linear combinations of the measurements themselves ($\boldsymbol{\ell}_n$), the B_n matrix is made up entirely of the values +1, -1, and 0. For example, suppose that there is a very small network with three receivers (a, b, and c), each generating measurements from three satellites (x, y, and z). The measurement vector in this case is

$$\boldsymbol{\ell}_n = \begin{bmatrix}\bar{\phi}_a^x & \bar{\phi}_a^y & \bar{\phi}_a^z & \bar{\phi}_b^x & \bar{\phi}_b^y & \bar{\phi}_b^z & \bar{\phi}_c^x & \bar{\phi}_c^y & \bar{\phi}_c^z\end{bmatrix}^T \tag{3.21}$$

One possible double difference vector is

$$\Delta\nabla\boldsymbol{\ell}_n = \begin{bmatrix}\Delta\nabla\bar{\phi}_{ab}^{xy} & \Delta\nabla\bar{\phi}_{ab}^{xz} & \Delta\nabla\bar{\phi}_{ac}^{xy} & \Delta\nabla\bar{\phi}_{ac}^{xz}\end{bmatrix}^T. \tag{3.22}$$

(There are other possible sets of four linearly independent double differences, but the results would be the same). Then, according to Equation 3.20, the B_n matrix is

$$\mathrm{B}_n = \begin{bmatrix} 1 & -1 & 0 & 1 & -1 & 0 & 0 & 0 & 0 \\ 1 & 0 & -1 & 1 & 0 & -1 & 0 & 0 & 0 \\ 1 & -1 & 0 & 0 & 0 & 0 & 1 & -1 & 0 \\ 1 & 0 & -1 & 0 & 0 & 0 & 1 & 0 & -1 \end{bmatrix}. \tag{3.23}$$

Note that the B_n matrix is of size $n_{dd} \times n_m$, where n_{dd} is the number of double differences and n_m is the number of measurements. For a network in which all receivers receive signals from a common set of satellites

$$n_m = (n_{rec})(n_{sv}) \tag{3.24}$$

$$n_{dd} = (n_{rec} - 1)(n_{sv} - 1). \tag{3.25}$$

Note also that the double difference vector can be formed by multiplying the measurement vector by the B_n matrix

$$\Delta\nabla\ell_n = B_n\ell_n. \tag{3.26}$$

For this reason, the B_n matrix is called a "double difference matrix."

3.2 Derivation of NetAdjust Method

3.2.1 Definition of Differential Measurement Errors

In this section, the GPS measurement errors are expressed in such a way as to separate out errors which are canceled during double differencing from those that are not canceled when double differencing. In Chapter 2, Equation 2.16, the phase measurement was given as

$$\phi = \frac{1}{\lambda}(\mathbb{R} + T - \frac{I}{f^2} + c\delta t_{rec} - c\delta t_{sv} + m + v) + N. \tag{3.27}$$

If the calculated range is subtracted from this measurement, and a nominal value of T is removed using a tropospheric error model, then, from Chapter 2, the measurement-minus-range observable is

$$\bar{\phi} = \frac{1}{\lambda}(T' - \frac{I}{f^2} + c\delta t_{rec} - c\delta t_{sv} + m + v - \delta p_{sv}) + N. \tag{3.28}$$

Note that there would also be a receiver position error term δp_{rec} were it not for the assumption stated in Section 1.2.3.1 that the receiver coordinates are known. Note also

that the tropospheric error is denoted as T', indicating the *residual* tropospheric error, after subtracting the modeled error. Equation 3.28 can be broken into four parts

$$\bar{\phi} = \delta\phi_{\text{clock}} + \delta_c\phi(\boldsymbol{p}_{rec}) + \delta_u\phi + N \tag{3.29}$$

where

$$\delta\phi_{\text{clock}} \triangleq \frac{1}{\lambda}(c\delta t_{rec} - c\delta t_{sv}) \tag{3.30}$$

$$\delta_c\phi(\boldsymbol{p}_{rec}) \triangleq \frac{1}{\lambda}(T' - \frac{I}{f^2} - \delta p_{sv}) \tag{3.31}$$

$$\delta_u\phi \triangleq \frac{1}{\lambda}(m + v). \tag{3.32}$$

The first term, $\delta\phi_{\text{clock}}$, includes the clock errors which will be completely canceled in the double differencing process. The $\delta_c\phi(\boldsymbol{p}_{rec})$ is the *correlated* error term, and it includes all of the errors which are purely a function of the receiver position $\boldsymbol{p}_{rec}$. These are called correlated errors, because they are correlated between receivers that are close together. Correlated errors include satellite position error, ionospheric error, and tropospheric error. The third term, $\delta_u\phi$, is the *uncorrelated* error term. This includes all errors which are not canceled in the double differencing process and which are not a function of receiver position (hence uncorrelated). Uncorrelated errors include multipath and measurement noise. The integer ambiguity N is the fourth term. Note that $\delta_c\phi(\boldsymbol{p}_{rec})$ and $\delta_u\phi$ are *absolute* errors. That is, they are the whole valued errors before any differential canceling occurs.

Next, the point $\boldsymbol{p}_0$ is defined as a fixed position from which all of the differential errors will be referenced. It will be called the "zero-point". It should be chosen to be somewhere near the center of the network, in order to minimize the distances to the reference receivers (and any mobile receiver position). The results are not very sensitive to the location of $\boldsymbol{p}_0$, however. Define the *relative* error term

$$d_c\phi(\boldsymbol{p}_{rec}, \boldsymbol{p}_0) \triangleq \delta_c\phi(\boldsymbol{p}_{rec}) - \delta_c\phi(\boldsymbol{p}_0). \tag{3.33}$$

Combining Equation 3.29 and 3.33 yields

$$\bar{\phi} = \delta\phi_{\text{clock}} + \delta_c\phi(\boldsymbol{p}_0) + d_c\phi(\boldsymbol{p}_{rec}, \boldsymbol{p}_0) + \delta_u\phi + N. \tag{3.34}$$

Everything done up to this point has involved a single measurement from a single receiver, and the goal was to separate out errors which are canceled when double differencing from those which are not canceled when double differencing. If a double difference measurement is formed between *any* two receivers and *any* two satellites, the double difference equation is

$$\Delta\nabla\bar{\phi} = \Delta\nabla\delta\phi_{\text{clock}} + \Delta\nabla\delta_c\phi(\boldsymbol{p}_0) + \Delta\nabla d_c\phi(\boldsymbol{p}_{rec}, \boldsymbol{p}_0) + \Delta\nabla\delta_u\phi + \Delta\nabla N. \tag{3.35}$$

Note, however, that $\Delta\nabla\delta\phi_{\text{clock}} = 0$, because the clock terms cancel out (reference Section 2.1.1.1). Also, $\Delta\nabla\delta_c\phi(\boldsymbol{p}_0) = 0$, because it is the whole valued error at the reference point $\boldsymbol{p}_0$, and as such it is not a function of the receiver position. When double differencing is performed, this term will be common to both receivers, so it will cancel. Therefore,

$$\Delta\nabla\bar{\phi} = \Delta\nabla d_c\phi(\boldsymbol{p}_{rec}, \boldsymbol{p}_0) + \Delta\nabla\delta_u\phi + \Delta\nabla N. \tag{3.36}$$

Equation 3.36 includes all of the relevant errors when double differencing GPS measurements. If these errors can be estimated (and corrected), then the double difference measurements will be perfect (i.e. have zero error). Of the three terms on the right hand side of Equation 3.36, only the $\Delta\nabla d_c\phi(\boldsymbol{p}_{rec}, \boldsymbol{p}_0)$ and $\Delta\nabla\delta_u\phi$ terms will be estimated by NetAdjust. The integer ambiguity term $\Delta\nabla N$ will be assumed to be known (in the case of the reference network–see Section 1.2.3.4) or will be the quantity that the mobile user will attempt to determine. Solving for the integer ambiguities between a reference receiver and the mobile user becomes easier the more the other two error terms are reduced.

3.2.1.1 Relationship Between Measurements and Errors

The measurements involved in a differential GPS network are either measurements from the network (reference) receivers or measurements from a mobile receiver. The position

of the mobile receiver is called the 'computation point," because it is the point for which the differential errors should be computed.

All of the phase measurement-minus-range observables for measurements from the network are placed into the $\boldsymbol{\ell}_n$ vector (as described in Section 3.1.2). In a similar manner, all of the measurement-minus-range values that would be generated by a mobile receiver are placed into a vector $\tilde{\boldsymbol{\ell}}_{cp}$. The subscript *cp* stands for "computation point", and the tilde (~) above the measurement denotes that it is a measurement that is unavailable for use in the network estimation process (i.e. it exists, but it cannot be used except by the mobile user). These two vectors can then be combined to form the complete measurement vector

$$\boldsymbol{\ell} = \begin{bmatrix} \boldsymbol{\ell}_n \\ \tilde{\boldsymbol{\ell}}_{cp} \end{bmatrix}. \tag{3.37}$$

Note that $\boldsymbol{\ell}$ is a combination of available measurements ($\boldsymbol{\ell}_n$) and unavailable measurements ($\boldsymbol{\ell}_{cp}$).

Combining the definition of $\boldsymbol{\ell}$ (Equation 3.21) with Equation 3.34 yields

$$\boldsymbol{\ell} = \delta\boldsymbol{\phi}_{\text{clock}} + \delta_c\boldsymbol{\phi}(\boldsymbol{p}_0) + d_c\boldsymbol{\phi}(\boldsymbol{p}, \boldsymbol{p}_0) + \delta_u\boldsymbol{\phi} + \boldsymbol{N}, \tag{3.38}$$

where the boldface error terms are now vector quantities corresponding to each phase measurement from the network. Note that the position at which the measurement was taken is denoted $\boldsymbol{p}$, whether it was at a reference receiver ($\boldsymbol{p}_{rec}$) or a computation point ($\boldsymbol{p}_{cp}$). The clock errors and ambiguities keep the raw $\boldsymbol{\ell}$ vector from being directly useful. However, double differencing yields (following Equation 3.36)

$$\Delta\nabla\boldsymbol{\ell} = \Delta\nabla d_c\boldsymbol{\phi}(\boldsymbol{p}, \boldsymbol{p}_0) + \Delta\nabla\delta_u\boldsymbol{\phi} + \Delta\nabla\boldsymbol{N}, \tag{3.39}$$

where the boldface error terms are again vector quantities. Define $\Delta\nabla\delta\boldsymbol{\ell}$ as the double difference errors to be eliminated (see Equation 3.36)

$$\Delta\nabla\delta\boldsymbol{\ell} = \Delta\nabla d_c\boldsymbol{\phi}(\boldsymbol{p}, \boldsymbol{p}_0) + \Delta\nabla\delta_u\boldsymbol{\phi}. \tag{3.40}$$

Then, from Equation 3.39,

$$\Delta\nabla\delta\boldsymbol{\ell} = \Delta\nabla\boldsymbol{\ell} - \Delta\nabla\boldsymbol{N}. \tag{3.41}$$

Equation 3.41 is key, because it states that the double differenced measurement-minus-range observables $\Delta\nabla\boldsymbol{\ell}$ are *equivalent* to the double difference errors $\Delta\nabla\delta\boldsymbol{\ell}$, after correcting for the integer ambiguities $\Delta\nabla\boldsymbol{N}$.

3.2.2 Definition of Network Optimal Estimization Problem

When performing differential positioning or ambiguity resolution between the mobile receiver and one or more reference receivers, selected measurements from $\boldsymbol{\ell}$ will be combined to form the double difference observables $\Delta\nabla\boldsymbol{\ell}_{cp}$. Using the double difference operator notation presented in Section 3.1.2, this can be written

$$\Delta\nabla\tilde{\boldsymbol{\ell}}_{cp} = \mathrm{B}_{cp}\boldsymbol{\ell}, \tag{3.42}$$

where B_{cp} represents the linear combinations of $\boldsymbol{\ell}$. Because $\Delta\nabla\boldsymbol{\ell}_{cp}$ is used for positioning or ambiguity resolution of the mobile receiver, all of the double difference measurements will be formed using two measurements from a network reference receiver (from $\boldsymbol{\ell}_n$) and two measurements from the mobile receiver (from $\tilde{\boldsymbol{\ell}}_{cp}$). Therefore, B_{cp} can be separated into two parts, such that

$$\Delta\nabla\tilde{\boldsymbol{\ell}}_{cp} = \begin{bmatrix}\mathrm{B}_{cp_1} & \mathrm{B}_{cp_2}\end{bmatrix}\begin{bmatrix}\boldsymbol{\ell}_n \\ \tilde{\boldsymbol{\ell}}_{cp}\end{bmatrix} \tag{3.43}$$

where B_{cp_1} corresponds to the measurements from the network, and B_{cp_2} corresponds to the measurements from the mobile receiver. From Equation 3.41, the double difference measurements can be written instead in terms of double difference errors

$$\Delta\nabla\delta\tilde{\boldsymbol{\ell}}_{cp} + \Delta\nabla\boldsymbol{N}_{cp} = \begin{bmatrix}\mathrm{B}_{cp_1} & \mathrm{B}_{cp_2}\end{bmatrix}\begin{bmatrix}\boldsymbol{\ell}_n \\ \tilde{\boldsymbol{\ell}}_{cp}\end{bmatrix}. \tag{3.44}$$

The term $\Delta\nabla\delta\tilde{\boldsymbol{\ell}}_{cp}$ represents errors in the measurements that are not canceled by double differencing. Large $\Delta\nabla\delta\tilde{\boldsymbol{\ell}}_{cp}$ make ambiguity resolution difficult and reduce position accuracy.

The network algorithm will generate estimated measurement errors $\hat{\delta\boldsymbol{\ell}}$ for the measurements in $\boldsymbol{\ell}$, and applying them will give the corrected measurement vector $\hat{\boldsymbol{\ell}}$

$$\hat{\boldsymbol{\ell}} = \boldsymbol{\ell} - \hat{\delta\boldsymbol{\ell}}. \tag{3.45}$$

When these corrected measurements are double differenced, the resulting corrected double difference measurement vector $\Delta\nabla\hat{\tilde{\boldsymbol{\ell}}}_{cp}$ is then

$$\Delta\nabla\hat{\tilde{\boldsymbol{\ell}}}_{cp} = \mathrm{B}_{cp}\hat{\boldsymbol{\ell}} \tag{3.46}$$

$$= \mathrm{B}_{cp}[\boldsymbol{\ell} - \hat{\delta\boldsymbol{\ell}}]. \tag{3.47}$$

The error estimates can themselves be double differenced by

$$\Delta\nabla\hat{\delta\boldsymbol{\ell}}_{cp} = \mathrm{B}_{cp}\hat{\delta\boldsymbol{\ell}}, \tag{3.48}$$

and after combining this result with Equations 3.44 and 3.47, the corrected double difference measurements are

$$\Delta\nabla\delta\tilde{\boldsymbol{\ell}}_{cp} - \Delta\nabla\hat{\delta\boldsymbol{\ell}}_{cp} + \Delta\nabla\boldsymbol{N}_{cp} = \mathrm{B}_{cp}[\boldsymbol{\ell} - \hat{\delta\boldsymbol{\ell}}]. \tag{3.49}$$

Note that the vector $\Delta\nabla\tilde{\boldsymbol{\ell}}_{cp}$ cannot be directly calculated without access to the mobile receiver measurements (which the network does not have).

Equation 3.49 shows that after applying the corrections $\hat{\delta\boldsymbol{\ell}}$ to the measurements, the total double difference estimation error $\mathbf{err}(\Delta\nabla\delta\boldsymbol{\ell}_{cp})$ is

$$\mathbf{err}(\Delta\nabla\delta\boldsymbol{\ell}_{cp}) = \Delta\nabla\delta\tilde{\boldsymbol{\ell}}_{cp} - \Delta\nabla\hat{\delta\boldsymbol{\ell}}_{cp}, \tag{3.50}$$

and the covariance[6] of this estimation error is (by the definition of covariance)

$$\begin{aligned} \boldsymbol{C}_{\mathbf{err}(\Delta\nabla\delta\boldsymbol{\ell}_{cp})} &\triangleq E[\mathbf{err}(\Delta\nabla\delta\boldsymbol{\ell}_{cp})\mathbf{err}(\Delta\nabla\delta\boldsymbol{\ell}_{cp})^T] \\ &= E[(\Delta\nabla\delta\tilde{\boldsymbol{\ell}}_{cp} - \Delta\nabla\hat{\delta\boldsymbol{\ell}}_{cp})(\Delta\nabla\delta\tilde{\boldsymbol{\ell}}_{cp} - \Delta\nabla\hat{\delta\boldsymbol{\ell}}_{cp})^T] \end{aligned} \tag{3.51}$$

Note that the trace of the $\boldsymbol{C}_{\mathbf{err}(\Delta\nabla\delta\boldsymbol{\ell}_{cp})}$ matrix is the sum of the error variances.

The differential GPS network optimization problem can then be stated as follows: given only the *network* measurement-minus-range observables $\boldsymbol{\ell}_n$, generate an estimate of the differential measurement errors $\hat{\delta\boldsymbol{\ell}}$ that minimizes the trace of the error covariance matrix $\boldsymbol{C}_{\mathbf{err}(\Delta\nabla\delta\boldsymbol{\ell}_{cp})}$.

The operational concept is that the network is used to calculate measurement corrections $\hat{\delta\boldsymbol{\ell}}$, which are then transmitted in some form to the mobile user, who applies them in the process of generating double difference measurement-minus-range observables. In so doing, minimizes the double difference measurement errors.

3.2.3 Solution to Network Optimal Estimation Problem

The previous section dealt with the double difference matrix B_{cp} which generates double difference measurements between the mobile receiver at the computation point and one or more reference receivers. Recall from Section 3.1.2 that there is also a double difference matrix B_n which generates all possible linearly independent double difference combinations using measurements from only the network reference receivers. After the application of Equation 3.41, the double differenced network measurements are

$$\Delta\nabla\delta\boldsymbol{\ell}_n + \Delta\nabla\boldsymbol{N}_n = \mathrm{B}_n\boldsymbol{\ell}_n. \tag{3.52}$$

---

[6]This is the error covariance as long as the estimator that generates $\Delta\nabla\hat{\delta\boldsymbol{\ell}}_{cp}$ is an unbiased estimator (i.e. $E[\mathbf{err}(\Delta\nabla\delta\boldsymbol{\ell}_{cp})] = E[\Delta\nabla\delta\tilde{\boldsymbol{\ell}}_{cp} - \Delta\nabla\hat{\delta\boldsymbol{\ell}}_{cp}] = \mathbf{0}$). If this is not true, then Equation 3.51 is actually a correlation matrix. (The estimator used by NetAdjust (Section 3.1.1.3) is an unbiased estimator (Minkler and Minkler, 1993)).

This equation is important for two reasons. First, recall that the goal is to calculate $\delta\ell_n$ and $\delta\ell_{cp}$. Equation 3.52 provides observability to the $\delta\ell_n$ errors, albeit through a double difference. In fact, double differencing is really the only way that the differential errors $\delta\ell_n$ or $\delta\ell_{cp}$ can be directly observed. Secondly, this equation shows how $\Delta\nabla\delta\ell_n$ can be generated using data from the reference network. The $\Delta\nabla\ell_n$ term is made up of double differenced phase measurement-minus-range observables from the network reference receivers, and the $\Delta\nabla\boldsymbol{N}$ term represents the double difference integer ambiguities between the network reference receivers receivers (which are assumed to be known, as stated in Section 1.2.3.4). Therefore, because $\Delta\nabla\delta\ell_n$ can be generated using the network measurements and network ambiguities, and it is the only way to gain observability to the errors of interest, it then becomes the *observable* in the network estimation process (even though the ultimate goal is to calculate $\hat{\delta\ell}$).

Two different estimators will be derived. The first, called $\mathbf{e}_1(\cdot)$, uses observables $\Delta\nabla\delta\ell_n$ to generate estimates of the double difference error $\Delta\nabla\hat{\delta\ell}_{cp}$. The second estimator, $\mathbf{e}_2(\cdot)$ uses the same observables $\Delta\nabla\delta\ell_n$ to generate estimates of the measurement error vector $\hat{\delta\ell}$. It is necessary to derive these two estimators, because the relationship between them gives the final solution to the network estimation problem. Table 3.1 summarizes the two estimators.

Table 3.1: *Two estimators to be derived* ($\hat{\boldsymbol{x}} = \boldsymbol{e}(\boldsymbol{Y})$)

Estimator	Observables ($\boldsymbol{Y}$)	Parameters to be Estimated ($\boldsymbol{x}$)
$\mathbf{e}_1(\cdot)$	$\Delta\nabla\delta\ell_n$	$\Delta\nabla\delta\ell_{cp}$
$\mathbf{e}_2(\cdot)$	$\Delta\nabla\delta\ell_n$	$\delta\ell$

3.2.3.1 Characteristics of $\delta\ell$

In the derivations that follow, it will be useful to understand what the $\delta\ell$ vector is and what its statistical characteristics are. A combination of Equations 3.40 and 3.48 results in

$$\Delta\nabla d_c\phi(\boldsymbol{p},\boldsymbol{p}_0) + \Delta\nabla\delta_u\phi = \Delta\nabla\delta\ell = \mathrm{B}\delta\ell, \tag{3.53}$$

where B is a double difference matrix. This equation holds true if $\delta\ell$ is defined to be

$$\delta\ell \triangleq d_c\phi(\boldsymbol{p},\boldsymbol{p}_0) + \delta_u\phi. \tag{3.54}$$

The $d_c\phi(\boldsymbol{p},\boldsymbol{p}_0)$ term includes differential ionosphere, troposphere, and satellite position errors relative to point $\boldsymbol{p}_0$. The $\delta_u\phi$ term represents multipath and noise, which are uncorrelated between different measurements (so they do not cancel out in the double differencing). The following two assumptions will be made about the $\delta\ell$ vector:

1. It is well-described as a Gaussian random vector with covariance matrix $\boldsymbol{C}_{\delta\ell}$.
2. It is a zero-mean vector (i.e. $E[\delta\ell] = \mathbf{0}$).

Both of these assumptions will be discussed in the paragraphs that follow.

3.2.3.1.1 $\delta\ell$ is Gaussian Random Vector. There are two primary justifications for considering $\delta\ell$ to be a Gaussian random vector. First, it is a linear combination of many different independent error sources (satellite position, ionosphere, troposphere, multipath, noise), and a linear combination of independent noise sources tends toward a Gaussian distribution according to the central limit theorem.[7] Secondly, each of the error sources was separately analyzed in Chapter 2 using double differences, and sample probability distribution functions were generated for each of them (see Table 3.2 for figure reference information). All of the double differenced errors followed a Gaussian trend.

[7]The central limit theorem essentially states that the more independent error sources there are, the more the combination of them appears Gaussian (Maybeck, 1994).

Table 3.2: Locations of plots showing double difference error probability distribution

Error Type	Figure Number	Page Number
Satellite Position Error	2.17	50
Ionospheric Error	2.2	32
	2.3	32
Tropospheric Error	2.5	35
Multipath	2.14	47
Measurement Noise	2.9	40

3.2.3.1.2 $\delta\ell$ is Zero-Mean A necessary but not sufficient condition for $\delta\ell$ to be zero-mean is that any double differences $\Delta\nabla\delta\ell$ are zero-mean, because

$$E[\Delta\nabla\delta\ell] = E[\mathrm{B}\delta\ell] = \mathrm{B}E[\delta\ell]. \tag{3.55}$$

The double difference probability density plots referred to in Table 3.2 do show that the mean values of the double differenced errors are zero (or are very close). In addition, there is nothing inherent in the terms $\Delta\nabla d_c\boldsymbol{\phi}(\boldsymbol{p}, \boldsymbol{p}_0)$ and $\Delta\nabla\delta_u\boldsymbol{\phi}$ which would keep them from being zero-mean. For example, there is no reason that the tropospheric error at point $\boldsymbol{p}$ would always be greater than the tropospheric error at point $\boldsymbol{p}_0$. Therefore, the vector $\delta\ell$ will be considered to be zero-mean.

3.2.3.2 Covariance Transformations from $\boldsymbol{C}_{\delta\ell}$

In the previous section, the measurements error vector $\delta\ell$ was assumed to be Gaussian with covariance matrix $\boldsymbol{C}_{\delta\ell}$. This means that, by the definition of a covariance matrix,

$$\boldsymbol{C}_{\delta\ell} \triangleq E[(\delta\ell - E[\delta\ell])(\delta\ell - E[\delta\ell])^T]. \tag{3.56}$$

However, the vector $\delta\ell$ was also assumed to be zero-mean ($E[\delta\ell] = \mathbf{0}$), so the covariance equation reduces to

$$\boldsymbol{C}_{\delta\ell} = E[(\delta\ell)(\delta\ell)^T]. \tag{3.57}$$

In the derivations that follow, it will be useful to know the covariance matrix of measurements that are a linear combination of the measurements in $\delta\ell$. For example, the errors from double differencing the measurements from the network reference receivers are

$$\Delta\nabla\delta\ell_n = \mathrm{B}_n\delta\ell_n. \tag{3.58}$$

The covariance matrix of these double difference errors ($\boldsymbol{C}_{\Delta\nabla\delta\ell_n}$) is, by definition,

$$\boldsymbol{C}_{\Delta\nabla\delta\ell_n} \triangleq E[(\Delta\nabla\delta\ell_n - E[\Delta\nabla\delta\ell_n])(\Delta\nabla\delta\ell_n - E[\Delta\nabla\delta\ell_n])^T]. \tag{3.59}$$

This can be transformed using Equation 3.58, combined with the fact that the expectation operator $E[\cdot]$ is a linear operator, as follows:

$$\begin{aligned}
\boldsymbol{C}_{\Delta\nabla\delta\ell_n} &\triangleq E[(\Delta\nabla\delta\ell_n - E[\Delta\nabla\delta\ell_n])(\Delta\nabla\delta\ell_n - E[\Delta\nabla\delta\ell_n])^T]. \\
&= E[(\mathrm{B}_n\delta\ell_n - E[\mathrm{B}_n\delta\ell_n])(\mathrm{B}_n\delta\ell_n - E[\mathrm{B}_n\delta\ell_n])^T] \\
&= E[(\mathrm{B}_n\delta\ell_n - \mathrm{B}_nE[\delta\ell_n])(\mathrm{B}_n\delta\ell_n - \mathrm{B}_nE[\delta\ell_n])^T] \\
&= E[(\mathrm{B}_n\delta\ell_n)(\mathrm{B}_n\delta\ell_n)^T] \\
&= E[(\mathrm{B}_n\delta\ell_n)(\delta\ell_n^T\mathrm{B}_n^T)] \\
&= \mathrm{B}_nE[(\delta\ell_n)(\delta\ell_n)^T)]\mathrm{B}_n^T \\
&= \mathrm{B}_n\boldsymbol{C}_{\delta\ell_n}\mathrm{B}_n^T.
\end{aligned} \tag{3.60}$$

The same reasoning applies to cross-correlation matrices as well.

A summary of the relations between the various error vectors and error double-difference vectors discussed in the previous sections are shown in the following equation:

$$\Delta\nabla\delta\ell = \begin{bmatrix} \Delta\nabla\delta\ell_n \\ \Delta\nabla\delta\ell_{cp} \end{bmatrix} = \begin{bmatrix} \mathrm{B}_n & \mathbf{0} \\ \mathrm{B}_{cp_1} & \mathrm{B}_{cp_2} \end{bmatrix} \begin{bmatrix} \delta\ell_n \\ \delta\ell cp \end{bmatrix} = \mathrm{B}\delta\ell. \tag{3.61}$$

These relationships can be used to calculate two other cross-covariance matrices (all based upon the $\boldsymbol{C}_{\delta\boldsymbol{\ell}}$ matrix or a subset of it) which will be useful later:

$$\boldsymbol{C}_{\Delta\nabla\delta\boldsymbol{\ell}_{cp},\Delta\nabla\delta\boldsymbol{\ell}_n} = \begin{bmatrix} \mathrm{B}_{cp_1} & \mathrm{B}_{cp_2} \end{bmatrix} \boldsymbol{C}_{\delta\boldsymbol{\ell}} \begin{bmatrix} \mathrm{B}_n^T \\ \mathbf{0} \end{bmatrix} \tag{3.62}$$

$$\boldsymbol{C}_{\delta\boldsymbol{\ell},\Delta\nabla\delta\boldsymbol{\ell}_n} = \boldsymbol{C}_{\delta\boldsymbol{\ell}} \begin{bmatrix} \mathrm{B}_n^T \\ \mathbf{0} \end{bmatrix} \tag{3.63}$$

3.2.3.3 Solution for $\mathbf{e}_1(\cdot)$

Recall from Section 3.1.1 that for zero-mean, jointly Gaussian $\boldsymbol{x}$ (parameters) and $\boldsymbol{Y}$ (observations), the estimator $\mathbf{e}(\boldsymbol{Y})$ which minimizes the trace of the error covariance matrix is

$$\hat{\boldsymbol{x}} = \boldsymbol{C}_{\boldsymbol{x},\boldsymbol{Y}} \boldsymbol{C}_{\boldsymbol{Y}}^{-1} \boldsymbol{Y}, \tag{3.64}$$

where $C_{\boldsymbol{x},\boldsymbol{Y}}$ and $C_{\boldsymbol{Y}}$ are defined in Equation 3.17.

For this $\mathbf{e}_1(\cdot)$ filter, $\boldsymbol{Y} = \Delta\nabla\delta\boldsymbol{\ell}_n$ and $\boldsymbol{x} = \Delta\nabla\delta\boldsymbol{\ell}_{cp}$. In order to apply Equation 3.64, it must be shown that $\Delta\nabla\delta\boldsymbol{\ell}_n$ and $\Delta\nabla\delta\boldsymbol{\ell}_{cp}$ are zero-mean and jointly Gaussian. From Equation 3.61

$$\Delta\nabla\delta\boldsymbol{\ell} = \begin{bmatrix} \Delta\nabla\delta\boldsymbol{\ell}_n \\ \Delta\nabla\delta\boldsymbol{\ell}_{cp} \end{bmatrix} = \mathrm{B}\delta\boldsymbol{\ell}. \tag{3.65}$$

Therefore,

$$E[\Delta\nabla\delta\boldsymbol{\ell}] = E[\mathrm{B}\delta\boldsymbol{\ell}] = \mathrm{B}E[\delta\boldsymbol{\ell}] = \mathbf{0}, \tag{3.66}$$

so both $\Delta\nabla\delta\boldsymbol{\ell}_n$ and $\Delta\nabla\delta\boldsymbol{\ell}_{cp}$ are zero-mean. Requiring $\Delta\nabla\delta\boldsymbol{\ell}_n$ and $\Delta\nabla\delta\boldsymbol{\ell}_{cp}$ to be jointly Gaussian is equivalent to requiring the vector made from them (i.e. $\Delta\nabla\delta\boldsymbol{\ell}$) to be Gaussian. Since $\delta\boldsymbol{\ell}$ is assumed to be Gaussian, then $\Delta\nabla\delta\boldsymbol{\ell}$ must also be Gaussian, because it is a linear transformation of $\delta\boldsymbol{\ell}$ (Maybeck, 1994).

Now that it has been shown that the observation vector $\Delta\nabla\delta\boldsymbol{\ell}_n$ and the parameter vector $\Delta\nabla\delta\boldsymbol{\ell}_{cp}$ are zero-mean, jointly Gaussian random variables, a straightforward application of Equation 3.64 can be performed

$$\Delta\nabla\hat{\delta\boldsymbol{\ell}}_{cp} = \boldsymbol{C}_{\Delta\nabla\delta\boldsymbol{\ell}_{cp},\Delta\nabla\delta\boldsymbol{\ell}_n}(\boldsymbol{C}_{\Delta\nabla\delta\boldsymbol{\ell}_n})^{-1}\Delta\nabla\delta\boldsymbol{\ell}_n. \tag{3.67}$$

Applying Equations 3.60 and 3.62 results in the final form of the estimator $\mathbf{e}_1(\cdot)$

$$\mathbf{e}_1(\Delta\nabla\delta\boldsymbol{\ell}_n) = \Delta\nabla\hat{\delta\boldsymbol{\ell}}_{cp} = \begin{bmatrix}\mathrm{B}_{cp_1} & \mathrm{B}_{cp_2}\end{bmatrix}\boldsymbol{C}_{\delta\boldsymbol{\ell}}\begin{bmatrix}\mathrm{B}_n^T \\ \mathbf{0}\end{bmatrix}(\mathrm{B}_n\boldsymbol{C}_{\delta\boldsymbol{\ell}}\mathrm{B}_n^T)^{-1}\Delta\nabla\delta\boldsymbol{\ell}_n, \tag{3.68}$$

3.2.3.4 Solution for $\mathbf{e}_2(\cdot)$

For this $\mathbf{e}_2(\cdot)$ filter, $\boldsymbol{Y} = \Delta\nabla\delta\boldsymbol{\ell}_n$ (as before) and $\boldsymbol{x} = \delta\boldsymbol{\ell}$. In order to apply Equation 3.64, it must be shown that $\Delta\nabla\delta\boldsymbol{\ell}_n$ and $\delta\boldsymbol{\ell}$ are zero-mean and jointly Gaussian. Define

$$\boldsymbol{Z} \triangleq \begin{bmatrix}\delta\boldsymbol{\ell} \\ \Delta\nabla\delta\boldsymbol{\ell}_n\end{bmatrix} = \begin{bmatrix}\mathbf{I} \\ \begin{bmatrix}\mathrm{B}_n & \mathbf{0}\end{bmatrix}\end{bmatrix}\delta\boldsymbol{\ell} = \mathrm{B}_2\delta\boldsymbol{\ell}. \tag{3.69}$$

Then $\boldsymbol{Z}$ can be shown to be a zero-mean, Gaussian random vector using the same reasoning as presented for the $\mathbf{e}_1(\cdot)$ estimator, and therefore $\Delta\nabla\delta\boldsymbol{\ell}_n$ and $\delta\boldsymbol{\ell}$ are both zero-mean and jointly Gaussian.

Next, Equation 3.64 is applied

$$\hat{\delta\boldsymbol{\ell}} = \boldsymbol{C}_{\delta\boldsymbol{\ell},\Delta\nabla\delta\boldsymbol{\ell}_n}(\boldsymbol{C}_{\Delta\nabla\delta\boldsymbol{\ell}_n})^{-1}\Delta\nabla\delta\boldsymbol{\ell}_n. \tag{3.70}$$

Utilizing Equations 3.60 and 3.63 results in the final form of the estimator $\mathbf{e}_2(\cdot)$

$$\mathbf{e}_2(\Delta\nabla\delta\boldsymbol{\ell}_n) = \hat{\delta\boldsymbol{\ell}} = \boldsymbol{C}_{\delta\boldsymbol{\ell}}\begin{bmatrix}\mathrm{B}_n^T \\ \mathbf{0}\end{bmatrix}(\mathrm{B}_n\boldsymbol{C}_{\delta\boldsymbol{\ell}_n}\mathrm{B}_n^T)^{-1}\Delta\nabla\delta\boldsymbol{\ell}_n, \tag{3.71}$$

3.2.3.5 Comparison between $\mathbf{e}_1(\cdot)$ and $\mathbf{e}_2(\cdot)$ Estimators

Comparing Equations 3.68 and 3.71 shows that

$$\mathbf{e}_1(\Delta\nabla\delta\boldsymbol{\ell}_n) = \begin{bmatrix}\mathrm{B}_{cp_1} & \mathrm{B}_{cp_2}\end{bmatrix}\mathbf{e}_2(\Delta\nabla\delta\boldsymbol{\ell}_n), \tag{3.72}$$

or, equivalently

$$\Delta\nabla\hat{\delta\ell}_{cp} = \begin{bmatrix} \mathrm{B}_{cp_1} & \mathrm{B}_{cp_2} \end{bmatrix} \hat{\delta\ell}. \tag{3.73}$$

This equation shows that the individual measurement error estimates $\hat{\delta\ell}$, when double differenced via the $\begin{bmatrix} \mathrm{B}_{cp_1} & \mathrm{B}_{cp_2} \end{bmatrix}$ matrix, yield the optimal double difference error estimates (i.e. the estimates which minimize the trace of $\boldsymbol{C}_{\mathbf{err}(\Delta\nabla\delta\ell_{cp})}$). This is the exact goal of the differential network optimal estimation problem as stated in Section 3.2.2.

Note that it is not necessary to know the $\begin{bmatrix} \mathrm{B}_{cp_1} & \mathrm{B}_{cp_2} \end{bmatrix}$ matrix in order to solve the network optimal estimation problem, because *any* double difference vector formed from the $\hat{\delta\ell}$ vector will be an optimal estimate. Nowhere in the above derivation has the exact form of $\begin{bmatrix} \mathrm{B}_{cp_1} & \mathrm{B}_{cp_2} \end{bmatrix}$ been specified.

3.2.3.6 Final Form of Estimator

The estimator $\mathbf{e}_2(\Delta\nabla\delta\ell_n)$, then, is the estimator which will generate the estimates of the measurement errors $\hat{\delta\ell}$. When these errors are used to correct the measurements before double differencing, the double difference errors are minimized.

The covariance matrix $\boldsymbol{C}_{\delta\ell}$ in Equation 3.71 can be partitioned according to the errors from the network measurements $\delta\ell_n$ and the errors from the mobile receiver measurements $\delta\ell_{cp}$

$$\boldsymbol{C}_{\delta\ell} = \begin{bmatrix} \boldsymbol{C}_{\delta\ell_n} & \boldsymbol{C}_{\delta\ell_n,\delta\ell_{cp}} \\ \boldsymbol{C}_{\delta\ell_{cp},\ell_n} & C\delta\ell_{cp} \end{bmatrix}, \tag{3.74}$$

where $\boldsymbol{C}_{\delta\ell_n,\delta\ell_{cp}}$ and $\boldsymbol{C}_{\delta\ell_{cp},\delta\ell_n}$ are the cross covariances between the network and mobile receiver measurement errors ($\boldsymbol{C}_{\ell_n,\ell_{cp}} = \boldsymbol{C}^T_{\delta\ell_{cp},\delta\ell_n}$). The $\mathbf{e}_2(\cdot)$ equation can be broken into two parts (for calculating $\hat{\delta\ell}_n$ and $\hat{\delta\ell}_{cp}$) and simplified as

$$\hat{\delta\ell}_n = \boldsymbol{C}_{\delta\ell_n}\mathrm{B}_n^T(\mathrm{B}_n\boldsymbol{C}_{\delta\ell_n}\mathrm{B}_n^T)^{-1}\Delta\nabla\delta\ell_n \tag{3.75}$$

$$\hat{\delta\ell}_{cp} = \boldsymbol{C}_{\delta\ell_{cp},\delta\ell_n}\mathrm{B}_n^T(\mathrm{B}_n\boldsymbol{C}_{\delta\ell_n}\mathrm{B}_n^T)^{-1}\Delta\nabla\delta\ell_n. \tag{3.76}$$

Finally, combining with Equation 3.52, the final form of the network optimal estimator (i.e. the NetAdjust method) is obtained

$$\hat{\delta\boldsymbol{\ell}}_n = \boldsymbol{C}_{\delta\ell_n}\mathrm{B}_n^T(\mathrm{B}_n\boldsymbol{C}_{\delta\ell_n}\mathrm{B}_n^T)^{-1}(\mathrm{B}_n\boldsymbol{\ell}_n - \Delta\nabla\boldsymbol{N}_n) \tag{3.77}$$

$$\hat{\delta\boldsymbol{\ell}}_{cp} = \boldsymbol{C}_{\delta\ell_{cp},\delta\ell_n}\mathrm{B}_n^T(\mathrm{B}_n\boldsymbol{C}_{\delta\ell_n}\mathrm{B}_n^T)^{-1}(\mathrm{B}_n\boldsymbol{\ell}_n - \Delta\nabla\boldsymbol{N}_n). \tag{3.78}$$

All of the terms on the right hand side of Equations 3.77 and 3.78 can be generated without using the measurements from the mobile receiver. The measurement-minus-range vector $\boldsymbol{\ell}_n$ comes directly from the GPS measurements taken by the network reference stations (and the network station positions). The integer ambiguities between the network reference stations $\boldsymbol{N}_n$ are assumed to be known. The double difference matrix B_n generates all of the possible linearly independent double difference combinations of $\boldsymbol{\ell}_n$, as described in Section 3.1.2. B_n is formed based upon which measurements are available in $\boldsymbol{\ell}_n$. (Note that the actual values of the measurements in $\boldsymbol{\ell}_n$ are not needed–just their existence). The last terms are the covariance matrices $\boldsymbol{C}_{\delta\ell_n}$ and $\boldsymbol{C}_{\delta\ell_{cp},\delta\ell_N}$, which are actually part of the larger covariance matrix $\boldsymbol{C}_{\delta\ell}$. The $\boldsymbol{C}_{\delta\ell}$ matrix describes the second moments of the errors, and it can be calculated without knowing the actual measurement values (again, just their existence is needed). Calculation of $\boldsymbol{\ell}_n$, $\boldsymbol{N}_n$,[8] and B_n are straightforward and unequivocal, and the effectiveness of the NetAdjust approach is dependent upon an accurate $\boldsymbol{C}_{\delta\ell}$ matrix. The method used to calculate the $\boldsymbol{C}_{\delta\ell}$ matrix is presented in Section 3.4.

Note that the results presented in Equations 3.77 and 3.78 can also be obtained using a least squares condition adjustment (see Section 3.5.1, or least squares prediction (or collocation) (Moritz, 1989).

Equations 3.77 and 3.78 involve an inversion of the network double difference covariance matrix $\mathrm{B}_n\boldsymbol{C}_{\delta\ell_n}\mathrm{B}_n^T$, so this matrix must be non-singular for the method to work. For NetAdjust, the covariance function (presented in Section 3.4.1) generates a positive-definite $\boldsymbol{C}_{\delta\ell_n}$ matrix, and B_n is a full-rank matrix that transforms $\boldsymbol{C}_{\delta\ell_n}$ into double-

[8]It is not necessarily easy to calculate these integer ambiguities between reference stations, but there is a single, correct value for each one of them.

difference space, so the resulting matrix ($\mathrm{B}_n \boldsymbol{C}_{\delta\ell_n} \mathrm{B}_n^T$) will always be non-singular.

A flow chart showing the interrelationships between the various measurement and correction variables is shown in Figure 3.2. All of the operations shown within the dashed box are performed by NetAdjust, and all of the operations outside of this box are performed by the mobile receiver at the computation point. The $\boldsymbol{\ell}_n$ measurement vector is separated into individual measurement vectors for each of the reference receivers ($\boldsymbol{\ell}_{n_1}$, $\boldsymbol{\ell}_{n_2}$, etc.) As shown in the figure, there are two vectors generated by NetAdjust:

1. $\hat{\delta\boldsymbol{\ell}}_{cp}$ — The corrections to be applied to the measurements collected by the mobile receiver at the computation point ($\boldsymbol{\ell}_{cp}$).

2. $\hat{\boldsymbol{\ell}}_{n_1}$ — The corrected measurements from a *single* reference receiver (receiver 1 in this case). Only one set of reference receiver measurements is required because of the "data encapsulation" effect of NetAdjust, as described in Section 3.5.2. (While receiver 1 is shown in the figure, NetAdjust would perform equally well using any one of the reference receivers).

The vector $\hat{\boldsymbol{\ell}}_{n_1}$ is generated directly from the measurements from the reference receiver network, and it is independent of the computation point. The vector $\hat{\delta\boldsymbol{\ell}}_{cp}$ is generated from the measurements from the reference receiver network, but it is also a function of the computation point. If NetAdjust is used to calculate corrections for many different computation points (as described in Chapter 6), then the $\hat{\boldsymbol{\ell}}_{n_1}$ vector is calculated only once, and only the $\hat{\delta\boldsymbol{\ell}}_{cp}$ vector needs be recalculated for each computation point.

Note that, if desired, the $\hat{\delta\boldsymbol{\ell}}_{cp}$ and $\hat{\boldsymbol{\ell}}_{n_1}$ vectors can be combined by NetAdjust as follows:

$$\hat{\boldsymbol{\ell}}_{n_{1_{total}}} = \hat{\boldsymbol{\ell}}_{n_1} - \hat{\delta\boldsymbol{\ell}}_{cp}. \tag{3.79}$$

Then, $\hat{\boldsymbol{\ell}}_{n_{1_{total}}}$ represents the total corrections for the measurements from reference receiver 1, which, when double differenced with the *raw* measurements from the mobile receiver at the computation point ($\boldsymbol{\ell}_{cp}$), result in the same corrected double difference

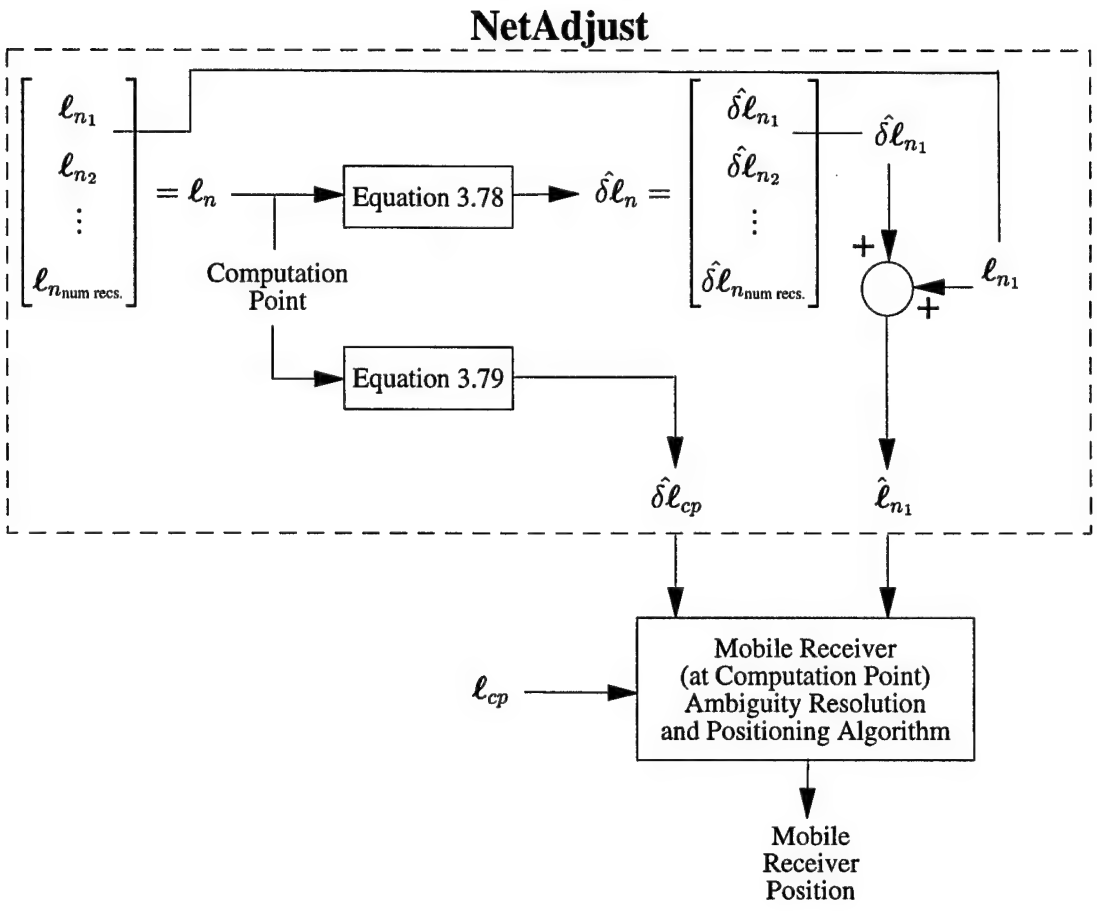

Figure 3.2: *Diagram of NetAdjust algorithm. Operations within dashed box are performed by NetAdjust, and operations outside this box are performed by the mobile receiver.*

measurements that would be obtained using the procedure shown in Figure 3.2. The only difference between the two approaches is that in the figure, $\hat{\delta\ell}_{cp}$ and $\hat{\ell}_{n_1}$ are differenced by the mobile receiver (in the double differencing process), whereas using Equation 3.79, the differencing is performed by NetAdjust prior to transmission to the mobile user. The advantage of using Equation 3.79 is that it requires less information to be transmitted to the mobile user.

3.3 Covariance Analysis Technique

In this section, a method for predicting differential positioning accuracy is developed based upon the estimators presented above, which are designed to minimize the covariance matrix of the double difference errors $\boldsymbol{C}_{\mathbf{err}(\Delta\nabla\delta\ell_{cp})}$ as defined in Equation 3.51. The goal in this section is to show how to calculate this covariance matrix, which will be used extensively in Chapter 5.

Before deriving the various error covariance matrices, it is useful to describe the so-called *covariance law* (Krakiwsky, 1990). The covariance law states that, given a functional relationship

$$\boldsymbol{y} = \boldsymbol{f}(\boldsymbol{z}) \tag{3.80}$$

between two Gaussian random vectors $\boldsymbol{y}$ and $\boldsymbol{z}$, along with the covariance matrix of $\boldsymbol{z}$ ($\boldsymbol{C}_{\boldsymbol{z}}$), the covariance matrix of $\boldsymbol{y}$ ($\boldsymbol{C}_{\boldsymbol{y}}$) is given by

$$\boldsymbol{C}_{\boldsymbol{y}} = \left(\frac{\partial \boldsymbol{f}}{\partial \boldsymbol{z}}\right) \boldsymbol{C}_{\boldsymbol{z}} \left(\frac{\partial \boldsymbol{f}}{\partial \boldsymbol{z}}\right)^{T}. \tag{3.81}$$

If

$$\boldsymbol{y} = \mathbf{A}\boldsymbol{z}, \tag{3.82}$$

where $\mathbf{A}$ is a real matrix, then from Equation 3.81

$$\boldsymbol{C}_{\boldsymbol{y}} = \mathbf{A}\boldsymbol{C}_{\boldsymbol{z}}\mathbf{A}^{T}. \tag{3.83}$$

This was previously demonstrated in Equation 3.60.

3.3.1 Calculation of $C_{\mathbf{err}(\delta\ell)}$

The goal here is to calculate the covariance matrix of the errors in the estimation of $\delta\ell$. This will then be used in the following section to calculate the covariance matrix of the double difference errors.

The estimation error of $\delta\ell$ is defined to be

$$\mathbf{err}(\delta\ell) \triangleq \delta\ell - \hat{\delta\ell}. \tag{3.84}$$

Since the estimator is an unbiased estimator, $E[\mathbf{err}(\delta\ell)] = \mathbf{0}$, and the covariance matrix of $\mathbf{err}(\delta\ell)$ is the same as the correlation matrix of $\mathbf{err}(\delta\ell)$.

Combining Equation 3.58 ($\Delta\nabla\delta\ell_n = \mathrm{B}_n\delta\ell_n$) with the $\mathbf{e}_2(\cdot)$ estimator (Equation 3.71) and recognizing that $\mathrm{B}_n C_{\delta\ell_n}\mathrm{B}_n^T = \mathrm{B}_1 C_{\delta\ell}\mathrm{B}_1^T$ yields

$$\hat{\delta\ell} = C_{\delta\ell}\mathrm{B}_1^T(\mathrm{B}_1 C_{\delta\ell}\mathrm{B}_1^T)^{-1}\mathrm{B}_1\delta\ell, \tag{3.85}$$

where

$$\mathrm{B}_1 \triangleq \begin{bmatrix}\mathrm{B}_n & \mathbf{0}\end{bmatrix}. \tag{3.86}$$

The estimation error can then be written

$$\begin{aligned}\mathbf{err}(\delta\ell) &= \delta\ell - C_{\delta\ell}\mathrm{B}_1^T(\mathrm{B}_1 C_{\delta\ell}\mathrm{B}_1^T)^{-1}\mathrm{B}_1\delta\ell \\ &= [\mathbf{I} - C_{\delta\ell}\mathrm{B}_1^T(\mathrm{B}_1 C_{\delta\ell}\mathrm{B}_1^T)^{-1}\mathrm{B}_1]\delta\ell\end{aligned} \tag{3.87}$$

where $\mathbf{I}$ is the identity matrix. Then, applying the covariance law, the covariance matrix of the errors can be calculated as

$$\begin{aligned}C_{\mathbf{err}(\delta\ell)} &= [\mathbf{I} - C_{\delta\ell}\mathrm{B}_1^T(\mathrm{B}_1 C_{\delta\ell}\mathrm{B}_1^T)^{-1}\mathrm{B}_1]C_{\delta\ell}[\mathbf{I} - C_{\delta\ell}\mathrm{B}_1^T(\mathrm{B}_1 C_{\delta\ell}\mathrm{B}_1^T)^{-1}\mathrm{B}_1]^T \\ &= C_{\delta\ell} \\ &\quad - C_{\delta\ell}\mathrm{B}_1^T(\mathrm{B}_1 C_{\delta\ell}\mathrm{B}_1^T)^{-1}\mathrm{B}_1 C_{\delta\ell} \\ &\quad - C_{\delta\ell}\mathrm{B}_1^T(\mathrm{B}_1 C_{\delta\ell}\mathrm{B}_1^T)^{-1}\mathrm{B}_1 C_{\delta\ell} \\ &\quad + C_{\delta\ell}\mathrm{B}_1^T(\mathrm{B}_1 C_{\delta\ell}\mathrm{B}_1^T)^{-1}\mathrm{B}_1 C_{\delta\ell}\mathrm{B}_1^T(\mathrm{B}_1 C_{\delta\ell}\mathrm{B}_1^T)^{-1}\mathrm{B}_1 C_{\delta\ell} \\ &= C_{\delta\ell} - C_{\delta\ell}\mathrm{B}_1^T(\mathrm{B}_1 C_{\delta\ell}\mathrm{B}_1^T)^{-1}\mathrm{B}_1 C_{\delta\ell}.\end{aligned} \tag{3.88}$$

This shows that the covariance of the errors in the estimates of $\delta\ell$ can be calculated from the $C_{\delta\ell}$ covariance matrix and the B_1 double difference matrix. (Note that $C_{\delta\ell_n}$ and B_n are submatrices of $C_{\delta\ell}$ and B_1).

3.3.2 Calculation of $C_{\mathbf{err}(\Delta\nabla\delta\ell)}$

Recall from Equation 3.61 that the relationship between $\Delta\nabla\delta\ell$ and $\delta\ell$ is

$$\Delta\nabla\delta\ell = \mathrm{B}\delta\ell \tag{3.89}$$

or, equivalently,

$$\mathbf{err}(\Delta\nabla\delta\ell) = \mathrm{B}\,\mathbf{err}(\delta\ell) \tag{3.90}$$

where

$$\mathrm{B} = \begin{bmatrix} \mathrm{B}_n & \mathbf{0} \\ \mathrm{B}_{cp_1} & \mathrm{B}_{cp_2} \end{bmatrix}. \tag{3.91}$$

The covariance matrix $C_{\mathbf{err}(\delta\ell)}$ is given in Equation 3.88, and the covariance law can be used to transform it into the covariance of the error estimates of the double difference measurements $C_{\mathbf{err}(\Delta\nabla\delta\ell)}$

$$C_{\mathbf{err}(\Delta\nabla\delta\ell)} = \mathrm{B}(C_{\delta\ell} - C_{\delta\ell}\mathrm{B}_1^T(\mathrm{B}_1 C_{\delta\ell}\mathrm{B}_1^T)^{-1}\mathrm{B}_1 C_{\delta\ell})\mathrm{B}^T \tag{3.92}$$

$$= \mathrm{B}C_{\delta\ell}\mathrm{B}^T - \mathrm{B}C_{\delta\ell}\mathrm{B}_1^T(\mathrm{B}_1 C_{\delta\ell}\mathrm{B}_1^T)^{-1}\mathrm{B}_1 C_{\delta\ell}\mathrm{B}^T. \tag{3.93}$$

This is the covariance for the estimation errors of the entire double difference vector $\Delta\nabla\delta\ell$, which includes the double differences exclusively between network reference receivers $\Delta\nabla\delta\ell_n$ and the double differences between the mobile receiver and the network receivers $\Delta\nabla\delta\ell_{cp}$. It is useful to examine each of these separately.

First, to evaluate the covariance of the estimation errors of $\Delta\nabla\delta\ell_n$ ($C_{\mathbf{err}(\Delta\nabla\delta\ell_n)}$), Equation 3.89 is changed to

$$\Delta\nabla\delta\ell_n = \mathrm{B}_1\delta\ell, \tag{3.94}$$

where B_1 is defined in Equation 3.86. Then the same development presented in Equations 3.90 through 3.93 is followed, substituting B_1 for B. The result is

$$\boldsymbol{C}_{\mathbf{err}(\Delta\nabla\delta\boldsymbol{\ell}_n)} = \mathrm{B}_1\boldsymbol{C}_{\delta\boldsymbol{\ell}}\mathrm{B}_1^T - \mathrm{B}_1\boldsymbol{C}_{\delta\boldsymbol{\ell}}\mathrm{B}_1^T(\mathrm{B}_1\boldsymbol{C}_{\delta\boldsymbol{\ell}}\mathrm{B}_1^T)^{-1}\mathrm{B}_1\boldsymbol{C}_{\delta\boldsymbol{\ell}}\mathrm{B}_1^T \tag{3.95}$$

$$= \mathbf{0}. \tag{3.96}$$

This shows that there are *no* errors in the estimated value of the double difference measurement errors $\Delta\nabla\hat{\delta\boldsymbol{\ell}}_n$, which is not surprising because the exact values of $\Delta\nabla\delta\boldsymbol{\ell}_n$ are actually the measurements used in the first place.

More useful is the analysis of the errors in the estimates of the double difference measurements between the mobile receiver at the computation point and the network reference receivers. Following the relation shown in Equation 3.73, Equation 3.89 is changed to

$$\Delta\nabla\delta\boldsymbol{\ell}_{cp} = \mathrm{B}_2\delta\boldsymbol{\ell}, \tag{3.97}$$

where B_2 is defined as

$$\mathrm{B}_2 \triangleq \begin{bmatrix} \mathrm{B}_{cp_1} & \mathrm{B}_{cp_2} \end{bmatrix}. \tag{3.98}$$

Then, as before, the B matrix in Equations 3.90 through 3.93 is changed to the B_2 matrix, yielding the final result

$$\boldsymbol{C}_{\mathbf{err}(\Delta\nabla\delta\boldsymbol{\ell}_{cp})} = \mathrm{B}_2\boldsymbol{C}_{\delta\boldsymbol{\ell}}\mathrm{B}_2^T - \mathrm{B}_2\boldsymbol{C}_{\delta\boldsymbol{\ell}}\mathrm{B}_1^T(\mathrm{B}_1\boldsymbol{C}_{\delta\boldsymbol{\ell}}\mathrm{B}_1^T)^{-1}\mathrm{B}_1\boldsymbol{C}_{\delta\boldsymbol{\ell}}\mathrm{B}_2^T. \tag{3.99}$$

This equation shows how $\boldsymbol{C}_{\mathbf{err}(\Delta\nabla\delta\boldsymbol{\ell}_{cp})}$ can be calculated using only the B matrix (of which B_1 and B_2 are submatrices) and the $\boldsymbol{C}_{\delta\boldsymbol{\ell}}$ matrix. Both the B and $\boldsymbol{C}_{\delta\boldsymbol{\ell}}$ matrices can be calculated without having the measurement realizations available, because all that is needed is knowledge of what measurements are available from each receiver. Equation 3.99, then, can be used to *predict* network performance under various network configurations (which result in different B and $\boldsymbol{C}_{\delta\boldsymbol{\ell}}$ matrices). This is called a covariance analysis procedure, and it is utilized extensively in Chapter 5.

3.4 Calculation of Covariance Matrix

The covariance matrix of the measurement differential errors $\boldsymbol{C}_{\delta\ell}$ is a key element in both the optimal estimation equations of Section 3.2 and the covariance analysis of Section 3.3. This section describes how the $\boldsymbol{C}_{\delta\ell}$ matrix can be expressed in a functional form, and then shows how field data was used to determine the covariance function.

3.4.1 Covariance Functional Form

The measurement differential error vector $\delta\boldsymbol{\ell}$ was defined in Equation 3.54, and it is restated here as

$$\delta\boldsymbol{\ell} \triangleq d_c\boldsymbol{\phi}(\boldsymbol{p}, \boldsymbol{p}_0) + \delta_u\boldsymbol{\phi}. \tag{3.100}$$

The correlated error term $d_c\boldsymbol{\phi}(\boldsymbol{p}, \boldsymbol{p}_0)$ includes the differential ionosphere, troposphere, and satellite position errors, relative to point $\boldsymbol{p}_0$. The uncorrelated error term $\delta_u\boldsymbol{\phi}$ includes multipath and measurement noise, which are assumed to be completely uncorrelated between measurements. (For more details, refer to Section 3.2.1). As stated in Section 3.2.3.1, this $\delta\boldsymbol{\ell}$ vector is assumed to be zero-mean ($E[\delta\boldsymbol{\ell}] = \boldsymbol{0}$) and well-described by a Gaussian distribution function. As such, it has a covariance matrix $\boldsymbol{C}_{\delta\ell}$ defined as

$$\begin{aligned}\boldsymbol{C}_{\delta\ell} &\triangleq E[(\delta\boldsymbol{\ell} - E[\delta\boldsymbol{\ell}])(\delta\boldsymbol{\ell} - E[\delta\boldsymbol{\ell}])^T] \\ &= E[(\delta\boldsymbol{\ell})(\delta\boldsymbol{\ell})^T].\end{aligned} \tag{3.101}$$

Each element in the $\boldsymbol{C}_{\delta\ell}$ matrix is the cross-covariance (or variance, if they are the same measurement) of two different scalar measurement errors. These two measurement errors are denoted $\delta\ell_a^x$ (for the measurement from receiver a to satellite x) and $\delta\ell_b^y$ (for the measurement from receiver b to satellite y). Then the element in the $\boldsymbol{C}_{\delta\ell}$ matrix corresponding to the two measurements $\delta\ell_a^x$ and $\delta\ell_b^y$ is

$$c_{ab}^{xy} = E[(\delta\ell_a^x)(\delta\ell_b^y)]. \tag{3.102}$$

This can be expanded into the actual error sources according to the definition found in Equation 3.100

$$c_{ab}^{xy} = E[(d_c\phi_a^x(\boldsymbol{p}_a, \boldsymbol{p}_0) + \delta_u\phi_a^x)(d_c\phi_b^y(\boldsymbol{p}_b, \boldsymbol{p}_0) + \delta_u\phi_b^y)], \tag{3.103}$$

where $\boldsymbol{p}_a$ and $\boldsymbol{p}_b$ are the positions of receivers a and b, respectively. This can be expanded to

$$\begin{aligned} c_{ab}^{xy} = E[&(d_c\phi_a^x(\boldsymbol{p}_a, \boldsymbol{p}_0))(d_c\phi_b^y(\boldsymbol{p}_b, \boldsymbol{p}_0)) \\ &+ (d_c\phi_a^x(\boldsymbol{p}_a, \boldsymbol{p}_0))(\delta_u\phi_b^y) \\ &+ (\delta_u\phi_a^x)(d_c\phi_b^y(\boldsymbol{p}_b, \boldsymbol{p}_0)) \\ &+ (\delta_u\phi_a^x)(\delta_u\phi_b^y)]. \end{aligned} \tag{3.104}$$

Recognizing that the expectation operator is a linear operator, it can be rewritten as the sum of four separate expectations

$$\begin{aligned} c_{ab}^{xy} =&E[(d_c\phi_a^x(\boldsymbol{p}_a, \boldsymbol{p}_0))(d_c\phi_b^y(\boldsymbol{p}_b, \boldsymbol{p}_0))] \\ &+E[(d_c\phi_a^x(\boldsymbol{p}_a, \boldsymbol{p}_0))(\delta_u\phi_b^y])] \\ &+E[(\delta_u\phi_a^x)(d_c\phi_b^y(\boldsymbol{p}_b, \boldsymbol{p}_0))] \\ &+E[(\delta_u\phi_a^x)(\delta_u\phi_b^y)]. \end{aligned} \tag{3.105}$$

The uncorrelated error terms are *by definition* uncorrelated with anything but themselves, so this reduces to

$$c_{ab}^{xy} = \begin{cases} E[(d_c\phi_a^x(\boldsymbol{p}_a, \boldsymbol{p}_0))(d_c\phi_b^y(\boldsymbol{p}_b, \boldsymbol{p}_0))] + E[(\delta_u\phi_a^x)(\delta_u\phi_b^y)] & \text{if } a = b \text{ and } x = y, \\ E[(d_c\phi_a^x(\boldsymbol{p}_a, \boldsymbol{p}_0))(d_c\phi_b^y(\boldsymbol{p}_b, \boldsymbol{p}_0))] & \text{otherwise.} \end{cases} \tag{3.106}$$

Furthermore, assume that the correlated differential errors are uncorrelated between satellites, i.e.

$$E[(d_c\phi_a^x)(d_c\phi_b^y)] = 0 \quad \text{if } x \neq y. \tag{3.107}$$

This is a reasonable assumption, considering the nature of the errors involved. Differential satellite position errors are certainly uncorrelated between satellites. Considering the ionospheric and tropospheric errors, there is nothing that would strongly indicate that differential atmospheric errors between satellites at different elevation and azimuth angles should be correlated.[9] Then, given this additional assumption, the equations for calculating a single element of the covariance matrix $\boldsymbol{C}_{\delta\ell}$ are

$$c_{ab}^{xy} = \begin{cases} E[(d_c\phi_a^x(\boldsymbol{p}_a,\boldsymbol{p}_0))(d_c\phi_b^y(\boldsymbol{p}_b,\boldsymbol{p}_0))] + E[(\delta_u\phi_a^x)(\delta_u\phi_b^y)] & \text{if } a = b \text{ and } x = y, \\ E[(d_c\phi_a^x(\boldsymbol{p}_a,\boldsymbol{p}_0))(d_c\phi_b^y(\boldsymbol{p}_b,\boldsymbol{p}_0))] & \text{if } a \neq b \text{ and } x = y, \\ 0 & \text{otherwise.} \end{cases} \tag{3.108}$$

In plain terms, the first line is for elements along the diagonal of the covariance matrix (i.e., the variances of each of the differential measurement errors), the second line calculates differential error *co*variances for measurements from two different receivers but the same satellite, and all other terms are zero.

It is desirable to be able to generate a functional form of c_{ab}^{xy}, which uses as independent variables the positions of the receivers ($\boldsymbol{p}_a$ and $\boldsymbol{p}_b$), the position of the zero-point ($\boldsymbol{p}_0$), the average satellite elevation (ε[10]), and the actual receivers used (a and b)

$$c_{ab}^{xy} = f(\boldsymbol{p}_a, \boldsymbol{p}_b, \boldsymbol{p}_0, \varepsilon, a, b). \tag{3.109}$$

If this function is known, then it can be used to generate each element in the $\boldsymbol{C}_{\delta\ell}$ matrix.

---

[9]There may be some situations where this assumption is not entirely true, such as when the tropospheric error model is significantly in error. Such second order effects are small and extremely difficult to characterize accurately, however, so they will not be considered here. (Remember that the tropospheric error is actually the residual tropospheric error, after removing an estimate of tropospheric error from a model.)

[10]The elevation of the satellite will be slightly different if the measurements are taken at different locations on earth. The elevation ε is the average of the two elevations. (When two different satellites are involved, the covariance term is defined to be zero, so the elevation doesn't matter)

It should be noted that there can be many different functional forms of the $\boldsymbol{C}_{\delta\ell}$ matrix, each with varying degrees of complexity and accuracy. The functional form presented in this research is intended to represent a reasonable trade-off between complexity and accuracy, and it is based upon insights into the overall characteristics of the errors. Other approaches could be taken that might improve the accuracy of $\boldsymbol{C}_{\delta\ell}$, but they would probably be significantly more complex.

In Chapter 2, each of the error sources (except for satellite position error) was shown to be elevation dependent—the magnitudes of the errors tended to increase as the elevation decreased. Because of this, it is useful to generate a functional form of the errors at the zenith, and then scale this variance or covariance term for the specific elevation involved. To this end, an elevation scaling factor $\mu(\varepsilon)$ is introduced. This factor relates the value of a covariance element with its zenith value ($c^{xy}_{ab_z}$) as follows:

$$c^{xy}_{ab} = \mu^2(\varepsilon) c^{xy}_{ab_z}. \tag{3.110}$$

This removes the elevation as an independent variable of the covariance function, so Equation 3.109 can be rewritten as

$$c^{xy}_{ab} = \mu^2(\varepsilon) f_z(\boldsymbol{p}_a, \boldsymbol{p}_b, \boldsymbol{p}_0, a, b). \tag{3.111}$$

Equation 3.108 shows that there are two types of errors involved in calculating each covariance matrix element—correlated errors (in $E[(d_c\phi^x_a(\boldsymbol{p}_a, \boldsymbol{p}_0))(d_c\phi^y_b(\boldsymbol{p}_b, \boldsymbol{p}_0))]$), and uncorrelated errors (in $E[(\delta_u\phi^x_a)(\delta_u\phi^y_b)]$). The f_z function can be separated into two different functions relating to the two types of errors

$$c^{xy}_{ab} = \mu^2(\varepsilon)[f_{z_c}(\boldsymbol{p}_a, \boldsymbol{p}_b, \boldsymbol{p}_0) + f_{z_u}(\text{receiver})]. \tag{3.112}$$

The function f_{z_c} is for the correlated (satellite position and atmospheric) errors, and the function f_{z_u} is for the uncorrelated errors (multipath and noise). Note that the same elevation scaling factor $\mu^2(\varepsilon)$ is applied to both the correlated and uncorrelated errors. This is a reasonable approach, because the uncorrelated errors elevation dependence follows a similar trend as that expected from the uncorrelated errors. This can be seen by comparing

the uncorrelated error standard deviations versus elevation plots shown in Figures 2.12 and 2.13 with the standard (model) ionospheric mapping function shown in Figure 2.1.

Note also that the correlated errors ($f_{z_c}(\boldsymbol{p}_a, \boldsymbol{p}_b, \boldsymbol{p}_0)$) are entirely a function of the positions of the receivers and the zero-point, while the uncorrelated errors (f_{z_u}(receiver)) are entirely a function of the receiver being used. The arguments a and b have been dropped from the notation and replaced with the word "receiver", because the uncorrelated error only applies to individual measurements at a single receiver (i.e., $a = b$). Both of these functions will be developed in the sections that follow.

3.4.1.1 Functional Form of Uncorrelated Errors at Zenith (f_{z_u})

The noise at zenith is primarily a function of the receiver design, although it may be somewhat affected by anything that reduces the signal-to-noise ratio of the GPS signal as well. The multipath is a function of the receiver design, but it is also a function of the environment surrounding the GPS antenna. Both the receiver design and the environment around the antenna are constant for each receiver, so the variance of the uncorrelated errors (multipath and noise) at zenith will be modeled as a constant, which can be different for each receiver. In equation form

$$f_{z_u}(\text{receiver}) = \sigma^2_{u_z}(\text{receiver}) = E[(\delta_u \phi_z \text{receiver})^2] = constant. \tag{3.113}$$

where $\sigma^2_{u_z}$(receiver) is the constant zenith uncorrelated error variance for the receiver.

3.4.1.2 Functional Form of Correlated Errors at Zenith (f_{z_c})

The goal in this section is to calculate

$$f_{z_c}(\boldsymbol{p}_a, \boldsymbol{p}_b, \boldsymbol{p}_0) = E[(d_c\phi_a(\boldsymbol{p}_a, \boldsymbol{p}_0)_z)(d_c\phi_b(\boldsymbol{p}_b, \boldsymbol{p}_0)_z)]. \tag{3.114}$$

Note that the errors correspond to zenith errors, hence the subscript z. Note also that the superscript indication of the satellite has been removed from the ϕ_a and ϕ_b terms. The atmospheric errors are not a function of the satellite. The realized satellite position errors

are different for different satellites, but it is assumed that the error *statistics* are the same for each satellite. Also, since the error is a zenith error, satellite elevation is not relevant. Therefore, the satellite is not relevant to the equation, so it is removed from the notation.

From the definition of the differential errors found in Equation 3.33, the above equation can be rewritten as

$$f_{z_c}(\boldsymbol{p}_a, \boldsymbol{p}_b, \boldsymbol{p}_0) = E[(\delta_c\phi_a(\boldsymbol{p}_a)_z - \delta_c\phi_0(\boldsymbol{p}_0))(\delta_c\phi_b(\boldsymbol{p}_b)_z - \delta_c\phi_0(\boldsymbol{p}_0))]. \tag{3.115}$$

After expanding the right hand side, collecting like terms, factoring, and taking advantage of the fact that the expectation operator is a linear operator, the equation becomes

$$\begin{aligned} f_{z_c}(\boldsymbol{p}_a, \boldsymbol{p}_b, \boldsymbol{p}_0) = &\frac{1}{2}E[(\delta_c\phi_a(\boldsymbol{p}_a)_z - \delta_c\phi_0(\boldsymbol{p}_0))^2] \\ &+ \frac{1}{2}E[(\delta_c\phi_b(\boldsymbol{p}_b)_z - \delta_c\phi_0(\boldsymbol{p}_0))^2] \\ &- \frac{1}{2}E[(\delta_c\phi_a(\boldsymbol{p}_a)_z - \delta_c\phi_b(\boldsymbol{p}_b))^2]. \end{aligned} \tag{3.116}$$

Note that each line in the above equation is a variance of the differential error between two different points. Define a function

$$\sigma^2_{c_z}(\boldsymbol{p}_m, \boldsymbol{p}_n) \triangleq E[(\delta_c\phi_z(\boldsymbol{p}_m) - \delta_c\phi_z(\boldsymbol{p}_n))^2] \tag{3.117}$$

to be the variance of the differential correlated errors between two arbitrary points $\boldsymbol{p}_m$ and $\boldsymbol{p}_n$. Combining Equations 3.116 and 3.117 yields

$$f_{z_c}(\boldsymbol{p}_a, \boldsymbol{p}_b, \boldsymbol{p}_0) = \frac{\sigma^2_{c_z}(\boldsymbol{p}_a, \boldsymbol{p}_0) + \sigma^2_{c_z}(\boldsymbol{p}_b, \boldsymbol{p}_0) - \sigma^2_{c_z}(\boldsymbol{p}_a, \boldsymbol{p}_b)}{2}. \tag{3.118}$$

Now all that is required is to specify a functional form of $\sigma^2_{c_z}(\boldsymbol{p}_m, \boldsymbol{p}_n)$ (which describes how the differential correlated errors grow with distance) in order to specify the correlated error covariance function f_{z_c} completely.

Define

$$\sigma^2_{c_z}(\boldsymbol{p}_m, \boldsymbol{p}_n) \triangleq c_1 d + c_2 d^2 \tag{3.119}$$

where d is the distance (magnitude) between $\boldsymbol{p}_m$ and $\boldsymbol{p}_n$, and c_1 and c_2 are fit coefficients.

This function states that the variance of the differential correlated (atmospheric and satellite position) errors grows according to the sum of second order polynomials in the east and north directions. This particular functional form (a truncated Taylor series expansion) was chosen because it provided a good fit to the data collected in the Norway network, as discussed in the following section.

3.4.2 Method for Calculating Covariance Parameters Using Field Data

These coefficients of the covariance function are time varying, because the characteristics of the errors themselves vary with time. For example, during periods of high ionospheric activity, the correlated error variances (which include the ionospheric error) would be larger than periods of low ionospheric activity. The same is true of tropospheric errors (such as the passage of a weather front). The multipath uncorrelated error could also vary according to changes in the environment around the antenna (such as rain decreasing or increasing the reflective properties of nearby reflecting objects).

It is useful, then, to devise a methodology for determining the covariance function coefficients using network reference station data over a particular time interval. The coefficients are valid for errors like those present in that time interval. As the error characteristics change over time, the covariance function coefficients can be recalculated, allowing them to adapt to the specific conditions at the time of interest.

In this section a method is described for estimating the covariance function coefficients using the data from the network. It is demonstrated using a 24-hour data set from the Norway network, which is described in Appendix A. These coefficients are then used in the NetAdjust algorithm to generate the results that are presented in Chapter 4.

There are two distinct phases used in calculating the covariance function coefficients.

1. Determination of the elevation mapping function $\mu(\varepsilon)$.

2. Determination of the constant zenith uncorrelated error variance $\sigma^2_{u_z}$ for each receiver and the coefficients of the zenith correlated error variance function $\sigma^2_{c_z}(\boldsymbol{p}_m, \boldsymbol{p}_n)$.

It is necessary to calculate the elevation mapping function first in order to scale the measured double difference errors to zenith, before calculating the coefficients of the zenith $\sigma^2_{u_z}$(receiver) and $\sigma^2_{c_z}(\boldsymbol{p}_m, \boldsymbol{p}_n)$ functions. These two phases are described in the sections that follow.

There are three independent covariance functions that are used in this research–L1 code, L1 phase, and WL phase. It should be noted that the derivations presented in this section are performed notationally on the L1 phase measurements. The same derivations apply equally well to the WL phase measurements and the code measurements, unless noted otherwise.

3.4.3 Determination of Elevation Mapping Function $\mu(\varepsilon)$

This section begins by defining the elevation mapping function. The mapping functions to convert double difference errors and double difference error variances to zenith values are then derived. After this background material, a method for determining the mapping function from network receiver data is presented.

3.4.3.1 Definition of $\mu(\varepsilon)$

Define the differential error δl^x_a of a phase measurement-minus-range observable between receiver a and satellite x as

$$\delta l^x_a \triangleq d_c \phi^x_a(\boldsymbol{p}_a, \boldsymbol{p}_0) + \delta_u \phi^x_a. \tag{3.120}$$

These represent the errors that are not directly canceled by double differencing, which are the errors of interest.

Next, the elevation mapping function $\mu(\varepsilon)$ is defined, which maps the error at elevation ε (δl_ε) to the zenith error δl_z (for any receiver or satellite)

$$\mu(\varepsilon) \triangleq \frac{\delta l_\varepsilon}{\delta l_z}, \tag{3.121}$$

or, equivalently,

$$\delta l_\varepsilon = \mu(\varepsilon)\delta l_z, \tag{3.122}$$

where ε is the elevation of the satellite (satellite x in the case of δl_a^x).

3.4.3.2 Use of $\mu(\varepsilon)$ to Map Double Difference Measurement Errors to Zenith

Define the double differenced differential errors between receivers a and b and satellites x and y as

$$\Delta\nabla\delta l_{ab}^{xy} \triangleq \delta l_a^x - \delta l_a^y - (\delta l_b^x - \delta l_b^y). \tag{3.123}$$

Converting each of the individual errors to zenith errors by Equation 3.122 yields

$$\Delta\nabla\delta l_{ab}^{xy} = \mu(\varepsilon^x)\delta l_{a_z}^x - \mu(\varepsilon^y)\delta l_{a_z}^y - (\mu(\varepsilon^x)\delta l_{b_z}^x - \mu(\varepsilon^y)\delta l_{b_z}^y) \tag{3.124}$$

$$= \mu(\varepsilon^x)[\delta l_{a_z}^x - \delta l_{b_z}^x] + \mu(\varepsilon^y)[\delta l_{b_z}^y - \delta l_{a_z}^y], \tag{3.125}$$

where ε^x and ε^y are the average elevations (between the two reference stations) of satellites x and y. Now, define the double differenced *zenith* differential errors as

$$\Delta\nabla\delta l_{ab_z}^{xy} \triangleq \delta l_{a_z}^x - \delta l_{a_z}^y - (\delta l_{b_z}^x - \delta l_{b_z}^y). \tag{3.126}$$

The goal is to determine a mapping function $\mu_{\Delta\nabla}(\varepsilon^x, \varepsilon^y)$ that maps the double difference of the errors ($\Delta\nabla\delta l_{ab}^{xy}$) to the double difference of the errors at zenith ($\Delta\nabla\delta l_{ab_z}^{xy}$), i.e.

$$\mu_{\Delta\nabla}(\varepsilon^x, \varepsilon^y) \triangleq \frac{\Delta\nabla\delta l_{ab}^{xy}}{\Delta\nabla\delta l_{ab_z}^{xy}}. \tag{3.127}$$

Substituting Equations 3.123 and 3.126 and rearranging terms yields

$$\mu_{\Delta\nabla}(\varepsilon^x, \varepsilon^y) = \frac{\mu(\varepsilon^x)(\delta l_{a_z}^x - \delta l_{b_z}^x) + \mu(\varepsilon^y)(\delta l_{b_z}^y - \delta l_{a_z}^y)}{(\delta l_{a_z}^x - \delta l_{b_z}^x) + (\delta l_{b_z}^y - \delta l_{a_z}^y)}. \tag{3.128}$$

This is not directly solvable as a function of $\mu(\varepsilon^x)$ and $\mu(\varepsilon^y)$. However, it can be reasonably assumed that *on average*

$$(\delta l_{a_z}^x - \delta l_{b_z}^x) = (\delta l_{b_z}^y - \delta l_{a_z}^y), \tag{3.129}$$

because these are the differential errors at the zenith, and the statistics of the errors are the same between different satellites. By making this assumption, Equation 3.128 can be reduced to

$$\mu_{\Delta\nabla}(\varepsilon^x, \varepsilon^y) = \frac{\mu(\varepsilon^x) + \mu(\varepsilon^y)}{2}. \tag{3.130}$$

Using this in Equation 3.127 and rearranging terms results in the mapping between the actual double difference errors and the double difference errors at the zenith

$$\Delta\nabla\delta l^{xy}_{ab} = \frac{\mu(\varepsilon^x) + \mu(\varepsilon^y)}{2}\Delta\nabla\delta l^{xy}_{ab_z}. \tag{3.131}$$

3.4.3.3 Use of $\mu(\varepsilon)$ to Map Double Difference Error Variances to Zenith

The variance $\sigma^2_{\Delta\nabla\delta l^{xy}_{ab}}$ of the double difference measurement $\Delta\nabla\delta l^{xy}_{ab}$ is, by definition,

$$\sigma^2_{\Delta\nabla\delta l^{xy}_{ab}} \triangleq E[(\Delta\nabla\delta l^{xy}_{ab})^2], \tag{3.132}$$

assuming that $\Delta\nabla\delta l^{xy}_{ab}$ is zero-mean, which is a reasonable assumption (see Section 3.2.3.1). This is expanded by Equation 3.123 and simplified (assuming that errors between satellites are uncorrelated)

$$\begin{aligned} E[(\Delta\nabla\delta l^{xy}_{ab})^2] =& E[(\delta l^x_a - \delta l^y_a - \delta l^x_b + \delta l^y_b)(\delta l^x_a - \delta l^y_a - \delta l^x_b + \delta l^y_b)] \\ =& E[(\delta l^x_a)^2 - 2(\delta l^x_a \delta l^x_b) + (\delta l^x_b)^2] \\ &+ E[(\delta l^y_a)^2 - 2(\delta l^y_a \delta l^y_b) + (\delta l^y_b)^2]. \end{aligned} \tag{3.133}$$

The differential errors δl can be rewritten using the definition of the mapping function (Equation 3.122) and then simplified

$$\begin{aligned} E[(\Delta\nabla\delta l^{xy}_{ab})^2] =& E[(\mu(\varepsilon^x)\delta l^x_{a_z})^2 - 2(\mu(\varepsilon^x)\delta l^x_{a_z}\mu(\varepsilon^x)\delta l^x_{b_z}) + (\mu(\varepsilon^x)\delta l^x_{b_z})^2] \\ &+ E[(\mu(\varepsilon^y)\delta l^y_{a_z})^2 - 2(\mu(\varepsilon^y)\delta l^y_{a_z}\mu(\varepsilon^y)\delta l^y_{b_z}) + (\mu(\varepsilon^y)\delta l^y_{b_z})^2] \\ =& \mu^2(\varepsilon^x)E[(\delta l^x_{a_z})^2 - 2(\delta l^x_{a_z}\delta l^x_{b_z}) + (\delta l^x_{b_z})^2] \\ &+ \mu^2(\varepsilon^y)E[(\delta l^y_{a_z})^2 - 2(\delta l^y_{a_z}\delta l^y_{b_z}) + (\delta l^y_{b_z})^2], \end{aligned} \tag{3.134}$$

where ε^x and ε^y are the elevations of satellites x and y, respectively. Next, the error variance of the double difference errors *at zenith* is (using the same approach as Equation 3.133)

$$\begin{aligned} E[(\Delta\nabla\delta l^{xy}_{ab_z})^2] =& E[(\delta l^x_{a_z})^2 - 2(\delta l^x_{a_z}\delta l^x_{b_z}) + (\delta l^x_{b_z})^2] \\ &+ E[(\delta l^y_{a_z})^2 - 2(\delta l^y_{a_z}\delta l^y_{b_z}) + (\delta l^y_{b_z})^2]. \end{aligned} \tag{3.135}$$

The goal is to determine a mapping function $\mu_{\sigma^2_{\Delta\nabla}}(\varepsilon^x, \varepsilon^y)$ that maps the double difference of the error variance ($E[(\Delta\nabla\delta l^{xy}_{ab})^2]$) to the double difference of the error variance at zenith ($E[(\Delta\nabla\delta l^{xy}_{ab_z})^2]$), i.e.,

$$\mu^2_{\sigma^2_{\Delta\nabla}}(\varepsilon^x, \varepsilon^y) \triangleq \frac{E[(\Delta\nabla\delta l^{xy}_{ab})^2]}{E[(\Delta\nabla\delta l^{xy}_{ab_z})^2]} \tag{3.136}$$

Substituting Equations 3.134 and 3.135 and rearranging terms yields

$$\mu^2_{\sigma^2_{\Delta\nabla}}(\varepsilon^x, \varepsilon^y) = \frac{\mu^2(\varepsilon^x)E[(\delta l^x_{a_z})^2 - 2(\delta l^x_{a_z}\delta l^x_{b_z}) + (\delta l^x_{b_z})^2] + \mu^2(\varepsilon^y)E[(\delta l^y_{a_z})^2 - 2(\delta l^y_{a_z}\delta l^y_{b_z}) + (\delta l^y_{b_z})^2]}{E[(\delta l^x_{a_z})^2 - 2(\delta l^x_{a_z}\delta l^x_{b_z}) + (\delta l^x_{b_z})^2] + E[(\delta l^y_{a_z})^2 - 2(\delta l^y_{a_z}\delta l^y_{b_z}) + (\delta l^y_{b_z})^2]} \tag{3.137}$$

This is not directly solvable as a function of $\mu^2(\varepsilon^x)$ and $\mu^2(\varepsilon^y)$. However, as in Section 3.4.3.2, it can be reasonably assumed that *on average*

$$E[(\delta l^x_{a_z})^2 - 2(\delta l^x_{a_z}\delta l^x_{b_z}) + (\delta l^x_{b_z})^2] = E[(\delta l^y_{a_z})^2 - 2(\delta l^y_{a_z}\delta l^y_{b_z}) + (\delta l^y_{b_z})^2], \tag{3.138}$$

because the statistics of the errors (at the zenith) are the same between different satellites. By making this assumption, Equation 3.137 can be reduced to

$$\mu^2_{\sigma^2_{\Delta\nabla}}(\varepsilon^x, \varepsilon^y) = \frac{\mu^2(\varepsilon^x) + \mu^2(\varepsilon^y)}{2}. \tag{3.139}$$

Using this in Equation 3.136 and rearranging terms results in the mapping between the double difference error variance and the double difference error variance at the zenith

$$E[(\Delta\nabla\delta l^{xy}_{ab})^2] = \frac{\mu^2(\varepsilon^x) + \mu^2(\varepsilon^y)}{2} E[(\Delta\nabla\delta l^{xy}_{ab_z})^2]. \tag{3.140}$$

3.4.3.4 Calculation of $\mu(\varepsilon)$ From Data

The procedure described below was performed using data from the Norway network, which consisted of 11 receivers spread throughout a 400 km x 600 km region of southern Norway. For a detailed description of this network, see Appendix A.

There is a total of 55 different baselines between these 11 receivers. First, numerical estimates of $\mu(\varepsilon)$ for a fixed set of elevations ε were calculated for each of the 55 baselines. Then, these results were combined together to generate a functional form of $\mu(\varepsilon)$ which fit the data generated in the first step. These two steps are described in the paragraphs that follow.

3.4.3.4.1 Calculating Numerical Estimates of $\mu(\varepsilon)$. First, all combinations of double differenced measurement-minus-range observables (with the integer ambiguities removed) were calculated once every minute over the 24-hour period described in Appendix A. This generated between 31,000 to 45,000 samples of the double differenced differential errors ($\Delta\nabla\delta l$), depending upon the baseline.[11] Next, any double difference measurement that did not have a satellite above 45° was rejected (for this calculation of $\mu(\varepsilon)$ only). Double difference measurements were then grouped into bins according to the elevation of the lower satellite. A bin size of 3° was used, so the first bin included all double difference measurements where the lower satellite was between 10°–13°, the second bin was from 13°–16°, and so on. The variance of the measurement errors was then calculated for each bin. A sample plot of the *standard deviations* of the measurements in each bin for the ALES-STAV (387 km) baseline is shown in Figure 3.3. The standard deviation (square root of the variance) is plotted rather than the variance, because the standard deviation relates directly to the measurement errors (in m) rather than the square of

[11] Some baselines had more double differences than others due to 1) variations in the number of measurements taken by each receiver, and 2) variations in the number of ambiguities that could be resolved between baselines. (If the integer ambiguity was not known for a particular double difference measurement, then that double difference measurement was rejected).

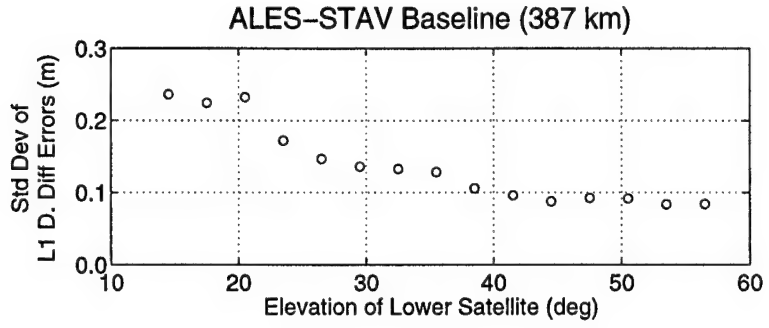

Figure 3.3: *Standard deviation of double differenced measurement errors for ALES-STAV baseline*

the measurement errors (in m^2).

Next, Equation 3.140 is used to solve for the value of $\mu(\varepsilon)$ for each of the elevation bins. In that equation, $\mu(\varepsilon^x)$ is considered the low elevation satellite and $\mu(\varepsilon^y)$ is considered the high elevation satellite. Then, solving for $\mu(\varepsilon^{low})$,

$$\mu(\varepsilon^{low}) = \sqrt{\frac{2E[(\Delta\nabla\delta l)^2]}{E[(\Delta\nabla\delta l_z)^2]} - \mu^2(\varepsilon^{high})}. \tag{3.141}$$

Each of the terms on the right side of the equation can be calculated from the data. The variance of the double differenced errors ($E[(\Delta\nabla\delta l)^2]$) is the variance of each bin (i.e., the squared values of each point in Figure 3.3). The variance of the double difference errors at zenith ($E[(\Delta\nabla\delta l_z)^2]$) represents an extrapolation of the data shown in Figure 3.3 to 90°. This is performed by fitting the data to a function g of the form

$$g(\varepsilon) = c_1 F_I(\varepsilon) + c_2 F_T(\varepsilon), \tag{3.142}$$

where

$$F_I(\varepsilon) = 1 + 16 * \left(0.53 - \frac{\varepsilon}{180^\circ}\right)^3 \tag{3.143}$$

$$F_T(\varepsilon) = \frac{1}{\sin\varepsilon} \tag{3.144}$$

(Note that the $F_I(\varepsilon)$ and $F_T(\varepsilon)$ are the ionospheric and tropospheric mapping functions used in Chapter 2). The constants c_1 and c_2 are calculated from the data, and then the

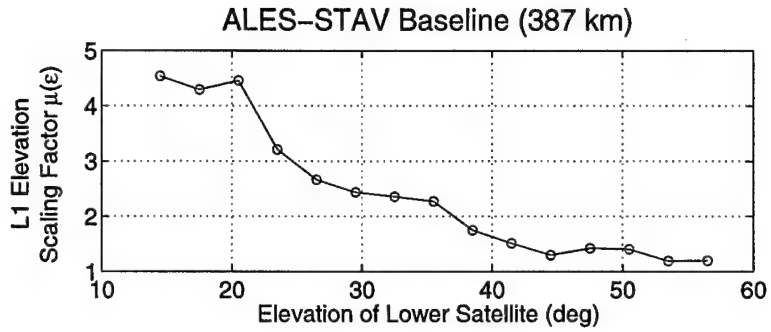

Figure 3.4: *Sample elevation scaling factor data points (for ALES-STAV baseline in Norway network)*

double difference error variance at zenith is calculated as

$$E[(\Delta\nabla\delta l_z)^2] = g(90°). \tag{3.145}$$

The standard deviation of the double difference measurement errors at zenith for the sample data shown in Figure 3.3 is 0.071 m. Finally, the elevation scaling factor of the high elevation satellite ($\mu(\varepsilon^{high})$) can be calculated using an average value of the high elevation satellite over the 24 hour period in the nominal elevation mapping function

$$\mu_{nominal}(\varepsilon) = \frac{F_I(\varepsilon) + F_T(\varepsilon)}{2} \tag{3.146}$$

which is an average of the ionospheric and tropospheric mapping functions.

Using this analysis, a value for $\mu(\varepsilon)$ can be calculated for each elevation bin. Figure 3.4 shows the calculated values of $\mu(\varepsilon)$ for the ALES-STAV baseline. Note that for elevations between 15°–20°, the errors are four to five times larger than for high elevation satellites.

The procedure described above was performed on all 55 baselines, and the resulting point-by-point measurements of $\mu(\varepsilon)$ are plotted together in Figure 3.5. All of the traces (except one) followed a very similar pattern. The one spurious trace above the others was between two receivers separated by only 43 m in a very high multipath environment (the TRYM-TRYR baseline in the Norway network – see Appendix A). The overall errors

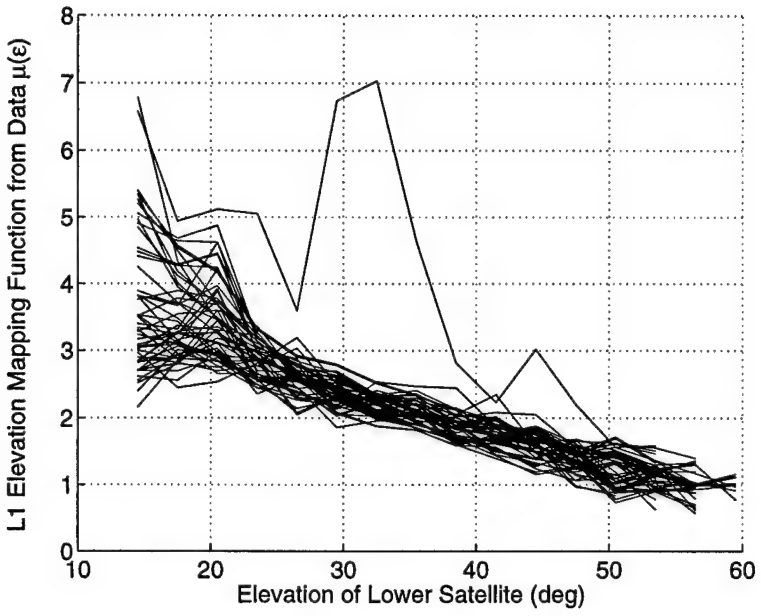

Figure 3.5: *Elevation scaling factor data points for all baselines*

were still very low but noisy (between 0.005 and 0.01 m), and it was difficult to establish an accurate value for the zenith error variance ($E[(\Delta\nabla\delta l_{ab_z}^{xy})^2]$) in this case.

Finally, the data represented in Figure 3.4 was used in a least-squares fit to determine the coefficients of the elevation mapping function which is of the form

$$\mu(\varepsilon) = \frac{1}{\sin\varepsilon} + c_\mu \left(0.53 - \frac{\varepsilon}{180^\circ}\right)^3. \tag{3.147}$$

This function is a combination of the $F_I(\varepsilon)$ and $F_T(\varepsilon)$ mapping functions, and it was chosen because a) both ionospheric and tropospheric errors are involved, and b) it seemed to provide a good fit for both code and carrier-phase measurements. The statistics of the calculated values of $\mu(\varepsilon)$ from the data is plotted along with the functional fit in Figure 3.6. The results are shown for L1 code,[12] L1 phase, and widelane (WL) phase measurements. The circles are the mean values from the 55 baselines, the lines show the 1σ range of the values from the 55 baselines, and the line shows the fit using the functional form

[12]L1 code measurements were CA-code for the Trimble receivers and semicodeless P-code for the Ashtech receivers (due to the high levels of multipath on the Ashtech CA code). See Chapter 4.

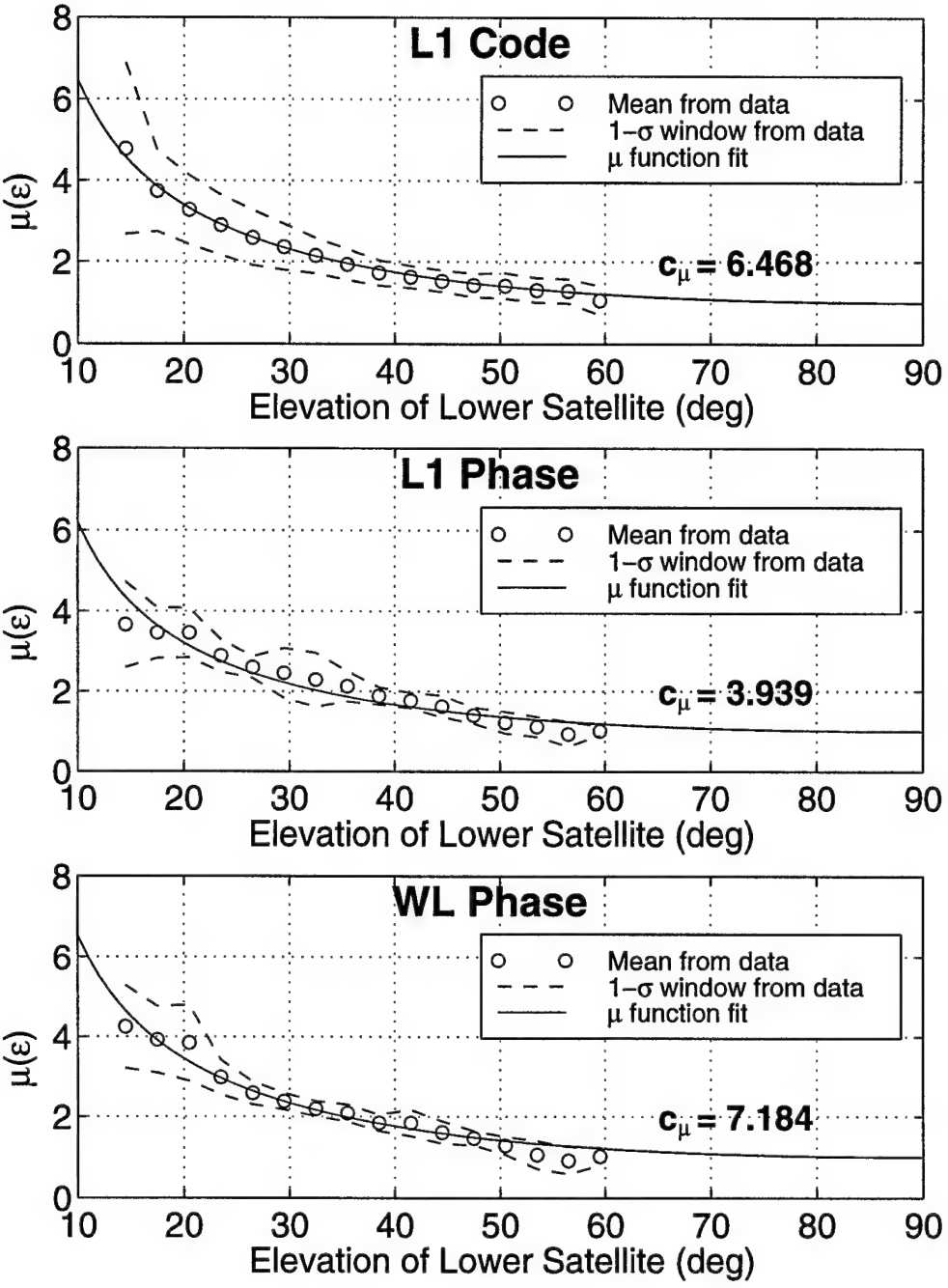

Figure 3.6: *Statistical values and functional fit of elevation mapping function $\mu(\varepsilon)$ for L1 code, L1 phase, and widelane phase measurements*

of Equation 3.147. The values of c_μ are shown on the plots, and they are 6.468, 3.939, and 7.184 for L1 code, L1 phase, and WL phase, respectively. All three curves show a reasonable fit for the data, so these elevation mapping functions will be used in all of the results that follow.

3.4.4 Determination of Zenith Error Variance Functions

This section describes how the zenith correlated and uncorrelated error variance functions are determined using data from the network reference stations. Due to the different natures of code and phase measurements, they will be discussed separately in the sections that follow.

3.4.4.1 Phase Measurement Variance Functions

The 24-hour double difference data set that was described in Section 3.4.3.4.1 was also used for determining the error variance functions. First, all of the double difference measurements were scaled to the zenith using Equation 3.131. Then, the variance of the zenith double differenced measurement error was calculated for each of the 55 different baselines. These zenith variance values are plotted against distance for L1 and WL phase measurements in Figures 3.7 and 3.8, where each dot represents the zenith variance of the errors in one baseline. There is a strong correlation between the error variance and distance for both the L1 and WL cases, as expected.

The goal is to calculate the differential measurement error variance, as shown in Equation 3.117 and restated here as

$$\sigma^2_{c_z}(\boldsymbol{p}_m, \boldsymbol{p}_n) \triangleq E[(\delta_c\phi_z(\boldsymbol{p}_m) - \delta_c\phi_z(\boldsymbol{p}_n))^2]. \tag{3.148}$$

The data represented in Figures 3.7 and 3.8 are the *double differenced* measurement error variances

$$E[(\Delta\nabla\delta l^{xy}_{ab_z})^2] \tag{3.149}$$

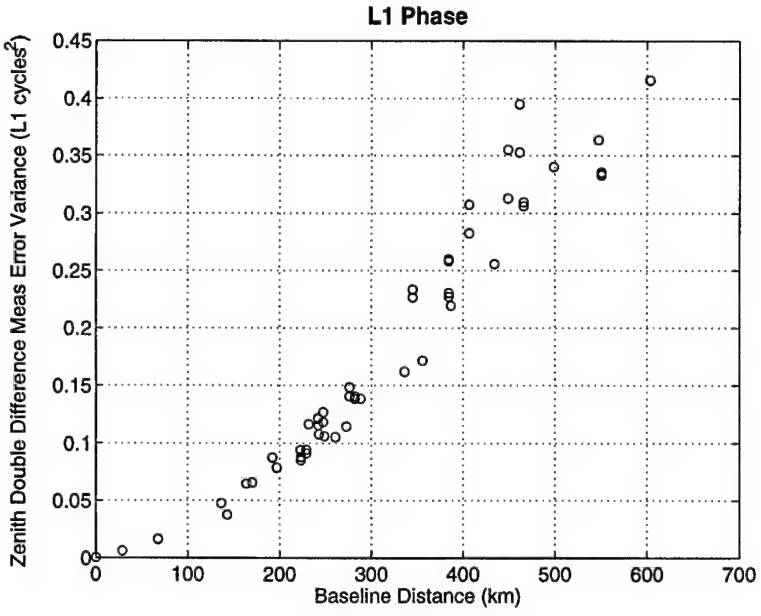

Figure 3.7: *Variance of L1 phase zenith double differenced measurement error for 55 baselines in Norway Network*

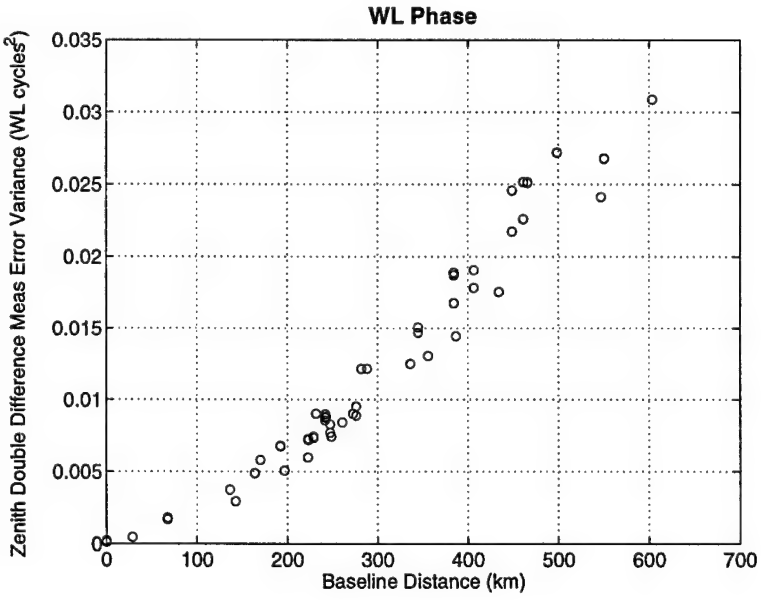

Figure 3.8: *Variance of WL phase zenith double differenced measurement error for 55 baselines in Norway Network*

for receivers a and b and satellites x and y. (It will be shown later that the actual satellites used are unimportant, but it is notationally useful to consider two satellites). The zenith measurement error is defined in a manner analogous to the actual measurement error (Equation 3.120) as

$$\delta l_{a_z}^{x} \triangleq d_c\phi_{a_z}^{x}(\boldsymbol{p}_a, \boldsymbol{p}_0) + \delta_u\phi_{a_z}^{x}. \tag{3.150}$$

Therefore, the relationship between the following two quantities must be established:

$$\underbrace{E[(\Delta\nabla\delta l_{ab_z}^{xy})^2]}_{\text{From double difference data}} \iff \underbrace{E[(\delta_c\phi_z(\boldsymbol{p}_m) - \delta_c\phi_z(\boldsymbol{p}_n))^2]}_{\text{For use in covariance function}} \tag{3.151}$$

Also, the uncorrelated zenith measurement error variances $E[(\delta_u\phi_z)^2]$ (which are modeled as a different constant for each receiver) need to be calculated. (See Section 3.4.1.1 on page 83).

Expanding the double difference measurement within the expectation yields

$$\begin{aligned} E[(\Delta\nabla\delta l_{ab_z}^{xy})^2] = E[\ (& d_c\phi_{a_z}^{x}(\boldsymbol{p}_a, \boldsymbol{p}_0) - d_c\phi_{a_z}^{y}(\boldsymbol{p}_a, \boldsymbol{p}_0) - d_c\phi_{b_z}^{x}(\boldsymbol{p}_b, \boldsymbol{p}_0) + d_c\phi_{b_z}^{y}(\boldsymbol{p}_b, \boldsymbol{p}_0) \\ & + \delta_u\phi_{a_z}^{x} - \delta_u\phi_{a_z}^{y} - \delta_u\phi_{b_z}^{x} + \delta_u\phi_{b_z}^{y}\ )^2\ ]. \end{aligned} \tag{3.152}$$

Recall that $d_c\phi_z(\boldsymbol{p}_a, \boldsymbol{p}_0) \triangleq \delta_c\phi_z(\boldsymbol{p}_a) - \delta_c\phi_z(\boldsymbol{p}_0)$ (Equation 3.33). All of the $\delta_c\phi_z(\boldsymbol{p}_0)$ terms cancel in the double differencing, so they can be neglected. Furthermore, all of the uncorrelated errors ($\delta_u\phi_z$) are by definition uncorrelated with the other error sources. Equation 3.152 can then be simplified to

$$\begin{aligned} E[(\Delta\nabla\delta l_{ab_z}^{xy})^2] = & E[\ (\ \delta_c\phi_{a_z}^{x}(\boldsymbol{p}_a) - \delta_c\phi_{a_z}^{y}(\boldsymbol{p}_a) - \delta_c\phi_{b_z}^{x}(\boldsymbol{p}_b) + \delta_c\phi_{b_z}^{y}(\boldsymbol{p}_b)\ )^2\ ] \\ & + E[(\delta_u\phi_{a_z}^{x})^2] + E[(\delta_u\phi_{a_z}^{y})^2] + E[(\delta_u\phi_{b_z}^{x})^2] + E[(\delta_u\phi_{b_z}^{y})^2] \end{aligned} \tag{3.153}$$

If the first line of Equation 3.153 is expanded, like terms canceled, and factored, it can be simplified to

$$\begin{aligned} E[(\Delta\nabla\delta l_{ab_z}^{xy})^2] = & E[\ (\ \delta_c\phi_{a_z}^{x}(\boldsymbol{p}_a) - \delta_c\phi_{b_z}^{x}(\boldsymbol{p}_b)\ )^2\ ] \\ & + E[\ (\ \delta_c\phi_{a_z}^{y}(\boldsymbol{p}_a) - \delta_c\phi_{b_z}^{y}(\boldsymbol{p}_b)\ )^2\ ] \\ & + E[(\delta_u\phi_{a_z}^{x})^2] + E[(\delta_u\phi_{a_z}^{y})^2] + E[(\delta_u\phi_{b_z}^{x})^2] + E[(\delta_u\phi_{b_z}^{y})^2]. \end{aligned} \tag{3.154}$$

Since all of the errors are zenith error, and the error statistics are assumed to be the same for each satellite, then

$$\begin{aligned} & E[\ (\ \delta_c\phi^x_{a_z}(\boldsymbol{p}_a) - \delta_c\phi^x_{b_z}(\boldsymbol{p}_b)\ )^2\ ] \\ =& E[\ (\ \delta_c\phi^y_{a_z}(\boldsymbol{p}_a) - \delta_c\phi^y_{b_z}(\boldsymbol{p}_b)\ )^2\ ] \\ =& E[\ (\ \delta_c\phi_z(\boldsymbol{p}_a) - \delta_c\phi_z(\boldsymbol{p}_b)\ )^2\ ] \end{aligned} \tag{3.155}$$

and

$$E[(\delta_u\phi^x_{a_z})^2] = E[(\delta_u\phi^y_{a_z})^2] = E[(\delta_u\phi_{a_z})^2] \tag{3.156}$$

$$E[(\delta_u\phi^x_{b_z})^2] = E[(\delta_u\phi^y_{b_z})^2] = E[(\delta_u\phi_{b_z})^2]. \tag{3.157}$$

Combining Equations 3.154 through 3.157 results in the desired relationship between the double difference variance and the correlated and uncorrelated differential errors:

$$E[(\Delta\nabla\delta l^{xy}_{ab_z})^2] = 2E[\ (\ \delta_c\phi_z(\boldsymbol{p}_a) - \delta_c\phi_z(\boldsymbol{p}_b)\ )^2\ ] + 2E[(\delta_u\phi_{a_z})^2] + 2E[(\delta_u\phi_{b_z})^2]. \tag{3.158}$$

In the notation from Section 3.4.1 (especially Equations 3.113 and 3.117), this can be written as

$$E[(\Delta\nabla\delta l^{xy}_{ab_z})^2] = 2\sigma^2_{c_z}(\boldsymbol{p}_a, \boldsymbol{p}_b) + 2\sigma^2_{u_z}(\mathrm{rec}_a) + 2\sigma^2_{u_z}(\mathrm{rec}_b), \tag{3.159}$$

where $\sigma^2_{u_z}(\mathrm{rec}_a)$ and $\sigma^2_{u_z}(\mathrm{rec}_b)$ are constants. Expanding the correlated error term using the function given in Equation 3.119 yields

$$E[(\Delta\nabla\delta l^{xy}_{ab_z})^2] = 2(c_1 d_{ab} + c_2 d^2_{ab}) + 2\sigma^2_{u_z}(\mathrm{rec}_a) + 2\sigma^2_{u_z}(\mathrm{rec}_b), \tag{3.160}$$

where d_{ab} is the distance between reference station a and b. Values of d_{ab} are calculated for each of the 55 baselines based upon the known receiver positions. The 55 double difference zenith measurement errors $E[(\Delta\nabla\delta l^{xy}_{ab_z})^2]$ (shown in Figures 3.7 and 3.8) are then *measurements* for Equation 3.160, and a standard least squares fit is used to determine the parameters c_1 and c_2, along with the constant $\sigma^2_{u_z}(\cdot)$ which is used for each of the 11

receivers.[13] Each of the 55 variances represented in Figures 3.7 and 3.8 (which are actually measurements for the least-squares fit) were assigned measurement variances proportional to d^2 for the least squares fit. This had the effect of assigning higher weights to the shorter baselines (which are more critical in the NetAdjust algorithm).

The results of these fits (for L1 and WL data) are given in Table 3.3 (which summarizes results) at the end of this section. Figures 3.9 and 3.10 show the zenith double difference *correlated* error variance functions for the L1 and WL phase measurements. They were generated by using the fit coefficients shown in Table 3.3, combined with the correlated error portion of Equation 3.160 (i.e., all but the $\sigma_{u_z}^2$ terms). The residuals[14] for the L1 and WL fits are shown in Figure 3.11, and they show a relatively good fit in both cases.

Other functional forms of Equation 3.160 were tried, such as one that included the vertical distance in addition to easting and northing distances. Some more complex functions gave smaller residuals, but this was a result of increased degrees of freedom rather than a better model. As a result, the more complicated functions tended to result in parameters which did not make any physical sense.[15] In many of the more complicated functions, the coefficients on the parameters failed to make any physical sense. In the end, Equation 3.160 was deemed to be the best fit for the Norway network at the time of the test. It is possible that, for other networks at other times, other functional forms would be better.

---

[13]Due to the long baseline distances between the network reference receivers, the correlated errors dominate the measurements, and it is not possible to determine uncorrelated errors on a station-by-station basis accurately.

[14]Residuals are defined as the measured variance values minus the variance values as generated by the covariance function.

[15]One example was a function that included vertical distance as one of the parameters. In this particular case the errors actually became more correlated as the vertical distance between receivers *increased.*

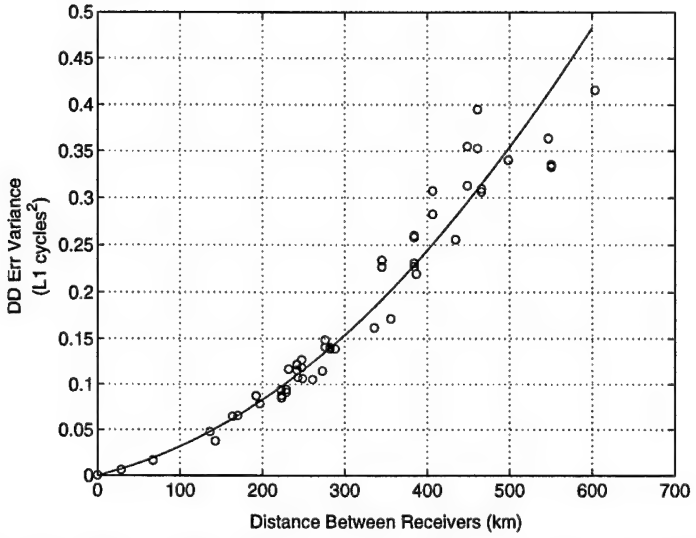

Figure 3.9: *Fit for zenith double difference correlated error variance of L1 phase measurements*

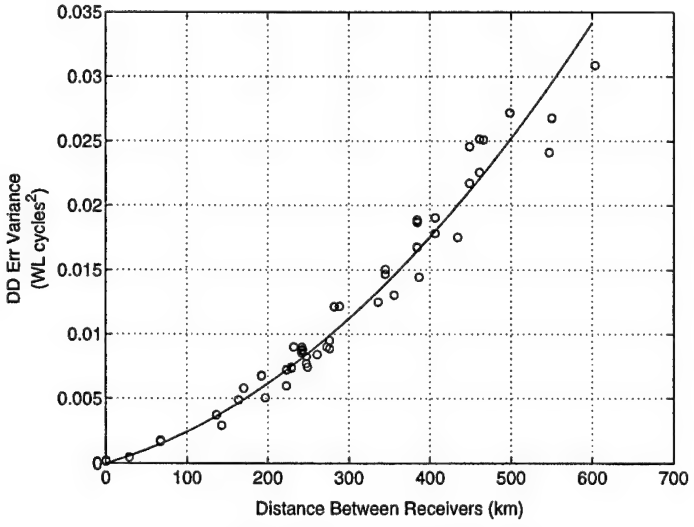

Figure 3.10: *Fit for zenith double difference correlated error variance of WL phase measurements*

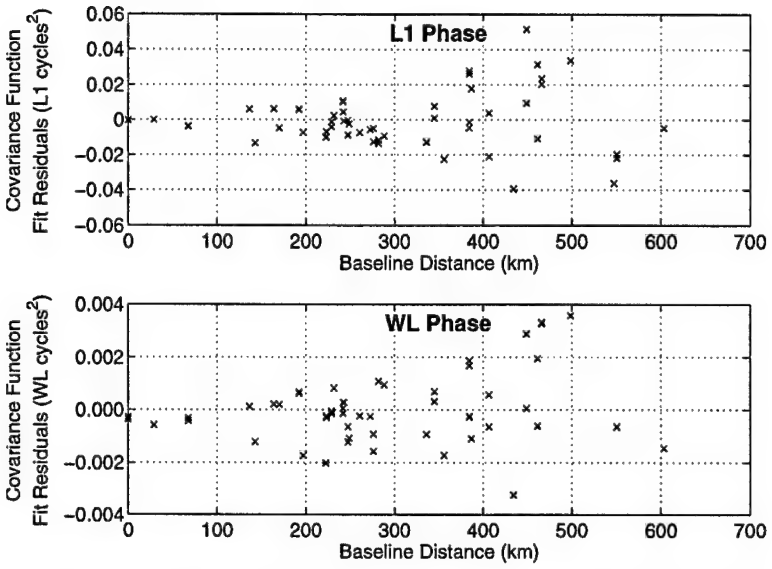

Figure 3.11: *Variance residuals of L1 and WL covariance function fits*

3.4.4.2 Code Measurement Variance Function

A plot showing the code measurement variance versus distance for all 55 baselines is shown in Figure 3.12, which shows no strong correlation with baseline distance. Unlike the phase measurements, the code measurements are dominated by multipath, and the correlated errors (atmospheric and satellite position errors) cannot be accurately determined. It is possible to determine the code correlated errors using the phase measurements, however.

In Chapter 2, two different dual frequency carrier-phase combinations were used to isolate the ionospheric and tropospheric errors. The $\phi_{\lambda_1,-\lambda_2}$ combination isolated the ionospheric errors (Equation 2.24), and the $\phi_{1,-f_2/f_1}$ combination isolated the tropospheric and satellite position errors.[16] After scaling these double difference errors appropriately and changing the sign on the ionospheric error (since it is a code delay rather than a phase advance), the errors are added together to yield a measure of the *code* measurement double difference zenith correlated errors. This process eliminates the impact of code multipath,

[16]In Chapter 2, precise orbits were used to eliminate the satellite position errors. For determining code correlated errors, standard broadcast orbits are used so that the satellite position errors remain (as desired).

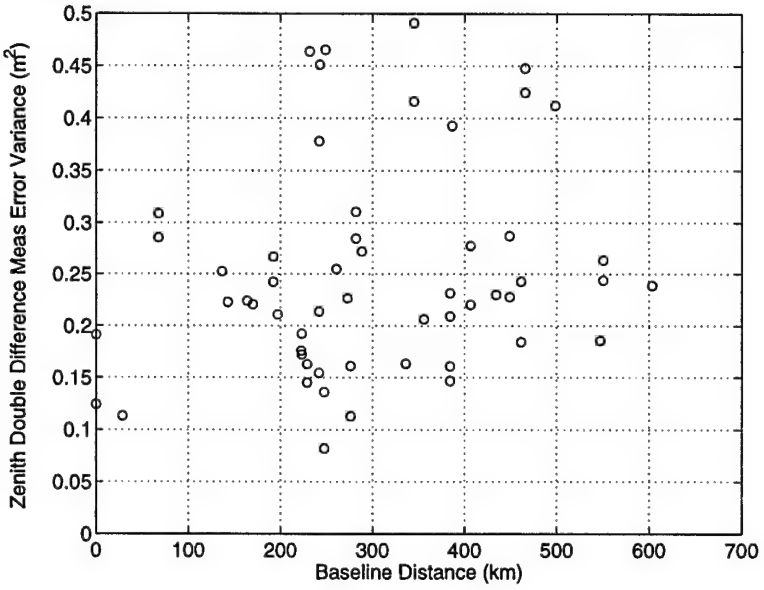

Figure 3.12: *Variance of L1 code zenith double difference errors for 55 baselines in Norway Network*

and the distance dependency of the correlated errors become much more evident, as shown in Figure 3.13.

Two different estimation processes were used to calculate the code measurement covariance parameters. The code errors from phase combinations were used to calculate the correlated error parameters (c_1 and c_2) using the same techniques as for the phase measurements (see Section 3.4.4.1). Then, in a separate estimation process, the code uncorrelated error variances ($\sigma^2_{u_z}$) were calculated by a least squares fit to

$$E[(\Delta\nabla\delta l^{xy}_{ab_z})^2] = 2\sigma^2_{u_z}(\mathrm{rec}_a) + 2\sigma^2_{u_z}(\mathrm{rec}_b). \tag{3.161}$$

(Note that this is the same as Equation 3.160, except that there are no correlated error terms ($c_1 d$, etc.). In this fit, the constant uncorrelated error variances $\sigma^2_{u_z}(\cdot)$ are given *a priori* values based upon the two short (less than 1 km) baselines in the Norway network.

The results are given in Table 3.3 in the summary section. The zenith double difference *correlated* error variance function, calculated from the fit coefficients is shown in Figure 3.14. The residuals for the code measurement variance fit are shown in Figure 3.15.

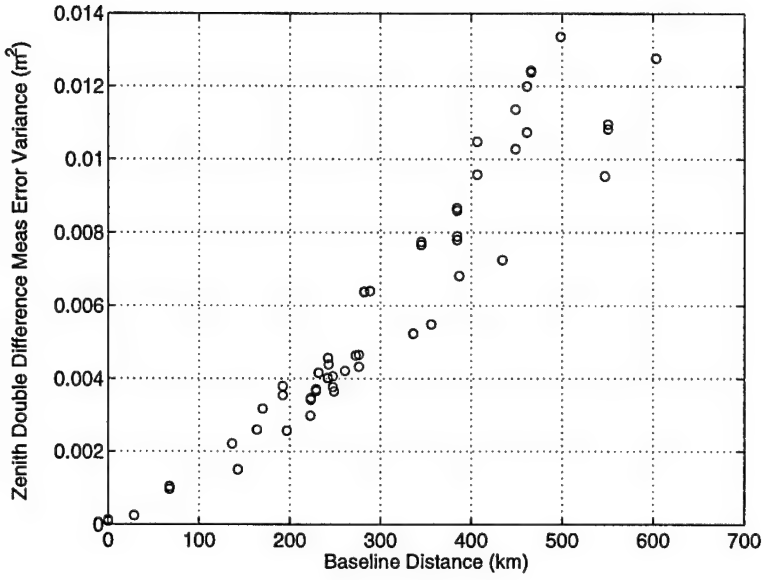

Figure 3.13: *Variance of L1 code zenith double difference correlated errors (from phase measurement combinations) for 55 baselines in Norway Network*

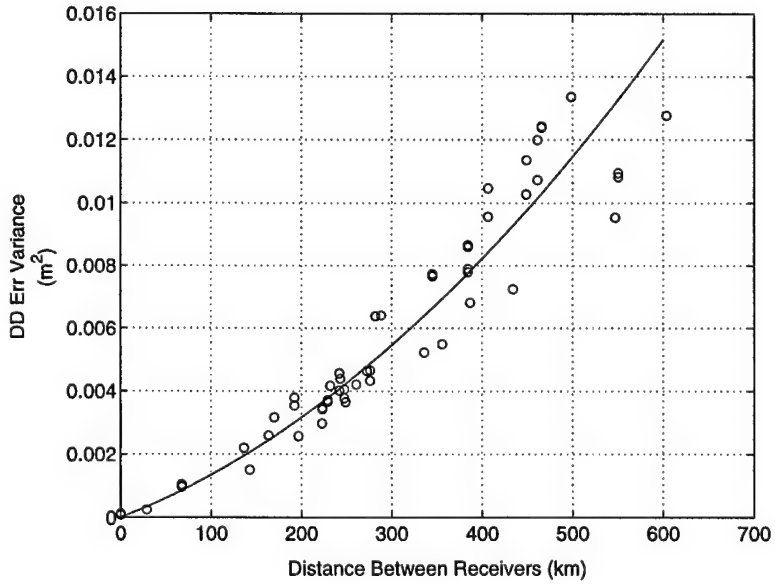

Figure 3.14: *Fit for zenith double difference correlated error variance of L1 phase measurements*

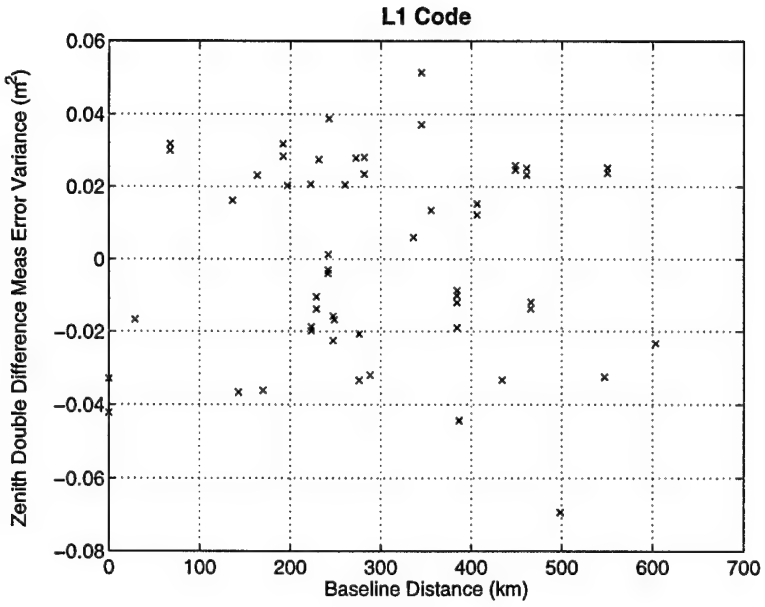

Figure 3.15: *Variance residuals of L1 code covariance function fits*

The residuals are small when compared with the magnitude of the overall error variances shown in Figure 3.12, indicating a good overall fit.

3.4.5 Summary of Covariance Function

The covariance function is summarized in this section, using the equations and results that have been generated in sections 3.4.1 through 3.4.4.

The covariance matrix $\boldsymbol{C}_{\delta\ell}$ is made up of individual elements c_{ab}^{xy} which correspond to the measurements $\delta\ell_a^x$ (from receiver a and satellite x) and $\delta\ell_b^y$ (from receiver b and satellite y as

$$c_{ab}^{xy} = E[(\delta\ell_a^x)(\delta\ell_b^y)]. \tag{3.162}$$

Receiver a is located at $\boldsymbol{p}_a$, and receiver b is located at $\boldsymbol{p}_b$.

There are three cases for the covariance function. The first case is when a=b and x=y

(i.e., it is the variance of the measurement). Then,

$$c_a^x = \mu^2(\varepsilon^x)[f_{z_c}(\boldsymbol{p}_a, \boldsymbol{p}_a, \boldsymbol{p}_0) + \sigma_{u_z}^2(\text{rec}_a)], \tag{3.163}$$

where $f_{z_c}(\boldsymbol{p}_a, \boldsymbol{p}_a, \boldsymbol{p}_0)$ is the correlated variance function (described below), $\mu^2(\varepsilon^x)$ is the elevation mapping function (described below), and $\sigma_{u_z}^2(\text{rec}_a)$ is taken from the Table 3.3. If the receiver is not one of the reference receivers (so it is not in the table), then a nominal value is chosen for $\sigma_{u_z}^2(\text{rec}_a)$ based upon expected levels of multipath and noise.

The second case is when both measurements are to the same satellite (x=y), but the measurements are from different receivers ($a \neq b$). In this case,

$$c_{ab}^x = \mu^2(\varepsilon^x) f_{z_c}(\boldsymbol{p}_a, \boldsymbol{p}_b, \boldsymbol{p}_0), \tag{3.164}$$

where $f_{z_c}(\boldsymbol{p}_a, \boldsymbol{p}_b, \boldsymbol{p}_0)$ is the correlated variance function (described below), and $\mu^2(\varepsilon^x)$ is the elevation mapping function (described below).

The third case involves measurements from different satellites ($x \neq y$), in which case

$$c_{ab}^{xy} = 0. \tag{3.165}$$

The correlated variance function is calculated as a combination of three uses of the differential variance function

$$f_{z_c}(\boldsymbol{p}_a, \boldsymbol{p}_b, \boldsymbol{p}_0) = \frac{\sigma_{c_z}^2(\boldsymbol{p}_a, \boldsymbol{p}_0) + \sigma_{c_z}^2(\boldsymbol{p}_b, \boldsymbol{p}_0) - \sigma_{c_z}^2(\boldsymbol{p}_a, \boldsymbol{p}_b)}{2}. \tag{3.166}$$

The differential variance function is described by

$$\sigma_{c_z}^2(\boldsymbol{p}_m, \boldsymbol{p}_n) \triangleq c_1 d + c_2 d^2 \tag{3.167}$$

where d is the distance between $\boldsymbol{p}_m$ and $\boldsymbol{p}_n$, and c_1 and c_2 are fit coefficients as found in Table 3.3.

Finally, the elevation mapping function is

$$\mu(\varepsilon) = \frac{1}{\sin\varepsilon} + c_\mu \left(0.53 - \frac{\varepsilon}{180^\circ}\right)^3, \tag{3.168}$$

where c_μ is taken from Table 3.3.

Table 3.3: *Summary of covariance function parameters for Norway network. (ALES, AREM, etc. are Norway network reference receivers).*

Parameter	L1 Code	L1 Phase	WL Phase
c_1 [a]	5.5554e-06	1.1024e-04	8.9407e-06
c_2 [b]	1.1820e-08	4.8766e-07	3.2532e-08
c_μ [c]	6.4680	3.9393	7.1839
$\sigma^2_{u_z}$(ALES) [d]	1.5983e-01	4.4273e-05	3.0794e-05
$\sigma^2_{u_z}$(AREM) [d]	4.2223e-02	4.4273e-05	3.0794e-05
$\sigma^2_{u_z}$(ARER) [d]	5.3479e-02	4.4273e-05	3.0794e-05
$\sigma^2_{u_z}$(BERG) [d]	6.8439e-02	4.4273e-05	3.0794e-05
$\sigma^2_{u_z}$(GEIM) [d]	3.6063e-02	4.4273e-05	3.0794e-05
$\sigma^2_{u_z}$(GEIR) [d]	1.6804e-02	4.4273e-05	3.0794e-05
$\sigma^2_{u_z}$(KRIS) [d]	8.7918e-02	4.4273e-05	3.0794e-05
$\sigma^2_{u_z}$(STAV) [d]	4.1489e-02	4.4273e-05	3.0794e-05
$\sigma^2_{u_z}$(TRON) [d]	4.9219e-02	4.4273e-05	3.0794e-05
$\sigma^2_{u_z}$(TRYM) [d]	1.6252e-02	4.4273e-05	3.0794e-05
$\sigma^2_{u_z}$(TRYR) [d]	4.5789e-02	4.4273e-05	3.0794e-05

[a] Units are m^2/km for code, $(cycles)^2$/km for phase

[b] Units are m^2/km^2 for code, $(cycles)^2/km^2$ for phase

[c] Unitless

[d] Units are m^2 for code and $(cycles)^2$ for phase

3.5 Interpretation As Least Squares Condition Adjustment

In previous sections of this chapter, the NetAdjust method was derived using optimal estimation theory based on minimizing the trace of the error covariance matrix (i.e., minimum squared error estimation). The NetAdjust method can also be *interpreted* in classical least squares terms as a "condition adjustment," and doing so will provide insight into how the method works.

Note that the NetAdjust method can also be interpreted as least squares collocation (or least squares prediction), which involves calculating the "signal" at a number of signal points, using measurements (which include the signal and noise) from other locations (Moritz, 1989). For NetAdjust, the signal is the correlated (satellite position and atmospheric) error, and the signal points are the computation points.

3.5.1 Description of Least Squares Condition Adjustment

In many applications, least-squares techniques are used to estimate one or more unknown parameters ($\boldsymbol{x}$) based upon one or more measurements or observations ($\boldsymbol{l}$). In the most general case, the parameters and the measurements are related through the function

$$\boldsymbol{f}(\boldsymbol{x}, \boldsymbol{l}) = \boldsymbol{0}. \tag{3.169}$$

This is often referred to as the "mixed model" or "combined" case. A subset of the combined case is a condition adjustment, in which there are no unknown parameters, but there are conditions placed upon the measurements as represented by the Equation (Bjerhammer, 1973; Krakiwsky, 1990; Leick, 1995)

$$\boldsymbol{f}(\boldsymbol{l}) = \boldsymbol{0}. \tag{3.170}$$

The least squares condition adjustment generates measurement corrections $\hat{\delta \boldsymbol{l}}$ which

are applied to the measurements using

$$\hat{\boldsymbol{l}} = \boldsymbol{l} + \hat{\delta}\boldsymbol{l}. \tag{3.171}$$

When this is done, the corrected measurements $\hat{\boldsymbol{l}}$ meet the conditions specified in Equation 3.170, i.e.,

$$\boldsymbol{f}(\hat{\boldsymbol{l}}) = \boldsymbol{0}. \tag{3.172}$$

In general, there are an infinite number of choices for $\hat{\delta}\boldsymbol{l}$ which will satisfy Equation 3.172. The *least squares* condition adjustment chooses the $\hat{\delta}\boldsymbol{l}$ that minimizes the quadratic form

$$(\hat{\delta}\boldsymbol{l})\boldsymbol{C}_{\boldsymbol{l}}(\hat{\delta}\boldsymbol{l})^T = \text{minimum}, \tag{3.173}$$

where $\boldsymbol{C}_{\boldsymbol{l}}$ is the covariance matrix of the measurements.

The solution for the least squares condition adjustment is then (Krakiwsky, 1990)

$$\hat{\delta}\boldsymbol{l} = -\boldsymbol{C}_{\boldsymbol{l}}\mathrm{B}^T(\mathrm{B}\boldsymbol{C}_{\boldsymbol{l}}\mathrm{B}^T)^{-1}\boldsymbol{w}, \tag{3.174}$$

where

$$\mathrm{B} \triangleq \frac{\partial \boldsymbol{f}(\boldsymbol{l})}{\boldsymbol{l}} \tag{3.175}$$

and

$$\boldsymbol{w} \triangleq \boldsymbol{f}(\boldsymbol{l}). \tag{3.176}$$

It can be seen that Equation 3.174 is similar to the NetAdjust solution given in Equation 3.77 on page 72, if the conditions are defined as

$$\boldsymbol{f}(\hat{\boldsymbol{\ell}}_n) = \Delta\nabla\hat{\boldsymbol{\ell}}_n - \Delta\nabla\boldsymbol{N}_n = \boldsymbol{0}, \tag{3.177}$$

where $\Delta\nabla\boldsymbol{N}_n$ is a vector of the double difference integer ambiguities between the network reference receivers. This states that the measurement corrections $\hat{\delta}\boldsymbol{\ell}_n$ are generated such that all of the *corrected* double differenced measurement-minus-range observables

between the reference receivers are zero (after removing the known ambiguities between reference receivers). This makes intuitive sense, because if there were no measurement errors in $\boldsymbol{\ell}_n$, the double differences would be zero.

This condition (that $\Delta\nabla\hat{\boldsymbol{\ell}}_n = \mathbf{0}$) also makes sense in terms of the covariance analysis presented in Section 3.3. Recall from Equation 3.96 that the covariance of the errors in the estimation of $\Delta\nabla\hat{\delta\boldsymbol{\ell}}_n$ is $\mathbf{0}$, which means that the estimated double difference errors $\Delta\nabla\hat{\delta\boldsymbol{\ell}}_n$ are known perfectly. Since they are known perfectly, then their double difference values between the network reference stations should be zero (after removing ambiguities), as stated in the condition adjustment.

3.5.2 Data Encapsulation Effect

The condition $\Delta\nabla\hat{\boldsymbol{\ell}}_n - \Delta\nabla\boldsymbol{N}_n = \mathbf{0}$ can be used to explain an important feature of the NetAdjust method. Presume phase measurements from satellites x and y are available from three different receivers—one mobile receiver at the computation point and two different receivers in the reference receiver network. The measurements from the network have been corrected using the NetAdjust method. The measurements are denoted as follows:

ϕ^x_{cp}, ϕ^y_{cp}	from mobile receiver at computation point
$\hat{\phi}^x_{n_1}$, $\hat{\phi}^y_{n_1}$	from network reference receiver 1
$\hat{\phi}^x_{n_2}$, $\hat{\phi}^y_{n_2}$	from network reference receiver 2

Two different double difference measurements are formed from these measurements, namely

$$\Delta\nabla\phi^{xy}_{cp1} = \phi^x_{cp} - \phi^y_{cp} - (\hat{\phi}^x_{n_1} - \hat{\phi}^y_{n_1}) \tag{3.178}$$

$$\Delta\nabla\phi^{xy}_{cp2} = \phi^x_{cp} - \phi^y_{cp} - (\hat{\phi}^x_{n_2} - \hat{\phi}^y_{n_2}) \tag{3.179}$$

Subtracting the two equations yields

$$\begin{aligned}\Delta\nabla\phi_{cp1}^{xy} - \Delta\nabla\phi_{cp2}^{xy} &= \hat{\phi}_{n_2}^{x} - \hat{\phi}_{n_2}^{y} - (\hat{\phi}_{n_1}^{x} - \hat{\phi}_{n_1}^{y}) \\ &= \Delta\nabla\hat{\phi}_{n_2 n_1}^{xy} \\ &= N_{n_2 n_1}^{xy} \quad \text{(from Equation 3.177).} \end{aligned} \tag{3.180}$$

This shows that, if the double difference measurement $\Delta\nabla\phi_{cp1}^{xy}$ is available, *there is no new information about the double difference errors* $\Delta\nabla\delta\phi_{cp1}^{xy}$ *to be gained by using another measurement from a different reference station* ($\Delta\nabla\phi_{cp2}^{xy}$). Therefore, since the goal of the network is to minimize the effect of the errors $\Delta\nabla\delta\phi_{cp1}^{xy}$, only the corrected measurements from one reference receiver are required at the mobile receiver.[17]

This is called data encapsulation, because the data from the entire network of reference receivers is "encapsulated" into the measurements of each individual reference receiver. This data encapsulation effect is very useful because it means that only one set of reference receiver measurements needs to be transmitted to the mobile receiver. Then the mobile user can use any standard differential processing algorithm[18] that relies only on one reference receiver to do the processing, and no special multiple reference algorithm is necessary.

---

[17]The mobile user will also need the estimated corrections at the mobile receiver computation point $\delta\ell_{cp}$, but these corrections are the same regardless of which reference receiver is used.

[18]While a single reference algorithm can be used, it may be desirable to tune it to account for the reduced errors brought about by the network.

Chapter 4

Analysis of NetAdjust Performance Using Field Data

In this chapter, data from two different GPS receiver networks is used to analyze the effectiveness of the NetAdjust method. The first network involved 24 hours of data from 11 stationary receivers in southern Norway, while the second network at Holloman Air Force Base, New Mexico, involved 4 stationary reference receivers and three mobile receivers. Both of these networks are described in detail in Appendix A.

Most of the analysis is focused on the Norway network, which is considered the primary network due to its large size and long observation duration. Much less analysis is performed on the Holloman network, due to its smaller size and the difficulty in determining the correct integer ambiguities of the mobile receivers.

4.1 Norway Network Performance Analysis

This section describes the specific manner in which the NetAdjust method was applied to the Norway network, and then seven different "test networks" are described. Each test network consists of a subset of the 11 receivers, chosen to represent a wide variety of network scenarios.

This is followed by four sections that describe NetAdjust performance, starting at the most basic level (individual measurements), progressing through positioning accuracy

and floating ambiguity positioning, and culminating in an analysis of the effect of NetAdjust on ambiguity resolution. This combination of analyses is used to establish the effectiveness of the NetAdjust method based upon the objectives stated in Chapter 1 (Section 1.2.1). These objectives state that the Network should improve the ability to resolve carrier-phase integer ambiguities, and the evidences for such improvement are restated here:

- Use of a network should improve the performance of ambiguity resolution algorithms, relative to the single reference case at the same distance. Performance is measured in terms of the ability to determine the correct ambiguities and the time required to do this.

- Use of a network should increase the distance over which ambiguities can be accurately resolved, relative to a single reference case.

- Use of the network should reduce the errors in the differential code and carrier-phase measurements for the mobile user. The differential errors that should be reduced are all errors that are not canceled in the double differencing process (except for the integer ambiguities). Reducing these errors improves the ability to resolve the carrier-phase ambiguities, and provides better positioning performance once the ambiguities are known.

Each of these will be shown in the analysis that is presented below.

4.1.1 Descriptions of Data Processing Technique

For all of the results shown below, NetAdjust was used to calculate corrections for L1 code, L1 phase, and widelane (WL) phase measurements using the methods and covariance function described in Chapter 3. These three sets of corrections were calculated independently from each other. Recall that NetAdjust generates error estimates for both the receiver measurements and for the unknown measurements at the computation point. The

total corrections were calculated as the sum of the estimated reference receiver errors and computation point errors. These corrections were then applied to the raw measurements to generate corrected measurements, which were then saved as corrected measurement files. A 12° elevation cut off angle was used for all measurements.[1]

A plot showing the GPS receivers used in the Norway network is given in Figure 4.1. A detailed description of the network is given in Appendix A.

L1 CA-code measurements were used from Trimble receivers (KRIS, STAV, BERG, ALES, and TRON), while L1 semicodeless P-code measurements were used from the Ashtech receivers (AREM, ARER, GEIM, GEIR, TRYM, TRYR). The Ashtech receivers also generated L1 CA-code measurements, but these were found to be extremely vulnerable to multipath, so they were not used. This is consistent with the short baseline results presented in Figure 2.13 in Chapter 2.

NetAdjust generated the L1 phase corrections, and these were applied directly to the L1 phase measurements.

The WL phase corrections were generated using the raw (uncorrected) WL phase measurements. These are by definition the *difference* between the L1 and L2 phase (see Section 2.1.3), so any WL correction could be applied to either the L1 or L2 phase measurements (or both). For this research, the WL corrections were applied directly to the L2 measurements only (after accounting for the previously applied L1 corrections). This is referred to as the L2 via WL approach.

Another approach would have been to use NetAdjust to estimate the L2 corrections directly, rather than correcting the L2 measurements through the WL correction. The differences between these two approaches, when implemented, are relatively minor, and the two approaches give nearly indistinguishable results. The L2 via WL approach was chosen in order to allow a straightforward WL covariance analysis (since the WL covariance

[1]Normally, elevation cutoff angles between 10° and 15° are used, balancing the tradeoff between more measurements versus increased atmospheric modeling error. The 12° value was chosen as a middle value in this tradeoff.

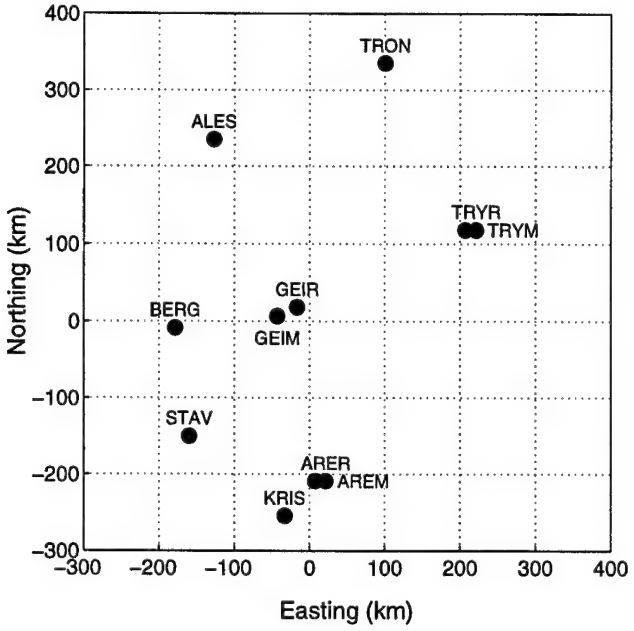

Figure 4.1: *Relative locations of Norway reference receiver sites*

matrix is explicitly calculated). If the L2 phase measurements are estimated directly (i.e., L2 via L2), then it is more difficult to predict WL performance, since no WL covariance matrix is explicitly calculated.

For all three types of measurements (L1 code, L1 phase, and WL phase), only *corrected* measurements were output to the corrected measurement file. Occasionally there was a phase measurement for which a correction could not be generated. This would occur when a) it was the only measurement from that satellite in the entire network, or b) when the integer ambiguities for all double difference phase measurements involving the measurements were not known.[2] In either case, the measurement was not part of any

[2]Appendix B shows that 10%–20% of the L1 integer ambiguities between reference stations were unknown at any given time. (The percentages are better for WL ambiguities). Also, a double difference measurement between network reference receivers was rejected, even if there was a valid ambiguity value, if the measurement exceeded a 4-σ value based upon the *a priori* double difference error covariance matrix $\mathrm{B}_n \boldsymbol{C}_{\boldsymbol{\ell}_n} \mathrm{B}_n^T$.

usable double difference measurements between network reference receivers, so its errors were unobservable, and no correction could be generated. Only measurements that were corrected were included in the output corrected measurement file.

While analyzing the error reduction brought about by NetAdjust, it is desirable to compare various results generated from corrected reference receiver measurements with results generated from raw reference receiver measurements. However, if some of the measurements are not available in the corrected measurement file (for reasons described above), then any differences in results with the raw data could be due to either reduced errors *or* differences in the available measurements. In order to facilitate a fair comparison between the raw and corrected measurements, NetAdjust generated a separate output file which included all of the measurements in the corrected measurement file, only without the corrections applied. This ensured that the same set of measurements were available in the raw and the NetAdjust corrected data files, and any differences between the two files can *only* be attributed to the NetAdjust corrections. When results are presented for the raw data in the sections that follow, they are referring to these raw data files which have the same measurements as the corrected measurement files (only without the corrections).

4.1.2 Description of Test Networks

To see the impact of network size and geometry on NetAdjust performance, seven different test networks will be used in the analyses that follow. For each test network, one receiver is specified as the "mobile" receiver to be positioned. The NetAdjust algorithm does not use the measurements from this receiver when generating the measurement corrections.

The mobile receiver is treated as though it were moving, even though it is actually stationary. This yields results which are very similar, if not identical, to results obtained if the receiver were actually moving, as long as any tuning parameters (such as process noise in a positioning Kalman filter) are set to the values for a moving receiver. This approach

can be taken because most of the differential GPS errors (atmospheric and satellite position errors) are independent of receiver dynamics. In general, multipath is *decreased* with dynamics (relative to a stationary receiver), so if anything, a stationary receiver treated as a mobile receiver represents a worst-case scenario.

Diagrams of each of the seven test networks are given in Figures 4.2 and 4.3. In these plots, circles represent reference receivers, and a diamond indicates the mobile receiver. Note that the ARER/AREM and TRYR/TRYM sites have two receivers located within 50 m of each other, so they show up as one circle. The four-letter designation of each of the receivers included in the network are on the diagram.

The networks are named using the mobile receiver four-letter designation followed by the distance to the nearest network reference receiver (in km). This distance is noteworthy, because it represents the minimum distance (i.e., best case) over which single reference positioning could be performed if there were no network, and this is the point of comparison for the NetAdjust results.

The first six test networks (ARER-0, GEIR-29, ARER-67, STAV-143, GEIR-164, and ALES-242) all involve either 9 or 10 reference receivers. The seventh test network (GEIR-223-sparse) has only three reference receivers, so it is also designated as "sparse." Table 4.1 summarizes the characteristics of each of the networks.

4.1.3 Effect of NetAdjust on Raw Double Difference Measurements

As stated above, one evidence of an improvement from the network is a reduction in the double difference measurement errors (once the ambiguities have been removed). These are the errors that reduce positioning accuracy and inhibit the ability to resolve carrier-phase integer ambiguities.

Individual double differenced L1 code, L1 phase, and WL phase measurement-minus-range observables were calculated over the 24-hour period using the Norway data. As shown in Equation 3.41, these observables are a direct measure of the double difference

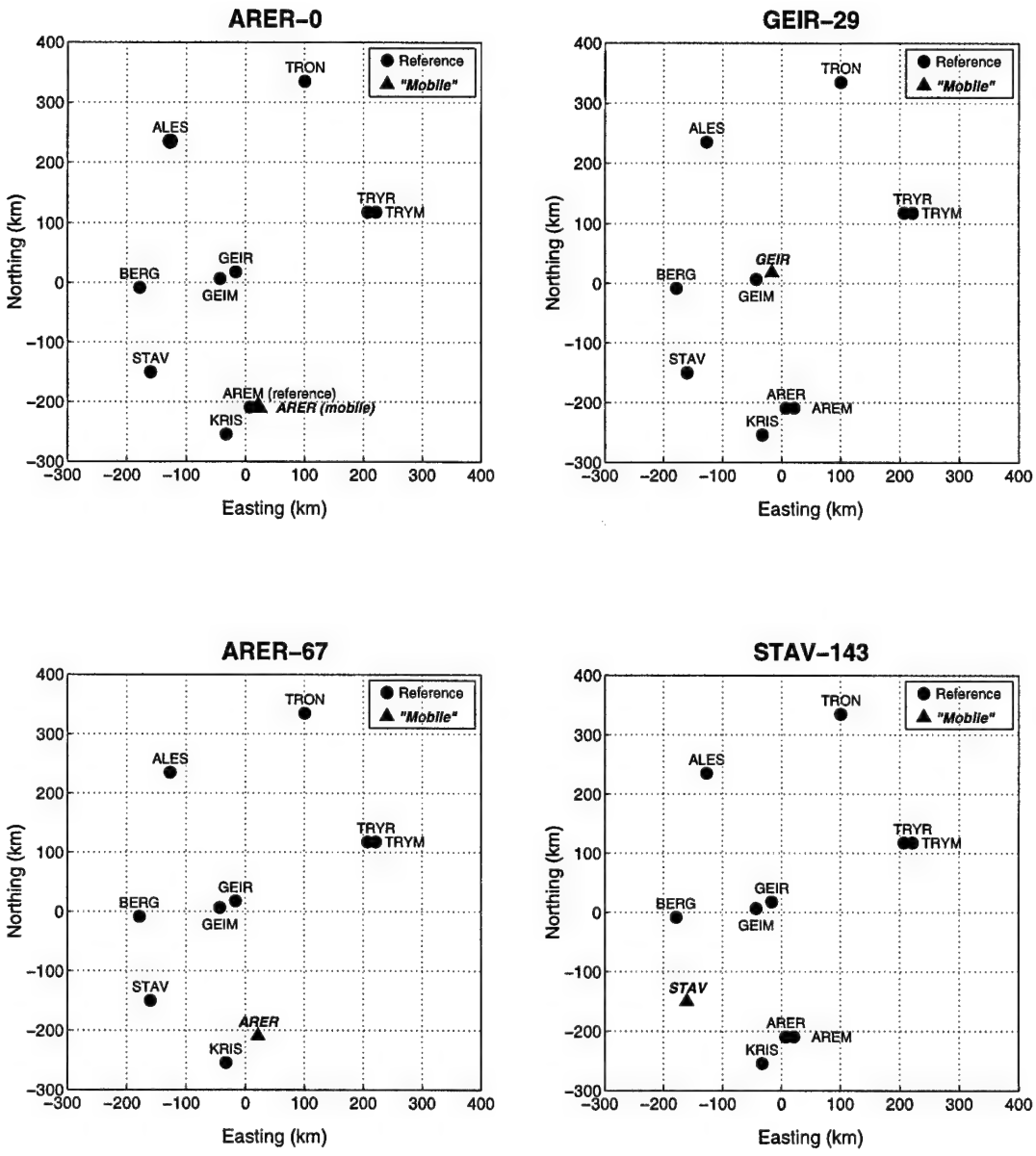

Figure 4.2: *Network maps for Norway networks ARER-0, GEIR-29, ARER-67, and STAV-143*

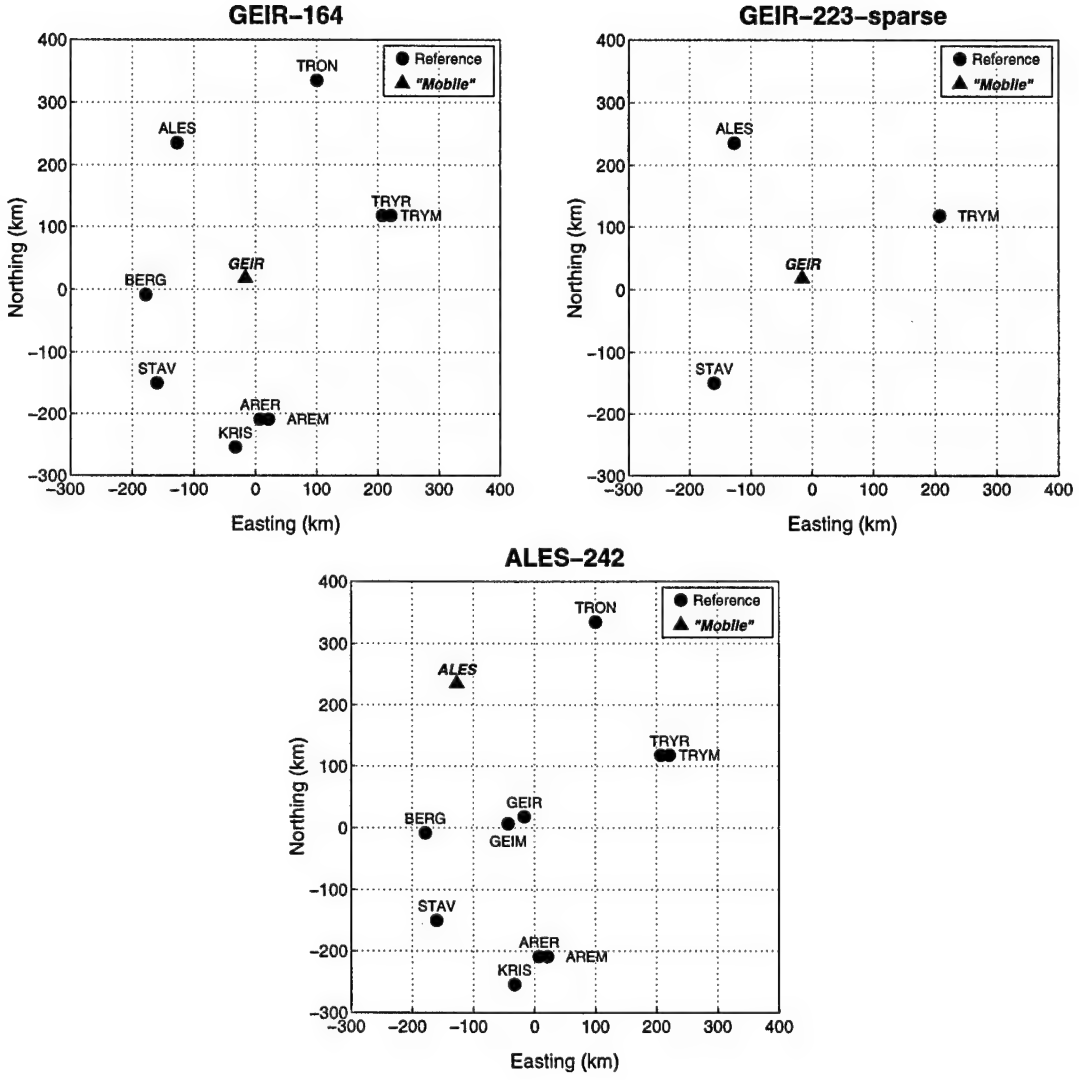

Figure 4.3: *Network maps for Norway networks GEIR-164, GEIR-223-sparse, and ALES-242*

Table 4.1: *Summary of test network characteristics*

Network	Nearest Reference Rec	Distance to Nearest Ref Rec	Network Reference Receivers
ARER-0	AREM	0.011	AREM KRIS STAV BERG ALES TRON TRYM TRYR GEIM GEIR
GEIR-29	GEIM	28.7	AREM ARER KRIS STAV BERG ALES TRON TRYM TRYR GEIM
ARER-67	KRIS	67.4	KRIS STAV BERG ALES TRON TRYM TRYR GEIM GEIR
STAV-143	BERG	142.8	AREM ARER KRIS BERG ALES TRON TRYM TRYR GEIM GEIR
GEIR-164	BERG	163.8	AREM ARER KRIS STAV BERG ALES TRON TRYM TRYR
GEIR-223-sparse	STAV	222.7	STAV ALES TRYM
ALES-242	GEIR	242.1	AREM ARER KRIS STAV BERG TRON TRYM TRYR GEIM GEIR

errors. The double difference observables were generated between the mobile receiver and the closest network receiver for each of the seven test networks using raw (uncorrected) data, and then repeated using the reference data file generated by NetAdjust (which included the NetAdjust corrections). Note that the mobile receiver data was the same in both cases.

A summary of results for all of these runs is presented at the end of this section, but it is useful to begin by examining the results from one of the test networks in greater detail. The GEIR-164 network was chosen for this, because it is the longest network which still has a reasonably good network geometry.[3]

Figure 4.4 shows a comparison between the raw and corrected double difference errors for the BERG-GEIR baseline (GEIR-164 network). The top two plots show the double

[3]Good network geometry means that there are reference receivers surrounding the mobile receiver. The ALES-242 network is longer, but it has poor geometry because most of the network receivers in that case lie to the south or west of ALES.

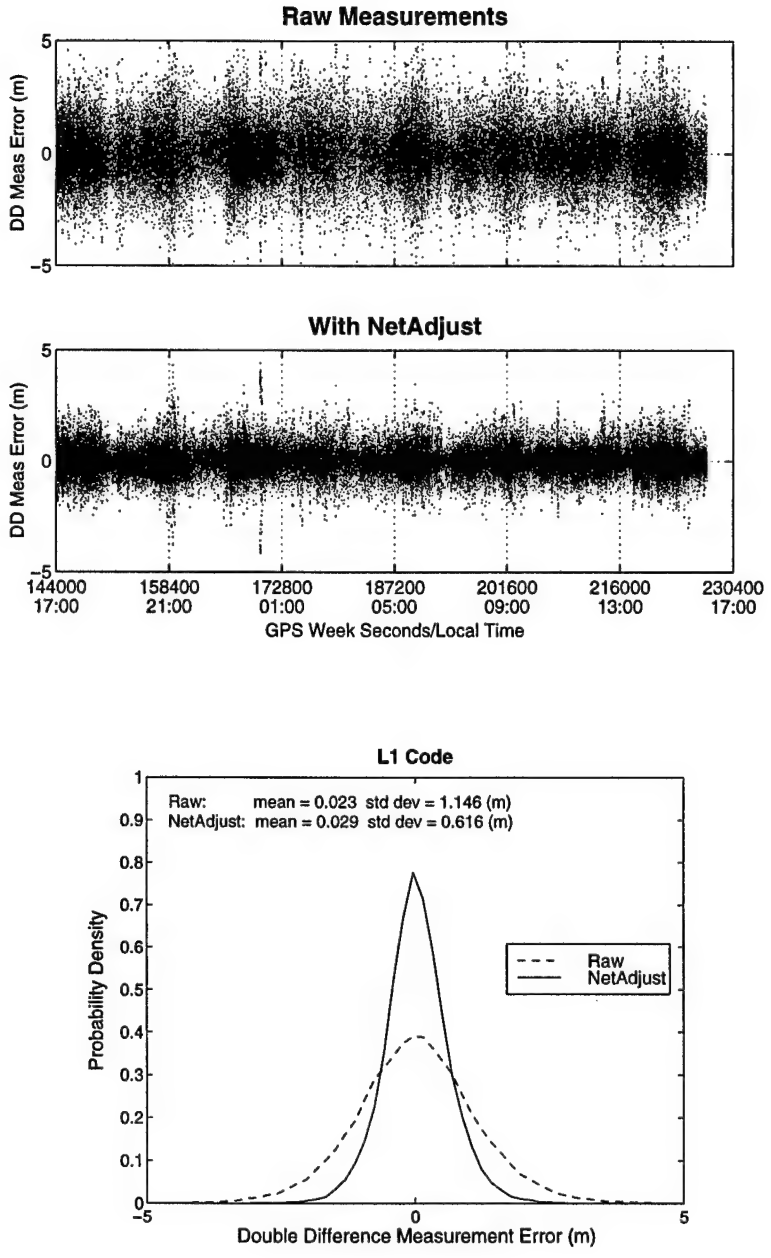

Figure 4.4: *Time series and Probability Distribution of L1 code double difference measurement errors for BERG-GEIR baseline (GEIR-164 network)*

difference code errors in a time series, and the improvement in the NetAdjust case can be clearly seen. Below that is a plot showing the probability density functions of the double difference code measurement errors for both the raw and NetAdjust cases. Both appear Gaussian, but the NetAdjust case has a much sharper peak, indicating smaller errors (and a smaller variance/standard deviation). The mean and standard deviations of the two cases are shown in the top of this plot, and these indicate that the standard deviation of the errors was cut in half by the use of NetAdjust.

Figures 4.5 and 4.6 present the same plots for the L1 phase and the WL phase measurements. The relatively large errors with NetAdjust during the first hour for the L1 case are a result of the lack of known integer ambiguities between the network reference receivers, which meant that NetAdjust had very few measurements to work with. Note the diurnal variation in the overall magnitude of the errors, especially in the raw cases. The lowest error periods appear during the night and early morning, and the peaks occur in the late afternoons. This can be attributed to the ionospheric errors, which normally follow this same pattern (see Section 2.2). Note also that when the NetAdjust corrections are applied, the errors are more consistent throughout the day. The improvement is evident as well in the probability density function plots, which show that the standard deviation of the double difference measurement error was reduced by approximately 45% for both L1 and WL phase measurements in this test network.

Note that these results are all using the reference receiver which is closest to the mobile receiver for the GEIR-164 network (BERG). If other, farther reference receivers were used, the raw data results would show even greater errors. The NetAdjust results, however, would be exactly the same, due to the data encapsulation effect discussed at the end of Chapter 3.

The results for all of the test networks are summarized in Table 4.2. Root-Mean-Square (RMS) values of the double difference measurement errors are shown for all three measurement types, along with the percentage of improvement. The test networks are listed in order of the network lengths, with the shorter length networks at the top of the ta-

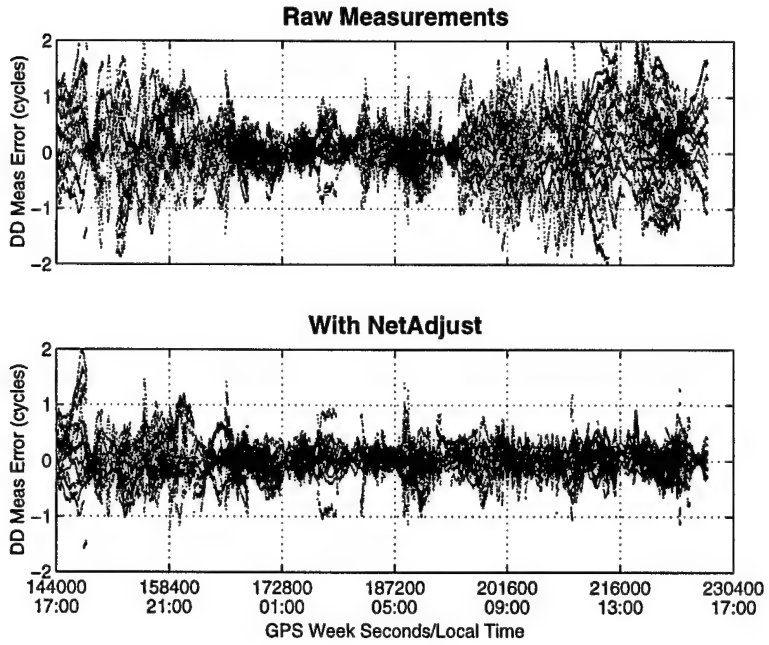

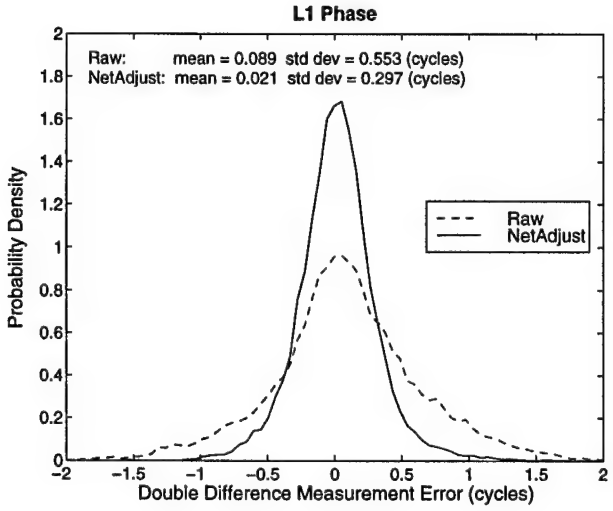

Figure 4.5: *Time series and Probability Distribution of L1 phase double difference measurement errors for BERG-GEIR baseline (GEIR-164 network)*

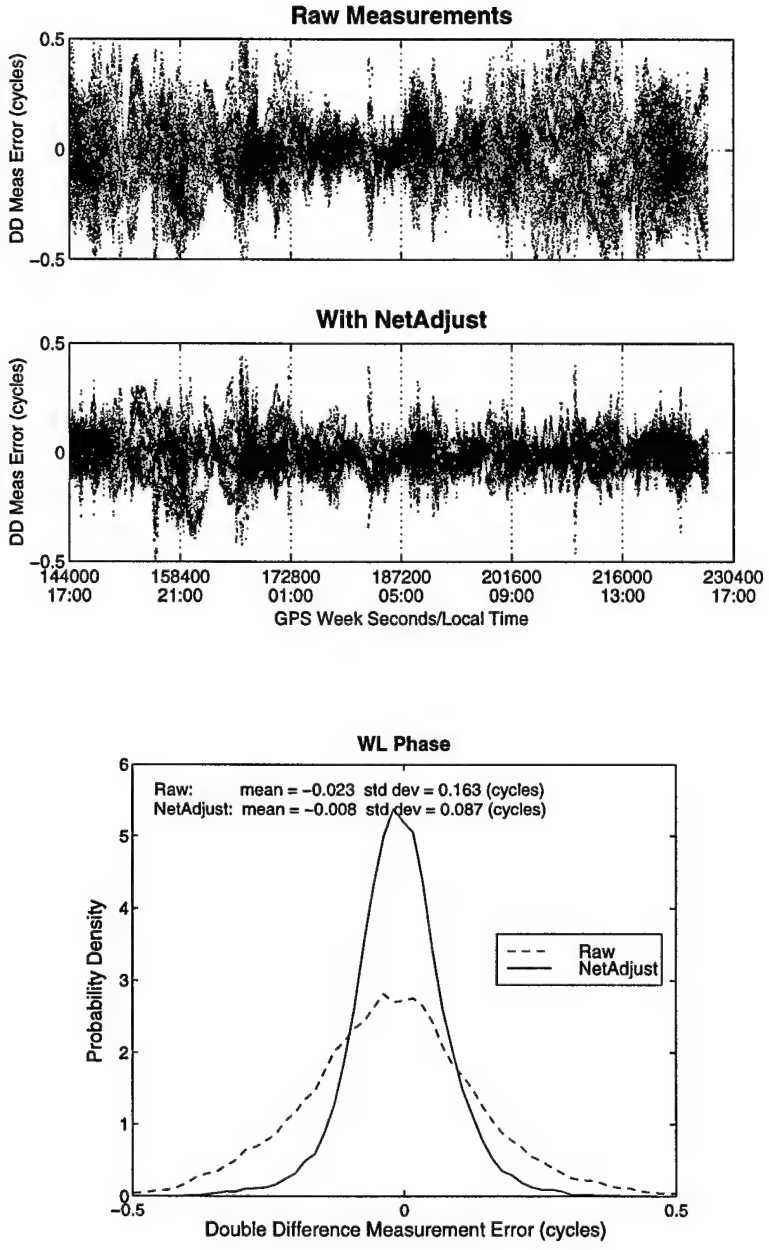

Figure 4.6: *Time series and Probability Distribution of WL phase double difference measurement errors for BERG-GEIR baseline (GEIR-164 network)*

Table 4.2: *Double difference RMS error comparison between raw and NetAdjust solutions for L1 code, L1 phase, and WL phase measurements*

Test	L1 Code (m)			L1 Phase (cycles)			WL Phase (cycles)		
Network	Raw	Cor	Imprv	Raw	Cor	Imprv	Raw	Cor	Imprv
ARER-0	1.089	0.888	18%	0.081	0.090	-10%	0.041	0.041	0%
GEIR-29	0.921	0.608	34%	0.180	0.154	15%	0.053	0.048	9%
ARER-67	1.338	0.899	33%	0.301	0.226	25%	0.096	0.077	20%
STAV-143	1.166	0.862	26%	0.455	0.260	43%	0.135	0.081	40%
GEIR-164	1.146	0.617	46%	0.560	0.297	47%	0.165	0.088	47%
GEIR-223-sparse	0.973	0.660	32%	0.707	0.332	53%	0.190	0.095	50%
ALES-242	1.957	1.885	4%	0.794	0.461	42%	0.236	0.134	43%

ble. These RMS errors are also plotted versus baseline distance in Figures 4.7 through 4.9.

Note that, for the L1 and WL phase measurements, the percentage improvement increases as the baseline length increases. For very short baselines (such as ARER-0 and GEIR-29), the differential errors are already low, and the additional network receivers (most of which are very far from the mobile receiver) do not provide much useful information. As the baseline length increases, then the differential errors grow, and the network reference receivers become more useful. Both the L1 and the WL phase measurements exhibit similar percentage improvements. The L1 errors grow much more quickly than the WL errors (both expressed in cycles), due to the L1 wavelength which is much shorter than the WL wavelength. As a result, use of NetAdjust keeps the WL RMS errors below 0.1 cycles for all but the longest networks, while the L1 RMS errors with NetAdjust grow to 0.3 cycles or more (even though they are still an improvement over the raw cases).

The double difference code measurement errors are reduced by NetAdjust for all of the test networks, but there is not a trend with network length as there was for the phase measurements, because the primary errors in the code measurement in this case are multipath

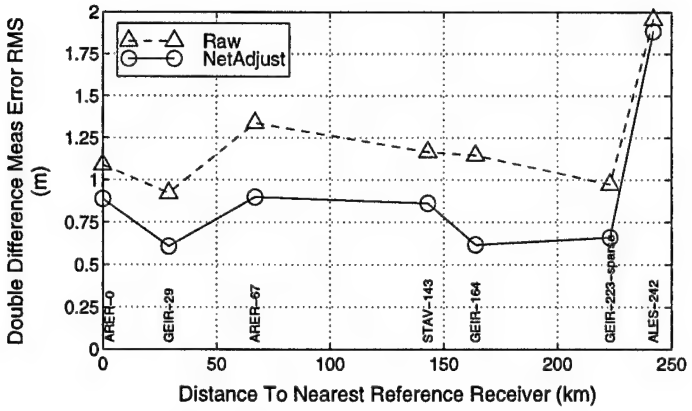

Figure 4.7: *L1 code double difference error RMS values for raw and NetAdjust corrected measurements*

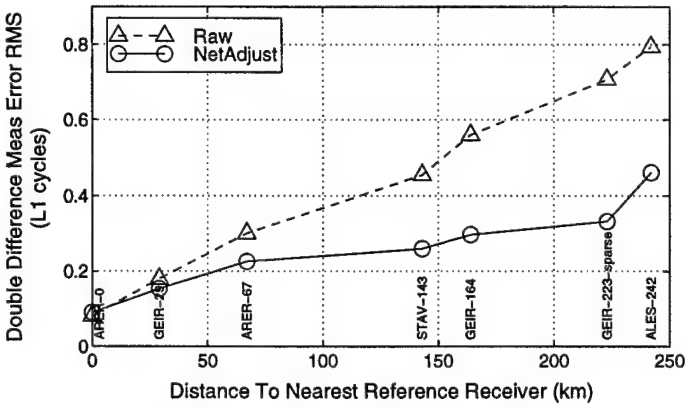

Figure 4.8: *L1 phase double difference error RMS values for raw and NetAdjust corrected measurements*

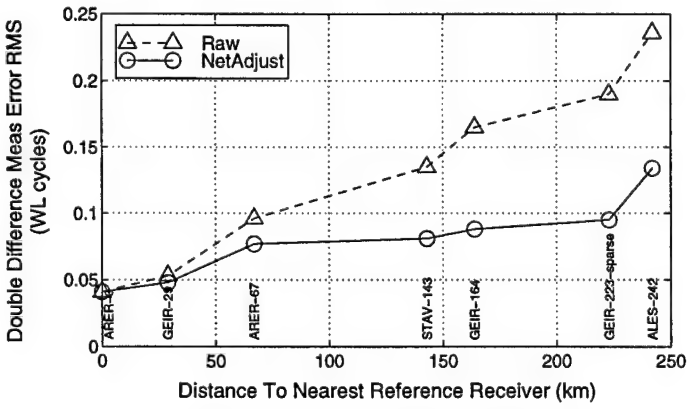

Figure 4.9: *WL phase double difference error RMS values for raw and NetAdjust corrected measurements*

and noise, which are not distance-dependent (see Section 3.4.4.2). If this test is repeated during periods of high solar activity (causing large ionospheric errors), code measurement errors could become correlated to distance.

4.1.4 Effect of NetAdjust on Differential Positioning Accuracy

An evaluation of the improvement in the individual double difference measurements brought about by NetAdjust was presented in the previous section. In the current section, the errors are evaluated in the position domain.

For any given time epoch, measurements from two receivers can be combined to form a set of linearly independent double difference measurements. (These are the measurements that were evaluated in the previous section). These double difference measurements are then used in a least-squares adjustment to calculate the position of the mobile receiver.

This was performed on an epoch-by-epoch basis (i.e., no filtering) for each of the test networks using L1 code, L1 phase, and WL phase measurements (raw and corrected). For the phase measurements, the previously calculated[4] integer ambiguities were applied, so the results in this section describe the positioning accuracy *after* the ambiguities have been resolved. (The effect of NetAdjust on ambiguity resolution is described in later sections). No carrier-phase smoothing of the code was used for the results in this section.

Figure 4.10 gives an analysis of the L1 code positioning results for the BERG-GEIR baseline and the GEIR-164 network over the 24-hour test period. The first three plots on the left show the position errors using the raw (uncorrected) measurements, and the first three on the right show the position errors after the NetAdjust corrections have been applied to the reference receiver measurements. The scales on the plots are held constant between the raw and the NetAdjust results to facilitate comparison between the two. Mean, standard deviation, and RMS value statistics are also provided on each of these plots.

---

[4]These ambiguities were calculated using the procedures described in Appendix B.

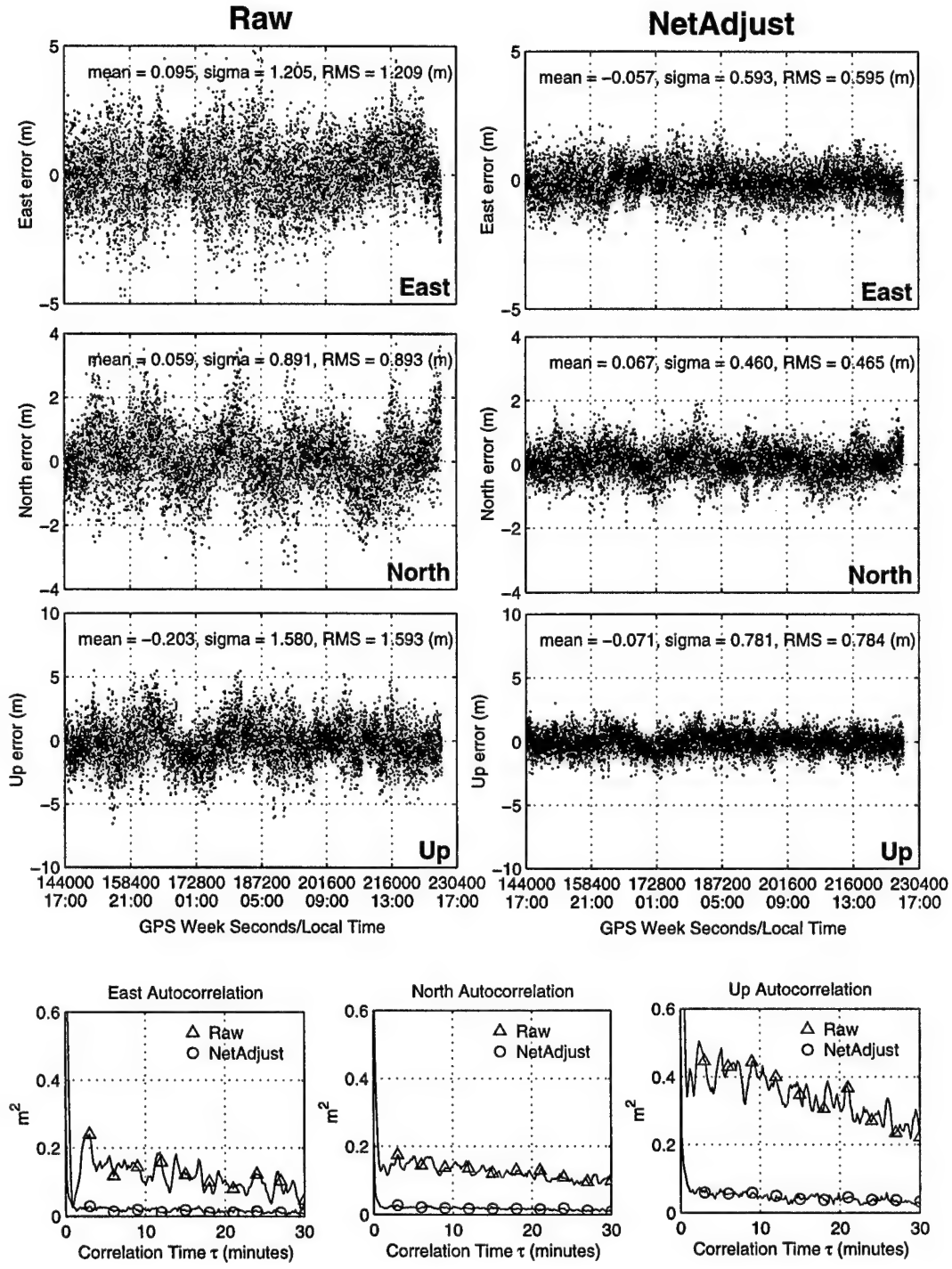

Figure 4.10: *Analysis of the epoch-by-epoch L1 code double difference positioning results on BERG-GEIR baseline. NetAdjust results used the GEIR-164 network.*

Note first of all that the code positioning errors are dominated by noise and multipath, although there are some longer time constant trends in the data as well. RMS errors for the raw positions varied between 0.9 and 1.6 m, but after the NetAdjust corrections were applied, the RMS errors varied between 0.47 and 0.8 m. Overall, application of the NetAdjust corrections reduced the RMS error by approximately 50% in each axis for this network. Note also that the NetAdjust corrections significantly reduced the vertical error bias (mean), from -20 cm raw to -7 cm corrected.

It is useful to examine the time constants of the errors in addition to the overall error statistics, and here this is done through the autocorrelation function. The general autocorrelation function $\Psi_{xx}(t_1, t_2)$ is defined as

$$\Psi_{xx}(t_1, t_2) \triangleq E[x(t_1)x(t_2)], \tag{4.1}$$

where $x(t_1)$ and $x(t_2)$ are random variables from the stochastic process x at times t_1 and t_2. If x is wide-sense stationary,[5] then this is simplified to

$$\Psi_{xx}(\tau) \triangleq E[x(t)x(t+\tau)]. \tag{4.2}$$

The autocorrelation function $\Psi_{xx}(\tau)$ then describes how the stochastic process x is correlated over time.

The bottom three plots show the autocorrelation functions for the position errors calculated using each of the 24 hour time series. The traces identified with triangles are the raw data autocorrelation functions, and the traces identified with circles are the NetAdjust autocorrelation functions. For all three axes, the NetAdjust position errors showed significantly less correlation. This appears to be primarily a result of the decreased error magnitudes and removal of long-term biases rather than a shortening of the time constants of the errors.[6] This makes sense, because the NetAdjust method, as implemented in this

[5]Wide-sense stationary essentially means that $E[x(t_1)x(t_2)]$ depends only on the time difference $\tau = t_2 - t_1$. A more precise definition is given in Maybeck (1994).

[6]If the time constants of the errors were significantly changed by NetAdjust, then the *shape* of the raw autocorrelation functions should be different from the *shape* of the NetAdjust autocorrelation functions.

research, performs epoch-by-epoch error estimations (i.e., no filtering).

Figure 4.11 shows the same family of plots, except for the fixed integer L1 phase position errors. In this case, the errors with longer time constants (atmospheric and satellite position errors) are dominant over the errors with short time constants (multipath and noise). This makes it easier to see the long term error trends than with the code position error plots from Figure 4.10. As in the code case, the NetAdjust corrections significantly reduced the total error RMS value. This is especially true in the east error component, for which the raw solution showed a -20 cm offset during daytime hours (which strongly suggests ionospheric errors), but the NetAdjust solution showed no such variation. Note also that, as in the code case, the autocorrelation functions differ in magnitude rather than shape, indicating that the NetAdjust corrections do not significantly change the error time constants.

For completeness, the fixed integer WL phase plots are shown in Figure 4.12. These also show a reduction in the error magnitudes, but no significant change in the error time constants.

Figures 4.10 through 4.12 represent the results from just one of the seven test networks (GEIR-164). The results from all of the test networks are summarized in Tables 4.3 through 4.8. Table 4.3 shows the statistics (mean, standard deviation, and RMS value) of the raw and NetAdjust code positioning errors, broken down into each axis. In every case, the NetAdjust solution resulted in a sizeable reduction in the RMS position errors. Tables 4.4 and 4.5 show the same statistics for the fixed integer L1 and WL phase position errors. Note that the NetAdjust corrections are very effective at reducing the mean errors (i.e., biases). For both L1 and WL position errors, the NetAdjust corrections generally keep the biases down to a few centimetres, in contrast to the raw position errors which have biases of up to 11 cm. The RMS errors are also reduced, especially on the longer networks.

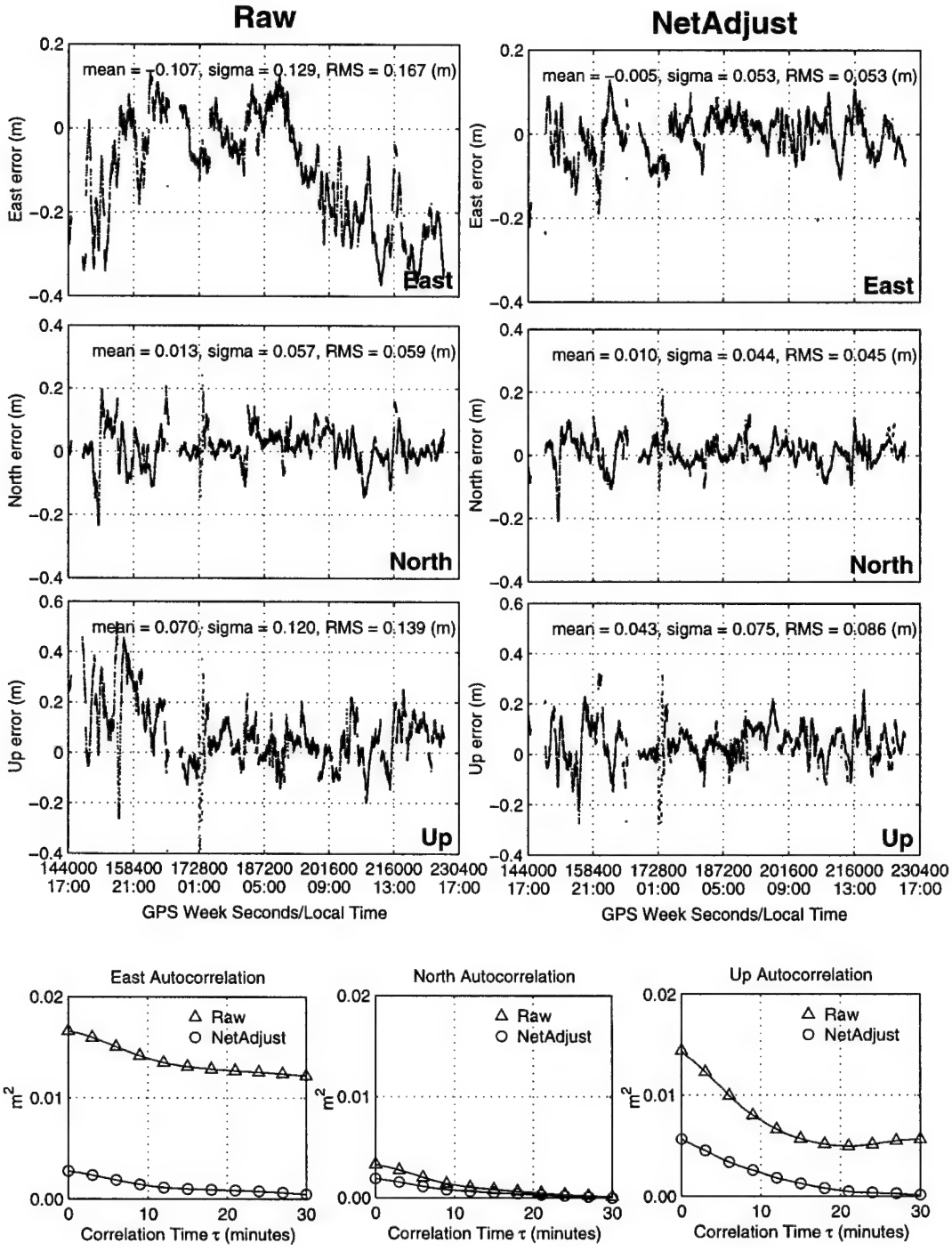

Figure 4.11: *Analysis of the epoch-by-epoch fixed integer L1 phase double difference positioning results on BERG-GEIR baseline. NetAdjust results used the GEIR-164 network.*

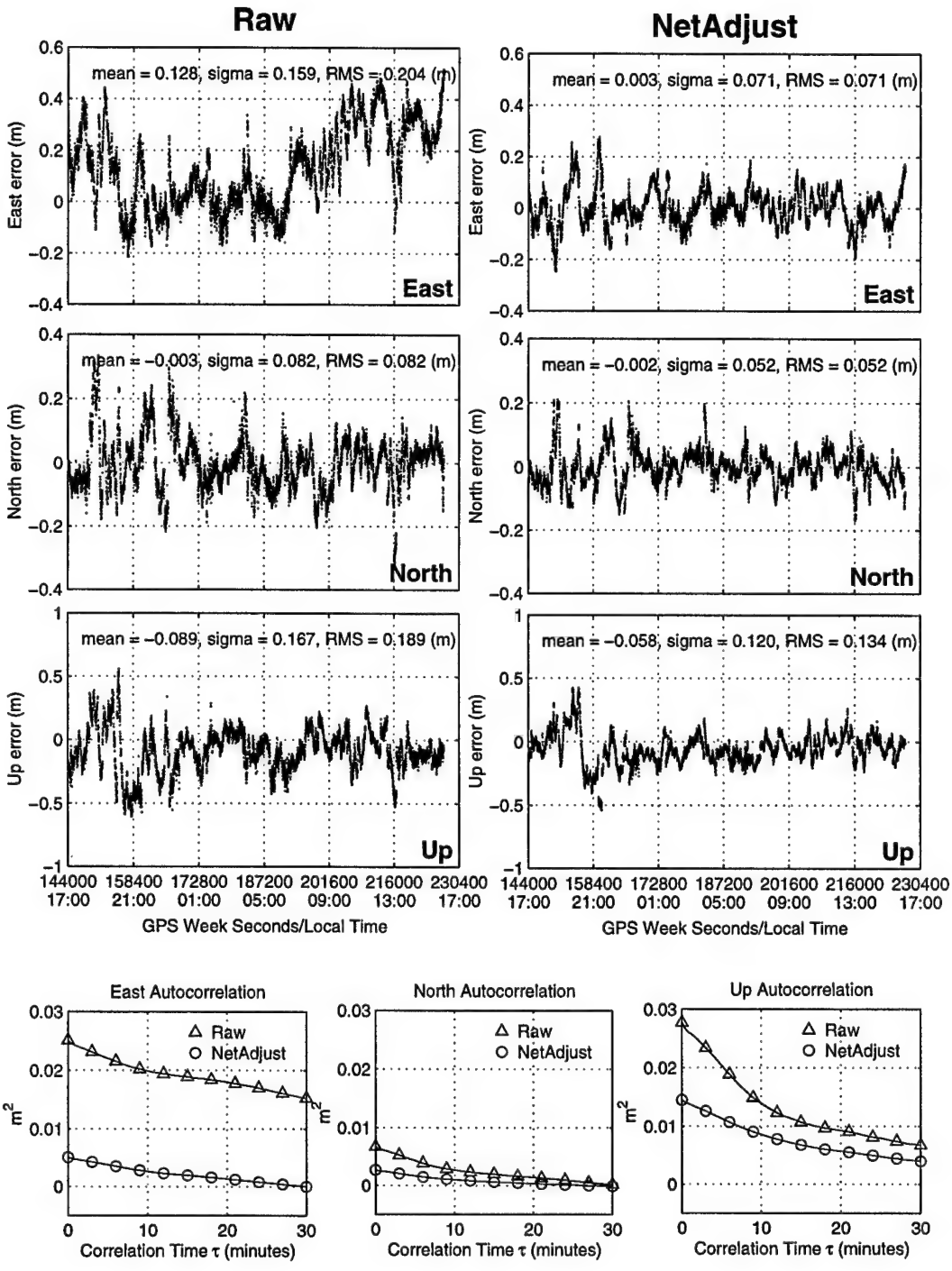

Figure 4.12: *Analysis of the epoch-by-epoch fixed integer WL phase double difference positioning results on BERG-GEIR baseline. NetAdjust results used the GEIR-164 network.*

Table 4.3: *Differential L1 code position error statistics over 24-hour period, Norway network*

		Raw Position Error (cm)			NetAdjust Position Error (cm)		
Network	Axis	Mean	Std Dev	RMS	Mean	Std Dev	RMS
ARER-0	East	11.0	98.8	99.4	1.0	78.8	78.8
ARER-0	North	-1.8	82.1	82.1	-19.1	64.7	67.5
ARER-0	Up	-6.1	137.8	137.9	-14.3	112.5	113.4
GEIR-29	East	1.8	84.1	84.1	-4.8	58.5	58.7
GEIR-29	North	3.1	65.8	65.9	6.1	45.0	45.4
GEIR-29	Up	-1.2	101.8	101.8	-6.5	75.4	75.7
ARER-67	East	0.1	124.1	124.1	0.6	80.1	80.1
ARER-67	North	-16.9	103.1	104.5	-22.5	66.7	70.3
ARER-67	Up	-21.0	176.2	177.4	-15.6	115.5	116.5
STAV-143	East	-0.5	113.1	113.1	-7.3	83.9	84.2
STAV-143	North	-2.5	88.6	88.7	-2.6	66.9	67.0
STAV-143	Up	3.4	154.8	154.9	18.9	114.3	115.9
GEIR-164	East	9.5	120.5	120.9	-5.7	59.3	59.5
GEIR-164	North	5.9	89.1	89.3	6.7	46.0	46.5
GEIR-164	Up	-20.3	158.0	159.3	-7.1	78.1	78.4
GEIR-223-sparse	East	8.4	98.2	98.5	-6.8	65.2	65.6
GEIR-223-sparse	North	9.2	80.2	80.7	2.9	51.9	52.0
GEIR-223-sparse	Up	-28.4	136.2	139.2	-10.5	86.3	87.0
ALES-242	East	8.3	126.4	126.6	1.5	112.2	112.2
ALES-242	North	-13.6	111.4	112.3	-10.5	100.8	101.3
ALES-242	Up	20.9	176.4	177.6	17.4	159.8	160.7

Table 4.4: *Differential fixed integer L1 phase position error statistics over 24-hour period, Norway network*

		Raw Position Error (cm)			NetAdjust Position Error (cm)		
Network	Axis	Mean	Std Dev	RMS	Mean	Std Dev	RMS
ARER-0	East	-0.1	0.5	0.5	-0.4	0.7	0.8
ARER-0	North	0.1	0.4	0.4	0.1	0.6	0.6
ARER-0	Up	0.7	0.7	1.0	0.5	1.1	1.2
GEIR-29	East	-1.5	3.9	4.2	0.3	2.9	2.9
GEIR-29	North	-0.1	2.1	2.1	-0.0	2.0	2.0
GEIR-29	Up	0.8	4.5	4.6	0.7	4.0	4.1
ARER-67	East	-5.1	4.7	7.0	-1.9	3.1	3.7
ARER-67	North	-0.9	3.5	3.6	0.3	2.8	2.8
ARER-67	Up	-1.9	6.5	6.8	-4.0	5.3	6.6
STAV-143	East	0.8	6.5	6.5	1.6	4.3	4.6
STAV-143	North	3.4	7.6	8.3	-0.2	3.5	3.5
STAV-143	Up	-1.9	8.8	9.0	0.1	6.0	6.0
GEIR-164	East	-10.7	12.9	16.7	-0.5	5.3	5.3
GEIR-164	North	1.3	5.7	5.9	1.0	4.4	4.5
GEIR-164	Up	7.0	12.0	13.9	4.3	7.5	8.6
GEIR-223-sparse	East	-11.3	14.3	18.2	-0.2	7.0	7.0
GEIR-223-sparse	North	-2.8	10.1	10.5	0.1	5.3	5.3
GEIR-223-sparse	Up	8.1	12.9	15.2	2.9	8.9	9.4
ALES-242	East	8.5	12.8	15.4	4.3	9.8	10.7
ALES-242	North	-5.0	13.0	14.0	-1.4	6.0	6.2
ALES-242	Up	-3.5	15.9	16.3	0.0	12.5	12.5

Table 4.5: *Differential fixed integer WL phase position error statistics over 24-hour period, Norway network*

		Raw Position Error (cm)			NetAdjust Position Error (cm)		
Network	Axis	Mean	Std Dev	RMS	Mean	Std Dev	RMS
ARER-0	East	-0.0	2.9	2.9	0.3	2.9	2.9
ARER-0	North	-0.1	2.3	2.3	-0.1	2.3	2.3
ARER-0	Up	-0.8	4.1	4.2	-0.4	4.1	4.1
GEIR-29	East	1.8	4.4	4.7	-0.2	4.1	4.1
GEIR-29	North	0.2	2.9	2.9	-0.1	2.6	2.6
GEIR-29	Up	-0.4	5.7	5.7	-0.7	5.5	5.5
ARER-67	East	4.3	8.6	9.6	1.5	6.9	7.0
ARER-67	North	1.8	6.7	6.9	-0.1	4.5	4.5
ARER-67	Up	2.4	9.6	9.9	4.8	8.6	9.8
STAV-143	East	1.9	9.3	9.5	-1.2	5.9	6.0
STAV-143	North	-4.0	10.0	10.8	-0.2	5.1	5.1
STAV-143	Up	0.6	12.6	12.6	-0.3	9.5	9.5
GEIR-164	East	12.8	15.9	20.4	0.3	7.1	7.1
GEIR-164	North	-0.3	8.2	8.2	-0.2	5.2	5.2
GEIR-164	Up	-8.9	16.7	18.9	-5.8	12.0	13.4
GEIR-223-sparse	East	11.8	16.2	20.0	0.9	8.0	8.0
GEIR-223-sparse	North	3.6	13.2	13.6	-0.7	6.5	6.6
GEIR-223-sparse	Up	-7.8	18.1	19.7	-3.7	12.5	13.1
ALES-242	East	-13.4	18.9	23.2	-6.6	10.8	12.6
ALES-242	North	5.2	16.4	17.2	1.8	7.7	7.9
ALES-242	Up	6.0	21.3	22.2	-1.3	15.0	15.0

Table 4.6: *Comparison of L1 code 3-D RMS position errors*

Network	3-D RMS Position Error (cm) Raw	NetAdjust	Percent Improvement
ARER-0	188.8	153.7	18.6%
GEIR-29	147.5	106.0	28.2%
ARER-67	240.4	158.0	34.3%
STAV-143	211.3	158.1	25.2%
GEIR-164	219.0	108.9	50.3%
GEIR-223-sparse	188.6	120.7	36.0%
ALES-242	245.3	220.6	10.0%
Avg. over short (< 100 km) networks	192.3	139.2	27.6%
Avg. over long (> 100 km) networks	216.1	152.1	29.6%

Table 4.7: *Comparison of fixed integer L1 phase 3-D RMS position errors*

Network	3-D RMS Position Error (cm) Raw	NetAdjust	Percent Improvement
ARER-0	1.2	1.6	-33.0%
GEIR-29	6.6	5.4	18.0%
ARER-67	10.4	8.1	22.2%
STAV-143	13.9	8.3	40.4%
GEIR-164	22.5	11.1	50.8%
GEIR-223-sparse	25.9	12.8	50.6%
ALES-242	26.4	17.6	33.2%
Avg. over short (< 100 km) networks	6.0	5.0	17.1%
Avg. over long (> 100 km) networks	22.2	12.5	43.9%

Table 4.8: *Comparison of fixed integer WL phase 3-D RMS position errors*

Network	3-D RMS Position Error (cm) Raw	NetAdjust	Percent Improvement
ARER-0	5.6	5.6	0.3%
GEIR-29	8.0	7.4	7.8%
ARER-67	15.4	12.9	16.1%
STAV-143	19.1	12.3	35.7%
GEIR-164	29.0	16.0	44.6%
GEIR-223-sparse	31.3	16.7	46.6%
ALES-242	36.4	21.2	41.9%
Avg. over short (< 100 km) networks	9.7	8.6	10.8%
Avg. over long (> 100 km) networks	28.9	16.5	42.8%

Table 4.6 shows the 3-D RMS[7] values of the L1 code position errors. Each of the networks showed an improvement when the NetAdjust corrections were used. The last two lines in the table show the average 3-D RMS values of the short (< 100 km) networks and the long (> 100 km) networks. Note that the improvement percentages given in the last two lines are calculated directly from the averaged 3-D RMS errors (not an average of the percentages for each network). For the code measurements, the short networks showed an average reduction in 3-D RMS errors of 27.6% when the NetAdjust corrections were applied, which was very similar to the average reduction of 29.6% for the long networks. This implies that the bulk of the L1 code errors reduced by NetAdjust are multipath and noise, and not distance-dependent errors (such as satellite position and atmospheric errors). This is consistent with the error analysis performed in conjunction with the generation of the covariance function in Chapter 3 (see Figure 3.12). In Figure 4.13, the 3-D RMS code position errors are plotted against the distance between mobile and reference receivers. This also shows that the NetAdjust corrections consistently reduce the errors, and that the total L1 code RMS position error (for both the raw and NetAdjust cases) is

[7]The 3-D RMS error is defined as the RMS value of the three-dimensional error magnitudes.

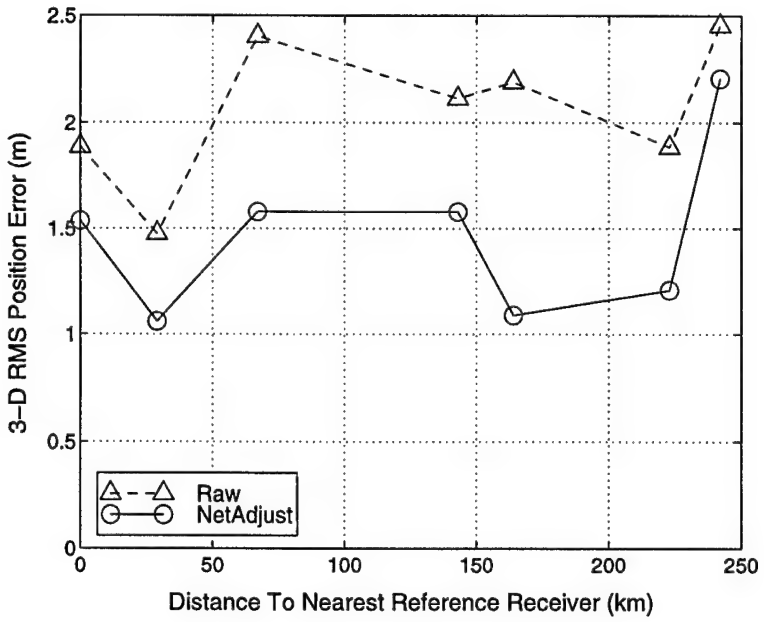

Figure 4.13: *L1 code 3-D RMS positioning error for seven test networks*

not related to the distance between the mobile and reference receivers.[8]

The same set of statistics are presented for the fixed integer L1 phase 3-D RMS position errors in Table 4.7. Note that the percentage improvement was 17% for short networks and 44% for long networks, demonstrating that the degree of phase measurement error reduction from NetAdjust is highly related to the network length. This is because, in contrast to code measurements, the dominant differential measurement errors for phase measurements are the errors which *are* distance-dependent (i.e., satellite position and atmospheric errors). If there is a reference receiver that is close to the mobile receiver (such as in the ARER-0 network, where there is only an 11 m separation between the receivers), then the correlated errors are very small, and the other reference receivers cannot help much. If, however, the mobile receiver is far from any reference receiver (as in the long networks), then the correlated errors dominate, and the other reference receivers are very valuable for reducing the errors. This is graphically demonstrated in Figure 4.14, which

[8]If this test were repeated during periods of high ionospheric activity (such as during a solar maximum), the errors could become correlated with distance.

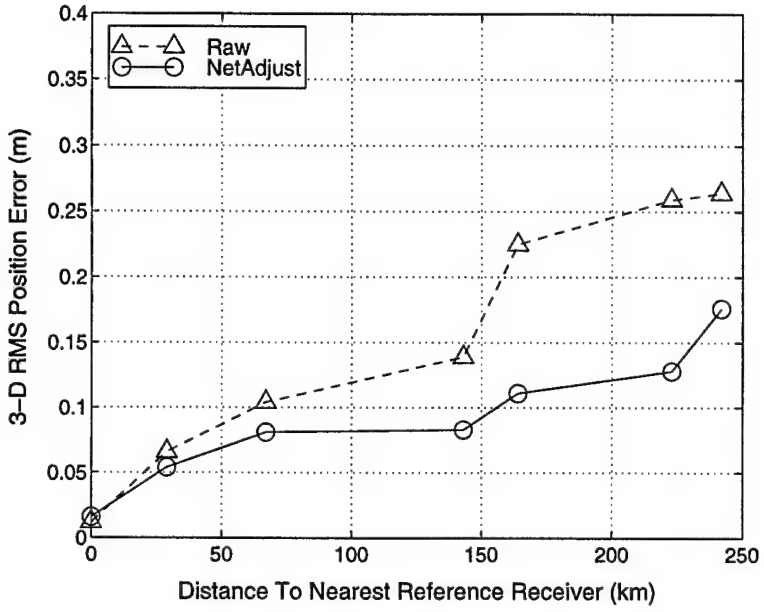

Figure 4.14: *Fixed integer L1 phase 3-D RMS positioning error for seven test networks*

shows a plot of the 3-D RMS errors against the distance between the mobile and reference receiver. Note how the improvement from NetAdjust grows as the distance between the mobile and reference receivers grows.

The same statistics are presented for the fixed integer WL case in Table 4.8 and Figure 4.15. Note that the trends are very similar to the L1 case, only with slightly larger errors. This is because a) the widelane observable is a combination of two measurements, which increases uncorrelated errors (multipath and noise) by a factor of $\sqrt{2}$, and b) the ionospheric errors, multipath, and noise are amplified in the widelane measurement *when expressed in metres*, as they are in this case (see Table 2.3).

4.1.5 Effect of NetAdjust on Integrated Floating Ambiguity Solution

The University of Calgary FLYKIN™ software was used to generate an integrated floating ambiguity solution. FLYKIN uses code and carrier-phase measurements together in a Kalman filter to estimate carrier-phase double-difference ambiguities along with three-dimensional position and velocity states. FLYKIN is designed primarily for kinematic

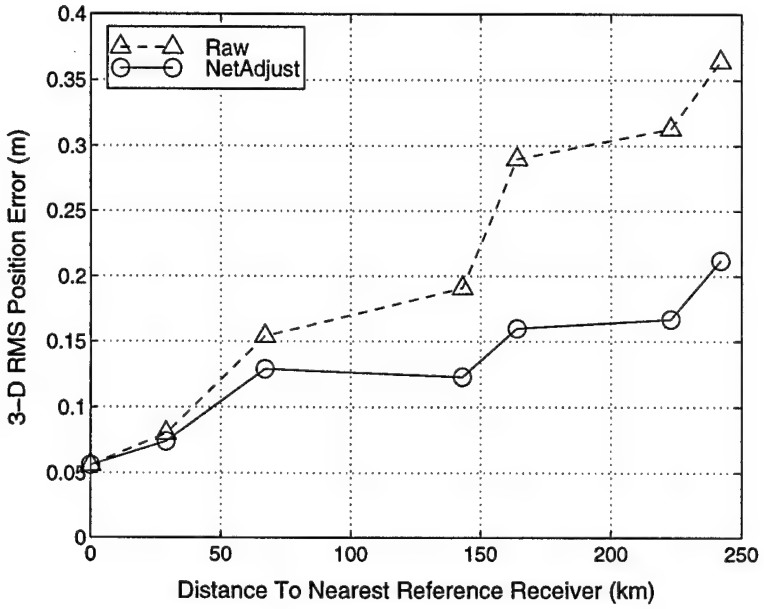

Figure 4.15: *Fixed integer WL phase 3-D RMS positioning error for seven test networks*

carrier-phase integer ambiguity resolution (as will be used in the next section), but it can also be used in a "floating" mode, whereby it never attempts to fix the carrier-phase ambiguities to integers. Instead, the ambiguities are allowed to take on any real (or floating) value.

All runs of FLYKIN in this section (and in Section 4.1.6) used a common set of filter tuning parameters. The L1 code, L1 phase, and WL phase (when used) were given measurement standard deviations of 1 m, 0.02 cycles, and 0.03 cycles.[9] The state vector is defined as

$$\boldsymbol{x} = \begin{bmatrix} p_x & p_y & p_z & v_x & v_y & v_z & \Delta\nabla N_1 & \ldots & \Delta\nabla N_n \end{bmatrix}^T, \tag{4.3}$$

where p_x, p_y, and p_z represent the mobile receiver position in ECEF coordinates (m), v_x, v_y, and v_z represent the mobile receiver ECEF velocity (m/s), and $\Delta\nabla N_1$ through $\Delta\nabla N_n$ are the integer ambiguity terms (cycles). Then, the process noise covariance matrix $\boldsymbol{Q}$ is

[9]These are values typically used for FLYKIN for single reference cases.

calculated as

$$Q = \begin{bmatrix} 3\Delta t^3 & 0 & 0 & 3\Delta t^2 & 0 & 0 & 0 & \cdots & 0 \\ 0 & 3\Delta t^3 & 0 & 0 & 3\Delta t^2 & 0 & 0 & \cdots & 0 \\ 0 & 0 & 3\Delta t^3 & 0 & 0 & 3\Delta t^2 & 0 & \cdots & 0 \\ 3\Delta t^2 & 0 & 0 & 3\Delta t & 0 & 0 & 0 & \cdots & 0 \\ 0 & 3\Delta t^2 & 0 & 0 & 3\Delta t & 0 & 0 & \cdots & 0 \\ 0 & 0 & 3\Delta t^2 & 0 & 0 & 3\Delta t & 0 & \cdots & 0 \\ 0 & 0 & 0 & 0 & 0 & 0 & 1E - 6\Delta t\lambda^2 & \cdots & 0 \\ \vdots & \vdots & \vdots & \vdots & \vdots & \vdots & \vdots & \ddots & \vdots \\ 0 & 0 & 0 & 0 & 0 & 0 & 0 & \cdots & 1E - 6\Delta t\lambda^2 \end{bmatrix}, \tag{4.4}$$

where Δt is the time interval between measurements (nominally 2 seconds for the Norway network) and λ is the L1 or WL wavelength, depending upon the phase measurement used in the processing. All of these tuning parameters are values typically used to provide the best results for integer ambiguity resolution, and they are not necessarily optimized for the conditions present in the Norway network. For more details on the FLYKIN algorithm, see Lachapelle et. al. (1992).

Because FLYKIN is a Kalman filter with an accuracy that improves as more measurements are obtained, it is useful to characterize its performance over time. Of special interest is the initialization period, defined as the time extending from filter initialization to filter steady state.[10] It is desirable to have a *statistical* measure of the filter accuracy that is based upon many repeated runs (samples), rather than just one or two sample runs. To this end, a test method was used which generated many repeated runs over the 24-hour test period, as described in the following section.

[10]Steady-state refers to the approximate time after which the filter errors no longer significantly decrease in magnitude, although they can fluctuate depending upon the number of measurements, geometry, etc.

4.1.5.1 Floating Ambiguity Test Methodology

FLYKIN was used in an iterative manner, starting at the beginning of the 24-hour test period. Each run had a duration of 20 minutes, and the runs were staggered at 10-minute intervals. At each epoch, the total position error was calculated relative to the known receiver position. Figure 4.16 shows the east position error of the BERG-GEIR baseline with NetAdjust (using the GEIR-164 network) for the first six iterations. Note how the errors vary from run to run (other than perhaps a negative bias for these six runs). Figure 4.17 is similar, only it shows the three-dimensional error magnitude rather than the east error.

This process was repeated until the end of the 24-hours was reached, for a total of 138 separate runs. Figures 4.18 and 4.19 show the east error and 3-D error magnitude, respectively, for each of the 138 runs. Note how the errors are large at the start, but they decrease rapidly until they appear to reach steady-state somewhere around 3–5 minutes. The occasional spikes in these plots show where the filter automatically reset itself in the middle of a 20 minute run.[11]

The data represented in Figures 4.18 and 4.19 can be presented more concisely as statistical values. Figure 4.20 shows the mean value and a window of $\pm$ one standard deviation about that mean calculated from the 138 samples. Likewise, Figure 4.21 shows the RMS value of the three-dimensional position errors.

The east, north, and vertical mean $\pm$ 1-σ window position errors for the GEIR-164 baseline, based on the 138 samples, are shown in Figure 4.22. The plots on the left were generated from the 138 iterations of the BERG-GEIR baseline using raw (uncorrected) data, and the plots on the right were generated for the BERG-GEIR baseline after the BERG code and phase measurements were corrected by NetAdjust (using the GEIR-164 baseline). FLYKIN was run in float mode using L1 code and L1 phase as measurements.

[11]Filter resets occur under various circumstances, such as if there are a large number of cycle slips or missing measurements.

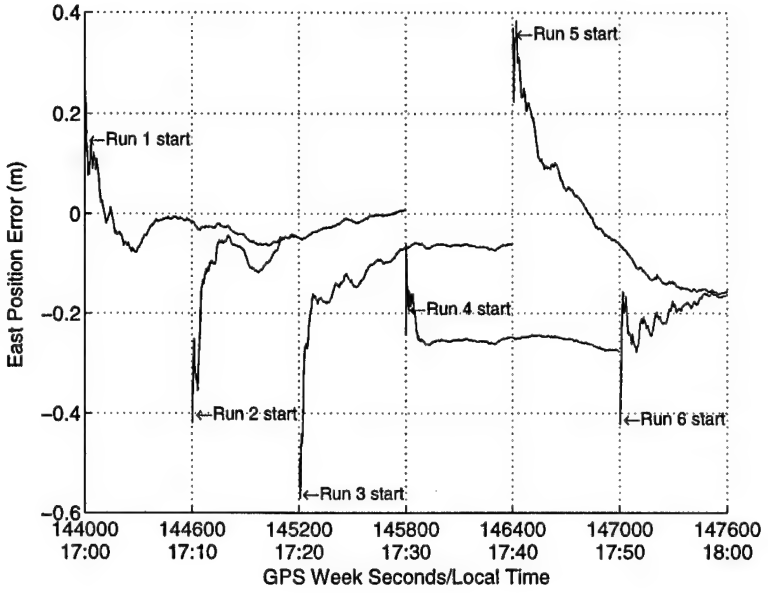

Figure 4.16: *East position error for first six runs of FLYKIN, in floating ambiguity mode, BERG-GEIR baseline, GEIR-164 network*

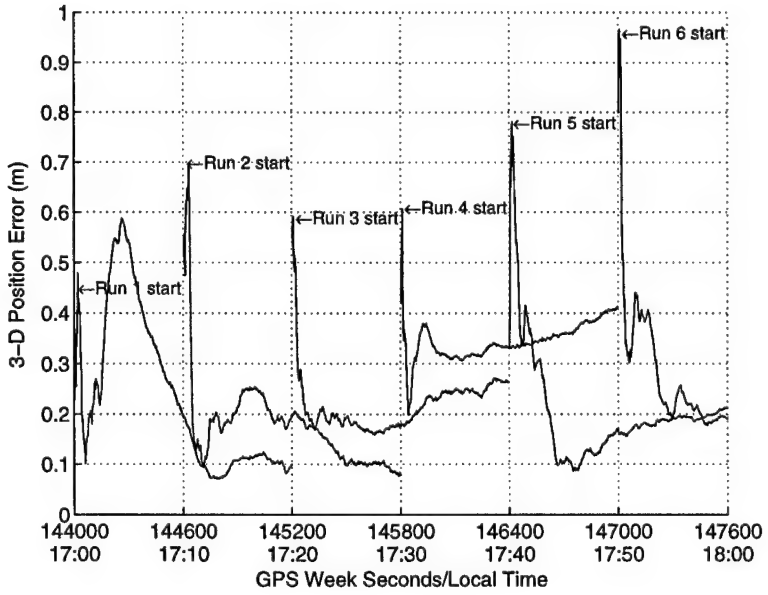

Figure 4.17: *3-D position error for first six runs of FLYKIN, floating ambiguity mode, BERG-GEIR baseline, GEIR-164 network*

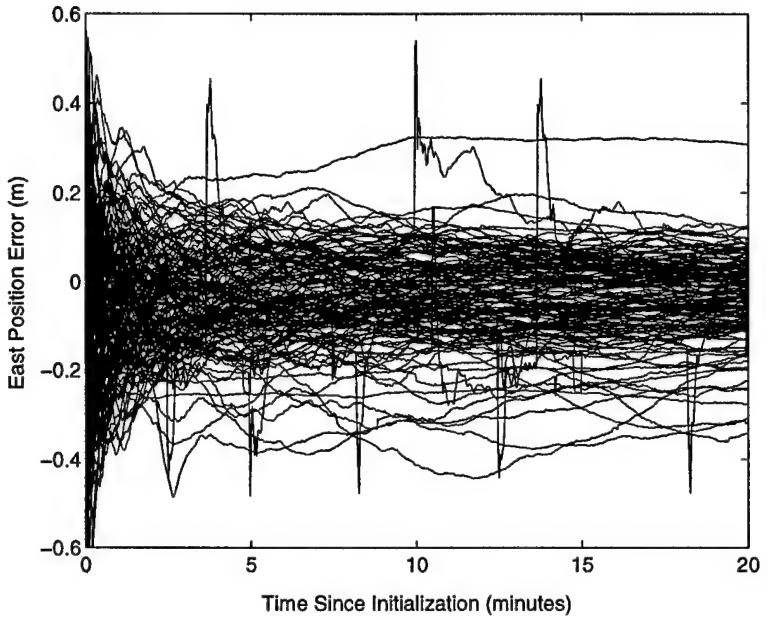

Figure 4.18: *East position error for 138 runs of FLYKIN referenced to initialization time, floating ambiguity mode, BERG-GEIR baseline, GEIR-164 network*

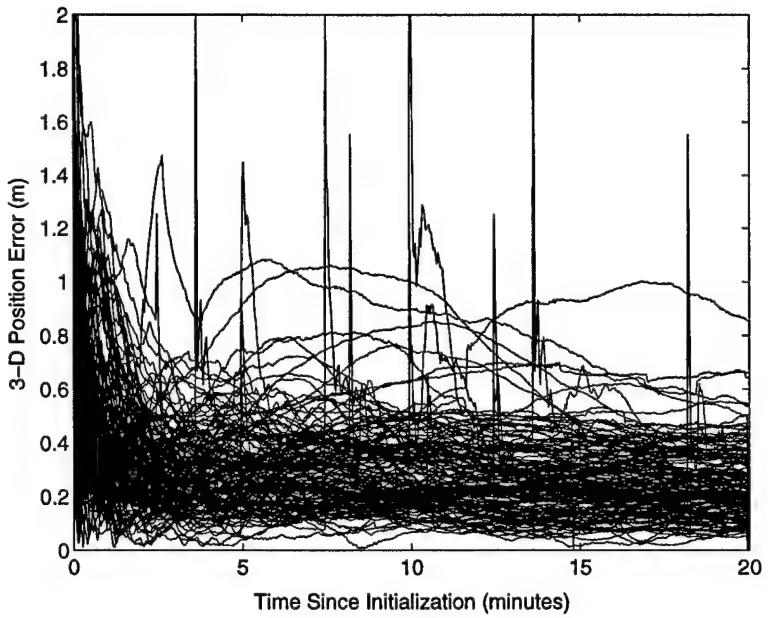

Figure 4.19: *3-D position error for 138 runs of FLYKIN referenced to initialization time, floating ambiguity mode, BERG-GEIR baseline, GEIR-164 network*

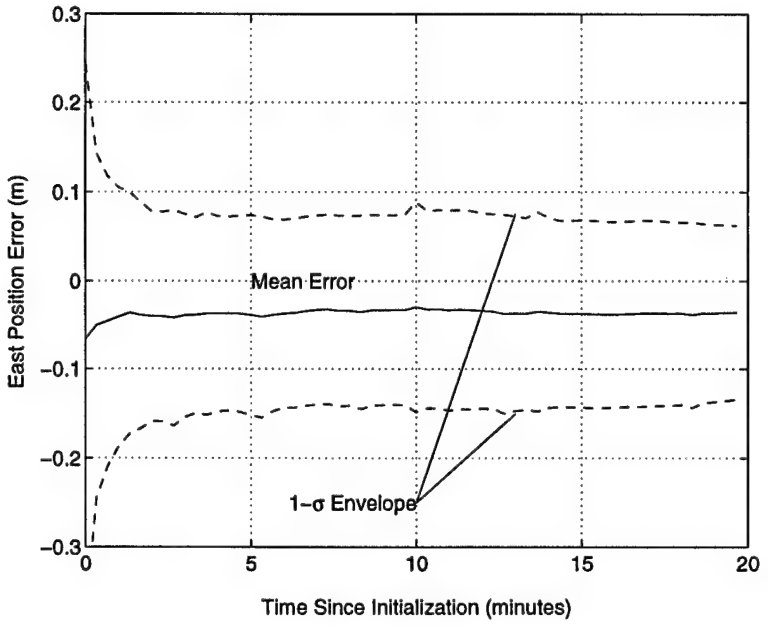

Figure 4.20: *East position error statistics using FLYKIN, floating ambiguity mode, BERG-GEIR baseline, GEIR-164 network*

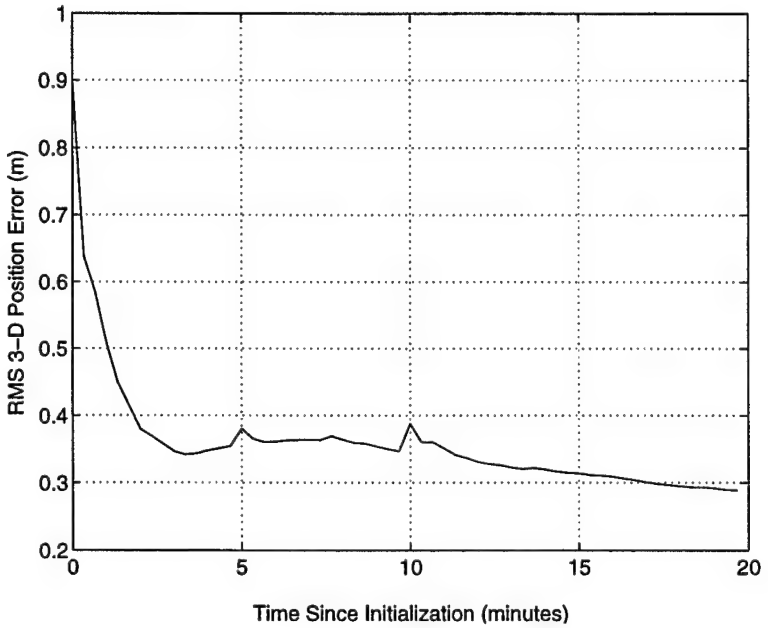

Figure 4.21: *RMS 3-D position error using FLYKIN, floating ambiguity mode, BERG-GEIR baseline, GEIR-164 network*

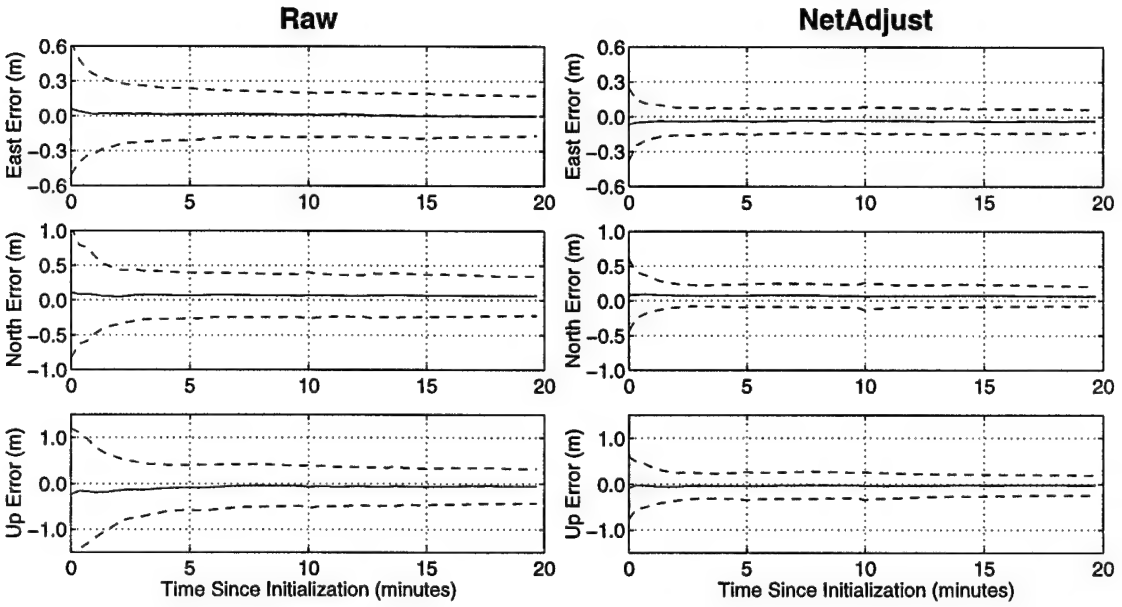

Figure 4.22: FLYKIN mean and 1-σ window position error statistics for BERG-GEIR (164 km) baseline, float mode, L1 phase and L1 code measurements. (NetAdjust corrections generated using GEIR-164 network.)

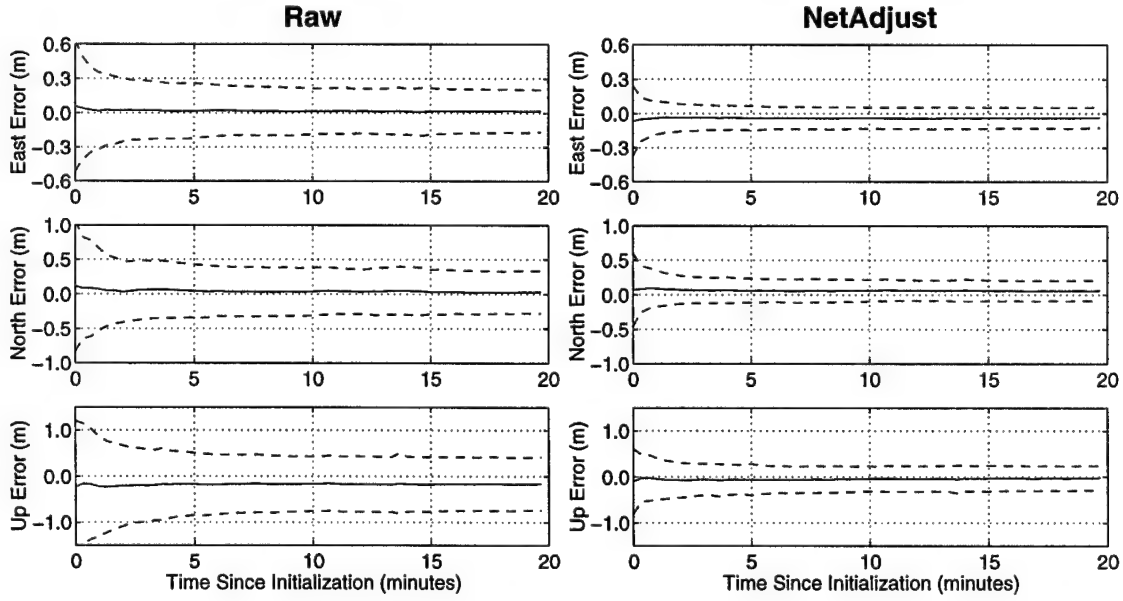

Figure 4.23: FLYKIN mean and 1-σ window position error statistics for BERG-GEIR (164 km) baseline, float mode, WL phase and L1 code measurements. (NetAdjust corrections generated using GEIR-164 network.)

Figure 4.23 shows a similar plot using WL phase measurements. Both of these figures demonstrate the improvement attained through the use of NetAdjust for this particular scenario.

The plots presented in Figures 4.22 and 4.23 only refer to the BERG-GEIR baseline (i.e., the GEIR-164 network). A summary of results for all of the networks is given in Tables 4.9 and 4.10. These tables present the mean and standard deviations of the position errors in each axis for each of the networks. Values are given after 3 minute and 15 minutes initialization time, for both raw and NetAdjust corrected values.

Note that, for these filtered position errors, use of the NetAdjust corrections always reduces the error standard deviation (compared to the raw case), but it is not so effective at removing the bias values. Possible explanations of this are discussed at the end of this section.

Figures 4.24 and 4.25 show the RMS values of the three-dimensional position errors for the 138 test runs after a 15-minute FLYKIN filter initialization period. Figure 4.24 was generated using L1 phase measurements, while Figure 4.25 was generated using WL phase measurements. The values are plotted for the raw measurements (triangles and dashed line), the NetAdjust corrected measurements (circles and solid line). A third line (boxes and dash-dot line) represents the results when using the *raw* L1 code measurements and the *corrected* phase measurements.

Note that correcting only the phase measurements yields almost no improvement for these floating ambiguity tests. This implies that the FLYKIN errors are primarily caused by code errors. This can be understood in terms of what the FLYKIN filter appears to be doing with this set of tuning parameters.

GPS phase measurements are implicitly used in a GPS positioning Kalman filter in two different ways.[12] First, the phase measurements act to smooth out the large, high fre-

[12]The two uses of phase measurements described here are *implicitly* part of the Kalman filter, meaning that the Kalman filter does not explicitly use them twice or in two ways—rather, the phase measurements improve the results in two distinct manners.

Table 4.9: *Mean position errors of 138 FLYKIN iterations after 3 and 15 minutes, float mode, L1 phase and L1 code measurements*

	Init.	Raw Mean Error (m)			NetAdjust Mean Error (m)		
Network	Time	East	North	Up	East	North	Up
ARER-0	3 min	0.056	-0.021	-0.022	-0.031	-0.164	-0.003
ARER-0	15 min	0.023	0.000	-0.017	-0.045	-0.120	0.054
GEIR-29	3 min	0.003	0.028	-0.016	-0.031	0.052	-0.051
GEIR-29	15 min	0.002	0.020	-0.025	-0.033	0.045	-0.046
ARER-67	3 min	-0.059	-0.125	-0.082	-0.033	-0.190	-0.012
ARER-67	15 min	-0.064	-0.111	-0.033	-0.047	-0.157	0.031
STAV-143	3 min	0.003	-0.008	0.003	-0.026	-0.027	0.164
STAV-143	15 min	0.004	-0.027	0.037	-0.018	-0.038	0.111
GEIR-164	3 min	0.021	0.075	-0.132	-0.041	0.067	-0.039
GEIR-164	15 min	0.002	0.066	-0.066	-0.042	0.072	-0.028
GEIR-223-sparse	3 min	0.006	0.105	-0.201	-0.055	0.047	-0.067
GEIR-223-sparse	15 min	-0.013	0.110	-0.116	-0.054	0.046	-0.027
ALES-242	3 min	0.052	-0.172	0.171	0.019	-0.132	0.193
ALES-242	15 min	0.072	-0.182	0.088	0.040	-0.152	0.153

Table 4.10: *Position error standard deviations of 138 FLYKIN iterations after 3 and 15 minutes, float mode, L1 phase and L1 code measurements*

	Init.	Raw Error Std Dev (m)			NetAdjust Error Std Dev (m)		
Network	Time	East	North	Up	East	North	Up
ARER-0	3 min	0.225	0.281	0.452	0.187	0.294	0.423
ARER-0	15 min	0.159	0.115	0.227	0.150	0.160	0.210
GEIR-29	3 min	0.095	0.136	0.236	0.098	0.136	0.243
GEIR-29	15 min	0.075	0.108	0.179	0.077	0.107	0.181
ARER-67	3 min	0.294	0.471	0.663	0.187	0.328	0.510
ARER-67	15 min	0.223	0.288	0.395	0.152	0.201	0.291
STAV-143	3 min	0.205	0.288	0.442	0.215	0.338	0.458
STAV-143	15 min	0.155	0.208	0.321	0.196	0.257	0.326
GEIR-164	3 min	0.243	0.350	0.582	0.109	0.142	0.274
GEIR-164	15 min	0.193	0.300	0.398	0.100	0.147	0.220
GEIR-223-sparse	3 min	0.235	0.390	0.547	0.113	0.171	0.326
GEIR-223-sparse	15 min	0.207	0.295	0.449	0.109	0.156	0.298
ALES-242	3 min	0.231	0.416	0.629	0.209	0.391	0.598
ALES-242	15 min	0.219	0.404	0.517	0.217	0.386	0.484

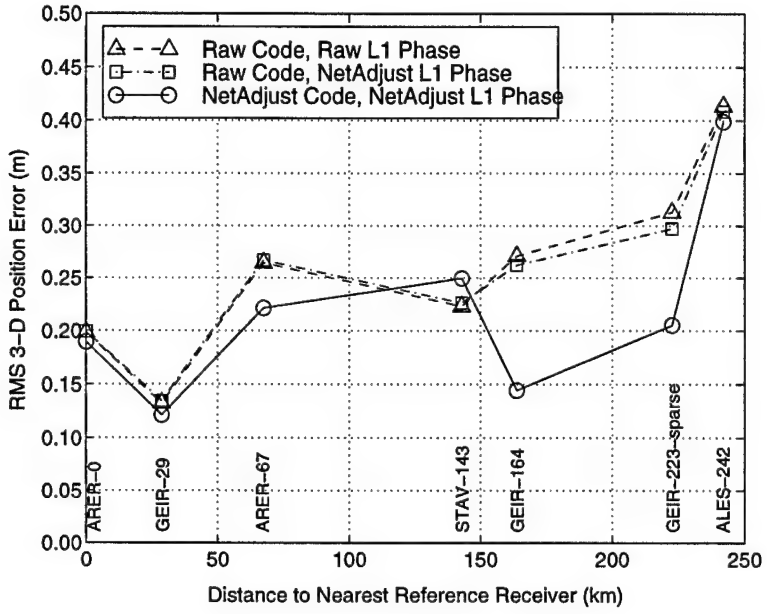

Figure 4.24: *RMS of three-dimensional position error for 138 iteration of FLYKIN, floating mode, L1 phase and L1 code measurements, 15 minute filter initialization time*

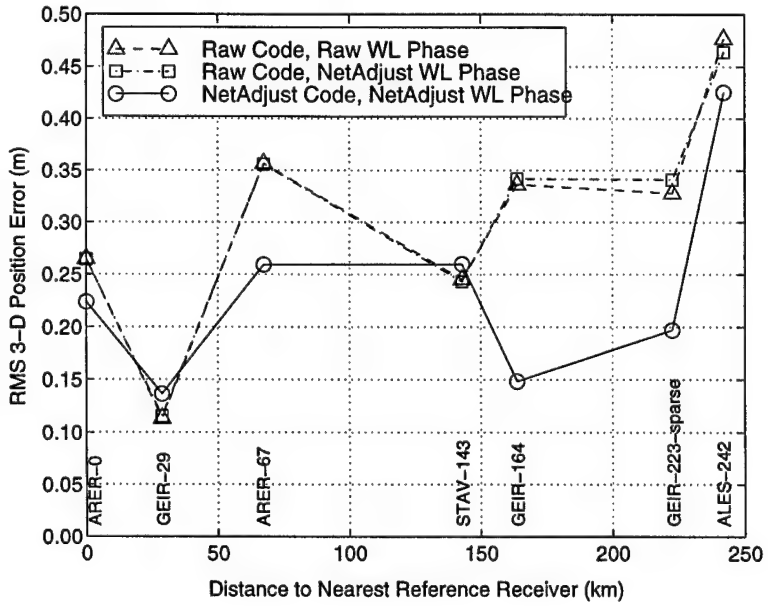

Figure 4.25: *RMS of three-dimensional position error for 138 iteration of FLYKIN, floating mode, WL phase and L1 code measurements, 15 minute filter initialization time*

quency errors in the code measurements (i.e., multipath and noise). This effect is known as carrier-phase smoothing of the code (Hatch, 1982), and benefits are gained after a very short period of time (on the order of minutes).

The second way carrier-phase measurements can improve positioning accuracy is more subtle, and it hinges on the idea that the ambiguities are *by definition* constant values. As the geometry of the satellite constellation changes over time, only one set of ambiguities (the true ones) fit the data. The longer the observation interval, the greater the observability of the carrier-phase ambiguities (and therefore position). It is even possible to attain centimetre level accuracies without the use of any code measurements using this approach, as in Cannon (1990). Because this effect depends upon changes in the satellite constellation, more time is required before positioning improvements are gained from this effect, when compared to carrier-phase smoothing of the code.

It appears from the performance of the FLYKIN filter in float mode (with the tuning parameters described above) essentially uses the phase measurements to smooth the code (the first use), but not to improve observability of the position (the second use). This assertion is backed up by the error plots in Figures 4.22 and 4.23, which show that the filter has reached steady state within 2–3 minutes. This time period is enough for carrier-phase smoothing, but not long enough for accurate ambiguity determination from changing satellite geometry.

Carrier-phase smoothing of the code does not significantly benefit in the short term from the improved phase accuracy gained by NetAdjust, because carrier-phase smoothing uses the phase *difference* over time to generate the corrections. Any low frequency[13] error in the phase measurement will have no effect on the carrier-phase smoothing results (other than to generate a slightly different ambiguity estimate, which cancels out in the positioning). NetAdjust generates absolute corrections which will yield only marginal improvements in the time differenced carrier-phase values, which means that NetAdjust

[13]Low frequency errors here imply a time constant on the order of approximately 5 minutes or more.

will not significantly improve carrier-phase smoothing results.[14]

Note that the RMS errors for the NetAdjust case (identified by circles/lines) in Figures 4.24 and 4.25 closely match the pattern of the NetAdjust corrected code-only differential positioning errors presented in Section 4.1.4 (Figure 4.13 on page 137). This again demonstrates that the errors in the FLYKIN floating solutions are dominated by the code measurement errors.

4.1.6 Effect of NetAdjust on Ambiguity Fixing

For this test, the FLYKIN software package was used to test the effect of NetAdjust on carrier-phase ambiguity resolution. The NetAdjust method enhances the ambiguity resolution process by reducing the differential errors, and such a reduction will aid *any* ambiguity resolution software package. The goal of this chapter, then, is not primarily to establish absolute performance levels when using NetAdjust, but rather to show the performance *improvement* resulting from the NetAdjust corrections relative to the raw (uncorrected) performance.

4.1.6.1 FLYKIN Ambiguity Resolution Algorithm

Understanding the algorithms used in the FLYKIN is essential to interpret the results in this section properly. The FLYKIN software combines the floating ambiguity Kalman filter described in Section 4.1.5 with the Fast Ambiguity Search Filter (FASF) described in Section B.1.1.1.5 on page 243. The FASF algorithm is essentially an efficient way to determine the integer ambiguity search space[15] using the information contained in the

[14] Also, to limit the effects of code-carrier divergence (caused by the ionosphere having opposite effects on the code and carrier-phase measurements), filters implementing carrier-phase smoothing of the code (either implicitly or explicitly) need to have short time constants. As a result, the code smoothing never completely converges to the carrier-phase values, and small differences (or corrections) in the phase measurements do not have a significant effect.

[15] The search space refers to the set of candidate integer ambiguity combinations, one of which is correct.

state covariance matrix generated by the Kalman filter. After determining the ambiguity search space, FLYKIN attempts to identify the correct ambiguity set from all of the sets in the search space. There are two ways that this identification can occur:

1. If there is only one candidate ambiguity set generated by FASF, then that one is deemed correct.

2. If there are multiple candidate ambiguity sets, then the ambiguity set which has the lowest residuals is chosen, *if* the ratio of the sum of squares of the residuals from this set to the sum of squares of the residuals from the next best set exceeds a prespecified threshold. This assures that an ambiguity set will not be chosen unless it stands out as being significantly better than all of the other candidate ambiguity sets. Note that the *phase* measurement residuals are the ones used for this ratio check.

Using NetAdjust to reduce the differential errors can then help the ambiguity resolution process of FLYKIN in two different ways. First, by having more accurate code measurements (and more accurate phase measurements to a lesser extent), the ambiguity search space will be made smaller and more accurate, which facilitates easier identification of the correct ambiguity. Secondly, more accurate phase measurements will improve the ability to distinguish the correct ambiguity set when using the ratio test. If the differential errors are small, then the correct ambiguity set will yield very small residuals, which make it easy to identify. As the differential phase errors grow, however, the residuals grow as well, and the correct set becomes indistinguishable from the other sets.

The emphasis of this research is to improve the ability to perform carrier-phase ambiguity resolution by reducing the phase errors (although the code errors are estimated and removed as well). As described above, any improvement in FLYKIN performance could be attributed to a combination of the improvement in the phase and the code measurements.

It is desirable to determine the impact of the NetAdjust phase measurement corrections on FLYKIN apart from the code corrections. To this end, a comparison is made between *three* different sets of results throughout this section, including

- Results using raw L1 code and raw phase measurements. These are called the *raw* results.
- Results using raw L1 code and NetAdjust-corrected phase measurements. (These results demonstrate the impact of phase measurement corrections only). These are called the *NetAdjust phase only* results.
- Results using NetAdjust-corrected L1 code and NetAdjust-corrected phase measurements. These are called the *NetAdjust* results.

4.1.6.2 Test Methodology

The iterative process (involving 138 FLYKIN runs) described in Section 4.1.5 was used here, only FLYKIN attempted to determine the integer ambiguities at each measurement epoch. As soon as a set of ambiguities was chosen (either by being the only one in the search space or by passing the ratio test), then the solution time and the ambiguity values were recorded, and the next iteration was begun. After all iterations were complete, the stored ambiguities were compared against the precalculated[16] ambiguities for that baseline to determine if they were correct. This analysis procedure was performed for L1 ambiguities and WL ambiguities, for each of the seven test networks, and for each of the three types of corrections (raw, NetAdjust phase only, and NetAdjust). As in the floating ambiguity case, a maximum of 20 minutes was allowed for resolving ambiguities.

Figure 4.26 is a bar chart showing, for each of the 138 runs, the time required to resolve the WL phase ambiguities between the BERG and GEIR receivers using raw data. Only the correct ambiguity solutions are plotted. Figure 4.27 shows the results after the

[16]This is described in Appendix B

NetAdjust corrections were applied to the BERG data. Note that the use of NetAdjust reduced the time required to resolve the ambiguities *and* increased the number of correct ambiguities.

Throughout the rest of this section, the results will be presented in terms of three performance measures which summarize the overall performance of the FLYKIN algorithm. The first performance measure is the **percentage of correct fixes**, which refers to the percentage of the 138 iterations that yielded a correct fixed ambiguity solution. For example, 94 correct ambiguities are represented in Figure 4.26, which means that the percentage of correct fixes in this case was 68.1% (100×94/138). Good performance results in a high percentage of correct fixes.

The second performance measure is the **percentage of incorrect fixes**, defined as the percentage of the 138 iterations where FLYKIN generated a fixed ambiguity solution, but it was incorrect. Figure 4.26 shows only the 94 runs in which the correct ambiguities were calculated. Of the remaining 44 runs, 18 were incorrect, yielding a percentage of incorrect fixes value of 13.0% (100×18/138). (No solutions were obtained for the remaining 26 runs). Good performance results in a low percentage of incorrect fixes.

The third and final performance measure is the **mean time to fix**, which is defined as the average time required to determine the ambiguities which were calculated correctly. Any incorrect ambiguities are not included in the mean time to fix. The results presented in Figures 4.26 and 4.27 had mean time to fix values of 4.1 minutes and 2.7 minutes, respectively. Good performance results in a low mean time to fix.

Each of these performance measures will be presented in the sections that follow.

4.1.6.3 Analysis of Percentage of Correct Fixes

Figure 4.28 shows the percentages of good fixes for the L1 phase ambiguities over the seven test networks. The raw results are presented using triangles and dashed lines, the NetAdjust phase only results are presented using squares and dash-dot lines, and the complete NetAdjust results are presented using circles and solid lines. This plot shows that

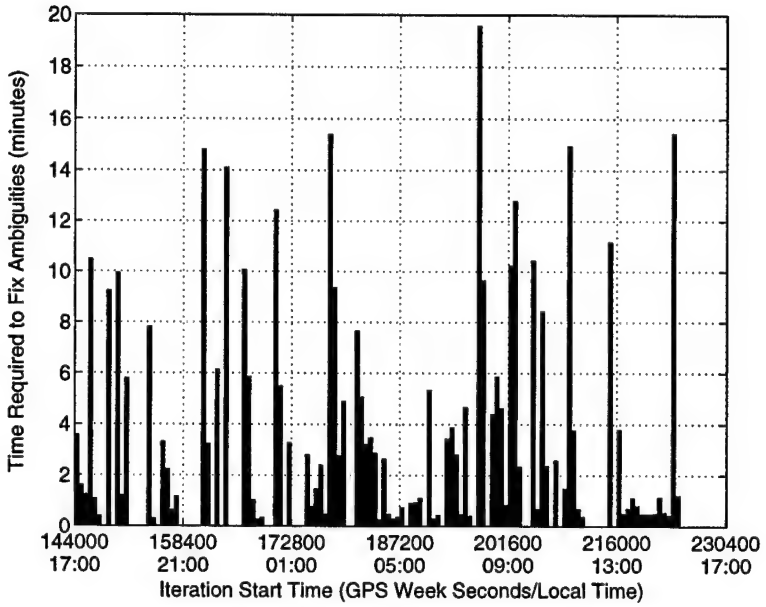

Figure 4.26: *Time required to resolve WL ambiguities for 138 iterations, BERG-GEIR baseline (164 km), raw data (only correct ambiguities plotted)*

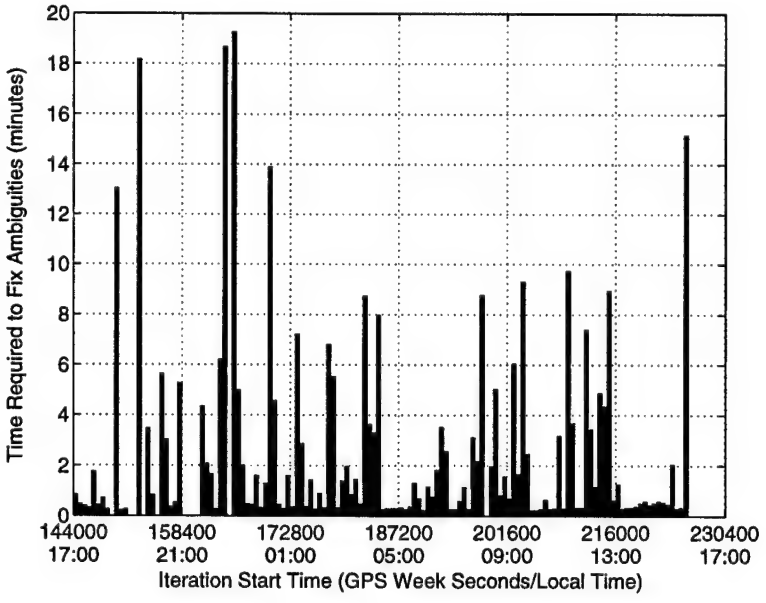

Figure 4.27: *Time required to resolve WL ambiguities for 138 iterations, BERG-GEIR baseline (164 km), NetAdjust data, GEIR-164 network (only correct ambiguities plotted)*

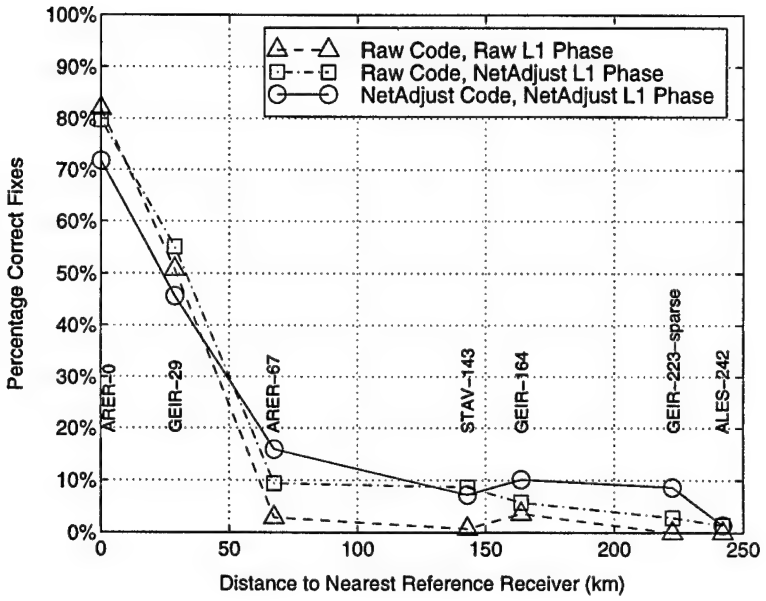

Figure 4.28: *Percentage of correct fixes for L1 ambiguities over seven test networks*

the L1 ambiguities were almost never determined correctly for baselines greater than 50 km when using the raw data. The NetAdjust (and NetAdjust phase only) results show a slight improvement to around 10% correct ambiguities, but this is still very poor from an absolute performance perspective. These results indicate that the L1 phase NetAdjust corrections generated from the Norway network were not sufficiently accurate enough to resolve the phase ambiguities reliably using FLYKIN. This is due primarily to the large distances between the reference stations in the Norway network. Note that the L1 phase errors were reduced by NetAdjust (see Figure 4.8 for example), but enough error still remained after the corrections to inhibit the ambiguity resolution process. These results are discussed further in Chapter 5.

The percentages of correct fixes for the WL phase ambiguities are shown in Figure 4.29. Here, the percentage of correct fixes when using raw measurements decreases from nearly 100% over short distances to around 50% at 242 km. In contrast, the NetAdjust results show a fairly consistent 90% correct fixes until the last reference network.

It is not surprising that the last network (ALES-242) has poor results even with NetAdjust, because in addition to the long distance between the mobile and reference re-

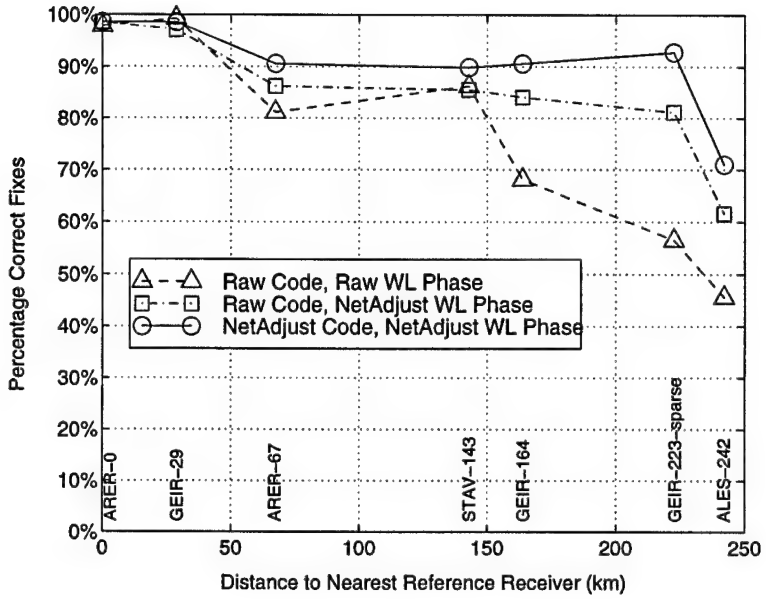

Figure 4.29: *Percentage of correct fixes for WL ambiguities over seven test networks*

ceivers, the network geometry is poor. The bulk of the Norway network is located far to the southeast of the ALES receiver, and the one network reference receiver located to the north (TRON) may have been less useful, due to the difficulty in calculating the network ambiguities between TRON and the other receivers resulting from the long baselines involved.

Note that the NetAdjust phase only results are only slightly inferior to the full NetAdjust results, and that they follow a similar patter. Clearly the majority of the improvement from using NetAdjust is a direct result of the phase measurement corrections.

4.1.6.4 Analysis of Percentage of Incorrect Fixes

Figure 4.30 shows the percentage of incorrect L1 ambiguities for each of the seven test networks. The NetAdjust corrections provide an overall reduction in the percentage of incorrect fixes. As before, these L1 results were not as notable as the WL results which are shown in Figure 4.31. Here, the percentage of incorrect fixes grows to between 10%–15% for the raw case, but it consistently stays at or below 5% for the NetAdjust case.

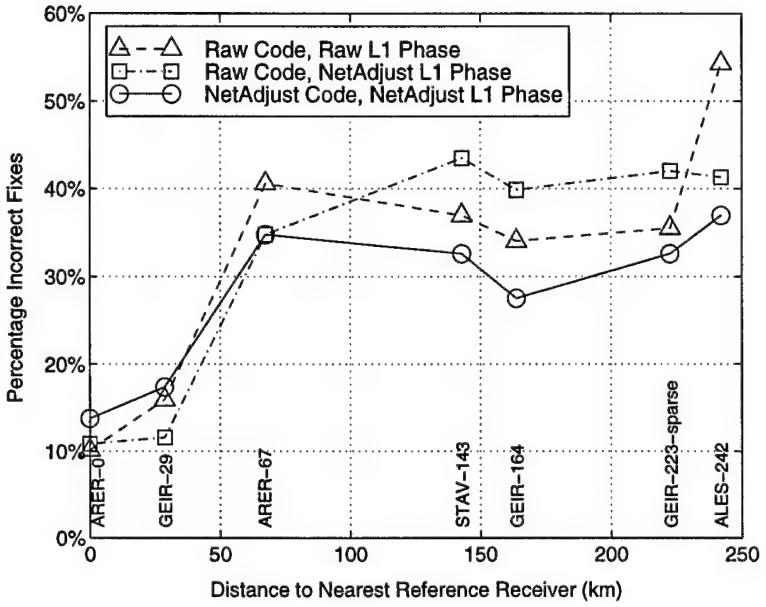

Figure 4.30: *Percentage of incorrect fixes for L1 ambiguities over seven test networks*

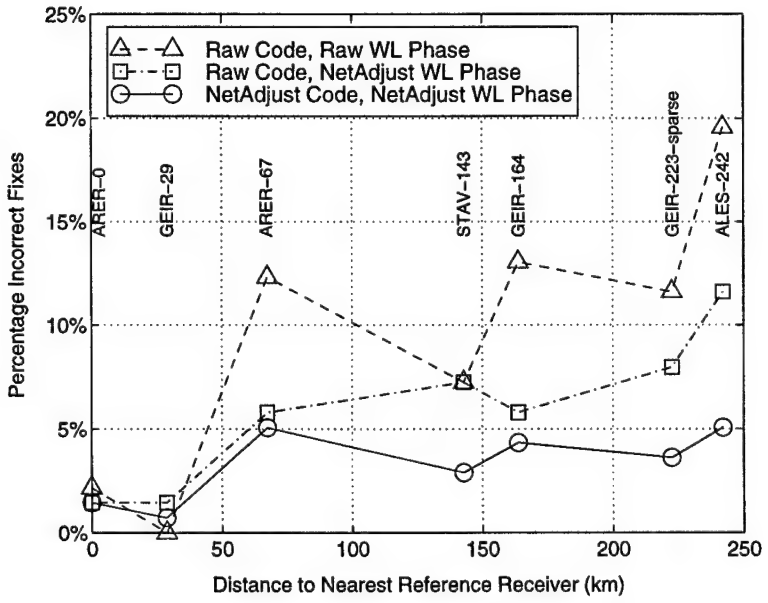

Figure 4.31: *Percentage of incorrect fixes for WL ambiguities over seven test networks*

Again, the NetAdjust phase only results are between the NetAdjust and the raw results, and they track the trends in the NetAdjust results.

It should be noted that the high percentage of incorrect fixes in the L1 case (both raw and NetAdjust) is partly due to the fact that FLYKIN is not currently tuned to calculate L1 ambiguities beyond a 50 km baseline.[17] This percentage could be reduced, if desired, by using different filter tuning and more robust algorithms for flagging incorrect ambiguities.

4.1.6.5 Analysis of Mean Time to Resolve Ambiguities

Figure 4.32 shows the mean time to resolve the WL ambiguities for each of the seven test networks. (A plot for the L1 ambiguities is not given, because so few ambiguities were resolved correctly). The NetAdjust results show a significant reduction in the time to resolve the WL ambiguities when compared with the raw results, and the NetAdjust improvement grows as the network length increases. Note that once again, the NetAdjust phase only results closely follow the full NetAdjust results.

4.1.6.6 Summary of Ambiguity Resolution Results

The preceding sections have shown that use of the NetAdjust corrections significantly improves each of the performance measures for the WL ambiguities. In general, the performance level when using NetAdjust at 200 km mobile/reference receiver separations was similar to the performance level when using the raw measurements over a 50 km separation. A significant portion of this improvement can be attributed to the WL phase measurement corrections.

The L1 results show that Norway network and the NetAdjust corrections generated from it are not sufficient for reliable L1 carrier-phase ambiguity resolution, unless the user is very close to one of the reference receivers. It would be useful to determine if

[17] In fact, some versions of FLYKIN do not even attempt to resolve the L1 ambiguities if the mobile/reference receiver separation exceeds 50 km.

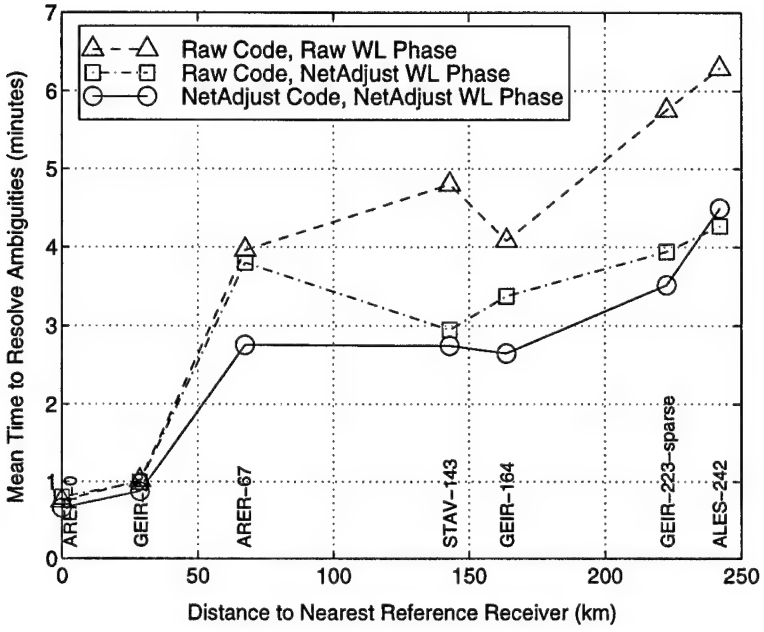

Figure 4.32: *Mean time to resolve WL ambiguities over seven test networks*

a more densely populated reference receiver network would make reliable L1 ambiguity resolution possible. The covariance analysis technique is used in Chapter 5 to help answer this question.

4.2 Holloman Network Performance Analysis

Analysis of the application of NetAdjust in a completely different network is presented here to demonstrate that NetAdjust can yield positive results in a variety of conditions. Data from the Holloman network was used for preliminary testing of the NetAdjust concept, and the results are based on an older, less refined NetAdjust algorithm (specifically a different covariance function). These results are still useful, however, because they show that the NetAdjust algorithm is effective even if the covariance $\boldsymbol{C}_{\delta\ell}$ is not very accurate.

The Holloman network consisted of four reference receivers and three mobile receivers. Data was collected over a nine hour period at a one Hz rate. The positions of the reference receivers and the trajectory of the mobile receivers are shown in Figure 4.33. A

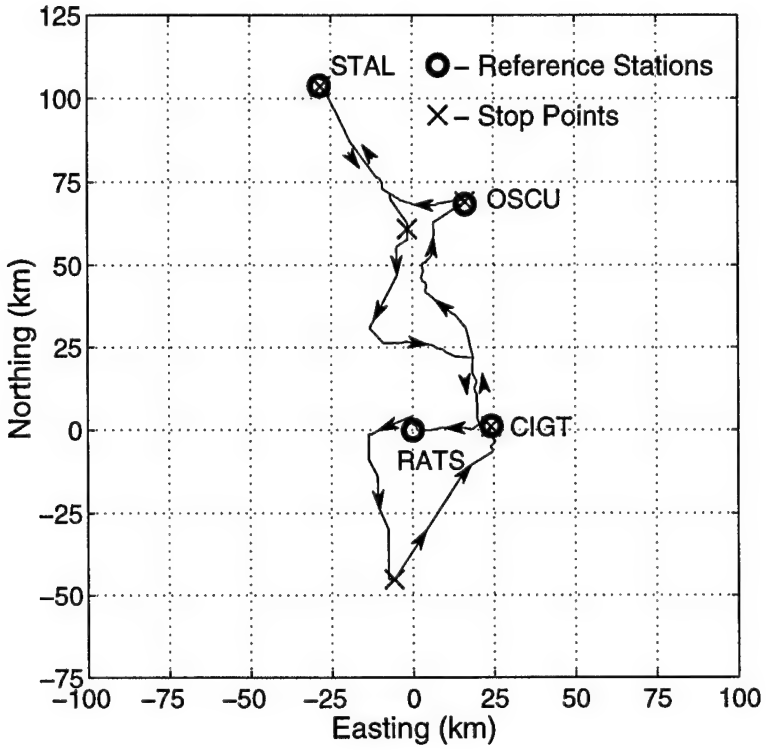

Figure 4.33: *Holloman network configuration and van test route*

detailed description of the test configuration is given in Appendix A.

4.2.1 Description of Covariance Function Used for Holloman Network

The covariance function described in this section is completely different from the more refined covariance function used on the Norway network (and described in Chapter 3). The notation used to describe the Holloman covariance function is therefore intentionally different from the Norway covariance function, in order to avoid confusion. A more detailed description of the Holloman covariance function can be found in Raquet (1997).

The Holloman network covariance function for calculating the covariance term between a measurement from receiver a and satellite x and another measurement from re-

ceiver b and satellite y is

$$E[\delta\phi_a^x \delta\phi_b^y] = \underbrace{c_1^2 \mu_x \mu_y \Omega_{x,y} (\Delta'_a \cdot \Delta'_b)}_{\text{correlated term}} + \underbrace{\delta_{ab} \mu_x \mu_y \sigma^2_{\text{uncorrelated}_{a,b}}}_{\text{uncorrelated term}}. \tag{4.5}$$

Each term in this equation will be explained in the paragraphs that follow.

Correlated term. In this term, c_1 is a scaling constant. (All c_x terms are constants, with values given in Table 4.11). μ_x and μ_y are mapping functions for satellites x and y which increase the magnitude of the correlation at low satellite elevations:

$$\begin{aligned} \mu_x &= e^{\frac{c_2}{\text{elev}_x - c_3}} - c_4 \\ \mu_y &= e^{\frac{c_2}{\text{elev}_y - c_3}} - c_4 \end{aligned} \tag{4.6}$$

(elevation is in degrees).

The $\Omega_{x,y}$ function decorrelates measurements from satellites that are in different directions:

$$\Omega_{x,y} = \mathrm{e}^{-c_5 D_{x,y} \mu_x \mu_y}, \tag{4.7}$$

where $D_{x,y}$ is the "angular distance" between satellites x and y, calculated by

$$D_{x,y} = \arccos\{\sin(\text{elev}_x)\sin(\text{elev}_y) + \cos(\text{elev}_x)\cos(\text{elev}_y)\cos(\Delta\text{azim})\}, \tag{4.8}$$

where Δazim is the difference in azimuth between satellites x and y.

Finally, the term $(\Delta'_a \cdot \Delta'_b)$ is the dot product of rescaled vectors from the computation point ($\boldsymbol{p}_{cp}$) to the positions of receivers a and b ($\boldsymbol{p}_a$ and $\boldsymbol{p}_b$), expressed in local level (east-north-up, abbreviated as e,n,u) coordinates:

$$\begin{aligned} \Delta'_a &= \begin{bmatrix} c_6\Delta_{a_e} & c_7\Delta_{a_n} & c_8\Delta_{a_u} \end{bmatrix} \\ &= \begin{bmatrix} c_6(p_{a_e} - p_{cp_e}) & c_7(p_{a_n} - p_{cp_n}) & c_8(p_{a_u} - p_{cp_u}) \end{bmatrix} \end{aligned} \tag{4.9}$$

$$\begin{aligned} \Delta'_b &= \begin{bmatrix} c_6\Delta_{b_e} & c_7\Delta_{b_n} & c_8\Delta_{b_u} \end{bmatrix} \\ &= \begin{bmatrix} c_6(p_{b_e} - p_{cp_e}) & c_7(p_{b_n} - p_{cp_n}) & c_8(p_{b_u} - p_{cp_u}) \end{bmatrix}. \end{aligned} \tag{4.10}$$

Table 4.11: *Values for constants used in Holloman covariance function*

Constant	Value
c_1	5×10^{-7}
c_2	5
c_3	4
c_4	0.06
c_5	1.0
c_6	1.0
c_7	1.2
c_8	100.0

The rescaling constants c_6, c_7, and c_8 provide for the fact that the amount of correlated error is a function of both the magnitude and direction of the distance between the two receivers. For example, the correlated error introduced by an offset of 100 m in the vertical direction would probably be much larger than the correlated error introduced by an offset of 100 m in the east or north directions.

Note that the dot product will give covariance characteristics that are similar to the covariance function derived in Chapter 3 (see Equation 3.166). For example, if the computation point is located a large distance from two receivers that are relatively close to each other, then the corresponding covariance element will be large for both covariance functions. Likewise, if the computation point is close to one of the reference receivers but far from the other, the covariance element will be small for both covariance functions. While similar, the two covariance functions are not the same, and the one presented in Chapter 3 is considered superior because it is based upon a precise definition of the differential errors and the definition of a covariance matrix.

Uncorrelated term. The uncorrelated term in Equation 4.5 is defined as follows:

$$\delta_{ab} = \begin{cases} 0 & \text{if } a \neq b, \\ 1 & \text{if } a = b. \end{cases} \tag{4.11}$$

$$\sigma^2_{\text{uncorrelated}_{a,b}} = (\sigma^2_{\text{noise}_a} + \sigma^2_{\text{noise}_b} + \sigma^2_{\text{multipath}_a} + \sigma^2_{\text{multipath}_b}), \tag{4.12}$$

where $\sigma^2_{\text{noise}_a}$, $\sigma^2_{\text{noise}_b}$, $\sigma^2_{\text{multipath}_a}$, and $\sigma^2_{\text{multipath}_b}$ are the nominal variances of the measurement noise and the multipath for receivers a and b.

4.2.2 Holloman Network Test Methodology

The primary goal of this test was to determine how much, if any, the NetAdjust method would improve the ability to perform carrier-phase ambiguity resolution for the mobile receivers. First, the raw (uncorrected) measurement data was used to establish a baseline level of performance. The University of Calgary FLYKIN software (Lachapelle et al., 1992) was used to calculate the ambiguities in kinematic mode for all of the results that follow.

The ability to perform carrier-phase ambiguity resolution successfully depends upon many different time-varying factors (such as multipath), so a large sample size is required to obtain a statistically valid indication of improved performance. A total of 87 FLYKIN samples were generated for each mobile receiver using the following iteration procedure:

1. Set start time to the beginning of the run.
2. Run FLYKIN until the ambiguities are determined, or the time exceeds a maximum time (30 minutes past the start time).
3. At the point that the ambiguities are determined (or the maximum time is exceeded), use these ambiguities to calculate the position of the mobile receiver.
4. Save the run start time, fix time, and fix position to a data file as one sample.

5. Increment the start time by six minutes. If not at the end of the run, go back to step 2.

The above procedure was repeated for each of the three mobile receivers and the results were combined to give a total of 261 samples for each set of runs.

The correctness of each integer ambiguity solution was evaluated by comparing the position saved at the end of the run with the "truth" position at the matching time. If the magnitude of the 3-dimensional error of a fixed ambiguity position relative to the truth was less than 2/3 of the ambiguity wavelength, then the ambiguity was deemed to be correct. Because the truth data was not always accurate (as described above), this method is only an approximate measure of the correctness of the ambiguities.

4.2.3 Holloman Network Test Results

In order to investigate various aspects of the NetAdjust algorithm as applied to this particular test, a number of different run sets were accomplished, varying the following parameters:

- Mobile receiver used (Ashtech, NovAtel1, NovAtel2)
- Type of ambiguities resolved (L1 or widelane)
- Whether the corrections were applied (Raw or NetAdjust)
- Reference receiver used (the closest receiver at the start of each iteration, CIGT only, RATS only, STAL only, or OSCU only)
- FLYKIN filter tuning (default, tuned for network)

It would be confusing to present all of the above variations simultaneously, so all results presented will be averages for each of the three mobile receivers.

4.2.3.1 Results When Using Closest Reference Receiver

Table 4.12 shows a summary of results when the reference receiver used was the receiver that was closest to the mobile receiver at the start of each iteration. It compares the results when the uncorrected (raw) reference data is used with the results when the NetAdjust corrections are applied. If there were no network algorithm available, it would make sense to use the reference station closest to the mobile receiver when performing ambiguity resolution. This table represents the best that can be done using the four receivers *without* using a network algorithm for the uncorrected (raw) case.

The first column of Table 4.12 shows the frequency used in the ambiguity resolution (L1 or widelane), and the second column shows whether or not the NetAdjust corrections were applied. The percentage of good fixes is the percentage of tests in which FLYKIN solved for the correct ambiguity set. The mean time to fix represents the average time it took to fix the ambiguities for those that were correct. As explained above, each line in this table represents results from 261 separate runs of the FLYKIN program.

It is clear that the use of the NetAdjust corrections improved the results when using the closest reference receiver to perform the double-differencing. In the L1 case, there was a 12% increase in the number of good fixes, and the mean time to fix was reduced by 12% when the NetAdjust corrections were applied. Results were even better for the WL case, in which there was a 15% increase in the number of good fixes and a 19% reduction in the mean time to fix. Note that under operational conditions, the NetAdjust method would not use the closest reference receiver, but would just choose any one reference receiver and stay with it (as in the next section). The purpose of Table 4.12 is to show the improvement using NetAdjust when the baselines are relatively short, as is the case when the nearest reference receiver is selected. Under these conditions, the uncorrelated errors (multipath and measurement noise) tend to dominate.

Based upon past experience with ambiguity resolution (and the results presented for the Norway network), the mean time to fix values were surprisingly high, especially for

Table 4.12: Holloman network results when using closest reference receiver

Freq	Network Corrections Applied to Ref Data	Pct Good Fixes	Mean time to fix (minutes)
L1	None (Raw)	31.8%	15.03
L1	NetAdjust	44.1%	13.28
WL	None (Raw)	58.2%	12.44
WL	NetAdjust	73.2%	10.12

the widelane case. (The percentage of good fixes seems slightly low as well). The same raw data sets were processed in an identical manner using the Ashtech PNAV™ software in widelane mode, resulting in 60.3% good fixes with a mean time to fix of 14.21 minutes. These results are very similar to the FLYKIN results shown in Table 4.12, which would imply that the long time to fix values are reasonable for this particular data set.

4.2.3.2 Results When Using Single Reference Receiver

Table 4.13 shows the results for runs in which a single reference receiver was used throughout the 9-hour mission (as opposed to selecting the closest receiver). For these runs, the baseline length between the mobile and the reference receiver could be as large as 150 km.

There are a number of observations that can be made about the results shown in Table 4.13. First, there was a dramatic improvement in the percentage of good fixes when the NetAdjust corrections were applied in the L1 cases. This makes sense, because L1 ambiguity resolution is highly sensitive to even small systematic errors that arise with longer baselines. These results show how helpful the network approach can be for solving ambiguities over long baselines. Also, note that while there were substantial improvements in the percentage of good fixes in the widelane cases, there was also a significant reduction in the mean time to fix.

Table 4.13: *Holloman network results when using a single reference receiver for the entire 9 hour test*

Freq	Ref Station Used	Network Corrections Applied to Ref Data	Pct Good Fixes	Mean time to fix (minutes)
L1	CIGT	None (raw)	15.9%	17.49
L1	RATS	None (raw)	8.0%	16.39
L1	STAL	None (raw)	15.9%	14.42
L1	OSCU	None (raw)	13.5%	15.47
L1	CIGT	NetAdjust	40.6%	14.24
L1	RATS	NetAdjust	29.9%	14.89
L1	STAL	NetAdjust	36.8%	14.37
L1	OSCU	NetAdjust	39.9%	14.57
WL	CIGT	None (raw)	71.7%	9.99
WL	RATS	None (raw)	62.8%	12.41
WL	STAL	None (raw)	59.4%	12.90
WL	OSCU	None (raw)	39.9%	14.93
WL	CIGT	NetAdjust	70.5%	9.70
WL	RATS	NetAdjust	78.5%	9.58
WL	STAL	NetAdjust	79.7%	8.92
WL	OSCU	NetAdjust	74.0%	8.73

Finally, when the NetAdjust corrections were applied, the results were very similar between each of the reference receivers for both the L1 and widelane cases. This demonstrates that once the NetAdjust corrections are applied to each of the reference receivers, *any* one of the corrected reference receivers can be used to get the benefit of the entire network (see Section 3.5.2). Variations that do exist between the corrected values in Table 4.13 are primarily due to the reference receivers not always tracking the same number of satellites. The most notable difference between the results for the corrected receivers was the L1 results from the "RATS" reference station, which had only a 30% fix rate. This can be explained by the fact that, for a reason unknown at this time, the "RATS" reference receiver consistently tracked fewer satellites than the other reference receivers during this test, as shown in Table 4.14.

4.2.3.3 Effect of Filter Tuning

The Holloman network results presented thus far were generated using the FLYKIN filter with a standard set of tuning parameters (see Section 4.1.5). The version of FLYKIN[18] used for the Holloman network has an adaptive noise algorithm which increased noise values as the distance between the reference and mobile receivers increases, in order to account for the increased error over long baselines. Some other ambiguity resolution software packages attempt to model atmospheric errors rather than increase noise values. The net result of either of these approaches (increasing noise or modeling) is that the filter ambiguity state variances decrease more slowly than they would in a short baseline case, resulting in a longer time to resolve the ambiguities (if they can be resolved at all). This is necessary for the standard two-receiver case, because the errors really do grow as the baseline distance increases.

For a carrier-phase network, however, the errors should not grow significantly with

[18]The Norway network data was processed using the standard version of FLYKIN. The Holloman data was processed by a modified version of FLYKIN called SFLY, developed by Weisenburger (1997).

Table 4.14: *Average number of tracked satellites for Holloman network*

Reference Station	Average Number of Tracked Satellites
CIGT	8.34
RATS	6.70
STAL	8.19
OSCU	8.11

distance (as long as the mobile receiver is within the area covered by the network). As a result, when using NetAdjust, the filter tuning parameters should be adjusted to reduce this baseline distance dependency in order to achieve improved performance.

In order to test this concept, the calculated distance between the reference and mobile receivers was divided by 4 in the FLYKIN software before using it to calculate the noise values. This would effectively reduce the distance dependency of the filter noise terms by a factor of 4 in order to "tune" the filter for the network. While this approach is not optimized in any way, it did result in significant performance improvements for the L1 case as shown in Table 4.15. Results in this table are given for the case in which a single reference receiver was used for the entire 9-hour test, as in Table 4.13, except that the values are also averaged between the reference receivers. (For example, the first line in Table 4.15 is an average of the first four lines of Table 4.13).

For the L1 case, tuning the filter for the network increased the percentage of good fixes and decreased the mean time to fix (by 14%) when the network was used. However, when the network was not used, tuning the filter for the network did not yield a performance improvement (as expected).

It is interesting to note that tuning the filter for the network in the widelane case did not have a significant impact on the results regardless of whether or not network corrections were applied. This seems to imply that the errors in the widelane case are not dominated by distance-dependent errors to the same extent as the L1 case, for this particular network.

Table 4.15: *Effect of filter tuning for Holloman network (averaged results when using single reference receiver for entire 9 hour test)*

Freq	Tuned For Network?	Network Corrections Applied to Ref Data	Pct Good Fixes	Mean time to fix (minutes)
L1	no	None (raw)	13.3%	15.90
L1	yes	None (raw)	14.2%	16.25
L1	no	NetAdjust	36.8%	14.49
L1	yes	NetAdjust	40.2%	12.50
WL	no	None (raw)	58.3%	12.44
WL	yes	None (raw)	54.8%	12.57
WL	no	NetAdjust	73.2%	10.12
WL	yes	NetAdjust	73.2%	10.84

Chapter 5

Performance Prediction by Covariance Analysis

In this chapter, the covariance analysis technique described in Chapter 3 (Section 3.3) is applied using the Norway network covariance function. Covariance analysis is a powerful tool for *predicting* the double difference code or phase error statistics for a given network configuration. A similar approach has been proposed for network differential code positioning (Pullen et al., 1995).

From Chapter 3, the covariance matrix of the double difference measurement errors between a receiver located at a computation point and a corrected reference receiver is

$$\boldsymbol{C}_{\mathrm{err}(\Delta\nabla\delta\ell_{cp})} = \mathrm{B}_2\boldsymbol{C}_{\delta\ell}\mathrm{B}_2^T - \mathrm{B}_2\boldsymbol{C}_{\delta\ell}\mathrm{B}_1^T(\mathrm{B}_1\boldsymbol{C}_{\delta\ell}\mathrm{B}_1^T)^{-1}\mathrm{B}_1\boldsymbol{C}_{\delta\ell}\mathrm{B}_2^T. \tag{5.1}$$

Each of the terms on the right hand side can be calculated without knowing the values of any of the measurements—all that is required is knowledge of which measurements are available, plus the information needed to calculate the covariance function for generating $\boldsymbol{C}_{\delta\ell}$.

In a real GPS receiver network, the number of visible satellites and the satellite elevations are constantly changing, so the resulting error covariance matrix $\boldsymbol{C}_{\mathrm{err}(\Delta\nabla\delta\ell_{cp})}$ is actually a function of time. The goal of covariance analysis as presented here is not, however, to determine the precise error covariance at a given time instant. Rather, the goal is to determine an average or typical error level for a given set of (constant) conditions.

To this end, some assumptions can be made to simplify the process, without significantly degrading the results. A description of each of the terms on the right side of Equation 5.1 and related assumptions are given in the paragraphs that follow.

The B_2 term is the double difference matrix used to form the double difference measurements between one or more reference stations and the the mobile receiver at the computation point. Because of the data encapsulation property of NetAdjust (see Section 3.5.2), it is only useful to form double difference measurements between the mobile receiver and *one* reference receiver. When forming the B_2 matrix, it is assumed that the same set of satellites is visible for both the reference and mobile receivers.

The other double difference matrix (B_1) generates a maximal set of linearly independent double difference measurements between all of the reference receivers. When generating this, it is assumed that all of the reference receivers obtain measurements from the same set of satellites. For a large network, this is usually not true, because low elevation satellites are often above the elevation cutoff angle for some receivers but not for others, or because a receiver simply fails to obtain a good measurement from a satellite that is visible. However, in a real network, there normally would only be a difference of one or possibly two satellites between reference receivers, so assuming that all receivers have the same measurements is not completely unrealistic.

The covariance matrix $\boldsymbol{C}_{\delta\ell}$ requires the satellite elevations and reference receiver positions, in addition to the set of available measurements. For the covariance analysis results presented in this section, all satellites are assumed to have the same elevations for all of the reference receivers. Although this is not true in a real network, the elevation differences are small (depending on the size of the network). Furthermore, the satellite elevations are set at predetermined, fixed values, as indicated in Table 5.1. These sets of elevations are based on actual elevations for GPS satellites relative to one of the receivers in the Norway network, so they are realistic, in that they represent the situation for a specific epoch.[1]

[1]For example, to select the set of 5 elevations, a set of epochs was found in which there were 5 visible satellites, and one of them was chosen to be the 5-satellite set presented in Table 5.1.

Table 5.1: Predetermined sets of satellite elevations used in covariance analysis

Number of Satellites	Predetermined Satellite Elevations (deg)							
5	25.7	15.1	59.9	38.4	48.3			
6	34.5	16.7	15.1	59.9	38.4	48.3		
7	29.9	39.1	63.7	59.0	27.3	15.6	54.0	
8	36.5	30.5	68.0	16.0	69.4	25.1	29.6	44.5

By making the assumptions stated above, it is relatively easy to generate the B_1, B_2, and $C_{\delta\ell}$ matrices, because they follow a regular pattern. This is demonstrated in Figure 5.1, which is a diagram of the matrix structure of the B_1 matrix. The x-axis represents the columns of B_1, and the y-axis represents the rows. All of the elements of the B_1 matrix are zero except for the ones shown as dots, which have values of either +1 or -1. Each row of the matrix generates a single double difference measurement, using measurements from two different reference receivers. The purpose behind Figure 5.1 is to demonstrate that, if the same satellites are visible to all receivers, then the B_1 matrix (and the B_2 matrix as well) can be easily calculated according to the pattern. If there are different satellites visible at each receiver, then the matrix does not follow this pattern, and computation becomes more involved.[2]

Note that Equation 5.1 describes the covariance matrix of the double difference measurement errors *after* the reference receiver measurements have been corrected by NetAdjust. The covariance matrix of the *raw* (uncorrected) measurements $C_{\Delta\nabla\delta\ell_{cp}}$ is obtained by a straightforward application of the covariance law (see Section 3.3)

$$C_{\Delta\nabla\delta\ell_{cp}} = B_2 C_{\delta\ell} B_2^T. \tag{5.2}$$

[2]It should be emphasized that the assumption of common visible satellites for all reference receivers applies only to the covariance analysis technique. The NetAdjust software is able to handle different satellites for each reference receiver.

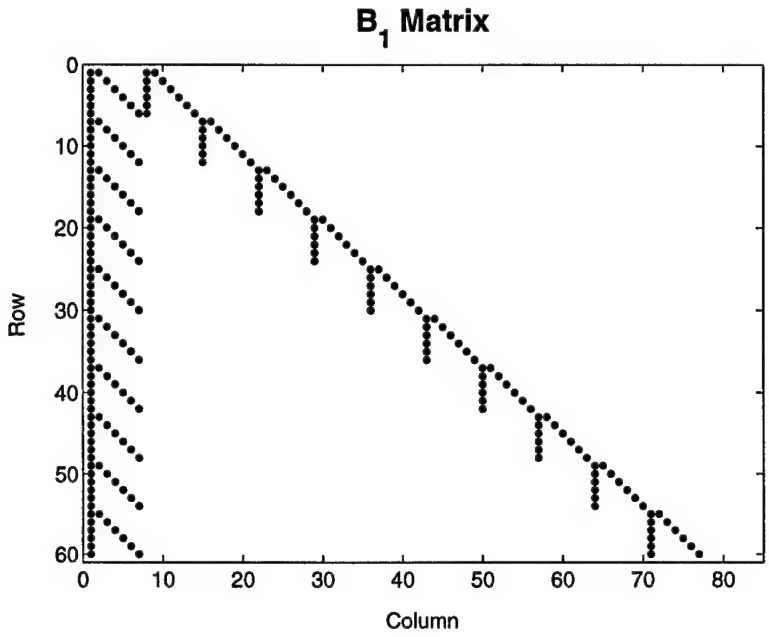

Figure 5.1: *Non-zero values of B_1 matrix (each dot is either +1 or -1)*

5.1 Covariance Analysis Validation

Before using the covariance analysis technique to predict performance, it is important to validate it against data from a real network. To this end, a covariance analysis was performed for each of the seven test networks described in Chapter 4.

The average number of satellites received by the real network varied between five and ten over the 24-hour test durations, as shown in Figure A.3 on page 230. The covariance analyses were performed assuming seven visible satellites for all reference receivers, at the elevations given in the third row of Table 5.1. For the covariance analysis of a given test network, the computation point was located at the position of the mobile receiver for that network. The same sets of reference receivers were used in the covariance analysis as in each of the seven test networks.

These covariance analyses generated seven different NetAdjust double difference error covariance matrices, corresponding to the seven different test networks. These represent predictions of the errors when forming double difference observables using measurements

from a receiver at the computation point and NetAdjust-corrected measurements from the reference receiver. Additionally, seven different *raw* double difference error covariance matrices were generated, using Equation 5.2. These represent predictions of the double difference errors when forming double difference measurements using raw (uncorrected) measurements from both the receiver at the computation point and the reference receiver.

In Section 4.1.3 of Chapter 4, double difference error statistics are presented for both raw and corrected double difference measurements. Specifically, Figures 4.8 and 4.9 show the double difference error RMS for the L1 and WL measurements, raw and corrected, for the seven test networks. Since the double difference measurement errors are zero-mean, these scalar RMS values represent the sample standard deviation for all of the double difference measurement errors.

The covariance analysis technique, however, provides an error covariance *matrix*, with diagonal elements representing the variances corresponding to each of the satellites. In order to relate the covariance analysis matrix with the scalar RMS values from the actual measurements, the diagonal elements of the covariance analysis matrix are combined to form the RMS_p (for RMS-predicted) value using

$$\text{RMS}_p = \sqrt{\frac{\sum_{i=1}^{n} \boldsymbol{C}(i,i)}{n}}, \tag{5.3}$$

where n is the number of satellites (7 in this case), and $\boldsymbol{C}(i,i)$ are the diagonal elements of the covariance matrix generated by the covariance analysis. Note that RMS_p is essentially the square root of the average variance (across each of the satellites). (It's also the root-mean value of the diagonal terms of the covariance matrix). As such, it can be thought of as the average (predicted) RMS value for comparison with the RMS values generated by the data.

A comparison between the L1 double difference RMS errors using the raw data and the covariance analysis predictions is shown in Figure 5.2. The traces marked with triangles show the double difference error RMS for the raw (uncorrected) measurements, and

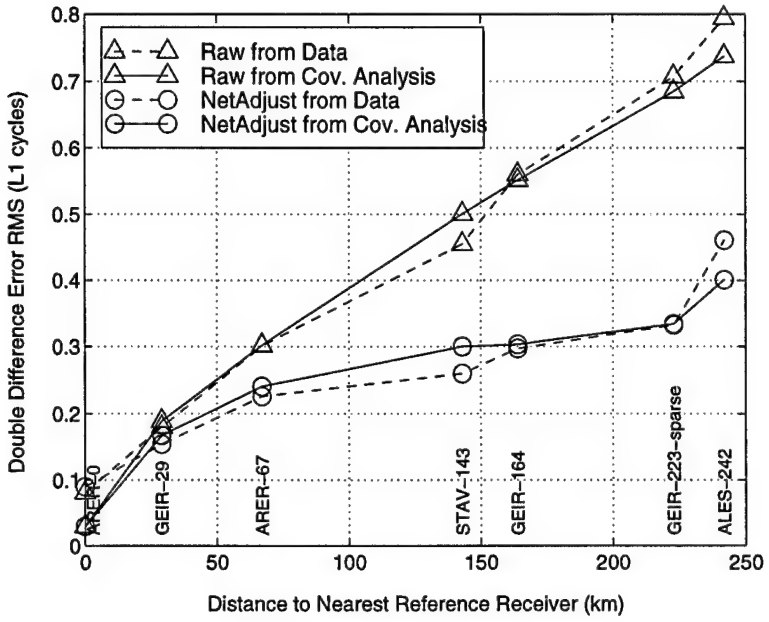

Figure 5.2: *Comparison of double difference L1 error RMS between data and covariance analysis predictions for seven test networks (raw and NetAdjust-corrected)*

the traces marked with circles show the double difference error RMS for the NetAdjust-corrected measurements. Also, the dashed-lines and the solid lines represent results obtained from the data and the covariance analysis, respectively.

Note first of all that for the raw measurements (traces with triangles), the covariance analysis generated very accurate predictions of the errors, when compared to the errors generated from the data. This is one indicator that the $\boldsymbol{C}_{\delta\ell}$ matrix is indeed correct for the Norway network during the test period.

The covariance analysis also did a very good job of predicting the corrected measurement error RMS values, indicating that the improvement brought about by NetAdjust is accurately predicted by the covariance analysis.

The same type of plot for WL phase measurements is given in Figure 5.3. Note that once again the covariance analysis did an excellent job of predicting both the raw and the NetAdjust errors, when compared to the real data.

Overall, the covariance analysis method generates accurate predictions for the L1 and

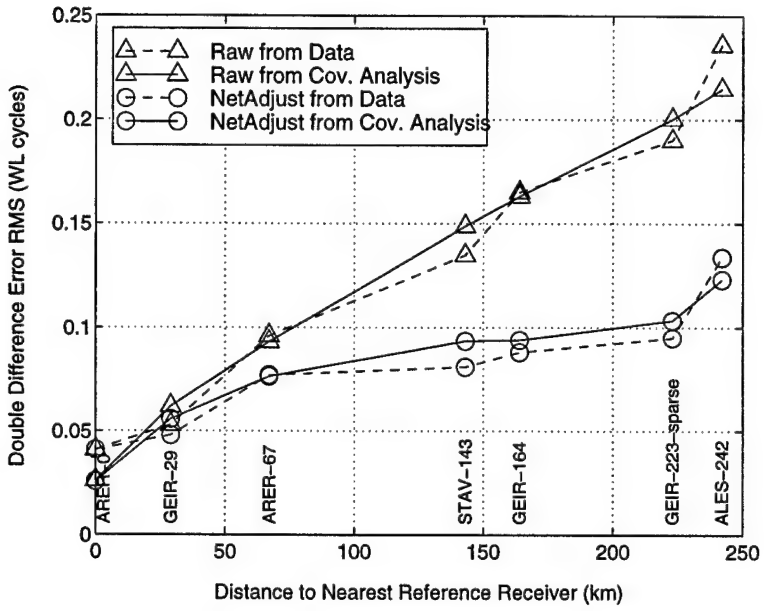

Figure 5.3: *Comparison of double difference WL error RMS between data and covariance analysis predictions for seven test networks (raw and NetAdjust-corrected)*

WL measurement accuracies, when compared with real-world data. It should be stressed that these results are as anticipated, given that the covariance functions were generated using the same data. The results, however, clearly validate the algorithms and developed software.

5.2 Development of Differential Error Specification

Since the output of the covariance analysis method is an estimate of the double difference error RMS value, then any specifications for network performance need to be stated in terms of this predicted RMS value. Specifically, for predicting carrier-phase ambiguity resolution performance, it is necessary to determine the relationship between ambiguity resolution performance and the RMS errors. Once this relationship is defined, then a level of performance for ambiguity resolution can be expressed in terms of predicted RMS error values.

Figure 5.4 shows the standard deviations of the L1 and WL phase zenith double differ-

ence measurement errors for each of the 55 baselines between reference receivers in the Norway network (represented as circles). The solid line in each of the plots is the value generated from the covariance function as described in Chapter 3. Figure 5.5 shows an expanded view of the curve fits for short baseline distances (which is useful in the discussion that follows). These plots show the same information as Figures 3.7 and 3.8 in Chapter 3, only here the errors are expressed in terms of error standard deviations (rather than variances).

Because ambiguity resolution is a complex process, it is difficult to parameterize ambiguity resolution performance directly in terms of error characteristics. However, ambiguity resolution performance is known to be closely linked to the distance between the reference and mobile receivers (i.e., the baseline distance) (Weisenburger and Cannon, 1997). If a specification for ambiguity resolution is given in terms of the baseline distance, then the fit lines in Figure 5.5 can be used to relate this distance to actual error values.

For example, suppose that L1 ambiguity resolution performance was evaluated (in terms of time to fix, percentage of good fixes, etc.) over baseline lengths varying between 1 km and 50 km, and it was found that acceptable performance[3] was assured as long as the baseline length was 25 km or less. Then, the left plot in Figure 5.5 can be used to translate this requirement into a requirement about the maximum allowable zenith double difference error standard deviation. For performance at the level of a baseline of 25 km or less, the zenith error standard deviations must be less than 0.079 L1 cycles.

Note that the error standard deviations shown in Figures 5.4 and 5.5 are *zenith* errors, which need to be converted to the actual satellite elevations. Since the satellite elevations in a real network vary over time, it is best to use an average mapping factor to map the

[3]What constitutes acceptable performance is application dependent—some applications (such as precision landing) may require extremely high good-fix percentages and low time-to-fix values, while less stringent applications (such as ground vehicle navigation) can settle for lower good fix percentages and longer time to fix values.

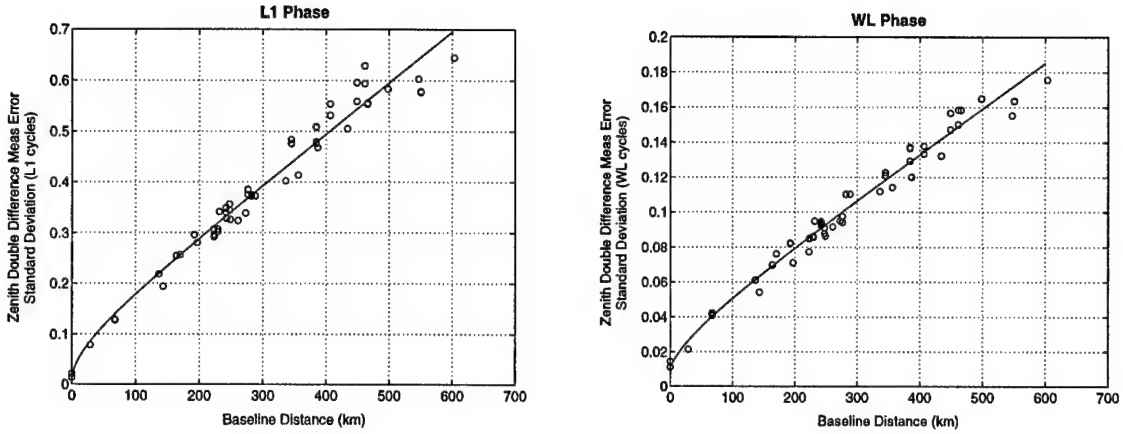

Figure 5.4: *L1 and WL zenith double difference measurement error standard deviations, data points from 55 baselines in Norway network, line from covariance function*

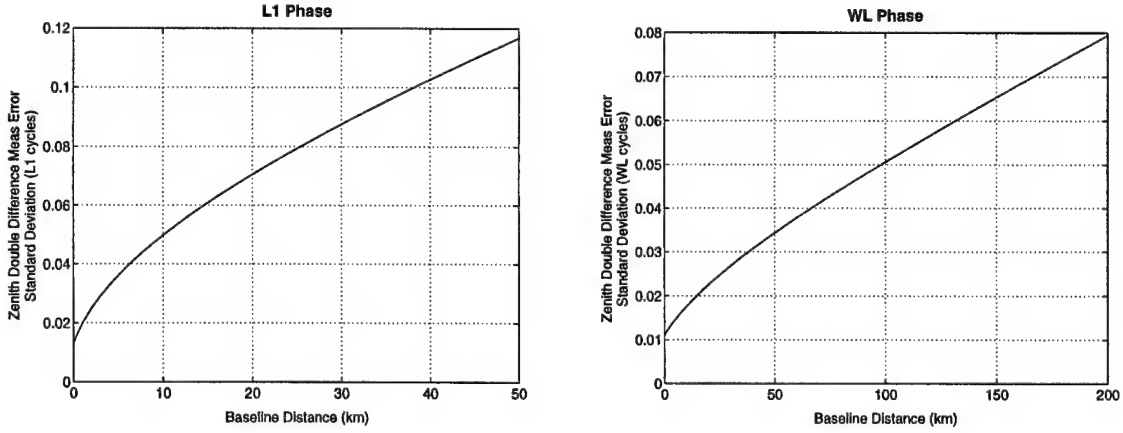

Figure 5.5: *Expanded view of covariance function of L1 and WL zenith double difference measurement error standard deviation*

errors from zenith. This average mapping factor is generated as follows:

1. Randomly sample a large number of discrete satellite elevations from 24-hours of Norway network data. (20,000 were sampled in this case.)

2. Calculate the elevation mapping function $\mu(\varepsilon)$ for each of the 20,000 elevations, using the c_μ coefficients for each measurement as described in Chapter 3.

3. Calculate the average of all of the mapping function values. This is the average mapping factor.

Using this procedure, the average mapping factors were 2.30 and 2.44 for L1 phase and WL phase measurements, respectively. The final error specification is then the zenith error multiplied by the average mapping factor. For the L1 phase example described above, the maximum error standard deviation would be $0.079 \times 2.30 = 0.182$ cycles.

Note that the error standard deviation is the same as the predicted RMS (RMS_p), as long as the double difference errors are zero-mean (which is a basic assumption of the NetAdjust method).

Table 5.2 shows the relationship between the baseline distance (for a single reference case) and the double difference measurement error RMS values for L1 phase measurements. The values given in this table are valid for the conditions present during the Norway test. The same information for WL phase measurements is given in Table 5.3.

Unless stated otherwise, the L1 error specification used throughout the rest of this chapter is that the performance with the network must meet or exceed the performance obtained in a 25 km baseline single reference case. This means that the double difference error RMS value, as generated by the covariance analysis, cannot exceed 0.182 L1 cycles for the results to be acceptable. Likewise, the WL specification is that the performance of the network must meet or exceed the performance obtained in a 60 km baseline single reference case, so the double difference RMS value must not exceed 0.092 WL cycles.

These specifications are arbitrary, since no specific application has been stated. For an

Table 5.2: *Relationship between single reference baseline distance and measurement error RMS value for L1 phase measurements (based on conditions present in Norway network)*

Distance Between Reference and Remote Receivers (km)	Zenith Double Difference Measurement Error Std Deviation (L1 cycles)	Double Difference Measurement Error RMS (L1 cycles)
5	0.036	0.083
10	0.050	0.115
15	0.061	0.140
20	0.071	0.162
25	0.079	0.182
30	0.088	0.201
35	0.095	0.219

application that required better or worse performance, the above specifications could be adjusted. The covariance analysis *procedure* is still valid, however.

Only phase measurements are considered for this covariance analysis, since phase measurements are the key error to be removed for ambiguity resolution. More complicated error specifications could be developed that would involve both code and phase errors, if desired.

5.3 Covariance Analysis of Norway Network

The results presented in the covariance analysis validation above (Section 5.1) were generated using a single computation point (located at the mobile receiver position) for each test network. The covariance analysis can be used to predict double difference error RMS values *anywhere* within or near the network, so it is possible to generate a map which shows the error as a function of position.

An evenly spaced rectangular grid of computation points with a grid spacing of 20 km was generated over the Norway network. The covariance analysis method (seven satellite case) was used to predict the double difference error RMS values at each of these

Table 5.3: *Relationship between single reference baseline distance and measurement error RMS value for WL phase measurements (based on conditions present in Norway network)*

Distance Between Reference and Remote Receivers (km)	Zenith Double Difference Measurement Error Std Deviation (WL cycles)	Double Difference Measurement Error RMS (WL cycles)
20	0.023	0.055
40	0.031	0.075
60	0.038	0.092
80	0.044	0.108
100	0.051	0.124
120	0.057	0.138
140	0.062	0.152

computation points.[4]

The results of this analysis are presented graphically in Figure 5.6. This "coverage map" needs to be explained in detail, because most of the results in the remainder of this chapter will be presented in this form.

The round, black dots on the coverage map represents the locations of each of the reference receivers available to the network. The dashed line that encircles the network delineates a desired region of coverage for the network. The overall goal is to assure that mobile receivers within this region will have ambiguity resolution performance that meets the requirements. The lines with the numbers overlaid are contour lines that show the predicted double difference error RMS values (in cycles) over the entire coverage map. The white and grey shading indicates the regions where the performance requirements

[4]Note that, when calculating these error RMS values using Equation 5.1, only the computation point changes. The matrix that needs to be inverted ($B_1 C_{\delta\ell} B_1^T$) does not involve the computation points, because the B_1 matrix forms double difference measurements only between the network reference receivers (which remain the same for each computation point). As a result, once the $(B_1 C_{\delta\ell} B_1^T)^{-1}$ matrix has been calculated once, it can be used for all of the computation points, drastically speeding up the computation process.

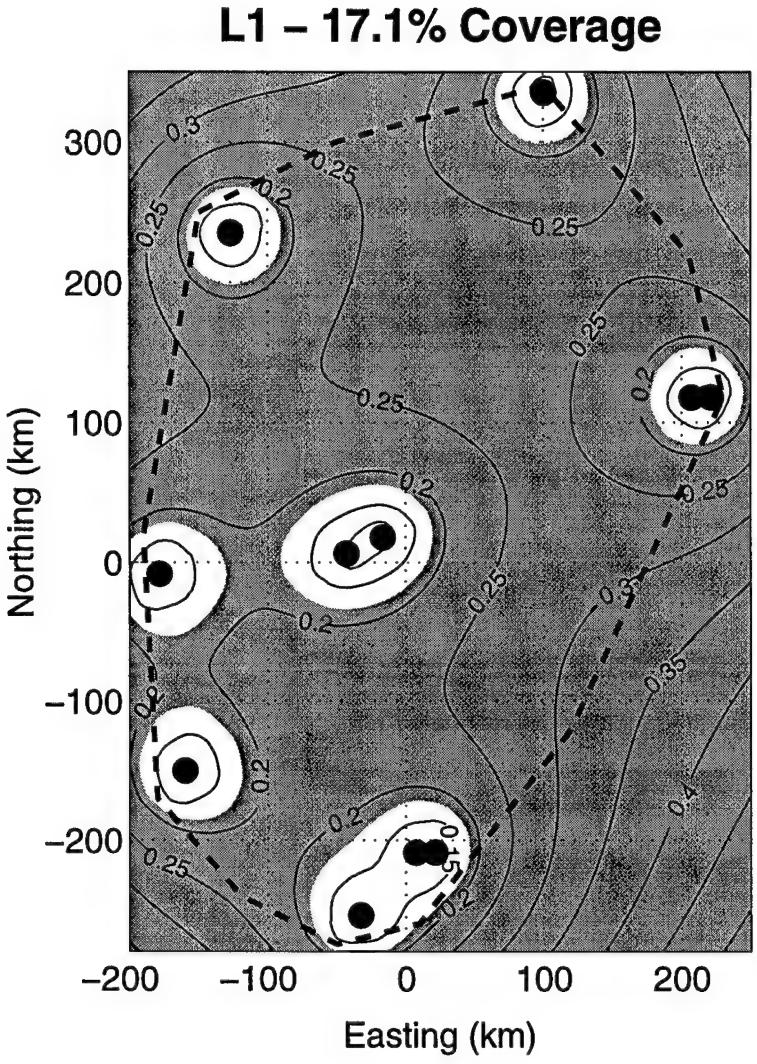

Figure 5.6: *L1 phase ambiguity resolution coverage map for Norway network configuration during test, 11 reference receivers, 7 satellites, contours are predicted double difference error RMS values (L1 cycles)*

have been met—white areas show where performance is acceptable, and grey areas show regions of sub-standard performance. Finally, at the top of the plot, a coverage percentage is given. This indicates what percentage of the desired region of coverage (i.e., the area within the dotted lines) meets the ambiguity resolution requirements. In Figure 5.6, there is only 17.1% coverage, meaning that, of all of the area within the desired region of coverage, only 17.1% is white. The goal is to have 100% coverage, meaning that there are no grey areas within the dotted lines.

This L1 coverage map demonstrates that the existing Norway network is not sufficient for performing L1 ambiguity resolution under the conditions present during the test. This conclusion matches the L1 ambiguity resolution test results presented in Section 4.1.6.

Figure 5.7 shows the WL coverage map. In this case, there is 98.1% coverage within the desired area, which is a significant improvement over the L1 case, and nearly up to the specifications given above (100%).

5.4 Using Covariance Analysis to Analyze Alternatives

The covariance analysis method is a powerful tool that can be used to study the effect of varying the parameters of the problem, as demonstrated in the sections that follow.

5.4.1 Re-positioning Reference Receivers

The eleven receivers in the Norway network were not evenly spaced throughout southern Norway, and the covariance analysis can be used to study alternative receiver placements. One such alternative placement is shown in the L1 and WL coverage maps shown in Figures 5.8 and 5.9.

The coverage has nearly doubled for L1 ambiguity resolution, but it is still at only 30.7%. The WL coverage, however, has attained 100%. This means that, for the error conditions present during this particular test, having reference receivers at the indicated

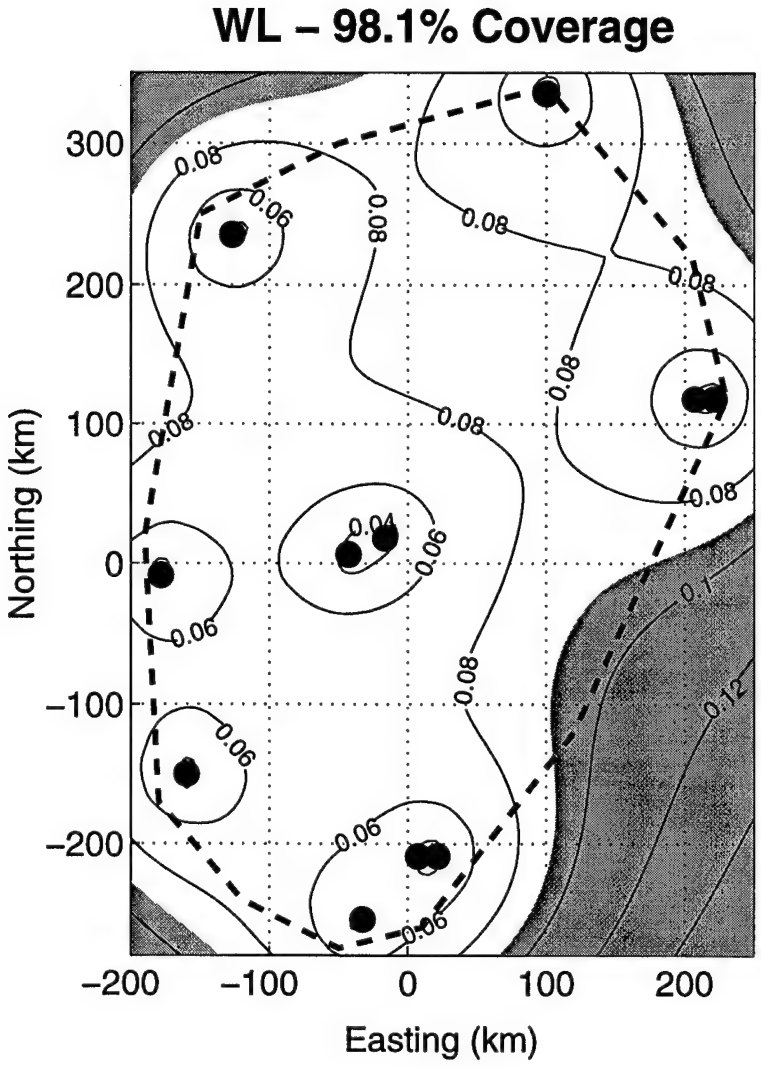

Figure 5.7: *WL phase ambiguity resolution coverage map for Norway network configuration during test, 11 reference receivers, 7 satellites, contours are predicted double difference error RMS values (WL cycles)*

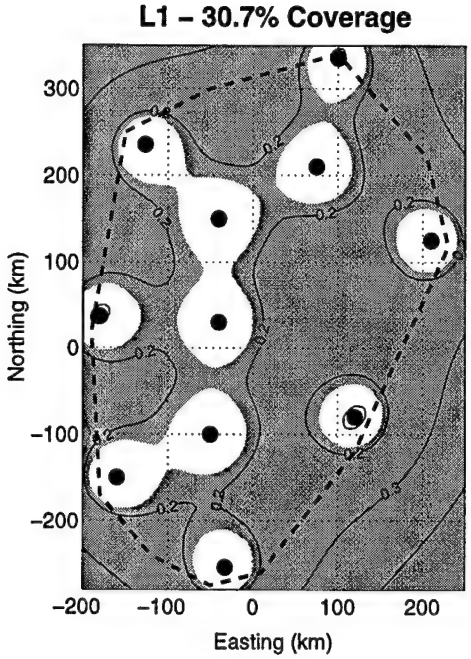

Figure 5.8: *L1 phase ambiguity resolution coverage map for re-positioned reference network configuration, 11 reference receivers, 7 satellites, contours are predicted double difference error RMS values (L1 cycles)*

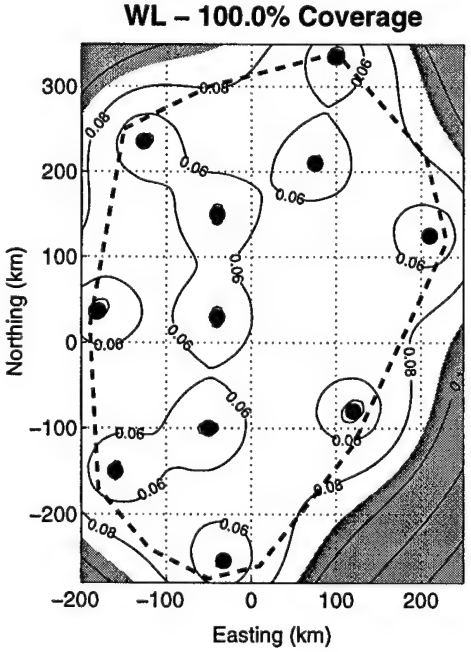

Figure 5.9: *WL phase ambiguity resolution coverage map for re-positioned reference network configuration, 11 reference receivers, 7 satellites, contours are predicted double difference error RMS values (WL cycles)*

locations is predicted to enable WL carrier-phase ambiguity resolution at the required performance level *everywhere* within the desired coverage region.

If the number of receivers is doubled (to 22), then the L1 coverage increases to 91.4% as shown in Figure 5.10. This is fairly good coverage for these error conditions. For completeness, the WL coverage for the 22 receiver network is given in Figure 5.11.

5.4.2 Varying the Number of Satellites

The results presented thus far have all used the seven satellite model shown in Table 5.1. L1 coverage maps for 5, 6, 7, and 8 satellites are shown in Figure 5.12. These were generated from the re-positioned 11-reference-receiver network described in the previous section. Note that, as expected, the coverage improves as the number of satellites increases. Even with 8 satellites, there is only 46% coverage, however.

WL results for 5, 6, 7, and 8 satellites are shown in Figure 5.13. Note that there is not 100% coverage even if there are only 5 satellites, for this test. (Increasing the number of satellites will still improve performance above the specification, however).

5.4.3 Increased Ionospheric Activity

The covariance analysis results presented to this point have used the correlated error covariance function that was generated by the data from the Norway network. It therefore represents only the error conditions presented during the Norway test, when the ionosphere was stable and at the mid-point in the 11 year solar cycle.

If data were to be collected at a different time, then a new covariance function could be calculated based on that data. Any covariance analysis using this new covariance function would generally be different from the results presented here, because the correlated errors change over time.

In order to demonstrate in a simple manner the effect of increased ionospheric errors, the covariance analysis for the 7 satellite, re-positioned reference receiver case was

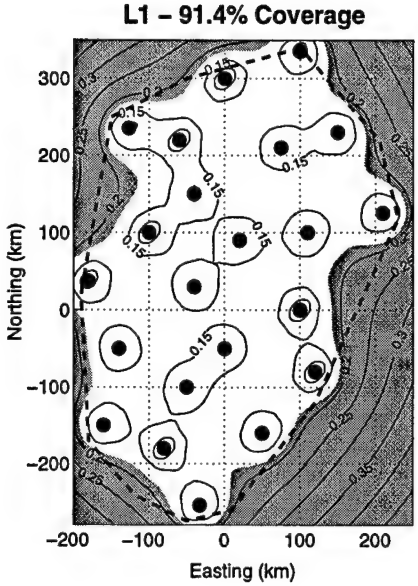

Figure 5.10: *L1 phase ambiguity resolution coverage map for re-positioned and enlarged reference network configuration (22 reference receivers), 7 satellites, contours are predicted double difference error RMS values (L1 cycles)*

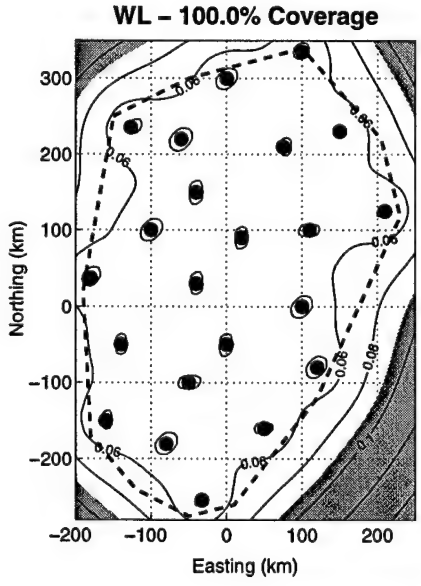

Figure 5.11: *WL phase ambiguity resolution coverage map for re-positioned and enlarged reference network configuration (22 reference receivers), 7 satellites, contours are predicted double difference error RMS values (WL cycles)*

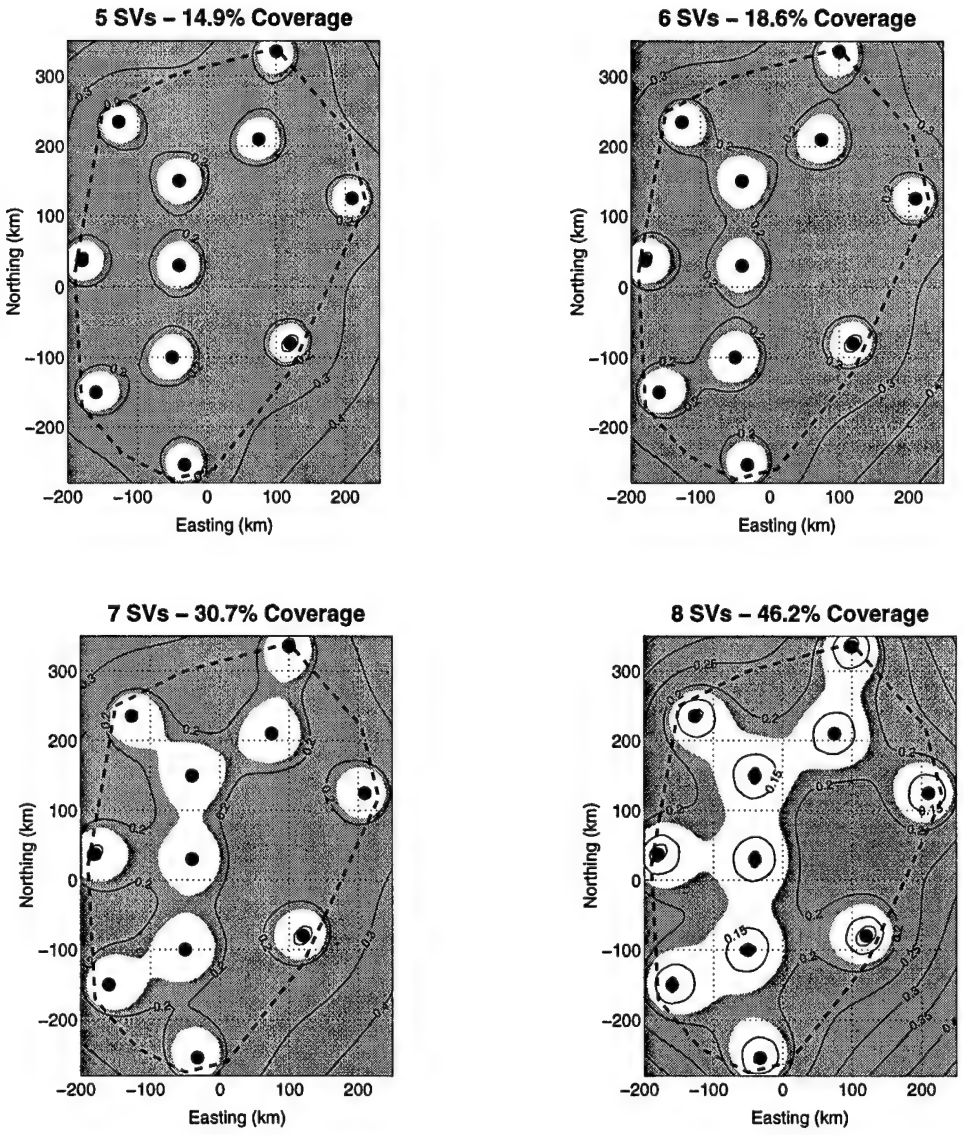

Figure 5.12: *L1 phase ambiguity resolution coverage map for 5, 6, 7, and 8 satellites, re-positioned reference network configuration (11 reference receivers), contours are predicted double difference error RMS values (L1 cycles)*

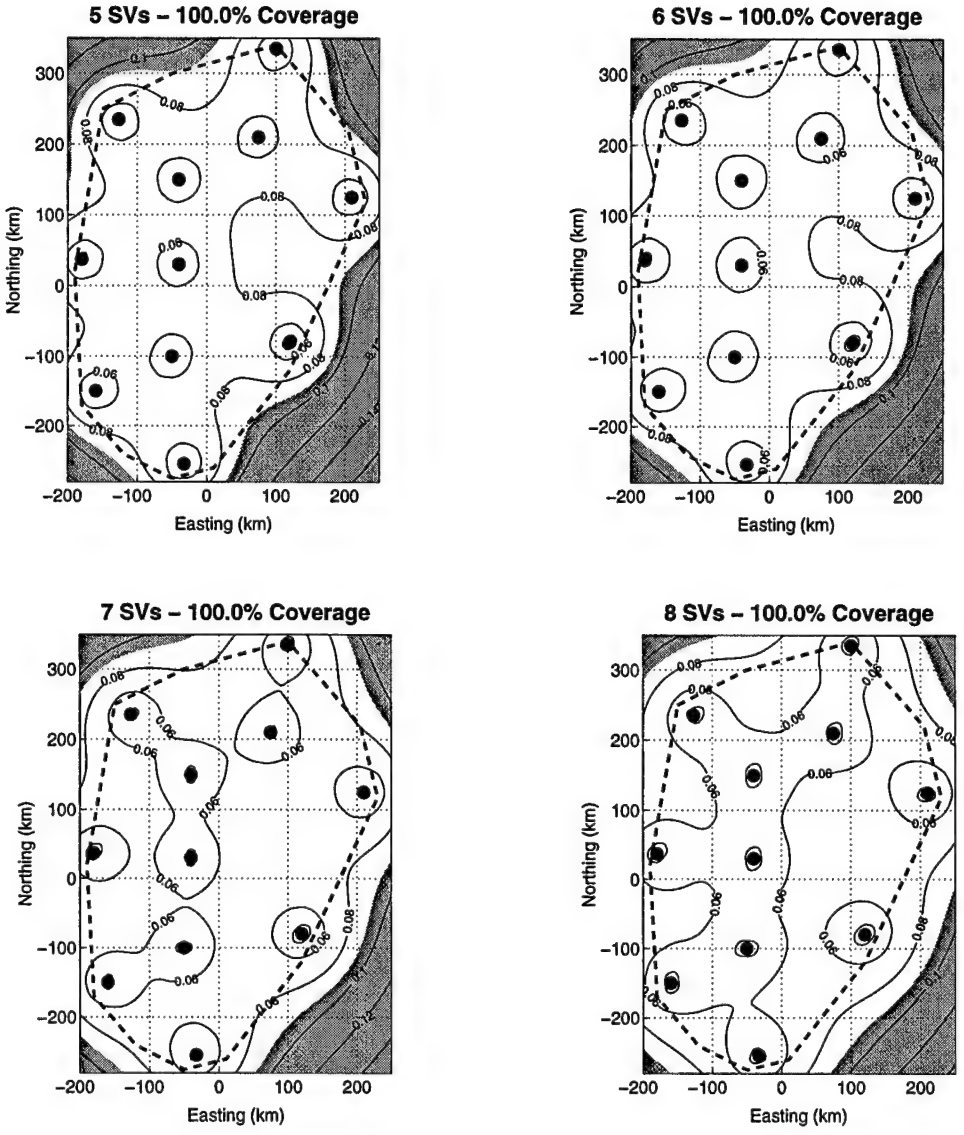

Figure 5.13: *WL phase ambiguity resolution coverage map for 5, 6, 7, and 8 satellites, repositioned reference network configuration (11 receivers), contours are predicted double difference error RMS values (WL cycles)*

repeated using correlated errors that were 50% larger than in the original covariance function.[5] This would simulate a situation in which the ionosphere is more active than during the Norway test. A 50% larger error means that the error magnitudes are 1.5 times as large as the Norway test. (The error variances would then be $1.5^2 = 2.225$ times larger).

Coverage maps showing the comparison between the normal and increased ionospheric ambiguity resolution performance are shown in Figures 5.14 and 5.15 for the L1 and WL ambiguities, respectively. In both cases, the performance of this network degrades dramatically. For an operational network to operate satisfactorily under these increased ionospheric conditions, the number of reference stations would have to increase significantly. Figures 5.16 and 5.17 show the coverage maps for the increased ionospheric conditions using the enlarged, 22 receiver network discussed previously (see Figures 5.10 and 5.11). By increasing the number of receivers in this way, there was nearly complete (96.2%) for WL ambiguity resolution, but only 10.3% coverage for L1 ambiguity resolution.

5.4.4 Limitations

There are many other ways to use the covariance analysis to predict network performance. It is important to remember that the accuracy of any covariance analysis prediction is dependent upon the accuracy of the covariance matrix and the assumptions that are made in the covariance analysis. The covariance analysis technique should not be used as an *absolute proof* of system performance, because a) many factors can be present in a real network that are not modeled by the covariance analysis and b) real networks operate under vastly different conditions (number of satellites, atmospheric conditions, etc.) over time, while the covariance analysis lends itself toward a single set of conditions. Nonethe-

[5]Note that the *total* correlated errors (including satellite position, tropospheric, and ionospheric errors) were increased by 50%. If the increase is to be attributed to ionosphere alone (i.e., the tropospheric and satellite position errors remain constant), then the increase in the *ionosphere* would be more than 50% for this example.

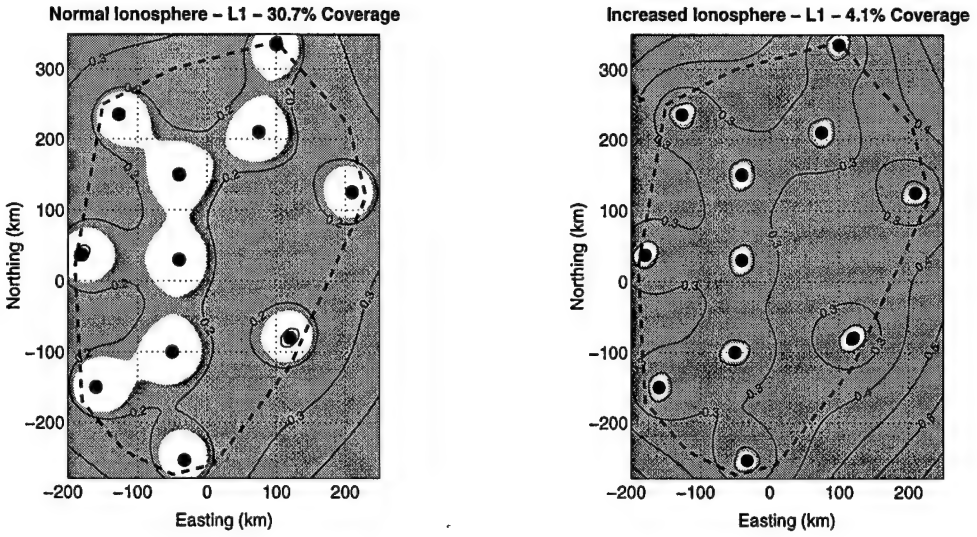

Figure 5.14: *Coverage maps for normal and increased ionospheric errors (50% increase in total correlated error), L1 ambiguities, 7 satellites, re-positioned reference receivers, contours are predicted double difference error RMS values (L1 cycles)*

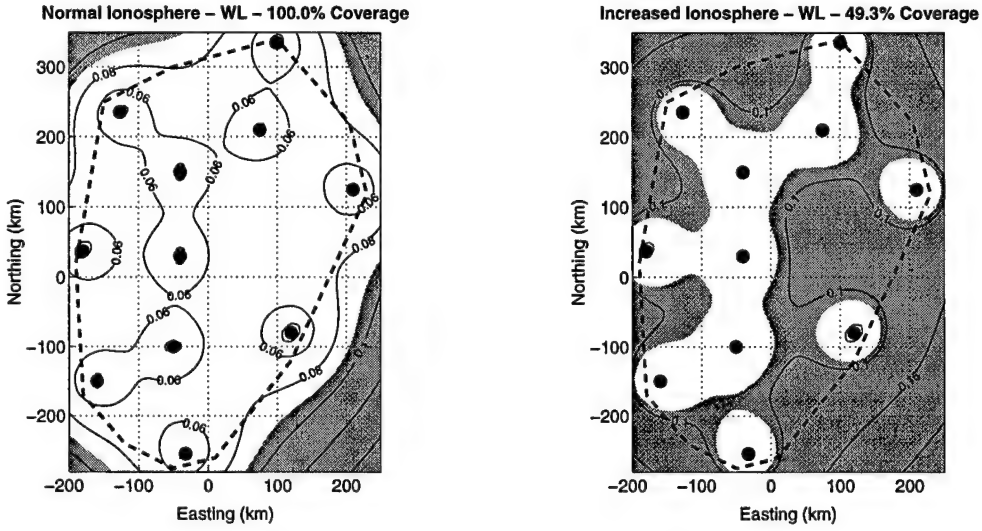

Figure 5.15: *Coverage maps for normal and increased ionospheric errors (50% increase in total correlated error), WL ambiguities, 7 satellites, re-positioned reference receivers, contours are predicted double difference error RMS values (WL cycles)*

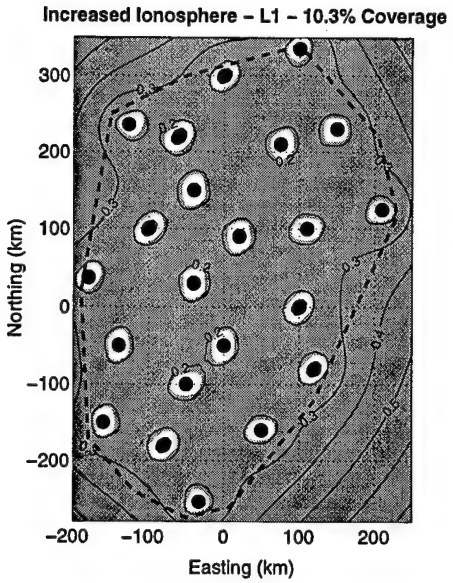

Figure 5.16: *L1 phase ambiguity resolution coverage map for increased ionospheric errors (50% increase in total correlated error), enlarged reference network configuration (22 reference receivers), 7 satellites, contours are predicted double difference error RMS values (L1 cycles)*

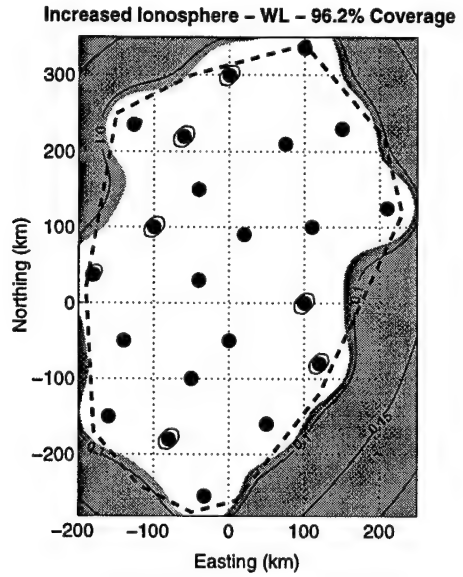

Figure 5.17: *WL phase ambiguity resolution coverage map for increased ionospheric errors (50% increase in total correlated error), enlarged reference network configuration (22 reference receivers), 7 satellites, contours are predicted double difference error RMS values (WL cycles)*

less, covariance analysis does provide a very useful tool for studying the effects of various parameters in the network differential problem, and the predictive results that it generates can be expected to be reasonable estimates of real-world performance.

Chapter 6

Operational Considerations

While results presented in this thesis demonstrate the *capabilities* of the NetAdjust approach for kinematic carrier-phase ambiguity resolution using multiple reference receivers, there are a number of additional issues to be considered for *implementation* of such a system in real-time. The key real-time implementation issues are addressed in the sections that follow. The purpose of this chapter is to highlight these real time implementation issues and briefly discuss methods for dealing with them.

6.1 Real-time Calculation of Ambiguities Between Reference Receivers

One of the initial assumptions for this thesis was that the carrier-phase integer ambiguities between all the reference receivers in the network are known. For the tests involving the Norway and Holloman networks, ambiguity resolution between reference receivers was performed using post-processing batch processing techniques, as described in Appendix B. The NetAdjust method provided good results for the Norway network data, even though not all of the integer ambiguities were available. This demonstrates that it is not absolutely necessary to know all of the ambiguities within the reference receiver network. Nonetheless, determination of these ambiguities is a challenging and important real-time implementation issue.

In contrast to post-processing methodologies, a real-time implementation of NetAdjust

does not have all of the measurements available ahead of time, so the ambiguities need to be estimated in real-time. Recall that the carrier-phase integer ambiguities are true constants, which implies that longer observation times can only improve the results.[1] Ambiguities between satellites that have been visible for a long time are therefore much easier to determine than satellites that have just come into view. It is these low elevation, rising satellites that pose the largest problem for real-time network ambiguity resolution.

When comparing real-time ambiguity resolution with the batch mode ambiguity resolution process described in Appendix B, the batch mode has the obvious advantage that it can use all measurements (past and future) to calculate the ambiguities at a given time epoch. Recall, however, that the batch mode process attempted to solve for the ambiguities on a *baseline by baseline* basis. Using this approach, no information about the correlated (satellite position and atmospheric) errors is available, making the ambiguity resolution algorithm more difficult.

Attempting to solve for the ambiguities simultaneously for the whole network (rather than on a baseline by baseline basis) would provide a means to take full advantage of the error correlations, improving the ability to resolve ambiguities. This network ambiguity resolution approach is normally applied in large batch processing algorithms, as shown in Blewitt (1989) and Dong and Bock (1989).

The same approach can be used in an iterative, sequential processing algorithm (such as a Kalman filter). Such a filter performs carrier-phase ambiguity resolution, but it also estimates the correlated errors and other "nuisance" parameters. After an initialization period, this filter will have solved the integer ambiguities for a subset of the measurements (normally including the satellites that have been visible for a while). Fixing these ambiguities increases the accuracy of the correlated error estimates, which then improves the ability to determine the ambiguities on the newly rising satellites.

---

[1] If the ambiguities were random processes rather than constants, then the estimates of the ambiguities would change over time, and the autocorrelation function of the errors would tend to decrease over large time intervals.

As stated in Appendix B, 80%–90% of the L1 ambiguities and 90%–100% of the WL ambiguities in the Norway network could be determined on a baseline by baseline basis in batch mode. A real-time Kalman filter as described above would have the advantage of calculating the ambiguities in a true network sense, which should improve performance. On the other hand, a real-time Kalman filter has the distinct disadvantage (compared to a post-processing batch technique) of only having measurements up to the current time available, which would degrade performance. The overall performance of the Kalman filter will depend on a combination of these two effects.

6.1.1 Use of Combination of Floating and Fixed Ambiguities

At any moment in time, the network ambiguity resolution Kalman filter will have some of the ambiguities solved as integers, and other ambiguities that it has not yet solved. While these unsolved *integer* ambiguities are not known, the Kalman filter will have *floating* (i.e., non-integer) ambiguity estimates.

Floating ambiguity estimates are not as good as fixed integer ambiguity estimates, but they still provide some amount of information. The NetAdjust procedure as described in this thesis requires fixed integer ambiguities, but it could be easily modified to be able to incorporate floating ambiguity estimates as well. The primary modification would be to make sure that the double difference measurement error covariance matrices used in the estimator reflect the reduced accuracies of the double difference measurements generated from the floating ambiguities.

6.2 Parameterizing Corrections as a Function of Mobile Receiver Position

When NetAdjust was applied to each of the seven test networks in Chapter 4, corrections were generated for one computation point (the location of the mobile receiver). If the mobile receiver location is known, then this single computation point approach is adequate.

However, if the location of the mobile receiver is not known, or there are too many mobile receivers to monitor, then the single computation point scheme will not work. In these cases, some other method must be used to express the NetAdjust corrections in such a form that a mobile receiver *at any location within the desired coverage area* is able to determine the corrections for its specific location.

In a real-time system, the NetAdjust corrections are transmitted by some means to the mobile user (typically through a radio data link). It is often desirable to minimize the amount of data that needs to be sent to the mobile user, so that data link bandwidth limits are not exceeded.

To devise a method for transmitting the NetAdjust corrections over the whole network, it is important to understand how the corrections change over the desired coverage area. Figure 6.1 shows the NetAdjust correction for PRN 23 at a single time epoch over the entire Norway network area. The plots on the left show the three-dimensional surfaces of the NetAdjust L1 code, L1 phase, and WL phase corrections. The plots on the right show contour plots of the same surfaces. The black dots represent the locations of the eleven reference receivers used by NetAdjust.[2] The dotted line marks the border of the desired coverage area for the network. Note that the information on the contour plots is also shown directly underneath each of the three-dimensional surfaces, in order to help in relating the two types of plots. The corrections are for using GEIR (the dot closest to the origin) as the reference receiver. (Using a different reference receiver would not change the shape of the plots, but would only add a constant offset to the corrections).

The same types of plots are shown for PRN 3 and PRN 21 in Figures 6.2 and 6.3, respectively. All of these plots are shown to give a sampling of the "shapes" of the NetAdjust corrections over the Norway network. Note that, in many cases, the total correction is very close to the shape of a flat plane. There are some that are not at all planar, however (such as the WL phase for PRN 3 and the L1 phase for PRN 21), so transmitting the

[2]Only nine distinct dots appear on the plots, because there are two pairs of co-located receivers—see Appendix A.

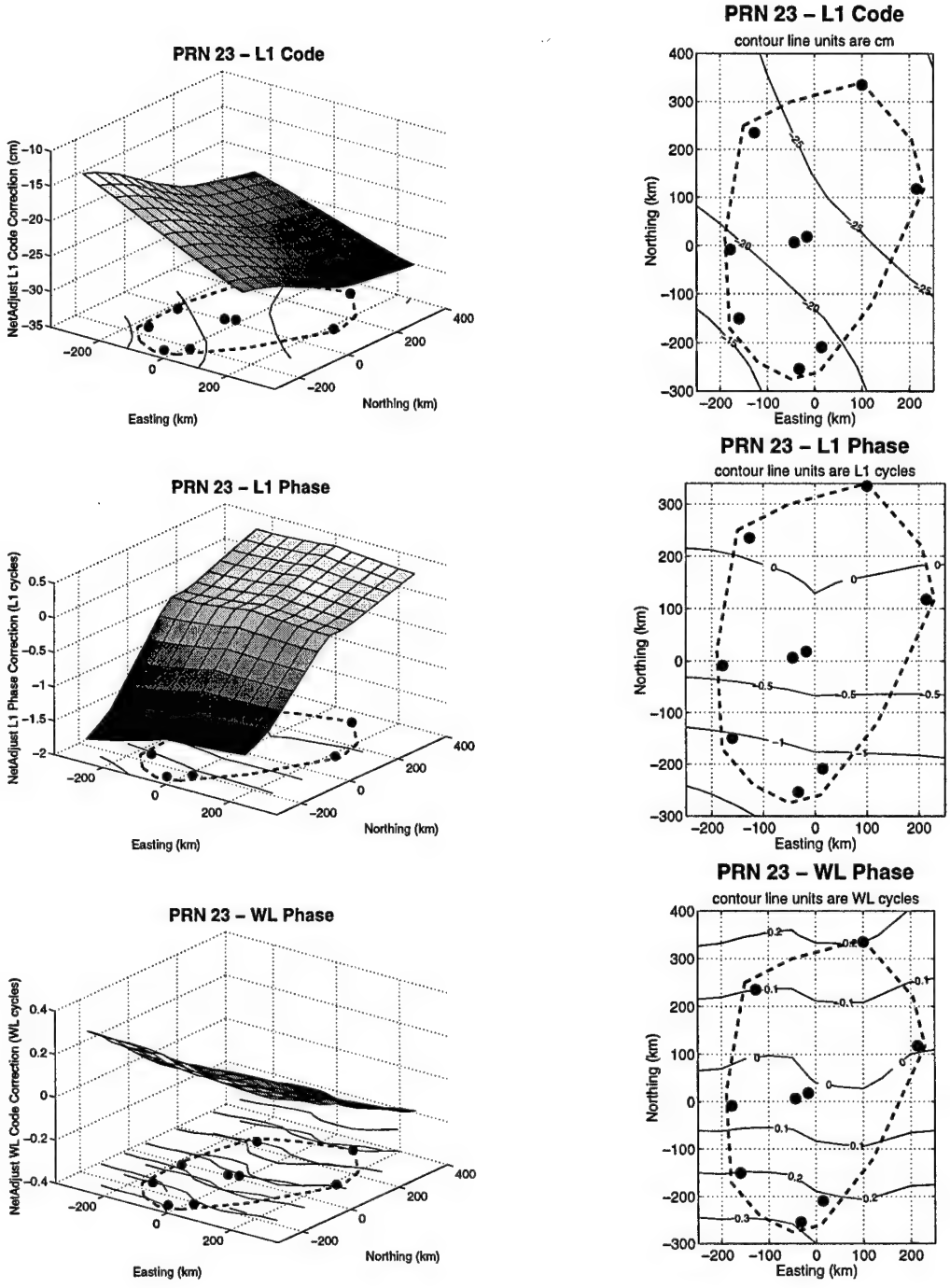

Figure 6.1: *Three-dimensional surface and contour plots of NetAdjust correction values over desired coverage area for a single time epoch, Norway network, PRN 23 (18° elevation)*

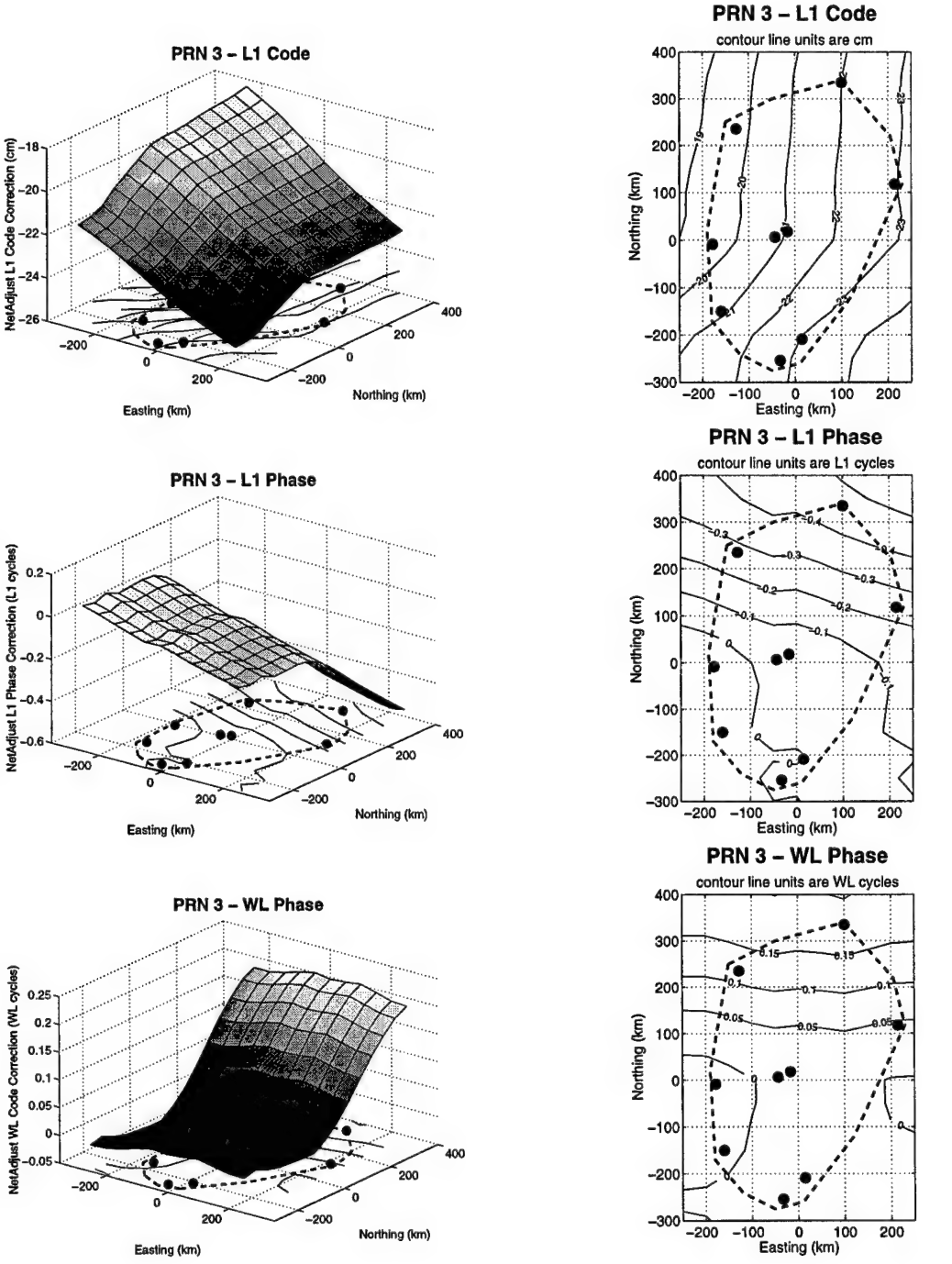

Figure 6.2: *Three-dimensional surface and contour plots of NetAdjust correction values over desired coverage area for a single time epoch, Norway network, PRN 3 (30° elevation)*

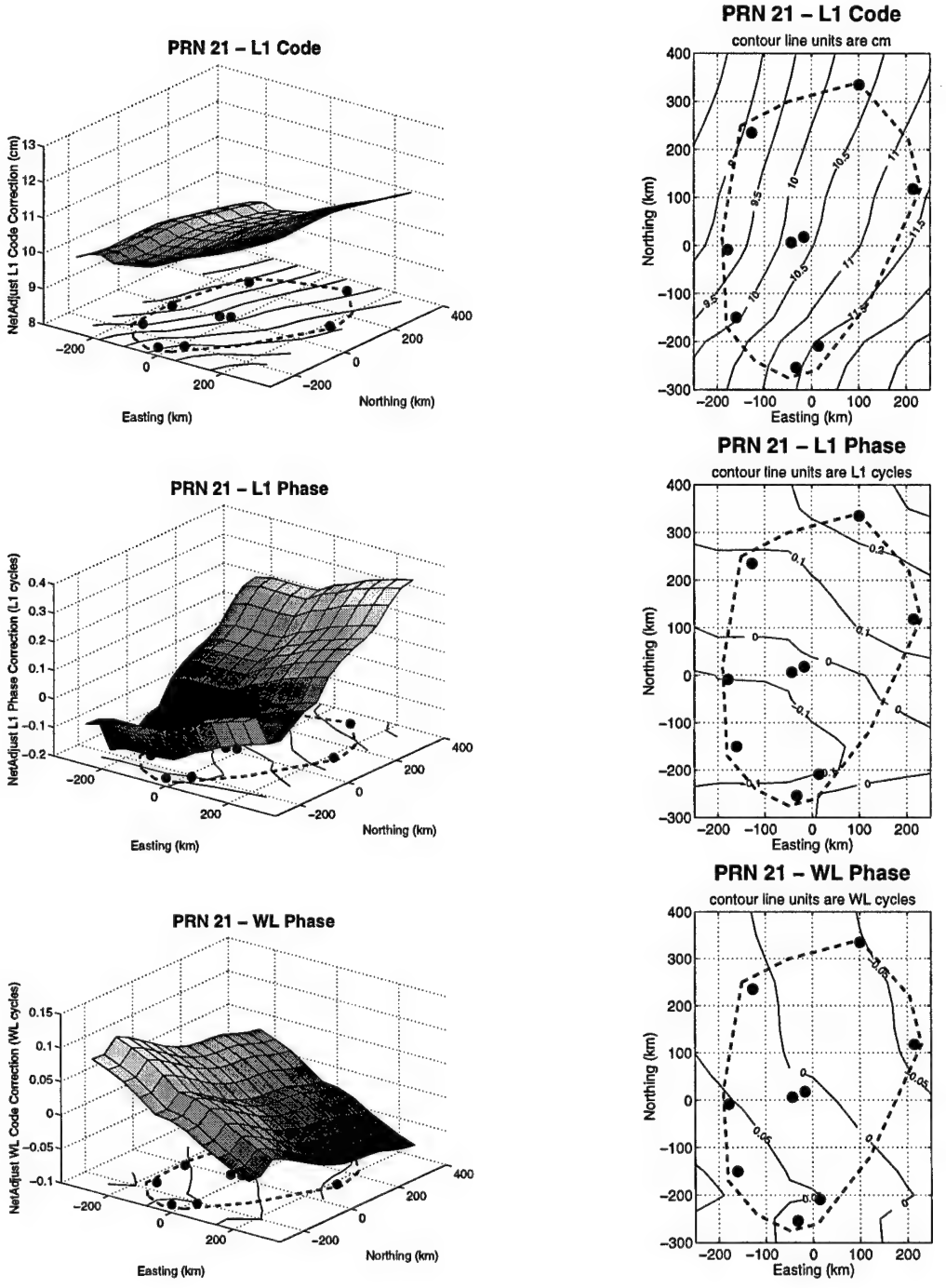

Figure 6.3: *Three-dimensional surface and contour plots of NetAdjust correction values over desired coverage area for a single time epoch, Norway network, PRN 21 (51° elevation)*

corrections as a simple plane (i.e., gradient) is probably not sufficient.

Given the nature of the errors shown in Figures 6.1 through 6.3, three different methods for transmitting measurement corrections to a mobile user are proposed:

1. Transmit the corrections as an algebraic function of user position. Coefficients of this function are calculated from the data shown in the correction surfaces. An example of this approach is to transmit the coefficients c_1 through c_7 of the following function

$$\text{correction} = c_1 + c_2 d_e + c_3 d_e^2 + c_4 d_e^3 + c_5 d_n + c_6 d_n^2 + c_7 d_n^3, \qquad (6.1)$$

   where d_e and d_n are the east and north approximate coordinates of the mobile user. This idea has been proposed by Varner (1997) and Wübbena (1996).

2. Transmit the discrete correction values at a number of computation points throughout the desired area of coverage. The mobile user then interpolates the correction value to the desired location, using the computation points that are closest to that location (Raquet, 1997a).

3. Use a combination of methods 1 and 2. Instead of transmitting a number of discrete correction values at the computation points, or transmitting a correction function, both correction values *and* local gradient information (i.e., a correction function) are transmitted for a smaller set of computation points. Then the mobile user interpolates the corrections to the desired location using the correction values and the gradient information.

Each of these methods has advantages and disadvantages. Method 1 potentially has very low bandwidth requirements (because only the function coefficients are transmitted), but it may be difficult to arrive at a function form that will provide sufficiently accurate fits to all of the correction "shapes" that are present.

Method 2 does not force the corrections into a certain functional form, so more unusual correction shapes can be accommodated (like the WL phase correction for PRN 3). This

method may require transmitting a large number of measurement corrections at many computation points, which could result in very high data link bandwidth requirements.

Method 3 is the most flexible, and it utilizes the advantages of methods 1 and 2. It is much easier to generate an accurate and simple functional form of the correction if the area to cover is small (such as one sixth of the total Norway network). At the same time, it is not necessary to transmit the information for as many grid points as with method 2, because the gradient information enables much more accurate interpolation between computation points.

Each of these three methods should be considered when designing an operational, real-time network. Any one of the three could be the best, depending upon the requirements such as the size of the network, the data link bandwidth requirements, accuracy requirements, and projected differential error levels. Once these requirements are established, then a decision can be made as to the best method to use for that particular case.

6.3 Correction Data Thinning

It may not be possible to transmit corrections for every satellite at every epoch, due to data link bandwidth constraints. A simple approach to handle such cases is to transmit the NetAdjust corrections only at periodic intervals, rather than at each epoch. It is important to understand what information is lost when doing this, however.

Figure 6.4 shows the NetAdjust L1 phase measurement corrections to be applied to the BERG reference receiver measurements for positioning the GEIR receiver. A 2-hour interval is shown (rather than the complete 24-hour interval) so that the correction time correlation can be clearly seen. This plot shows that the L1 phase measurement corrections do not change very quickly. The largest consistent rate of change is around 0.5 cycles/15 minutes (between 13:30 and 13:45), which works out to around 0.0005 cycles per second. If NetAdjust measurement corrections are sent every 20 seconds, and then treated as constants between 20 second updates, then the maximum expected data thin-

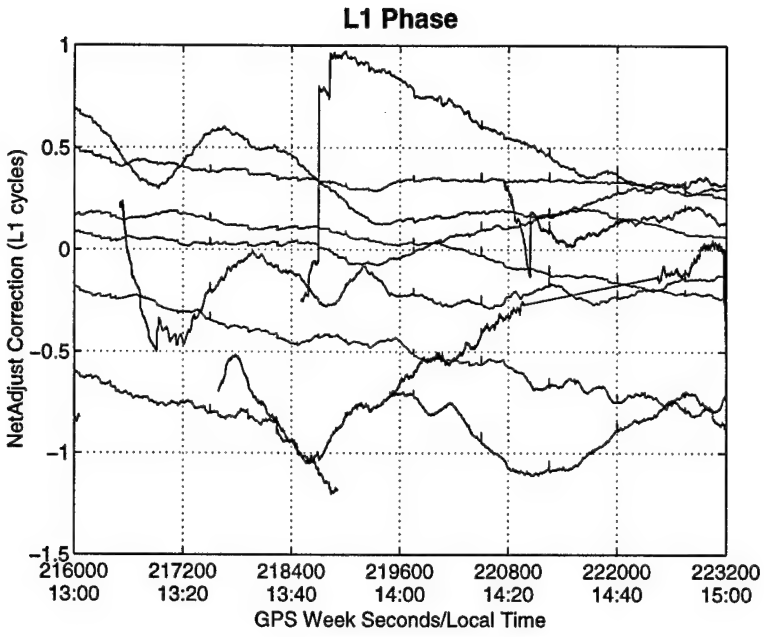

Figure 6.4: *NetAdjust L1 phase corrections for BERG-GEIR (164 km) baseline, GEIR-164 network, 2 hour period*

ning error is only 0.01 cycles. Such a small error is on the order of magnitude of the measurement noise, and it is insignificant.

A similar plot for the WL corrections over the same time period and baseline is given in Figure 6.5. Here, the maximum long term (low frequency) rate of change is about 0.0003 cycles per second (between 13:40 and 13:50), which would give an error of only 0.006 cycles with 20 second data thinning. Note, however, that there are some higher frequency components to these WL corrections. These are probably due to carrier-phase multipath, and they are much more evident for WL corrections than for L1 corrections, because multipath is amplified when forming the WL observable (see Section 2.1.3 in Chapter 2). Data thinning will act as a low-pass filter, and will prevent the NetAdjust corrections from reducing some of this higher frequency error. The high frequency error magnitude is usually small, however, so this is not much of a problem.

Finally, the NetAdjust L1 code measurement corrections are plotted for the same 2-hour period in Figure 6.6. These corrections are dominated by high frequency errors,

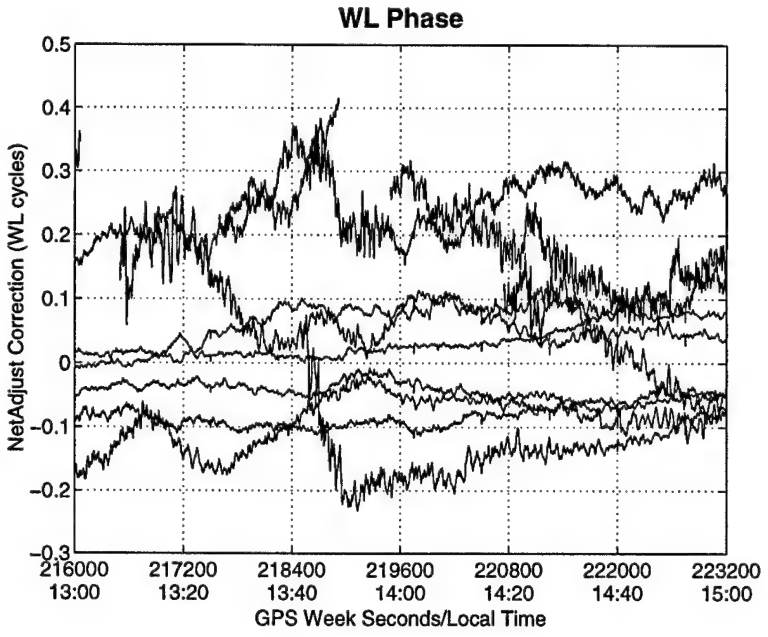

Figure 6.5: *NetAdjust WL phase corrections for BERG-GEIR (164 km) baseline, GEIR-164 network, 2 hour period*

relative to the phase measurements. This is because the code measurements are dominated by multipath and noise errors, which have much higher frequencies than the correlated (satellite position and atmospheric) errors. Figure 6.7 presents the NetAdjust L1 code corrections for just the first 5 minutes, in order to be able to see the time transients in the data more clearly.

Unlike the phase measurements, it is not possible to remove the majority of the code error if the NetAdjust corrections are thinned by anything more than a few seconds. Fortunately, high frequency code errors can often be tolerated in a carrier-phase ambiguity resolution process, and lower frequency code errors (e.g., from multipath) would still be reduced by a thinned code correction.

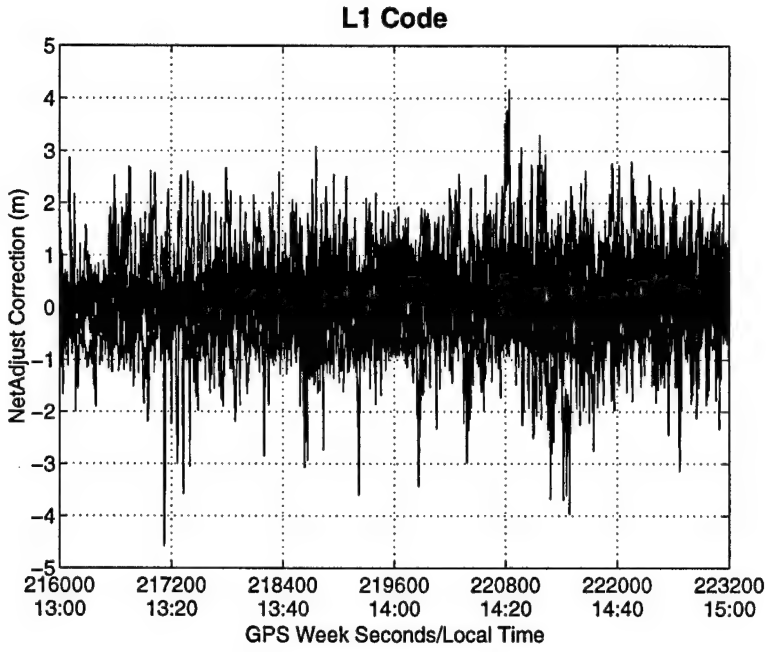

Figure 6.6: *NetAdjust L1 code corrections for BERG-GEIR (164 km) baseline, GEIR-164 network, 2-hour period*

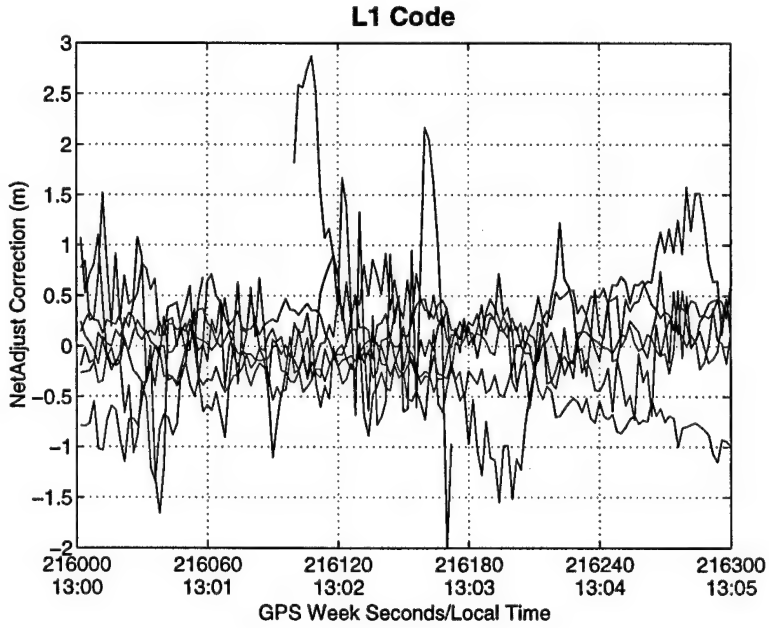

Figure 6.7: *NetAdjust L1 code corrections for BERG-GEIR (164 km) baseline, GEIR-164 network, 5-minute period*

6.4 Near Real-Time Calculation of Covariance Parameters

The covariance matrix used in this thesis was calculated using the entire 24-hour Norway data set, as described in Chapter 3. This single covariance matrix was used for the entire period, with the implicit assumption that the errors during this period were constant (since the covariance function remains the same). In reality, the error characteristics do change over time. Recall, for example, the diurnal variation in double difference phase errors due to the daily change in ionosphere (see Figures 4.5 and 4.6). Error characteristics can change over periods of days, months, and years as well, due to changes in the network environment (including weather patterns, seasonal variations, and the 11-year solar cycle).

A real-time, operational system must be able to monitor the error characteristics continuously, and change the covariance model accordingly.

Chapter 7

Conclusions and Recommendations

7.1 Conclusions

7.1.1 The NetAdjust Method

The goal of this research has been to develop a method for using a network of reference receivers which reduces the differential errors, and in so doing improves the ability to perform carrier-phase ambiguity resolution. The NetAdjust method proposed herein, which is based upon a linear minimum error variance estimator, is an effective means of using a reference receiver network to estimate and remove uncorrelated and correlated differential errors for both code and phase measurements, and for improving ambiguity resolution performance. If the double difference errors are zero-mean and Gaussian, then the NetAdjust algorithm provides the *optimal* error estimates (in the sense that the sum of the corrected measurement error variances is minimized). At the heart of the NetAdjust algorithm is the differential error covariance matrix, which describes the error variance and cross-correlation for all of the measurements received by network reference receivers *and* measurements that would be received by a mobile receiver at a predefined computation point. A perfectly true error covariance matrix guarantees optimality (as described above). The degree to which the implemented error covariance matrix matches the true error covariance matrix is the degree to which the NetAdjust algorithm, as implemented,

is optimal with respect to the defined criterion.

This differential error covariance matrix is expressed using a covariance function, which is generated using data from the reference receiver network. The covariance function used in this thesis generates variance and covariance elements using the distance between the two relevant receivers (expressed in the east and north directions) and the satellite elevation. Other covariance functions could be used as well, depending upon the network size, error characteristics, and desired degree of complexity.

One benefit of the NetAdjust approach is that all of the error information from the entire reference receiver network is "encapsulated" into the measurements of a single reference receiver. This is of great benefit, because it permits the use of standard single-reference differential processing techniques which, when used with the corrected reference receiver measurements, give network-quality results.

The NetAdjust method was tested using an 11-receiver network covering a 400 km $\times$ 600 km region in southern Norway. Seven different test networks, of varying baseline lengths, were used to evaluate various aspects of NetAdjust performance.

Measurement domain. The improvement in differential double difference phase measurements was proportional to the distance between the reference and the remote receivers. For short baselines (less than 30 km), NetAdjust yielded no significant improvement. As distances grew, the improvement from NetAdjust grew, so that the phase double difference RMS error was reduced by up to 50% at distances around 225 km. The NetAdjust method yielded approximately 30% reduction in code double difference error RMS values, and this improvement for code measurements was not dependent upon baseline length.

Position domain. A comparison was made between the differential position accuracy using raw data and data corrected by NetAdjust. The phase measurement integer ambiguities were removed in this test, resulting in a fixed ambiguity position. For L1 and WL phase measurements, NetAdjust reduced the 3-D RMS position errors by approximately 10% for short networks (less than 100 km distance) and 40% for long networks (greater

than 100 km distance). These results show that NetAdjust is effective in reducing the correlated phase errors. NetAdjust also reduced the L1 code position errors by an average of 28%, and the reduction was not dependent on distance.

Integrated code/carrier solution, floating ambiguities. A Kalman filter used both code and carrier-phase measurements to perform differential positioning with floating (non-fixed) carrier-phase ambiguities. Using NetAdjust to correct the code and phase measurements only yielded a moderate improvement in position accuracy in this case. As explained in Chapter 4, for the filter tuning parameters used in this test, phase measurement error reductions had almost no impact on the solution. Also, code measurements are significantly reduced for *both* the raw and NetAdjust cases, because the Kalman filter is implicitly performing carrier-phase smoothing of the code. Overall performance with NetAdjust corrections could be improved by tuning the Kalman filter to have longer time constants for the ambiguity states.

Ambiguity resolution performance. Use of NetAdjust significantly enhanced the ability to perform WL carrier-phase ambiguity resolution. The percentage of correct fixes when using raw (uncorrected) data decreased from 100% at short distances to 50%–60% for 225 km distances. After applying the NetAdjust corrections, however, the percentage of correct fixes generally remained above 90%. (The one exception involved a test network with poor network geometry, which prevented NetAdjust from generating highly accurate error estimates). Likewise, NetAdjust kept the percentage of incorrect fixes below 5% (compared with 10%–20% for the raw data), and NetAdjust reduced the mean time to resolve the WL ambiguities by up to 40%. Because of the size of the reference receiver network and the nature of the L1 measurement errors, ambiguity resolution performance for L1 ambiguities was extremely poor for both raw and NetAdjust-corrected measurements for all but the shortest baselines. Nonetheless, NetAdjust did yield slight improvements in the percentage of correct fixes and the percentage of bad fixes for L1 ambiguity resolution.

The NetAdjust method was also applied to a network of four reference receivers and

three mobile receivers covering a 50 km × 150 km region in southern New Mexico. (This analysis was performed using a preliminary version of the covariance function which is different from the one used for the Norway network). In this case, NetAdjust yielded significant reductions in the time to resolve ambiguities and the percentage of good fixes for *both* WL and L1 ambiguity resolution.

7.1.2 Covariance Analysis

The covariance function used by the NetAdjust method can also be used to determine the covariance matrix of the corrected measurements. This is useful, because it provides a means to predict the performance of the NetAdjust corrections, without having the measurements available. A method for relating the corrected measurement covariance matrix with carrier-phase ambiguity resolution is presented, which makes it possible to predict the carrier-phase ambiguity resolution performance as well.

This covariance analysis technique was first validated against the data from the Norway network. It was then used to determine the areas where the NetAdjust method would attain a reasonable level of ambiguity resolution performance. Using the covariance analysis, the percentage of the desired coverage area (i.e., the area within the network) with acceptable predicted ambiguity resolution performance was 78% for WL ambiguities, but only 12% for L1 ambiguities. This demonstrated in another way why the L1 ambiguities could not be accurately determined for many of the reference networks, as described above.

A number of different covariance analysis scenarios were calculated, varying the number of reference receivers, the number of satellites, and the level of ionospheric activity. These demonstrate that the covariance analysis is a powerful tool for studying NetAdjust performance as it relates to these environmental parameters.

7.1.3 Parameterization of NetAdjust Corrections

Using the NetAdjust method, it would be possible to generate the value of the code and phase measurement corrections over the entire network. Then, the "shape" of these corrections could be evaluated in order to determine the best method for parameterizing the corrections as a function of the user position. Such analysis is not possible with other network methods that assume an *a priori* functional form relating errors to position, and then fit the coefficients of this function to the network data.

7.2 Recommendations

While the NetAdjust derivation and analysis presented in this thesis cover a wide range of topics, there are many more related research avenues that can (and should) be pursued. Some of these include

- Derivation and testing of other statistically sound covariance functions. All of the results from the Norway network used a single covariance function that was generated from the data collected by the network. Areas to examine are
  - Calculation of cross-correlation terms between different satellites. (These were assumed to be zero for the current covariance function).
  - More comprehensive study of the best functional form of the correlated error term (i.e., the one that relates to distance) in the covariance function.
  - More comprehensive validation of the covariance function using real data.
  - Development and testing of a methodology for generating a covariance function which changes in real-time in order to track the real-time changes of the errors themselves (such as the atmospheric errors).
- Analysis using different networks in different environments. The analyses presented in this thesis primarily involved a 24-hour period of the Norway network.

The NetAdjust method should be applied to other networks at other locations and other times in order to gain a better understanding of its capabilities and limitations. Of special interest is the performance during periods of high ionospheric activity (especially during the solar maximum) and extreme tropospheric conditions.

- Study of the effects of filter tuning when using a network of reference receivers. The filter tuning parameters used for the ambiguity resolution process in this thesis were nominal parameters which work well under a variety of conditions. Since the NetAdjust method reduces many of the errors, the filter should be tuned to account for these reduced errors. This concept was briefly explored for the Holloman network, but it needs much more analysis and testing.

- Enhancement to use both fixed *and* floating ambiguities between reference receiver networks (as discussed in Section 6.1.1).

- Analysis of issues regarding real-time transmission of NetAdjust correction, including

  - Analysis of the best method for parameterizing the corrections as a function of the mobile user position (as discussed in Section 6.2).
  - Analysis of NetAdjust performance when using data thinning (see Section 6.3).
  - Analysis of data link bandwidth requirements and correction coding schemes.

- Use of covariance analysis to perform a comprehensive study of the relationship between L1 and WL ambiguity resolution performance and the number of reference receivers, network geometry, differential error levels (especially ionospheric errors), number and elevation of satellites, and differential error levels (especially ionospheric errors).

- Study of the effectiveness of using NetAdjust corrections when the mobile receiver is at a high altitude relative to the network (such as an aircraft). It is likely that the

form of the covariance function would need to be changed to adapt to this type of situation.

The large number of significant recommendations given above is indicative of the fact that this thesis represents the starting point for the NetAdjust approach to the multiple reference carrier-phase ambiguity resolution problem. Overall, the NetAdjust results presented in this thesis are very promising, and they indicate that further research in this area is warranted.

Bibliography

Abidin, H. Z. (1991). New Strategy for On-the-Fly Ambiguity Resolution. In *Proceedings of the 4th International Technical Meeting of the Satellite Division of the Institute of Navigation (ION GPS-91)*, pages 875–886. Albuquerque, New Mexico.

Ashkenazi, V. and Hill, C. (1992). Wide Area Differential GPS: A Performance Study. In *Proceedings of the 5th International Technical Meeting of the Satellite Division of the Institute of Navigation (ION GPS-92)*, pages 589–598. Albuquerque, New Mexico.

Ashtech (1994). *PRISM: Process User's Guide (software manual), pp. 29–30.*

Axelrad, P., Comp, C. J., and MacDoran, P. A. (1996). SNR-Based Multipath Error Correction for GPS Differential Phase. *IEEE Transactions on Aerospace and Electronic Systems*, 32(2):650–659.

Baby, H. B., Gole, P., and Lavergnat, J. (1988). A Model for the Tropospheric Excess Path Length of Radio Waves from Surface Meteorological Measurements. *Radio Science*, 23(6):1023–1038.

Bjerhammer, A. (1973). *Theory of Errors and Generalized Matrix Inverses.* Elsevier Scientific Publishing Company, Amsterdam.

Blewitt, G. (1989). Carrier Phase Ambiguity Resolution for the Global Positioning System Applied to Geodetic Baselines up to 2000km. *Journal of Geophysical Research*, 94(B8):10187–10203.

Borge, T. and Forssell, B. (1994). A New Real-Time Ambiguity Resolution Strategy Based on Polynomial Identification. In *Proceedings of the 1994 International Symposium on Kinematic Systems in Geodesy, Geomatics, and Navigation (KIS-94)*, pages 233–240. Banff, Canada.

Bowen, R., Swanson, P. L., Winn, F. B., Rhodus, N. W., and Feess, W. A. (1986). Global Positioning System Operational Control System Accuracies. In *Global Positioning System Papers, Vol. III*, pages 241–247. Institute of Navigation.

Brown, A., VanDiggelen, F., Kelecy, T., and Brown, P. (1995). Flight Test Results Using Carrier Phase Kinematic Solutions for Aircraft Approach and Landing. *SPN, Journal for Satellite-Based Positioning, Navigation and Communication*, pages 19–27.

Brunner, F. K. and Gu, M. (1991). An Improved Model for the Dual Frequency Ionospheric Correction of GPS Observations. *manuscripta geodaetica*, 16(3):205–214.

Cannon, M. E. (1990). High-Accuracy GPS Semikinematic Positioning: Modeling and Results. *NAVIGATION: Journal of the Institute of Navigation*, 37(1):53–64.

Chen, D. (1993). Fast Ambiguity Search Filter (FASF): A Novel Concept for GPS Ambiguity Resolution. In *Proceedings of the 6th International Technical Meeting of the Satellite Division of the Institute of Navigation (ION GPS-93)*, pages 781–787. Salt Lake City, Utah.

Chen, D. and Lachapelle, G. (1995). A Comparison of the FASF and Least-Squares Search Algorithms for On-the-Fly Ambiguity Resolution. *NAVIGATION: Journal of the Institute of Navigation*, 42(2):371–390.

Cohen, C. E. (1992). *Attitude Determination Using GPS*. PhD thesis, Stanford University, Department of Aeronautics and Astronautics.

Cohen, C. E., Pervan, B., and Parkinson, B. W. (1992). Estimation of Absolute Ionospheric Delay Exclusively through Single-Frequency GPS Measurements. In *Pro-*

ceedings of the 5th International Technical Meeting of the Satellite Division of the Institute of Navigation (ION GPS-92), pages 325–330. Albuquerque, New Mexico.

Colombo, O. L. (1991). Errors in Long Distance Kinematic GPS. In *Proceedings of the 4th International Technical Meeting of the Satellite Division of the Institute of Navigation (ION GPS-91)*, pages 673–680. Albuquerque, New Mexico.

Committee on the Future of the Global Positioning System (1995). The Global Positioning System, a Shared National Asset: Recommendations for Technical Improvements and Enhancements. Technical report, National Research Council.

Counselman, C. C. and Gourevitch, S. A. (1981). Miniature Interferometer Terminals for Earth Surveying: Ambiguity and Multipath for the Global Positioning System. *IEEE Transactions on Geoscience and Remote Sensing*, GE-19(4):244–252.

Dong, D.-N. and Bock, Y. (1989). Global Positioning System Network Analysis With Phase Ambiguity Resolution Applied to Crustal Deformation Studies in California. *Journal of Geophysical Research*, 94(B4):3949–3966.

Enge, P. (1997). WAAS Messaging System: Data Rate, Capacity, and Forward Error Correction. *NAVIGATION: Journal of the Institute of Navigation*, 44(1):63–76.

Enge, P. and Van Dierendonck, A. J. (1996). *Global Positioning System: Theory and Applications*, Volume II, Chapter 4: Wide Area Augmentation System, pages 117–142. American Institute of Aeronautics and Astronautics, Inc.

Enge, P., Walter, T., Pullen, S., Kee, C., Chao, Y., and Tsai, Y. (1996). Wide Area Augmentation of the Global Positioning System. *Proceedings of the IEEE*, 84(8).

Euler, H. J. and Landau, H. (1992). Fast GPS Ambiguity Resolution On-the-Fly for Real-Time Applications. In *Proceedings of the Sixth International Symposium on Satellite Positioning*, pages 650–659. Columbus, Ohio.

Frei, E. and Beutler, G. (1990). Rapid Static Positioning Based on the Fast Ambiguity Resolution Approach "FARA": Theory and First Results. *manuscripta geodaetica*, 15:325–356.

Gao, Y., Li, Z., and McLellan, J. (1997). Carrier Phase Based Regional Area Differential GPS for Decimeter-Level Positioning and Navigation. In *Proceedings of the 10th International Technical Meeting of the Satellite Division of the Institute of Navigation (ION GPS-97)*, pages 1305–1313. Kansas City, Missouri.

Goad, C. C. (1990). Optimal Filtering of Pseudoranges and Phases from Single Frequency GPS Receivers. *NAVIGATION: Journal of the Institute of Navigation*, pages 249–262.

Goad, C. C. and Goodman, L. (1974). A Modified Hopfield Tropospheric Refraction Correction Model. In *Proceedings of the Fall Annual Meeting of the American Geophysical Union*. San Francisco, California.

Hajj, G. A. (1990). The Multipath Simulator: A Tool Toward Controlling Multipath. In *Proceedings of the 2nd Symposium on GPS Applications in Space*, pages 229–243. Hanscom Air Force Base, Massachusetts.

Han, S. (1996). Quality Control Issues Relating to Instantaneous Ambiguity Resolution for Real-Time GPS Kinematic Positioning. In *Proceedings of the 9th International Technical Meeting of the Satellite Division of the Institute of Navigation (ION GPS-96)*, pages 1419–1430. Kansas City, Missouri.

Han, S. (1997). Carrier Phase-Based Long-Range GPS Kinematic Positioning. Reports from School of Geomatic Engineering UNISERV S-49, The University of New South Wales.

Han, S. and Rizos, C. (1996). Integrated Method for Instantaneous Ambiguity Resolution Using New Generation of GPS Receivers. In *Proceedings of the IEEE Position,*

Location, and Navigation Symposium (IEEE PLANS-96), pages 254–261. Atlanta, Georgia.

Hansen, A. J., Walter, T., and Enge, P. (1997). Ionospheric Correction Using Tomography. In *Proceedings of the 10th International Technical Meeting of the Satellite Division of the Institute of Navigation (ION GPS-97)*. Kansas City, Missouri.

Hardwick, C. D. and Liu, J. (1995). Characterization of Phase and Multipath Errors for an Aircraft GPS Antenna. In *Proceedings of the 8th International Technical Meeting of the Satellite Division of the Institute of Navigation (ION GPS-95)*, pages 491–498. Palm Springs, California.

Hatch, R. (1982). The Synergism of GPS Code and Carrier Measurements. In *Proceedings of the Third International Geodetic Symposium on Satellite Doppler Positioning*, pages 1213–1232. DMA, Las Cruces, New Mexico.

Hatch, R. (1989). Ambiguity Resolution in the Fast Lane. In *Proceedings of the 2nd International Technical Meeting of the Satellite Division of the Institute of Navigation (ION GPS-89)*, pages 45–52. Colorado Springs, Colorado.

Hatch, R. (1990). Instantaneous Ambiguity Resolution. In Schwarz and Lachapelle, editors, *Kinematic Systems in Geodesy, Surveying, and Remote Sensing*. IAG Symposia 107, Springer Verlag.

Hofmann-Wellenhof, B., Lichtenegger, H., and Collins, J. (1994). *Global Positioning System: Theory and Practice*. Springer-Verlag.

Hopfield, H. S. (1969). Two-quartic Tropospheric Refractivity Profile for Correcting Satellite Data. *Journal of Geophysical Research*, 74(17):4487–4499.

ICD-GPS-200C (1993). GPS Signal Specification Interface Control Document, Revision C.

Johnson, G. and King, D. (1996). Low Cost Multipath Mitigation in a Single Frequency Environment for a DGPS Station. In *Proceeding of the National Technical Meeting of the Institute of Navigation*, pages 899–904. Santa Monica, California.

Kee, C. (1996). *Global Positioning System: Theory and Applications*, Volume II, Chapter 3: Wide Area Differential GPS, pages 81–116. American Institute of Aeronautics and Astronautics, Inc.

Kee, C. and Parkinson, B. (1992). Algorithms and Implementations of Wide Area Differential GPS. In *Proceedings of the 5th International Technical Meeting of the Satellite Division of the Institute of Navigation (ION GPS-92)*, pages 565–572. Albuquerque, New Mexico.

Klobuchar, J. A. (1987). Ionospheric Time-Delay Algorithm for Single-Frequency GPS Users. *IEEE Transactions on Aerospace and Electronic Systems*, AES-23(3):325–331.

Klobuchar, J. A. (1996). *Global Positioning System: Theory and Applications*, Volume I, Chapter 12: Ionospheric Effects in GPS, pages 485–515. American Institute of Aeronautics and Astronautics, Inc.

Kouba, J., Tetrault, P., Ferland, R., and Lahaye, F. (1993). IGS Data Processing at the EMR Master Active Control System Centre. In *Proceedings of the 1993 IGS (International GPS Service for Geodynamics) Workshop*, pages 122–132. University of Bern.

Krakiwsky, E. (1990). The Method of Least Squares: A Synthesis of Advances. Technical report, UCGE Reports Number 10003, Department of Geomatics Engineering, The University of Calgary.

Kumar, R. and Lau, K. (1996). Deconvolution Approach to Carrier and Code Multipath

Error Elimination in High Precision GPS. In *Proceeding of the National Technical Meeting of the Institute of Navigation*, pages 729–737. Santa Monica, California.

Lachapelle, G. (1994). High Accuracy GPS Positioning. Navtech Seminars Course 330 Lecture Notes.

Lachapelle, G., Cannon, M. E., and Lu, G. (1992). High Precision GPS Navigation with Emphasis on Carrier Phase Ambiguity Resolution. *Marine Geodesy*, 15(4):253–269.

Lachapelle, G., Sun, H., Cannon, M. E., and Lu, G. (1994). Precise Aircraft-to-Aircraft Positioning Using a Multiple Receiver Configuration. In *Proceeding of the National Technical Meeting of the Institute of Navigation*, pages 793–799. San Diego, California.

Lapucha, D. and Barker, R. (1996). Dual Baseline Real-Time OTF Kinematics GPS. In *Proceedings of the 9th International Technical Meeting of the Satellite Division of the Institute of Navigation (ION GPS-96)*, pages 883–888. Kansas City, Missouri.

Lapucha, D. and Huff, M. (1992). Multi-Site Real-Time DGPS System Using Starfix Link; Operational Results. In *Proceedings of the 5th International Technical Meeting of the Satellite Division of the Institute of Navigation (ION GPS-92)*, pages 581–588. Albuquerque, New Mexico.

Leick, A. (1995). *GPS Satellite Surveying*. John Wiley and Sons, Inc., 2nd edition.

Loomis, P., Sheynblatt, L., and Mueller, T. (1991). Differential GPS Network Design. In *Proceedings of the 4th International Technical Meeting of the Satellite Division of the Institute of Navigation (ION GPS-91)*, pages 511–520. Albuquerque, New Mexico.

Lu, G. (1995). *Development of a GPS Multi-Antenna System for Attitude Determination*. PhD thesis, UCGE Report No. 20073, Department of Geomatics Engineering, The University of Calgary.

Lu, G., Cannon, M. E., and Lachapelle, G. (1995). Improving the Reliability of OTF Ambiguity Resolution with Dual Frequency GPS Observations. In *Proceedings of the 8th International Technical Meeting of the Satellite Division of the Institute of Navigation (ION GPS-95)*, pages 1111–1116. Palm Springs, California.

Mader, G. L. (1990). Ambiguity Function Techniques for GPS Phase Initialization and Kinematic Solution. In *Proceedings of the 2nd International Symposium on Precise Positioning with GPS*, pages 1234–1247. Canadian Institute of Surveying and Mapping, Ottawa.

Marini, J. W. (1972). Correction of Satellite Tracking Data for an Arbitrary Tropospheric Profile. *Radio Science*, 7(2):223–231.

Maybeck, P. S. (1994). *Stochastic Models, Estimation, and Control*, Volume 1. Navtech Book and Software Store.

Mendes, V. B. and Langley, R. B. (1994). A Comprehensive Analysis of Mapping Functions Used in Modelling Tropospheric Propagation Delay in Space Geodetic Data. In *Proceedings of the 1994 International Symposium on Kinematic Systems in Geodesy, Geomatics, and Navigation (KIS-94)*, pages 87–98. Banff, Canada.

Minkler, G. and Minkler, J. (1993). *Theory and Application of Kalman Filtering*. Magellan Book Company, Palm Bay, Florida.

Moritz, H. (1989). *Advanced Physical Geodesy*. Wichmann.

Mueller, T. (1994). Minimum Variance Network DGPS Algorithm. In *Proceedings of the IEEE Position, Location, and Navigation Symposium (IEEE PLANS-94)*, pages 418–425. Las Vegas, Nevada.

Pratt, M., Burke, B., and Misra, P. (1997). Single-Epoch Integer Ambiguity Resolution with GPS L1-L2 Carrier-Phase Measurements. In *Proceedings of the 10th Interna-*

tional Technical Meeting of the Satellite Division of the Institute of Navigation (ION GPS-97), pages 1737–1746. Kansas City, Missouri.

Pullen, S., Enge, P., and Parkinson, B. (1995). A New Method for Coverage Prediction for the Wide Area Augmentation System (WAAS). In *Proceedings of the 51st Annual Meeting of the Institute of Navigation*, pages 501–513. Colorado Springs, Colorado.

Raquet, J. (1996). Multiple Reference GPS Receiver Multipath Mitigation Technique. In *Proceedings of the 52nd Annual Meeting of the Institute of Navigation*, pages 681–690. Cambridge, Massachusetts.

Raquet, J. (1997a). Multiple Use Network Carrier Phase Ambiguity Resolution. In *Proceedings of the 1997 International Symposium on Kinematic Systems in Geodesy, Geomatics, and Navigation (KIS-94)*, pages 45–55. Banff, Alberta, Canada.

Raquet, J. (1997b). A New Approach to GPS Carrier-Phase Ambiguity Resolution Using a Reference Receiver Network. In *Proceeding of the National Technical Meeting of the Institute of Navigation*, pages 357–366. Santa Monica, California.

Raquet, J. and Lachapelle, G. (1996). Determination and Reduction of GPS Reference Station Multipath Using Multiple Receivers. In *Proceedings of the 9th International Technical Meeting of the Satellite Division of the Institute of Navigation (ION GPS-96)*, pages 673–681. Kansas City, Missouri.

Remondi, B. W. (1991). Pseudo-Kinematic GPS Results using the Ambiguity Function Method. *NAVIGATION: Journal of the Institute of Navigation*, 38(1).

Rothacher, M. (1997). *Geodetic Applications of GPS: Lecture Notes for Nordic Autumn School*, Chapter GPS Satellite Orbits, Orbit Determination, and the IGS, pages 55–108. National Land Survey of Sweden.

Santerre, R. (1987). Modification to the Goad and Goodman Tropospheric Refraction

Model. Unpublished internal report of the Department of Surveying Engineering, University of New Brunswick, 1987.

Skone, S., Cannon, M. E., Lochhead, K., Héroux, P., and Lahaye, F. (1996). Performance Evaluation of the NRCAN Wide Area System. In *Proceedings of the 9th International Technical Meeting of the Satellite Division of the Institute of Navigation (ION GPS-96)*, pages 1793–1801. Kansas City, Missouri.

Sonntag, J. G., Martin, C. F., and Krabill, W. B. (1995). Ambiguity Resolution Over Long Baselines for Airborne Differential GPS Positioning. In *Proceedings of the 8th International Technical Meeting of the Satellite Division of the Institute of Navigation (ION GPS-95)*, pages 1117–1126. Palm Springs, California.

Spilker Jr., J. J. (1996a). *lobal Positioning System: Theory and Applications*, Volume I, Chapter 13: Tropospheric Effects on GPS, pages 517–546. American Institute of Aeronautics and Astronautics, Inc.

Spilker Jr., J. J. (1996b). *lobal Positioning System: Theory and Applications*, Volume I, Chapter 3: GPS Signal Structure and Theoretical Performance, pages 57–120. American Institute of Aeronautics and Astronautics, Inc.

Spradley, L. (1993). Performing Precise, Seamless Hydrographic Surveys over Extended Areas Through Use of Integrated DGPS Reference Networks. In *Proceeding of the National Technical Meeting of the Institute of Navigation*, pages 233–240. San Francisco, California.

Szabo, D. J. and Tubman, A. M. (1994). Kinematic DGPS Positioning Strategies for Multiple Reference Station Coverage. In *Proceedings of the 1994 International Symposium on Kinematic Systems in Geodesy, Geomatics, and Navigation (KIS-94)*, pages 173–183. Banff, Alberta, Canada.

Tang, W., Johnson, N., and Graff, J. (1989). Differential GPS Operation with Multiple Ground Reference Stations. In *Proceedings of the 2nd International Technical Meeting of the Satellite Division of the Institute of Navigation (ION GPS-89)*, pages 319–323. Colorado Springs, Colorado.

Teunissen, P. J. G. (1994). A New Method for Fast Carrier Phase Ambiguity Estimation. In *Proceedings of the IEEE Position, Location, and Navigation Symposium (IEEE PLANS-94)*, pages 562–573. Las Vegas, Nevada.

Townsend, B. and Fenton, P. (1994). A Practical Approach to the Reduction of Pseudorange Multipath Errors in a L1 GPS Receiver. In *Proceedings of the 7th International Technical Meeting of the Satellite Division of the Institute of Navigation (ION GPS-94)*, pages 21–23. Salt Lake City, Utah.

Townsend, B., Fenton, P., and Van Dierendonck, K. (1995). Performance Evaluation of the Multipath Estimating Delay Lock Loop. *NAVIGATION: Journal of the Institute of Navigation*, 42(3):503–514.

Tranquilla, J. M., Carr, J. P., and Al-Rizzo, H. M. (1994). Analysis of a Choke Ring Groundplane for Multipath Control in Global Positioning System (GPS) Applications. *IEEE Transactions on Antennas and Propagation*, 42(7):905–911.

Van Dierendonck, A. J. (1994). Understanding GPS Receiver Terminology: A Tutorial on What Those Words Mean. In *Proceedings of the 1994 International Symposium on Kinematic Systems in Geodesy, Geomatics, and Navigation (KIS-94)*, pages 15–24. Banff, Alberta, Canada.

Van Direndonck, A. J., Fenton, P., and Ford, T. (1992). Theory and Performance of Narrow Correlator Spacing in a GPS Receiver. *NAVIGATION: Journal of the Institute of Navigation*, 39(3):265–283.

Varner, C. (1997). The Application of Multiple Reference Stations to the Determination of Multipath and Spatially Decorrelating Errors. In *Proceeding of the National Technical Meeting of the Institute of Navigation*, pages 323–333. Santa Monica, California.

Wanninger, L. (1995). Improved Ambiguity Resolution by Regional Differential Modeling of the Ionosphere. In *Proceedings of the 8th International Technical Meeting of the Satellite Division of the Institute of Navigation (ION GPS-95)*, pages 55–62. Palm Springs, California.

Wei, M. and Schwarz, K. P. (1995). Fast Ambiguity Resolution Using an Integer Nonlinear Programming Method. In *Proceedings of the 8th International Technical Meeting of the Satellite Division of the Institute of Navigation (ION GPS-95)*, pages 1101–1110. Palm Springs, CA.

Weisenburger, S. and Cannon, M. E. (1997). Performance Improvements Using Constraints in Marine OTF Ambiguity Resolution. In *Proceeding of the National Technical Meeting of the Institute of Navigation*, pages 585–594. Santa Monica, California.

Weisenburger, S. D. (1997). Effect of Constraints and Multiple Receivers for On-The-Fly Ambiguity Resolution. Master's thesis, The University of Calgary.

Wübbena, G., Bagge, A., Seeber, G., Boder, V., and Hankemeier, P. (1996). Reducing Distance Dependant Errors for Real-Time Precise DGPS Applications by Establishing Reference Station Networks. In *Proceedings of the 9th International Technical Meeting of the Satellite Division of the Institute of Navigation (ION GPS-96)*, pages 1845–1852. Kansas City, Missouri.

Zumberge, J. F. and Bertiger, W. I. (1996). *Global Positioning System: Theory and Applications*, Chapter 16: Ephemeris and Clock Navigation Message Accuracy, pages 585–599. American Institute of Aeronautics and Astronautics.

Appendix A

Description of Reference Network Data Sets

Two different data sets are used throughout this thesis, and this appendix describes both of them. The first is called the Norway network, and it involves eleven stationary receivers spaced throughout southern Norway. Due to the quality and size of this network, it is the primary network used in the analysis of the NetAdjust method.

A secondary network is called the Holloman network, which involves four stationary reference receivers and three mobile receivers.

A.1 Norway Network

The Norway network consists of eleven stationary receivers spaced throughout the southern portion of Norway, indicated by a box in Figure A.1. The relative locations of the reference receivers are shown in Figure A.2, which approximately covers the area of the box in Figure A.1.

Each receiver is identified by a four letter designation. The BERG, ALES, and TRON receivers are located in Bergen, Ålesund, and Trondheim, respectively. (This is useful for relating Figures A.1 and A.2). Note that there are two receivers at the TRYM and TRYR site, and two receivers at the ARER and AREM site. They are very close together (with 40 m), so they would normally appear as a single dot. They are placed in the figure

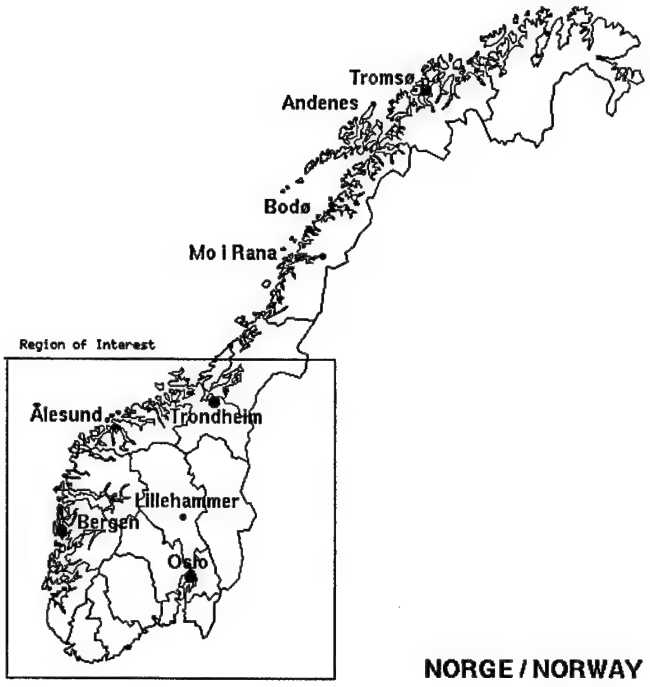

Figure A.1: *Map of Norway. The Norway network is located within the box.*

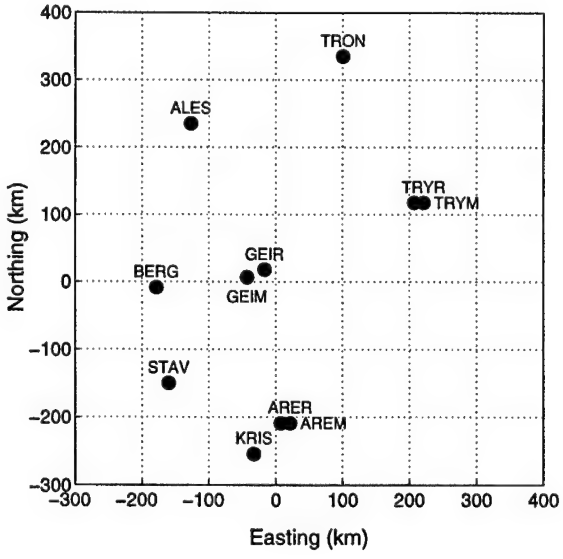

Figure A.2: *Relative locations of Norway reference receiver sites*

slightly offset from each other, however, in order to show that there are two receivers at these sites.

Five of the receivers (KRIS, STAV, BERG, ALES, and TRON) were part of the existing Norwegian SATREF system currently used for code differential GPS inland and in the waterways around Norway. These were all Trimble 4000 SSi dual frequency (semi-codeless) receivers using permanently mounted groundplane antennas.

The other six receivers (AREM, ARER, GEIM, GEIR, TRYM, TRYR) were dual frequency (semicodeless) Ashtech Z-12 receivers which were temporarily set up for this test. The GEIM, GEIR, TRYM, and TRYR receivers used Dorne-Margolin groundplane antennas, and the AREM and ARER receivers used standard Ashtech dual frequency groundplane antennas. All of the Ashtech antennas were mounted on tripods. The Dorne-Margolin antennas have a specified L2 phase center offset (relative to the L1 phase center). All of the L2 measurements from these receivers were transformed to the L1 phase center by subtracting out the projection of the phase center offset onto the satellite line-of-sight vector, *prior* to all of the analysis that is presented in this thesis.

One other receiver was present during the test, located approximately halfway between the TRYM and AREM receivers. There were many cycle slips and data outages from this site, so it was not used.

Data was collected from all receivers at a 1 Hz rate over a 50-hour period starting at approximately 14:00 UTC (15:00 local) on September 29^{th}, 1997. In order to make the data set more manageable, a 24-hour subset of the data was selected extending from 16:00 UTC (17:00 local) on September 29^{th} to 16:00 UTC (17:00 local) on September 30^{th}, and it was also thinned to two second intervals (0.5 Hz). This thinned, 24-hour data set was then used for all of the analysis and results presented in this thesis. The data collection for this test was performed by Kværner Ships Equipment, a.s. in a research effort in conjunction with The University of Calgary.

Figure A.3 shows the number of visible satellites (averaged between the 11 reference receivers) over the 24-hour period. Visible satellites are defined as satellites which are

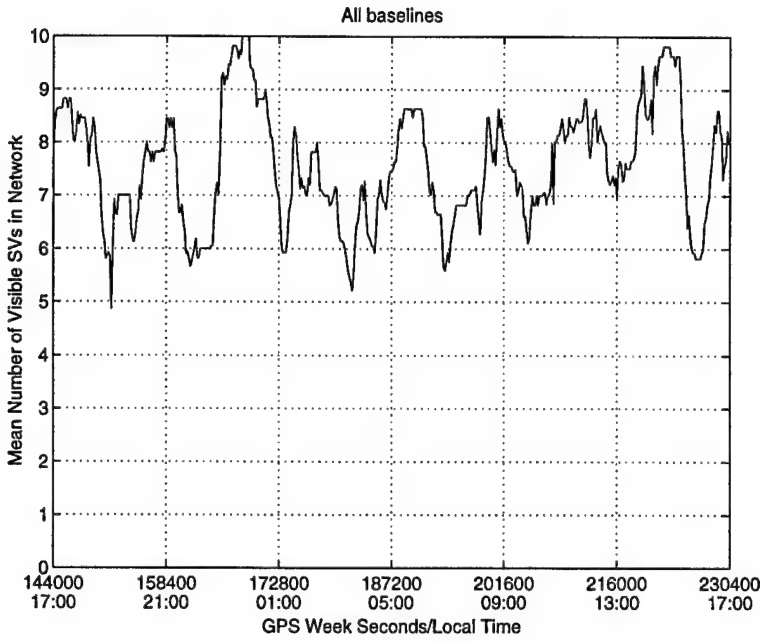

Figure A.3: *Number of visible satellites (averaged between the 11 receivers in the Norway network)*

above 12° elevation and have valid L1 and L2 phase measurements. The mean number of satellites was 7.7, averaged over time and among all 11 reference receivers.

In general, the weather over the 24-hour test period varied from cloudy to clear. No major storm fronts were present during this time. Table A.1 gives approximate (24-hour average) surface weather statistics obtained from the Norwegian Meteorological Institute.

Data from a ground-based magnetic observatory in Norway showed no unusual variations in the geomagnetic field during the 24-hour test period, indicating that the ionosphere was relatively stable. The test was performed in the 7^{th} year of the 11 year sunspot cycle (during the rising portion).

A.1.1 Calculation of Reference Receiver Positions

One of the assumptions when using a reference network is that the receiver antenna coordinates are precisely known (see Section 1.2.3.1). It is very important, then, to determine precise antenna coordinates. For a reference receiver network, precision (relative error) is

Table A.1: *Approximate Surface Weather Data for Selected Norway Reference Stations*

Site	Temperature (°C) Mean	Max	Min	Precipitation (mm)	Mean Rel. Humidity	Atm. Pressure at Sea Level (kPa)
ALES	11.5	12.6	9.3	1.6	73%	1013.0
BERG	10.4	13.1	8.0	0.8	92%	1020.6
STAV	10.9	14.3	8.7	0.3	90%	1021.3
AREM/ARER	9.0	15.9	2.3	0.1	75%	1019.8
GEIM/GEIR	5.7	9.5	2.0	·	64%	not avail.
TRYM/TRYR	4.4	10.3	0.8	·	74%	1016.9
TRON	9.6	14.0	6.2	·	83%	1016.2

more critical than accuracy (absolute error). If the coordinates are precise, but with a fixed offset for all of the receivers, then the estimated differential errors will be calculated (and removed) correctly, and the position result will simply be offset by the network offset. Any lack of precision within the network, however, will effect incorrect estimates of the differential errors, which will reduce position accuracy *and* inhibit the ability to resolve carrier-phase ambiguities.

Preliminary coordinates of each of the receivers were calculated by the Trimble GPSurvey™ surveying software using 6 hours of data thinned to 30-second intervals. The absolute positions of several of the SATREF receivers were provided by Kværner.

Next, a three-dimensional baseline vector was calculated for each baseline in the network[1] using positions calculated from the ionospheric free observable described in Section 2.1.3. This was done by first calculating an epoch by epoch relative position (i.e., baseline) at 30-second intervals over the 24-hour data period using fixed integer ionospheric free double difference residuals. (The integer ambiguities were calculated previously using the procedure described in Appendix B). Precise ephemeris obtained over the Internet from the U.S. National Geodetic Survey were used in order to minimize orbital error effects.

[1]There are a total of 55 baselines between the eleven receivers.

A sample plot showing the epoch-by-epoch three dimensional baseline between the BERG and STAV reference receivers is given in Figure A.4. This was calculated using fixed integer ionospheric free (dual frequency) phase measurements and precise satellite orbits. The mean and standard deviation were calculated for each axis using the 24-hours of data, and they are presented on the plots as well. This mean value was then considered the BERG-STAV baseline measurement, with the standard deviation calculated from the data.[2] This procedure was repeated for all 55 baselines, resulting in 55 three-dimensional baseline measurements and associated standard deviations. The standard deviations for each of the baseline measurements are plotted in Figure A.5.

The post-adjustment measurement residuals[3] provide a good indication of the overall precision of the adjustment, and they are plotted in Figure A.6. The residuals are generally less than 5 mm in the horizontal directions and 1 cm in the vertical direction, indicating that the measurements are probably more precise than the measurement standard deviations (shown in Figure A.5) indicate.

Finally, the post-adjustment error standard deviations of the receiver position errors were calculated for each of the receivers, using the error covariance (calculated from *a priori* measurement variances) scaled by the estimated variance factor $\hat{\sigma}_0^2$ (calculated from the residuals) (Krakiwsky, 1990). Normally, $\hat{\sigma}_0^2$ should be near one. In this case, it was 5.71×10^{-3}, due to the small residuals relative to the measurement error standard deviations. The post-adjustment error standard deviations for each of the reference receivers are shown in Table A.2. These values are probably somewhat optimistic, and data from a different day would be likely to generate slightly different coordinates. Nonetheless, the standard deviations do imply that the reference receiver locations are known to a precision

---

[2]While the results are presented here in the geodetic (east-north-up) frame, all of the calculations were performed in the Earth-Centered Earth-Fixed (ECEF) frame.

[3]The post-adjustment residuals are defined as the original baseline measurements (for the 55 baselines) minus the ranges calculated from the adjusted receiver coordinates. These residuals are calculated separately for each axis.

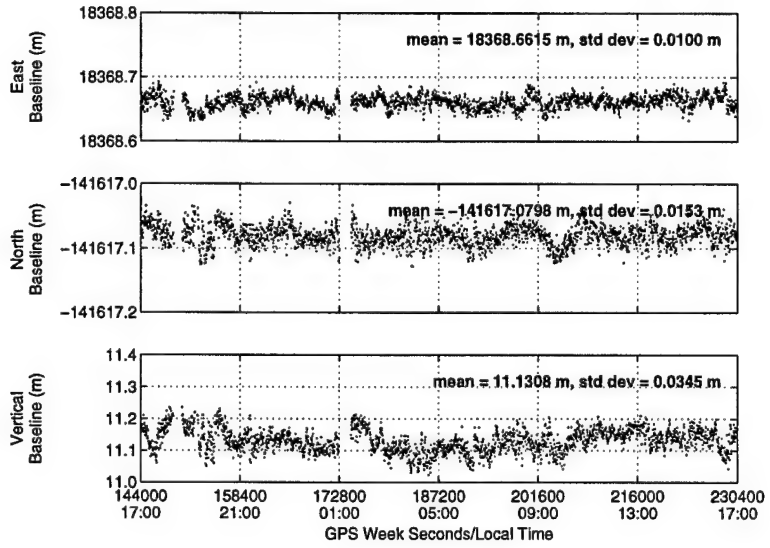

Figure A.4: *Epoch-by-epoch three-dimensional baseline between BERG and STAV receivers, calculated using fixed integer ionospheric free phase measurements and precise satellite orbits*

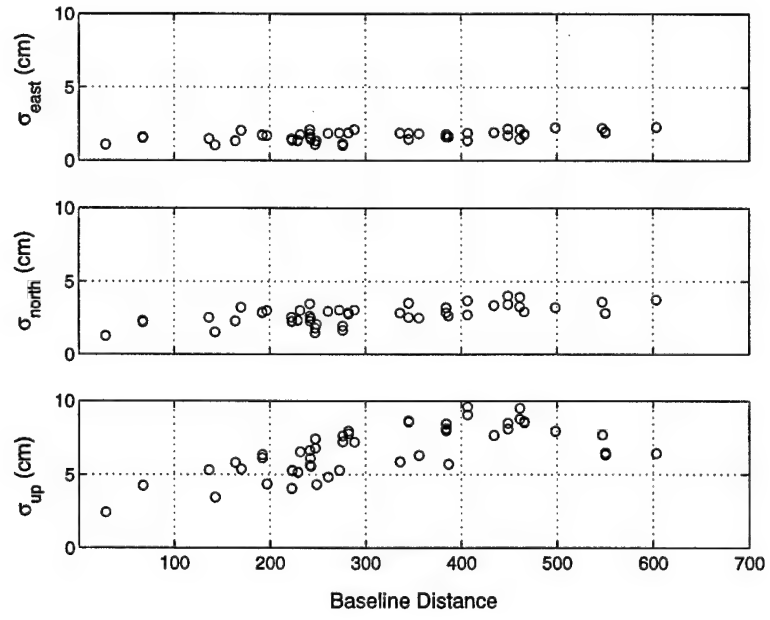

Figure A.5: *Three-dimensional baseline measurement standard deviations for all 55 baselines in Norway network*

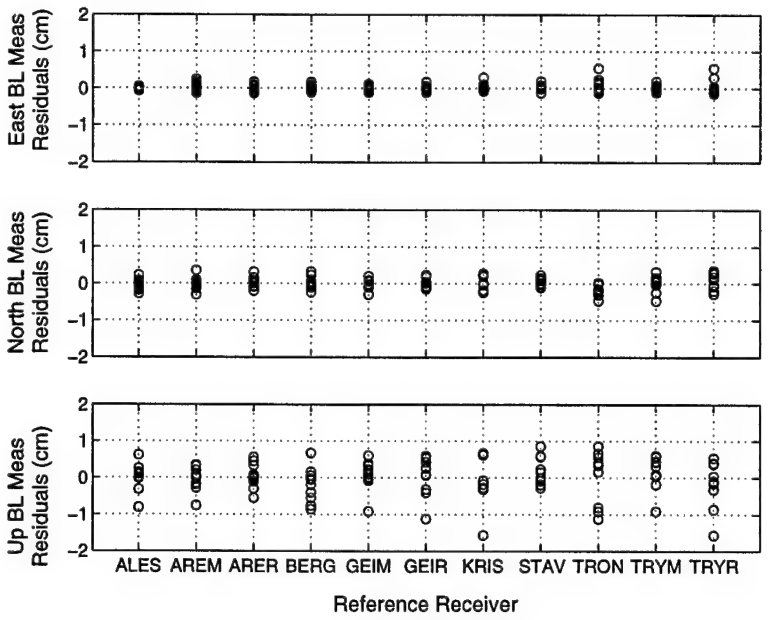

Figure A.6: *Post-adjustment measurement residuals for each reference receiver*

Table A.2: *Theoretical estimated position accuracy of reference receiver coordinates (post-adjustment, based partly upon adjustment residuals)*

	Estimated 1-σ Error (cm)		
Receiver	East	North	Up
ALES	0.05	0.12	0.17
AREM	0.05	0.13	0.16
ARER	0.05	0.12	0.16
BERG	0.05	0.12	0.15
GEIM	0.05	0.12	0.15
GEIR	0.05	0.12	0.15
KRIS	0.06	0.13	0.16
STAV	0.05	0.11	0.15
TRON	0.06	0.13	0.18
TRYM	0.05	0.13	0.17
TRYR	0.06	0.13	0.17

Table A.3: WGS-84 ellipsoidal coordinates of L1 phase centers for Norway network receivers

Receiver	Longitude (deg)	Latitude (deg)	Height (m)
ALES	6.198539697	62.476380742	194.982
AREM	8.759850207	58.489055592	104.511
ARER	8.759862588	58.489156739	104.123
BERG	5.266541503	60.288741923	98.916
GEIM	7.722183907	60.422093600	1247.947
GEIR	8.200342981	60.525564727	814.324
KRIS	7.907414342	58.082691975	152.801
STAV	5.598620273	59.017709092	110.059
TRON	10.319152630	63.371380847	322.810
TRYM	12.381637217	61.422832771	723.940
TRYR	12.381577927	61.423212395	724.795

of 1 cm or better.

The final computed positions of the reference receiver network are shown in Table A.3. These are expressed in WGS-84 ellipsoidal coordinates.

A.2 Holloman Network

In August 1996, four Ashtech Z-12 dual frequency all-in-view GPS receivers were set up at stationary points near Holloman Air Force Base, New Mexico (Raquet, 1997b). These receivers, shown as circles in Figure A.7, collected raw measurements at a 2-second interval continuously for over 54 hours. The receiver labeled "Cigt" was connected to a choke ring antenna which serves as the permanent differential GPS reference station antenna for the 746th Test Squadron Central Inertial Guidance Test Facility (CIGTF). The other three

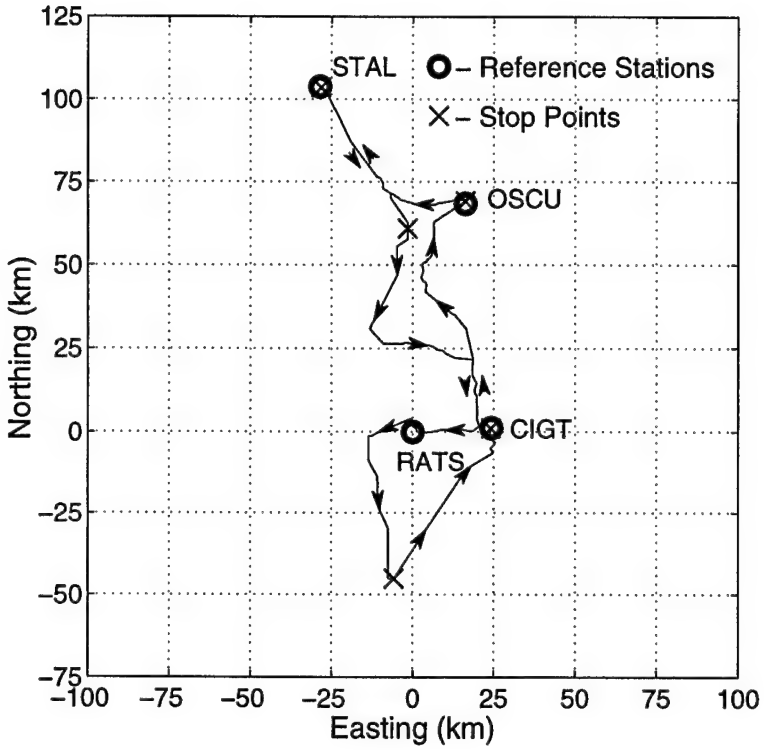

Figure A.7: *Holloman network configuration and van test route*

reference antenna established for this test were mounted on tripods approximately 1.5 m above flat building roofs. They each had an Ashtech antenna with groundplane, and their placement was not necessarily optimized for minimizing multipath.

A fifth receiver was placed 50 km south of the Rats receiver, but it was a very poor site because of a number of obstructions and multipath sources (such as large ventilation ducts). As a result, data from this receiver was not used for the NetAdjust analysis presented in this thesis. It was, however, used as part of the network to determine the positions of the reference receivers.

Three additional receivers were mounted on opposite corners of a 1.25 m square aluminum sheet on top of the 746th Test Squadron Van. One of the receivers was an Ashtech Z-12 with an Ashtech groundplane antenna identical to those used at the reference stations. The other two receivers were NovAtel MiLLennium dual-frequency all-in-view GPS receivers with choke ring antennas. The Ashtech Z-12 mobile receiver was on the

back left corner of the aluminum sheet (when looking from above), the first NovAtel mobile receiver was on the back right corner, and the second NovAtel mobile receiver was on the front right corner. These three receivers are referred to as Ashtech1, NovAtel1, and NovAtel2, respectively.

There were two days of kinematic testing. On the first day, four hours of data were collected as the bus traversed the south end of the test area. On the second day, a total of nine hours of continuous measurements were collected from all three receivers at a 2-second interval. During this period of time, the test van visited each of the reference receivers, following the route shown in Figure A.7. On six separate occasions (the van stopped twice at CIGT), the van remained stationary between for 30–45 minutes. These stationary periods are represented by an "X" in Figure A.7. The majority of the route was over the desert valley, and there were no significant obstructions to the signal of the mobile receivers over the entire 9-hour period. All of the results presented in this thesis were obtained from the data from this second day of testing.

A.2.1 Determination of truth trajectories

A "truth" trajectory was generated for each of the three mobile receivers. These trajectories were a weighted combination of four separate trajectories independently generated by using each of the four reference stations. These four trajectories were obtained by running the Ashtech PNAV software in forward/backward mode, attempting to fix ambiguities. During most of the 9-hour run, each of the four trajectories were in agreement to within 10 cm. However, during some portions of the test, the solutions differed by 1 m or more. Overall, the truth trajectories for the mobile receivers could be characterized as being accurate to within 10 cm 90% of the time, and accurate to within 1 m the remaining 10% of the time.

Appendix B

Calculation of Ambiguities Between Reference Stations

In order to apply the NetAdjust method, the ambiguities between each of the reference stations must be calculated. In an operational system, the ambiguities need to be calculated in real-time. To accomplish this for both widelane (WL) and single frequency (L1) ambiguities, a network approach is required which attempts to determine all ambiguities within the network simultaneously, as opposed to calculating the ambiguities separately for each baseline (see Section 6.1). Examples of the network approach are given in references (Blewitt, 1989) and (Dong and Bock, 1989). Such an extensive effort is outside the scope of this research, however, so a more ad-hoc approach was taken based upon baseline-by-baseline ambiguity determination methods, which are simpler to develop in the short term, but are computationally inefficient and are not optimal for real-time use.

The goal is to obtain integer ambiguity estimates for every possible double-difference measurement (between two receivers and two satellites). If integer ambiguities cannot be accurately determined, then the next best solution is to calculate floating ambiguities, which would introduce some level of error but should still result in an improvement over not using the double-difference measurement at all.

Different methods of calculating reference network ambiguities were used for the Holloman and the Norway data sets. The approach used in the Norway data set is more complex than the approach used in the Holloman data set, due to the large distances between

reference stations in the Norway data set. Both approaches are described in the sections below.

B.1 Norway Data Set

The Norway network had reference station baseline distances of up to 600 km, which necessitated the use of the network to calculate the double-difference ambiguities accurately. The procedure that was developed consists of the following stages of processing:

1. Calculation of the WL and L1 ambiguities separately for each of the baselines. This was done using an iterative method which attempted to calculate ambiguities in batch mode over various time intervals. The result was a highly redundant set of integer and floating ambiguity values from many different overlapping runs. Note that in this step, the L1 ambiguities were calculated using an ionospheric free observable which requires the WL integer ambiguities (so the WL ambiguities needed to be calculated first).

2. All of the redundant ambiguity values calculated in step 1 for each baseline were combined together to determine the best possible ambiguity estimate (integer or floating).

3. Using the ambiguities for each baseline calculated in step 2, the final ambiguities were determined by taking advantage of "chaining" together ambiguities from connecting baselines in the network. This step served as a cross-check as well as providing the ability to chain together short baseline ambiguities to get long baseline ambiguities.

Each of these three steps are described in the sections that follow.

B.1.1 Initial Iterative Ambiguity Calculation

In this step, repeated attempts were made to calculate the ambiguities between each reference receiver pair in batch mode, using different time segments and different base PRNs. Repeated attempts were necessary, because correctly resolving integer ambiguities is sensitive to many factors, including the selection of the base satellite and the length of data that is processed. If the fixed ambiguities are correct, then they should be consistent from run to run, within the same data set.

In order to eliminate the effect of satellite orbital errors, National Geodetic Survey precise orbits were used for all ambiguity calculations. These orbits have an advertised accuracy of 1.6–3.2 cm (1σ), based upon the information in the header of the precise orbit data files.

This portion of the method will be described by first explaining how the WL and L1 ambiguities were calculated for a given time segment of data and given base PRN. Then, the approach for determining which time segments and base PRNs to use is presented.

B.1.1.1 Calculation of WL ambiguities

The goal at this point is to calculate the WL and L1 ambiguities (integer, if possible) between two stationary receivers, using a specified base PRN and a specified time period. (The method for selecting the base PRN and the time period is given in the section that follows). One of the receivers was designated as the reference receiver, and the other as the remote receiver. Since the only purpose at this stage is to determine the ambiguities (rather than perform positioning), the selection of base and remote reference receivers was arbitrary, and reversing the base and remote receivers would only change the sign of all of the ambiguities.

B.1.1.1.1 Cycle Slip Detection and Correction. For every time epoch within the specified time interval, the L1 and L2 carrier-phase measurement-minus-range observable ($\Delta\nabla\bar{\phi}_{ab}^{xy}$) was generated between the base PRN (PRN x in this case) and each of the other

PRN measurements, as described in Section 2.1.2. This resulted in an epoch-by-epoch estimate of the L1 and L2 ambiguities. When a cycle slip occurred, a discrete jump was observed in this time series. (A threshold of 0.35 cycles was used). If the magnitude of the jump was within 0.22 cycles of an integer, and the time period between double-difference measurements before and after the jump was less than 300 seconds, then the cycle slip was corrected in the measurements that followed, and the slip was recorded for later output. If the cycle slip could not be fixed, then the double-difference data was split off at that epoch, and two separate ambiguity parameters were estimated. (The newly created one could be split again if there was another unfixable cycle slip later, if necessary).

B.1.1.1.2 Generation of WL observables. The widelane observable $\Delta\nabla\bar{\phi}_{WL}$ was then calculated as

$$\Delta\nabla\bar{\phi}_{WL} = \Delta\nabla\bar{\phi}_{\mathrm{L1}} - \Delta\nabla\bar{\phi}_{\mathrm{L2}}, \tag{B.1}$$

where $\Delta\nabla\bar{\phi}_{\mathrm{L1}}$ and $\Delta\nabla\bar{\phi}_{\mathrm{L2}}$ are the double differenced measurement-minus-range values of the L1 and L2 phase measurements. (This is the $\phi_{1,-1}$ combination, as expressed in Section 2.1.3.) Any WL cycle slips that occurred were a result of slips in either the L1 or L2 phase measurements (or both), and they were either corrected or split off into a new ambiguity, based upon the knowledge of the cycle slips in the single frequency measurements which had already been calculated.

B.1.1.1.3 Data Thinning. In order to reduce the number of data points to process (and to reduce the time correlation of the errors in the measurements), the data was thinned to 30-second intervals. In addition, the first and last double difference measurement were kept (if it didn't already fall on a 30-second interval), in order to keep track of the exact first and last epoch for that particular ambiguity.

B.1.1.1.4 Initial Floating WL Ambiguity Calculation. A batch least-squares algorithm was used to obtain initial ambiguity values (and the covariance matrix of those

values). First, the parameter vector was defined as

$$\boldsymbol{x} = \begin{bmatrix} \delta x & \delta y & \delta z & N_{1_{WL}} & N_{2_{WL}} & \dots & N_{n_{WL}} \end{bmatrix}^T, \tag{B.2}$$

where δx, δy, and δz are the errors in the nominal position of the remote receiver in the ECEF frame, and $N_{1_{WL}}$ through $N_{n_{WL}}$ are all of the double difference WL ambiguities that are to be estimated. The measurement vector $\boldsymbol{l}$ was comprised of all of the individual WL phase double differenced measurement minus range values for all epochs and all PRN combinations (involving the base PRN). The functional relationship between $\boldsymbol{l}$ and $\boldsymbol{x}$ is described by

$$\boldsymbol{l} = \boldsymbol{f}(\boldsymbol{x}). \tag{B.3}$$

Next, the design matrix $\boldsymbol{A}$ was calculated using

$$\boldsymbol{A} = \frac{\partial \boldsymbol{f}}{\partial \boldsymbol{l}}. \tag{B.4}$$

Each row of $\boldsymbol{A}$ corresponds to an individual measurement in the $\boldsymbol{l}$ vector. In this case, the first three columns of $\boldsymbol{A}$ (corresponding to δx, δy, and δz) were the unit line-of-sight vector from the mobile receiver to the satellite from which the measurements are taken, and the other columns (corresponding to the ambiguities) were 0, 1, or -1, depending upon the ambiguities involved in that particular measurement.

The initial floating ambiguity estimates were then calculated using the standard least-squares equation

$$\hat{\boldsymbol{x}} = (\boldsymbol{A}^T\boldsymbol{A})^{-1}\boldsymbol{A}^T\boldsymbol{l}. \tag{B.5}$$

Note that this equation assumes that the covariance matrix of the noise in the measurements is the identity matrix. This implies that the measurement errors were uncorrelated with each other (which is true for the primary measurement errors in question, namely the ambiguities), and that they are all equally accurate. It would be possible to refine this further (by increasing the covariance for low elevation satellites, for example), but such

improvements are not necessary to obtain the initial covariance estimates. The total scaling on the covariance matrix (one for an identity matrix) is not critical either, because it will be seen below that the covariance values of interests are the covariance of the estimated parameters *relative to each other*, but not in any absolute sense.[1] The covariance matrix of the estimated parameters ($C_{\hat{x}}$) is then

$$C_{\hat{x}} = (A^T A)^{-1}. \tag{B.6}$$

By definition, the ambiguity parameters are integers, so the nominal integer ambiguity estimates were the floating ambiguity estimates rounded to the nearest integer. For short baseline lengths (such as 10km or less), the correlated error terms (satellite position error, ionospheric errors, and tropospheric errors) are almost completely canceled in the double differencing process. As a result, the floating ambiguity estimates were very close (typically within 0.05) to the closest integer value. Over long baselines, however, the correlated error terms do not cancel as effectively, and the floating ambiguity estimates were often not very close to their true integer values. As a result, the algorithm needed to select the correct set of integer ambiguities. This involved two separate steps — determination of a set of integer ambiguity combinations to test (which should include the correct one), and determining which one is indeed the correct set of integer ambiguities. These steps are covered in the paragraphs that follow.

---

[1]It is understood that certain aspects of this whole ambiguity estimation procedure are not theoretically correct, because assumptions are made which are not true in the real world. In reality, there are cross-correlations in the measurement errors which should be reflected in the covariance matrix, and some measurements are more accurate than others. The cross-correlations are due to common errors in the same epoch, as well as time-correlated errors between observations at different epochs. While improving the measurement covariance matrix would improve the results, using an identity matrix worked sufficiently well for the purpose of this particular algorithm — to determine the integer ambiguities between reference stations.

B.1.1.1.5 Determination of Ambiguity Search Space. The technique used to determine the sets of integer ambiguity combinations to test was based on the Fast Ambiguity Search Filter developed by Chen and Lachapelle (Chen, 1993; Chen and Lachapelle, 1995). This algorithm uses the information embedded within the covariance matrix of the ambiguity parameters to select a set of ambiguities that are consistent in a very efficient manner.

The diagonals of the covariance matrix give the variances of each of the corresponding parameters, including the ambiguity parameters. First, the ambiguity parameter with the lowest variance was selected (designated as the n^{th} parameter). An integer search range was then specified for that ambiguity parameter, by selecting all integers that are within the range

$$\hat{x}_n - k\sigma_n \leq N_{n_{int}} \leq \hat{x}_n + k\sigma_n, \tag{B.7}$$

where $\hat{x}_n$ is the estimate of the n_{th} parameter, σ_n is the standard deviation of the n_{th} parameter, and k is a constant. (The method used to calculate k is described later).

Next, for each $N_{n_{int}}$ within the search range, a conditional mean and covariance for the parameters was calculated, conditioned on the fact the $\hat{x}_n$ has taken on the realized value $N_{n_{int}}$. This was implemented using the Equations (Lu, 1995; Weisenburger, 1997)

$$\tilde{\boldsymbol{x}} = \hat{\boldsymbol{x}} - \boldsymbol{c}_n(\hat{x}_n - N_{n_{int}})/\sigma_n^2 \tag{B.8}$$

$$\boldsymbol{C}_{\tilde{\boldsymbol{x}}} = C_{\hat{\boldsymbol{x}}} - (\boldsymbol{c}_n \boldsymbol{c}_n{}^T)/\sigma_n^2, \tag{B.9}$$

where

$\tilde{\boldsymbol{x}}$ is the estimated parameter vector conditioned upon $\hat{x}_n = N_{n_{int}}$,

$\boldsymbol{C}_{\tilde{\boldsymbol{x}}}$ is the covariance matrix conditioned upon $\hat{x}_n = N_{n_{int}}$,

$\boldsymbol{c}_n$ is the n^{th} column of the covariance matrix $C_{\hat{\boldsymbol{x}}}$, and

σ_n^2 is the scalar variance of the n^{th} parameter (taken from the diagonal of $C_{\hat{\boldsymbol{x}}}$).

Because there are correlations between the parameters, the diagonal elements of $\boldsymbol{C}_{\tilde{\boldsymbol{x}}}$ are less than or equal to the diagonal elements of $\boldsymbol{C}_{\hat{\boldsymbol{x}}}$. This effectively reduces the search ranges for each of the other ambiguities.

This process was repeated recursively, calculating conditional parameter estimates and covariances conditioned upon more than one fixed ambiguity. If all possible ambiguity parameters were set to integers in this recursive process, then this set of integer ambiguity estimates was considered a valid set to be considered as the possible correct set. This method is very efficient, because many incorrect integer ambiguity sets are rejected when at some layer in the recursion it is not possible to generate any integer values that meet the constraints given in Equation B.7. When all possible combinations have been exhausted, there are a number of candidate integer ambiguity sets, one of which is (hopefully) correct.

Most previous implementations of the FASF method (see Weisenburger (1997) for example), use a predetermined value for the parameter k given in Equation B.7. Typically, a value between 3 and 10 is chosen (Lu et al., 1995). If the parameters are jointly Gaussian and the covariance matrix is reflective of the true covariance (i.e., it is properly scaled, and all significant error sources have been modeled), then using a constant value of k is a reasonable approach, because for a Gaussian distribution, there is a specific probability that the realization of the random variable (an integer ambiguity in this case) will lie within a window of size $k\sigma$ about the mean. For example, if $k = 3$, then there is a 99.7% probability that the realization of the random variable will be within 3-σ of the mean. If, however, the covariance matrix is not reflective of the true covariance, then using a constant value of k can result in a candidate ambiguity set which is too pessimistic (resulting in many ambiguity sets, which makes it difficult to distinguish the correct one), or too optimistic (resulting in a small number of sets, but possibly excluding the correct ambiguity set).

In this research, a different approach was taken. Rather than fixing k and living with whatever ambiguity sets are generated, k was adjusted such that there would be between 30 and 700 candidate ambiguity sets. An initial value of k was chosen. If using that value of k generated fewer than 30 candidate ambiguity sets, then the entire process was repeated with a higher k value. Likewise, if more than 700 ambiguity sets were generated, then a lower k value was used. Using such an approach assured that there would be a

reasonable number of ambiguity sets to test.

B.1.1.1.6 Determination of Correct Ambiguity Set. The measurement residuals were used as a test to determine which of the candidate ambiguity sets was the correct one. First, the design matrix was partitioned into two submatrices

$$\boldsymbol{A} = [\boldsymbol{A}_{pos} | \boldsymbol{A}_{amb}], \tag{B.10}$$

where $\boldsymbol{A}_{pos}$ and $\boldsymbol{A}_{amb}$ are the columns of the $\boldsymbol{A}$ matrix which pertain to the position and ambiguity parameters, respectively. Next, the integer ambiguities were removed from the original double difference measurement vector by

$$\boldsymbol{l}(n) = \boldsymbol{l} - \boldsymbol{A}_{amb}\boldsymbol{x}_{int}(n), \tag{B.11}$$

where $\boldsymbol{x}_{int}(n)$ is the n^{th} candidate integer ambiguity set, and $\boldsymbol{l}(n)$ is the new vector of double difference measurements corrected for the ambiguities in $\boldsymbol{x}_{int}(n)$. At this point the effect of the ambiguities has been removed, so the residuals $\boldsymbol{r}(n)$ to a least squares fit in the position domain were calculated using

$$\hat{\boldsymbol{x}}_{pos}(n) = (\boldsymbol{A}_{los}^T \boldsymbol{A}_{los})^{-1} \boldsymbol{A}_{los} \boldsymbol{l}(n) \tag{B.12}$$

$$\boldsymbol{r}(n) = \boldsymbol{A}_{los}\hat{\boldsymbol{x}}_{pos}(n) - \boldsymbol{l}(n), \tag{B.13}$$

and the scalar sum of squares of the residuals (SOSr) was then calculated using

$$\text{SOSr}(n) = \boldsymbol{r}(n)^T \boldsymbol{r}(n). \tag{B.14}$$

Note that there exist alternative methods of calculating the SOSr values more efficiently in conjunction with Equations B.8 and B.9 (Weisenburger, 1997).

Once the SOSr values were calculated for each of the candidate integer ambiguity sets, then the ratio of the second best to the best SOSr values was calculated as

$$\text{SOS}_{\text{ratio}} = \frac{\text{SOSr}_{\text{2nd best}}}{\text{SOSr}_{\text{best}}}, \tag{B.15}$$

where the "best" is defined to be the lowest value. If this ratio exceeded 1.8, then the candidate ambiguity set corresponding with $SOSr_{2nd\ best}$ was deemed to be correct. Keep in mind that the residuals represented here were for all of the double difference measurements over every epoch (i.e. not just one epoch).

B.1.1.1.7 Removal of satellites when not correctly solved. Sometimes the above procedure would result in a SOS_{ratio} value of less than 1.8, which signified that with that particular set of measurements, no candidate ambiguity set was significantly better than any of the others. Sometimes this would be due to a satellite which had only a small number of measurements available in the specified time interval. Because there were only a small number of measurements, then different ambiguities for these satellites would only change relatively few measurements within the residual ($\boldsymbol{r}$) vectors, making the ratio test of Equation B.15 fail. Similar effects would occur if one satellite (or a few satellites) had significant atmospheric errors, which is typically the limiting factor over long baselines.

In order to prevent these types of situations, if the ambiguity search failed the ratio test, then measurements involving the ambiguity with the highest floating ambiguity variance (from the $\boldsymbol{C}_{\hat{\boldsymbol{x}}}$ matrix) were removed, and the entire process was restarted from the beginning. This iteration continued until either a) the ratio test was successful, or b) only three ambiguities remained (in which case they could not be solved).

If the ratio test was successful with a subset of the ambiguities (but not all the ambiguities), then floating ambiguity estimates were recalculated only for the ambiguities that were not successfully fixed. In this calculation, the fixed ambiguities were considered deterministic, resulting in fewer degrees of freedom than in the original floating solution (in which all ambiguities were stochastic).

Finally, the fixed or floating ambiguities for every possible PRN combination were then saved into a file for later processing. PRN combinations that do not involve the base PRN were calculated as well, using the equation

$$N^{xy} = N^{bx} - N^{by}, \tag{B.16}$$

where N^{bx} and N^{by} are the ambiguities between the base PRN and PRNs x and y, respectively, and N^{xy} is the ambiguity between PRNs x and y. If both N^{bx} and N^{by} are fixed integers, then N^{xy} is an integer as well, but if either N^{bx} or N^{by} (or both) are floating values, then N^{xy} is calculated as a floating ambiguity.

B.1.1.2 Calculation of L1 ambiguities

For long baselines[2], it becomes very difficult, if not impossible, to determine L1 or L2 integer ambiguities reliably using single frequency measurements. However, when dual frequency measurements are available, it is possible to calculate single frequency ambiguities using an ionospheric free L1/L2 measurement combination (which requires knowledge of the integer widelane ambiguity). The procedure described below is an adaptation of the algorithms given in Blewitt (1989) and Ashtech (1994).

Recall from Section 2.1.3 that the widelane and ionospheric free observables can be calculated as

$$\phi_{WL} = \phi_{L1} - \phi_{L2} \tag{B.17}$$

$$\phi_{IF} = \phi_{L1} - \frac{f_2}{f_1}\phi_{L2}, \tag{B.18}$$

and the corresponding ambiguity equations are

$$N_{WL} = N_{L1} - N_{L2} \tag{B.19}$$

$$N_{IF} = N_{L1} - \frac{f_2}{f_1}N_{L2}. \tag{B.20}$$

Recognizing from Equation B.19 that $N_{L2} = N_{L1} - N_{WL}$, Equation B.20 can be rewritten as

$$N_{IF} = N_{L1} - \frac{f_2}{f_1}\left(N_{L1} - N_{WL}\right), \tag{B.21}$$

[2]Many of the baselines in the Norway network were hundreds of kilometres long. It is generally difficult or impossible to determine integer ambiguities using single frequency data for baselines greater than 30–50 km.

or, equivalently,

$$N_{IF} = \left(1 - \frac{f_2}{f_1}\right) N_{L1} + \frac{f_2}{f_1} N_{WL}. \tag{B.22}$$

Finally, solving for N_{L1} yields

$$N_{L1} = \frac{N_{IF} - \frac{f_2}{f_1} N_{WL}}{\left(1 - \frac{f_2}{f_1}\right)}. \tag{B.23}$$

This equation shows how the L1 ambiguity can be calculated from the IF and WL ambiguities. At this point in the process, the WL integer ambiguities have been calculated (as described above), and they are here considered deterministic quantities. Equation B.23 then represents a linear transformation between the ionospheric free ambiguity N_{IF} to the L1 ambiguity N_{L1}. This means that, if the expected value (estimate) and covariance matrix are calculated for a jointly Gaussian random vector of ionospheric free ambiguities, then the expected value and covariance matrix of the random vector of L1 ambiguities can be easily determined using that linear transformation as follows (Maybeck, 1994):

$$\hat{\boldsymbol{N}}_{L1} = \frac{1}{\left(1 - \frac{f_2}{f_1}\right)} \hat{\boldsymbol{N}}_{IF} - \frac{\frac{f_2}{f_1} \boldsymbol{N}_{WL}}{\left(1 - \frac{f_2}{f_1}\right)} \tag{B.24}$$

$$\boldsymbol{C}_{\hat{N}_{L1}} = \frac{1}{\left(1 - \frac{f_2}{f_1}\right)^2} \boldsymbol{C}_{\hat{N}_{IF}}. \tag{B.25}$$

Taking this into account, the procedure used to calculate the L1 ambiguities from the IF observable is as follows:

1. The floating estimates ($\hat{\boldsymbol{N}}_{IF}$) and covariance matrix ($\boldsymbol{C}_{\hat{N}_{IF}}$) of the ionospheric free ambiguities were calculated using Equations B.5 and B.6, only in this case the $\boldsymbol{l}$ vector was comprised of IF observables (rather than WL observables). Because the IF observables included no ionospheric errors, the ionosphere did not introduce a bias into these floating ambiguity estimates.

2. Floating estimates of the L1 ambiguities ($\hat{\boldsymbol{N}}_{L1}$) and the related covariance matrix ($\boldsymbol{C}_{\hat{N}_{L1}}$) were calculated using Equations B.24 and B.25. These estimates were not

biased by ionospheric errors (which would not be true if we used single frequency measurements only).

3. The FASF procedure was used to calculate the candidate L1 integer ambiguity sets using $\hat{\boldsymbol{N}}_{L1}$ and $\boldsymbol{C}_{\hat{N}_{L1}}$.

4. The residuals for each L1 candidate integer ambiguity set were calculated by first transforming the integer L1 and WL ambiguities into an IF ambiguity using Equation B.22, then using the same procedure described in Equations B.11 through B.13.

5. The correct ambiguity set was determined by using the ratio test given in Equation B.15. As in the widelane case, a ratio of 1.8 was required for the search to be deemed successful.

6. If the search was unsuccessful, the ambiguity with the highest variance was removed, and the entire L1 search process was repeated until a successful ratio test or there were only three ambiguities left. (This is identical to the WL case).

7. If successful, then floating ambiguities were recalculated for those ambiguities that had not been successfully fixed. (This is identical to the WL case).

Using this procedure, ionospheric errors were eliminated. Using precise orbits essentially eliminated the satellite position errors. Errors that remained were tropospheric modeling errors, multipath, and measurement noise. Elimination of the ionospheric error was often sufficient to make it possible to determine integer ambiguities, even in the presence of these other errors.

B.1.1.3 Selection of Time Periods and Base PRNs

Even while using the above method for removing the ionospheric effect in calculating the L1 ambiguities, there were many situations in which it was not possible to determine the L1 (or even WL) ambiguities using a particular base PRN and data from a given time

period. However, in many of these cases it *was* possible to determine the ambiguities by using a different base PRN or by changing the time period of the data. As a result, it was useful to attempt to calculate the WL and L1 ambiguities using a variety of time periods and base PRNs. The sections that follow describe the algorithms used to select the different time periods and base PRNs.

B.1.1.3.1 Selection of Time Periods The total Norway data set consisted of 24 hours of data, starting at 17:00 local time (16:00 UTC) on 29 Sep 97. The goal was to determine the data time intervals over which calculations of the WL and L1 ambiguities would be attempted. For clarity, these data time intervals will be referred to as "windows."

First, the window length was set to three hours (i.e., three hours of data would be used for each batch estimation of WL and L1 ambiguities). The first window began at the start time (17:00 local) and ended three hours later (20:00 local). Then, the next window started at a time which was $1/10^{th}$ of a window length (18 minutes for a 3-hour window length) later than the first window start time. Additional 3-hour windows were then determined, each starting 18 minutes after the previous window started. This process continued until a window start time was within 1/2 of the window length of the end of the data set (1.5 hours for a 3-hour window). A diagram showing the all of the 3-hour time windows that were used is given in Figure B.1. Each line represents a time window. There are a total of 76 different windows.

The same procedure was followed for window lengths of 4 hours and 5 hours. Again, each window was delayed in time from the previous window by $1/10^{th}$ of the window length, which was 24 minutes for the 4-hour windows and 30 minutes for the 5-hour windows. This resulted in a total of 56 4-hour windows and 44 5-hour windows which, when combined with the 76 3-hour windows, resulted in a total of 186 different time windows used to calculate WL and L1 ambiguities for each baseline. Plots similar to Figure B.1 could also be drawn for the 4-hour and 5-hour length windows.

The primary purpose for trying such a variety of time windows was to give every

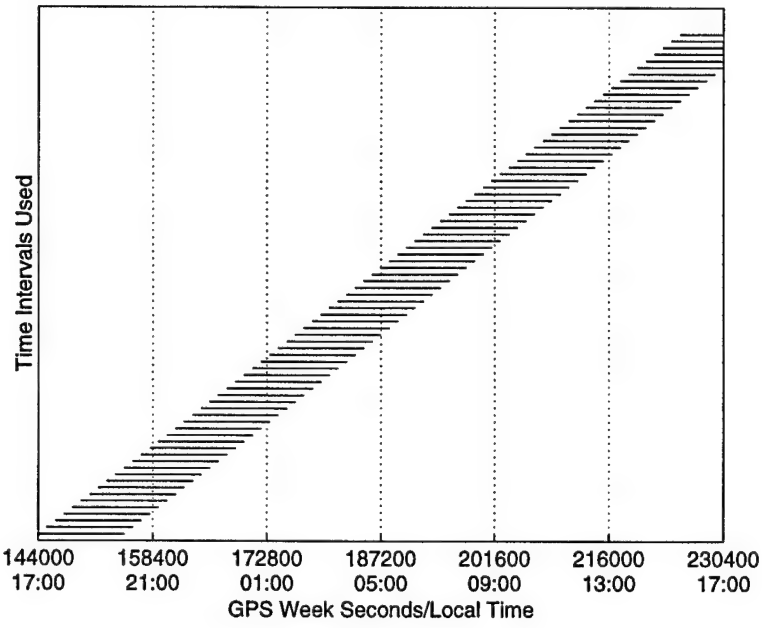

Figure B.1: *Set of 3-hour time windows used in the calculation of WL and L1 ambiguities*

possible opportunity to calculate all of the ambiguities. Because the differential GPS errors tend to vary with time, using different time periods would help to find periods in which the errors were low for any particular ambiguity.

B.1.1.3.2 Selection of Base PRNs When calculating the WL and L1 ambiguities as described in Section B.1.1, one satellite PRN is selected to be used as the base PRN in all double differenced measurement-minus-range values (i.e., the x in $\Delta\nabla\bar{\phi}_{ab}^{xy}$). It is generally accepted practice to select the highest elevation satellite as the base satellite (see Weisenburger (1997) for example), because this usually provides the best geometry, and the errors *tend* to be lower for high elevation satellites. While the highest elevation satellite is probably the best choice as a base satellite if only one must be used, there is no guarantee that using the highest elevation satellite is *always* the best.

To this end, for each time window selected, different runs of the WL and L1 ambiguity resolution procedure described in Section B.1.1 were performed for multiple base PRNs. For a particular time window, every satellite that provided cycle-slip-free measurements

for at least the first 1.5 hours of the data window was used as a base PRN. Using this method, there were an average of 2.74 base PRNs used for each time window.

It turned out that attempting to resolve ambiguities with different base PRNs was useful for obtaining more fixed integer ambiguities. In many cases, the integer ambiguities could not be determined using the highest elevation satellite, but they could be determined using a different base satellite.

It should be noted that using the described procedure for selecting base PRNs had the side-effect of using varying time windows as well. For example, for a particular 3-hour window, there might be a satellite which provides cycle-slip-free data for the first 2 hours of the window. This satellite would be selected as a base PRN, and when used would effectively have a time window of 2 hours (rather than the specified 3-hour window). In cases in which the integer ambiguities could be successfully calculated when using one base PRN but not another, it is not always clear whether the difference is the variations in time intervals between the PRNs or the different error characteristics of the PRNs were primarily responsible for the success or failure of the technique. Most likely, it is a combination of the two effects.

B.1.2 Combination of Redundant Ambiguity Calculations

Using the procedure described in the above section resulted in a total of 510 separate attempts to calculate ambiguities (on average) for each baseline, using different PRNs and different overlapping time periods. The next step was to combine the results of these attempts into a single set of results for the baseline.

First, the ambiguities were collected into groups according to the PRNs and the time periods. Each group corresponded to a single ambiguity value. If a cycle slip occurred, then there were multiple groups for the same PRN values, over different (but adjacent) time periods).

All of the integer ambiguities in a single group were the same if the ambiguity had

been calculated correctly at every instance. The ambiguity would then be selected as the correct ambiguity over the time period of the whole group. Occasionally, however, the integer ambiguities within a group would differ, which meant that one or more of them were wrong. In this case, the correct ambiguity was chosen by calculating a weighted average of the integer ambiguities. Ambiguities that passed the ratio test with large values and that were estimated using long time periods received high weightings. Ambiguities that were part of solutions from which a different ambiguity was found to be incorrect were given a very low weight. The weighted ambiguity was then rounded off to determine the integer ambiguity for that group. While there can be unusual situations in which this procedure results in an incorrect ambiguity, most of the time this method is very reliable at choosing the correct ambiguity from among the list of potential ambiguities. It works well because incorrect ambiguity calculations are rare, and they can usually be singled out easily from among a number of correct ambiguity choices.

For all groups, a pure floating ambiguity value was also calculated from all of the individual floating ambiguities weighted by their respective time intervals. As an example, a floating ambiguity calculated using three hours of data received three times the weighting of an ambiguity that was calculated using only one hour of data.

B.1.3 Generation of Final Ambiguity Values Using Reference Station Chaining

Equation B.16 showed how ambiguities between different PRNs can be combined together in order to calculate new ambiguities. In a similar manner, ambiguities between reference stations can be "chained" together in order to determine ambiguities over a long distance.

For example, suppose that there is a network with four receivers labeled a, b, c, and d. The symbol N_{ab} represents the ambiguity for a particular PRN pair between receivers a and b, N_{bc} represents the ambiguity between receivers b and c, and so forth. The ambiguity

between receivers a and c can be calculated using the relation

$$N_{ac} = N_{ab} + N_{bc}. \tag{B.26}$$

(This can be easily verified using Equation 2.17). If for some reason N_{ac} was unable to be calculated, then the above equation can be used to calculate it. If the ambiguity N_{ac} has already been calculated, then the above equation can be used as a cross check. Longer chains can be assembled as well, like this 3-link chain:

$$N_{ad} = N_{ab} + N_{bc} + N_{cd}. \tag{B.27}$$

For the Norway network, a computer program called NetAmb was developed which is able to use receiver chaining to determine some ambiguities that were not calculated on the direct baseline. It also serves as a cross-check of each of the ambiguities. For a given ambiguity between two receivers, NetAdjust attempts to recalculate it using every possible 2-link chain (using one intermediate receiver, as in Equation B.26) and every possible 3-link chain (using two intermediate receivers, as in Equation B.27).

Using the 11 receivers in the Norway network, there are a total of 9 possible 2-link chains and 72 possible 3-link chains. NetAdjust attempts to calculate the desired integer ambiguity using all of these different combinations, and then compares them with the direct ambiguity (with no chaining). If all of the ambiguities are correct, then all of the ambiguities will match. On occasions when they do not match, a scoring method is used to pick the correct ambiguity. This scoring method takes into account such factors as the frequency of occurrence (if almost every chain gives the same ambiguity, then the most common ambiguity is probably correct) and the number of chains used (shorter chains are weighted more highly than long chains).

In the process, NetAmb also determines whether or not a particular ambiguity could be in error due to a "single point failure". If there is any single link which is common to all of the chains that produced the ambiguity, then that ambiguity is completely dependent upon the accuracy of that single link. If the link is wrong, then all of the calculated ambiguities

will be wrong as well, and there would be no way to know that it was wrong. In most cases, however, NetAmb was able to establish at least two chains that were completely independent of each other (i.e., they shared no common links). In these cases, a high level of confidence can be placed upon the resulting ambiguity.

Despite the use of chaining, NetAmb was not able to determine every possible integer ambiguity. In cases in which it was not possible to determine the integer ambiguity, NetAmb calculated a floating ambiguity which was a weighted average of the floating ambiguities from each of the contributing chains (including the direct floating ambiguity between the two reference stations in question).

The NetAmb program was used to calculate/verify the ambiguities for each baseline in two iterations. For the first iteration, NetAmb used the ambiguities calculated using the procedure described in Section B.1.2, and output a new set of ambiguities for each baseline. For the second iteration, NetAmb used the newly calculated set of ambiguities, and output the final set of ambiguities. This second iteration was used because it allowed NetAmb to chain together ambiguities that had been calculated by the first iteration of NetAmb, which increased the total number of integer ambiguities. It should be noted that the second iteration of NetAmb only dealt with integer ambiguities. Any floating ambiguities calculated during the first iteration were kept at the same values, in order to prevent them from developing errors due to correlation problems. (Recalculating the floating ambiguities in the second iteration would be taking weighted averages of weighted averages).

Figure B.2 shows the total number of double difference measurements that can be generated between all of the reference stations in the Norway network, as a function of time. Note that this closely follows the number of satellites observed by the network, as shown in Appendix A (Figure A.3).

Figure B.3 shows the percentage of the total number of double difference ambiguities that have been successfully fixed to integer values by NetAmb. In general, the L1 ambiguity fix rate varies between 75% and 100%. The fix rate drops at the beginning and end of the 24-hour test period. This results from the fact that the ambiguity fixing process

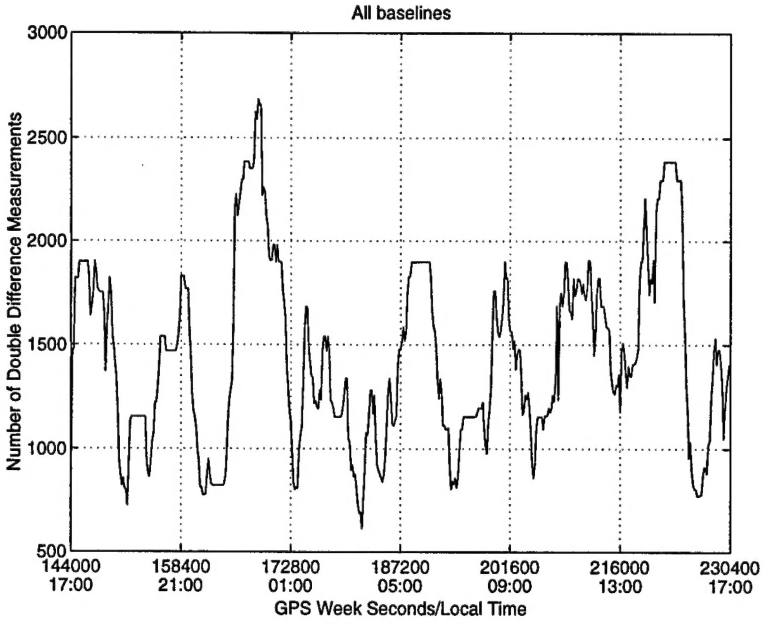

Figure B.2: *Total number of L1 double difference measurements between Norway network reference stations*

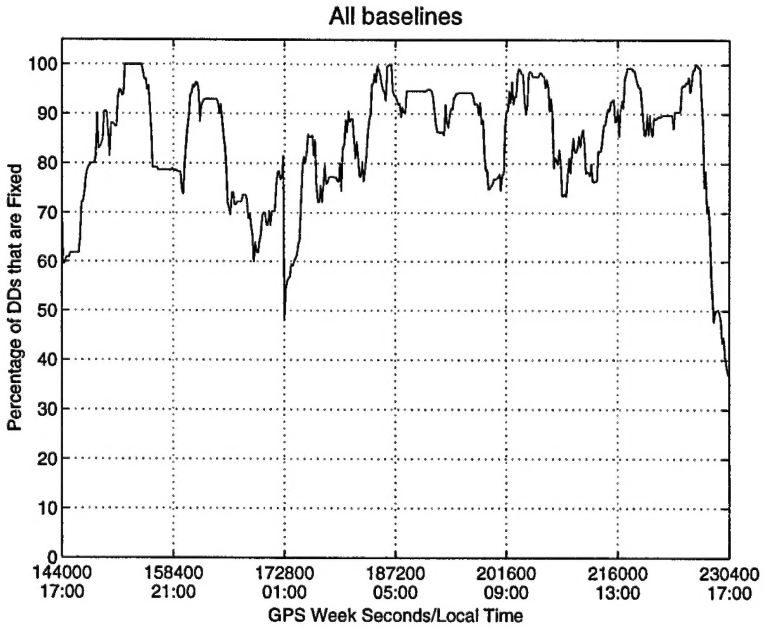

Figure B.3: *Percentage of L1 ambiguities that are fixed between between Norway network reference stations*

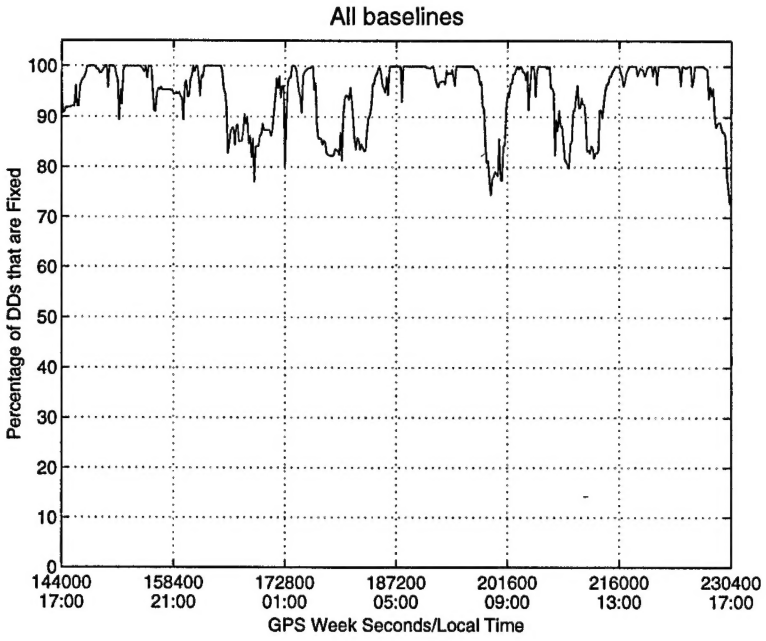

Figure B.4: *Percentage of WL ambiguities that are fixed between between Norway network reference stations*

is a batch process, and the ambiguities at any particular time epoch are calculated based on data before *and* after that epoch. At the beginning, however, data is only available after 17:00, so ambiguities calculated around 17:00 could only use measurements *after* that time, resulting in a reduced ambiguity fix rate. The same reasoning can be applied to explain the drop at the end of the 24-hour period as well. There is also a drop in the ambiguity fix rate at exactly 1:00 (which is midnight UTC). Because of an irregularity in the way that the raw data was recorded, all of the Trimble receivers experienced simultaneous cycle slips on all channels at that instant, causing the drop.

Figure B.4 shows the percentage of WL ambiguities that were successfully fixed.

B.2 Holloman Data Set

The Holloman data set was processed during the early stages of this research, and the process used for the Norway network had not been developed yet. It was a much smaller net-

work, however, so the ambiguities could be resolved using a slightly different approach.

The Ashtech PRISM™ software was used in an iterative manner to calculate both L1 and WL ambiguities. PRISM is a GPS positioning package designed to be used for surveying static receivers. It performs carrier-phase ambiguity resolution in a batch mode, which means it uses all of the data from two receivers over the run duration in a single least-squares adjustment (and ambiguity search).

For each baseline, PRISM was run over 3-hour time intervals which were staggered by one hour each, and the results from all of the separate runs were combined and cross-checked. The baseline-by-baseline ambiguities were then used in NetAmb (described in Section B.1.3) to generate the final set of ambiguities. Using this method, the L1 and WL (and therefore L2) ambiguities between the Holloman reference receivers were successfully determined almost 100% of the time.